R-8455

CORRELATION OF SPRAY DROPSIZE DISTRIBUTION AND INJECTOR VARIABLES

Rocketdyne
North American Rockwell

R-8455

CORRELATION OF SPRAY DROPSIZE DISTRIBUTION AND INJECTOR VARIABLES

by

L. J. Zajac

Prepared for

National Aeronautics and Space Administration
Jet Propulsion Laboratory
Pasadena, California

Contract NAS7-726

Rocketdyne
A Division of North American Rockwell Corporation
6633 Canoga Avenue, Canoga Park, California

FOREWORD

The work described herein was conducted for NASA, Jet Propulsion Laboratory, Pasadena, California, by Rocketdyne, a Division of North American Rockwell Corporation. The study was performed in accordance with Contract NAS7-726, G.O. 09162. This report supercedes the interim report originally issued as Rocketdyne document R-7995, September 1969.

Mr. R. M. Clayton of the Jet Propulsion Laboratory served as the NASA Technical Project Manager. The Rocketdyne Program Manager was Mr. T. A. Coultas. Technical guidance of the program was provided by Mr. S. D. Clapp.

Important contributions to the conduct of the program and to the preparation of the report material were made by the following Rocketdyne personnel: D. T. Campbell, W. H. Nurick, R. M. Knight, and E. A. Rojec.

ABSTRACT

An experimental investigation of the atomization characteristics of impinging stream rocket engine injection elements was conducted to determine the effects of a number of hydraulic and geometric parameters on the mass median dropsize. The parameters influencing atomization that were examined included: (1) those characterizing an individual jet such as injection velocity, jet (orifice) diameter, velocity profile, and turbulence level, (2) those characteristic of opposing jets such as dynamic pressure ratio, propellant miscibility, and diameter ratio, and (3) those parameters related to the injector design such as orifice length, free jet length, orifice entrance conditions, impingement angle, and degree of misimpingement. In addition, the possibility of an emulsion forming at the interface of jets flowing immiscible fluids was examined. The injector types utilized in this study included like and unlike-doublets, triplet and pentad elements.

A molten wax technique which provides a quantitative measure of the sprays was used to experimentally measure the dropsize distribution. In order to correlate the spray dropsizes with the internal characteristics of the free jets, the velocity profiles and turbulence levels of the jets were measured by a flat plate pressure probe.

The major conclusions that resulted from the atomization study are: (1) the velocity profile of impinging jets will effect the mean dropsize; this effect was found to be greater when the jets were laminar than when they were turbulent, (2) the dropsize/injection velocity dependence for turbulent jet impingement differs from that obtained with non-turbulent jets, (3) the level of (non-zero) turbulence intensity did not effect the mean dropsize, (4) the impingement of disintegrated or nearly disintegrated jets will substantially decrease atomization, and (5) even though an emulsion was formed when immiscible jets were impinged, the level of emulsification was small (1%). From the results of this investigation, empirical correlations relating the mean dropsize to the jet dynamic and geometric parameters were developed.

Several of the more important observations of the jet characteristics study are: (1) the disintegration of turbulent jets when the free jet length was greater than 5 orifice diameters, (2) sharp entrance orifices were susceptible to jet separation up to an orifice length of at least 10 diameters, (3) a long orifice length (greater than 15 to 20 diameters) was required to completely damp manifold effects, and (4) jet characteristics were severally degraded by cross-flow manifold effect when the orifice length was less than 6 diameters. The results of this study provide guidelines for the design of injection systems.

CONTENTS

ILLUSTRATIONS

TABLES

NOMENCLATURE

C_c	Contraction coefficient
C_D	Discharge coefficient
d_f	Fuel orifice diameter
d_j	Jet diameter
d_o	Oxidizer orifice diameter
D	Droplet diameter
$\bar{D}$	Mass median droplet diameter
$\bar{D}_f$	Fuel-side mass median dropsize
$\bar{D}_o$	Oxidizer-side mass median dropsize
$\bar{D}_\gamma$	Mass median dropsize at γ degrees
$\bar{D}_\Delta$	Mass median dropsize at Δ misimpingement
h	Sheet thickness
K	Sheet thickness parameter
K_f	Fuel sheet thickness parameter
K_o	Oxidizer sheet thickness parameter
L_j	Free jet length to impingement point
L_o	Orifice length
M_T	Total injected momentum
n	Number of impinging jets
N_R	Reynolds number
N_W	Weber number

p	Dynamic pressure
p_c	Dynamic pressure at center of jet
p_j	Mean dynamic pressure of jet
P_D	Dynamic pressure ratio, $(\rho V^2)_f/(\rho V^2)_o$
r	Radius
r_j	Jet radius
r_s	Separated jet radius
T	Turbulence intensity
V_c	Manifold cross velocity
V_f	Fuel injection velocity
V_j	Mean jet velocity
V_o	Oxidizer injection velocity
$\dot{w}$	Mass flowrate

Greek Letters

γ	Impingement angle
Δ	Misimpingement
μ	Viscosity
ν	Kinematic viscosity
ρ	Density
σ	Surface tension
ϕ	Mixing parameter, $(\rho V^2 d)_f/(\rho V^2 d)_o$
ψ	RMS value of pressure fluctuations
ψ_c	RMS value of pressure fluctuations at jet centerline

1.0 INTRODUCTION

Tne evaluation of rocket engine injector design criteria requires an understanding of the primary injection parameters which control the combustion process. Previous analytical and experimental work by Rocketdyne and other investigators has shown that one of the combustion-rate limiting processes in liquid rocket engines is vaporization of the liquid propellants, a process which is primarily dependent upon spray droplet size and propellant physical properties. Dropsize is, therefore, an important parameter in the determination of rocket engine combustion efficiency.

It is well known that when liquid jets impinge, liquid spray fans, or sheets, are formed. These sheets break down into ligaments which in turn form drops. Analytical solutions to the conservation equations governing the phenomena have been effected in only a small number of idealized cases in which specific assumptions were made regarding the forces acting upon the sheet and the method of sheet disintegration. The first theoretical contribution to this field was given by Rayleigh (Ref. 1) in his analysis of the instabilities associated with a single jet of liquid. Many other workers have extended the works of Rayleigh (e.g., Ref. 2 through 6); however, they have been unable to predict, to an adequate degree, the character of these spray droplet size distributions.

Although accurate quantitative predictions of dropsize have not been obtained from theory, these studies provide a physical insight into the mechanisms of the atomization process and serve to identify those parameters which influence droplet formation. For example, at very low injection velocities, the dropsize is primarily a function of the jet diameter or, more specifically, the energy associated with the surface tension forces of the jet. At higher injection velocities, aerodynamic shear forces between the liquid and the gaseous environment become important. At very high injection velocities, the liquid is exposed to rapid deceleration by the gaseous environment, and inertial forces thus become important. Some of these flow regimes have been observed experimentally (e.g., Ref. 6 through 9), and theoretical considerations of the existence of the different regimes have been recorded in the literature (Ref. 2, 3, and 10).

Because of the difficulties involved in the theoretical prediction of spray droplet sizes, many investigators have determined spray droplet sizes experimentally for various atomizer configurations and liquid physical properties (e.g., Ref. 11 through 18). However, the data reported in the literature are primarily for injection schemes and operating conditions which are not comparable to those found in contemporary rocket engines. Notable exceptions to this are the works of Dombrowski and Hooper (Ref. 12), Ingebo (Ref. 13), Kuykendal (Ref. 17) and a recent study at Rocketdyne (Ref. 14).

Dombrowski and Hooper conducted a study of the factors influencing the disintegration of sheets formed by the impingement of two water jets. The investigation was limited to like-doublet elements having an orifice L/d of 400. Impingement angle was varied and a dropsize correlation was developed. Kuykendal examined the effects of a variety of parameters including: injection velocity, orifice diameter, impingement angle, stream alignment, orifice length and orifice surface finish. As in the work of Dombrowski and Hooper, this investigation utilized like doublets with water as the propellant simulant. The work of Ingebo included effects of orifice diameter, jet velocity, and the velocity difference between the liquid jet and surrounding airstream; utilizing short orifice elements (L/d = 10) with n-heptane as the propellant simulant.

In all of the above investigations, a photographic method was used for measurement of the spray particle sizes. This technique has limitations since the results are generally dependent upon the size and location of the photographic field. In addition, reduction of data from the spray photographs is time consuming and costly. The works of Dickerson, et. al (Ref.14) and of Hasson and Mizrahi (Ref. 16) have shown that the molten wax technique could be successfully utilized to provide a quantitative measure of the sprays produced by impinging stream injector elements. This method has advantages in that the entire spray field is collected and particle sizes are determined using a relatively simple sieve analysis.

The Rocketdyne study (Ref. 14) was also instrumental in extending previous atomization work in the areas of rocket engine injector simulation. It was

demonstrated that two immiscible liquids (water and paraffin wax) could be used for simulation of unlike impinging injector elements. In addition, it was shown that the propellant atomization and mixing processes could be investigated separately and the results combined in computerized combustion models to predict overall combustion efficiency.

Although the Ref. 14 program added significantly to a better understanding of atomization, many areas of interest required investigation. For example, one area which had not been studied included the effects of propellant miscibility on droplet size and distribution and the possibility of forming an emulsion. In the realm of orifice geometry and injector design effects on dropsize, only limited work has been done. Also, little or no information was available to evaluate the influence of the internal hydraulic characteristics of the free jet. Consequently, an experimental program was conducted to investigate poorly understood aspects of the mechanisms of atomization and to extend the range of previous dropsize correlations. The experimental approach employed in the program was the molten wax technique successfully demonstrated by Dickerson, et al. (Ref. 14).

The program was divided into seven major tasks:

Task 1A Investigation of the Effect of Propellant Miscibility on Droplet Size Distribution Using Unlike Impinging Injector Elements

Task 1B Investigation of the Possible Occurrence of Emulsification Between Immiscible Liquid Propellants

Task IIA Droplet Size Determination at Low Injection Velocities

Task IIB Investigation of the Effects of Free Jet Geometry (Impingement Angle and Free Jet Length) on Spray Droplet Size Distribution

Task III Investigation of the Effects of Jet Disintegration, Turbulence Intensity and Velocity Profile on Droplet Size

Task IV Injector Design (Orifice entrance type and manifold cross velocity) Effects on Turbulence Intensity and Droplet Size

Task V Investigation of the Effect of Jet Dynamic Pressure Ratio on Spray Droplet Size

The data obtained during Tasks I and II of the program were presented in an interim report. This final report incorporates these data and supercedes the interim report originally issued as Rocketdyne document R-7995, September 1969.

From an analysis of the data conducted after the conclusion of Tasks I and II, it was apparent that parameters other than the gross characteristics of the impinging jets (i.e., injection velocity, impingement angle, etc.) were contributing to the median dropsize obtained from the spray. Specifically, in Task IIA, it was observed that significant variations in dropsize occurred when the length of the orifice was varied while all other parameters were held constant. It was postulated that internal characteristics of the jet (velocity and turbulence profiles) were responsible for the observed discrepancies in dropsize. In order to properly investigate these effects, an experimental program was initiated in Task III and continued through Tasks IV and V, to measure, in addition to droplet size distributions, the internal jet characteristics.

Although contractually, the program was divided into the seven aforementioned tasks, it is more appropriately described from a technical viewpoint in Table 1. As illustrated there, the program can be divided into three distinct parts on the basis of the type of experiments performed.

In the jet characteristic experiments, the dependent parameters were the free jet velocity and turbulence profiles. Single jets were used in conjunction with two different types of manifold configurations. The independent parameters and the range of investigation are listed in Table 1. In the majority of the impinging jet experiments, the mass median dropsize and droplet size distributions were quantitatively evaluated. A separate series of tests were performed in which the level of emulsification resulting from the impingement of immiscible propellants was examined. The range of the independent parameters for the atomization and emulsification experiments are also listed in Table 1. Although the orifice length was a variable in these tests, its effect is directly associated with the velocity and turbulence profiles and is therefore not considered to be an independent parameter.

TABLE 1. PARAMETERS AND RANGE OF INVESTIGATION

JET CHARACTERISTICS STUDY

	Range	
	Manifold Type	
	Parallel-Feed	Cross-Feed
Injection Velocity (ft/sec)	30 - 160	120
Orifice Diameter (inch)	0.060 - 0.120	0.060
Orifice Length/ Diameter	1.5 - 200	6 - 100
Free Jet Length/ Diameter	2 - 15	5
Orifice Entrance	Sharp and Round	Sharp and Round
Manifold Cross Velocity (ft/sec)	0	o - 20

TABLE 1. (Contd.) ATOMIZATION STUDY

Parameter	Range of Wax Jet(s)			
	Doublet	Unlike Doublet	Triplet	Pentad
Injection Velocity (ft/sec)	30-220	30-130	30-150	30-60
Orifice Diameter (inch)	0.060-0.081	0.060-0.120	0.067	0.063-0.086
Diameter Ratio	1.0	1.0-2.0	1.0	1.365
Velocity Profile	U-FDL* U-FDT	Laminar FDT	Laminar FDT	Laminar
Turbulence Level	0-FDT	0-FDT	0-FDT	0
Dynamic Pressure Ratio	1.0	0.5-4.0	1.7-2.0	0.5-0.8
Impingement Angle	45-90	60	60	60
Jet Misalignment (percent)	0-75	0	0	0
Free Jet Length/ Diameter	1.0-1.0	5	5	5
Orifice Length Diameter	1.5-200	1.5, 10, 50	50	10,50
Orifice Entrance	Sharp/Round	Round	Round	Round
Propellants Simulants	wax	wax/wax wax/H_2O wax/DEW	wax/H_2O	wax/H_2O

EMULSIFICATION STUDY

Total Momentum (ft-lb/sec)	-	7-40	-	10-50
Propellants Simulants	-	wax/DEW	-	wax/DEW

*U = Uniform Velocity Profile
FDL = Fully Developed Laminar
FDT = Fully Developed Turbulent

**DEW= Aqueous Solution of Diethanolamine

2.0 SUMMARY

This report contains the results of an 18-month applied research program. The overall goals of the program were to experimentally investigate the effects of a variety of injector hydraulic and geometric parameters on both atomization and the internal characteristics of the jets producing the sprayfield as well as the inter-relationship between atomization and the internal jet characteristics.

Experimentally, the program can be divided into three parts. In one, the velocity and turbulence profiles of the free jets were qualitatively evaluated by a technique which measures the pressure profiles produced by the impingement of the jet upon a flat plate. The velocity and turbulence profiles of the free jet are deduced from a comparison of the measured pressure profiles to those produced by jets with known internal characteristics.

In the second, the mean dropsize and the droplet size distribution produced by the impingement of liquid jets were quantitatively measured by a molten wax technique. With this technique, the entire spray field is collected and the mass fraction of droplets in a given size interval is determined from a sieve analysis.

The third series of tests investigated the possibility of an emulsion forming from the impact of immiscible jets.

The objectives of the internal jet characteristics investigation were twofold: (1) to evaluate the chracteristics of the jets produced by the injector elements subsequently used in the atomization experiments and (2) to investigate the influence of fluid velocity and orifice geometry on the free jet velocity and turbulence profiles.

Two manifold types were employed in the jet characteristics study. The majority of the measurements were obtained using a manifold which brought fluid to the orifice in a direction parallel to the orifice axis. In this series of tests, the principle independent variables were the injection velocity, free jet length,

orifice length, orifice diameter and the orifice entrance type. The remainder of the jet characteristics measurements were obtained with a manifold flow direction orthogonal to the orifice axis. Orifice length, entrance type and manifold cross velocity were the independent parameters in these tests.

The results of the jet characteristic studies with parallel-feed manifolds showed that, with round entrance orifices, a transition from laminar to turbulent flow occurred at Reynolds number of about 10,000. It was found that, in the laminar flow regime, the velocity profile could be correlated with theoretical predictions of velocity profile development by using the non-dimensional parameter $N_r\ d_j/L_o$. An orifice 200 diameters in length was required to obtain nearly fully developed laminar flow.

When the flow was turbulent, an orifice length of 50 diameters was sufficient to attain fully developed turbulent flow at Reynolds numbers above 10,000 while, an orifice length of 10 diameters was of insufficient length in the Reynolds number range of 10,000 to 15,000. Intermediate orifice lengths were not examined. In accordance with the measurements of other investigators, the absolute turbulence intensity level increased with both injection velocity and orifice length.

The measured tubulence intensity increased with the free jet length. However, this can be attributed to the measurement technique rather than to actual phenomena within the jet. The onset of jet disintegration occurred within free jet lengths of 5 to 10 orifice diameters when the jet was turbulent. Jet disintegration was not observed with laminar jets with free jet lengths up to 10 orifice diameters.*

With sharp entrance orifices and a parallel-feed manifold, the jets were found to completely separate from the orifice walls above a Reynolds number of about 4000 with orifice lengths up to 10 diameters. The separated jets were non-turbulent and had nearly uniform velocity profiles.

* Photographs obtained by Rupe, Ref.21, show that laminar jet disintegration will occur at free jet lengths above about 40 orifice diameters.

In the series of tests conducted with a manifold cross flow, the orifice velocity was held constant at 120 ft/sec; corresponding to a Reynolds number of 10740. As was the case with a parallel-feed manifold, the flow was turbulent at this Reynolds number. There were, however, significant differences in the flow obtained with the two manifold types, namely; (1) the jet did not separate when a sharp entrance orifice was used in conjunction with a cross-feed manifold and (2) in contrast to the results obtained with parallel-feed manifolds, the turbulence intensity passes through a minimum and then increases as the orifice length approaches zero. With respect to the latter statement, the high levels of turbulence encountered with orifice L_o/d_j's less than 6 (both orifice entrance types) precluded accurate measurements of the internal jet characteristics.

Additionally, these experiments showed that manifold cross flow with velocities, up to 20 ft/sec, will influence free jet characteristics when the orifice length is less than 25 diameters for a sharp entrance orifice and when it is less than 15 diameters for a round entrance orifice. There was no difference in the characteristics of the free jets produced by round or sharp entry orifices when the orifice length was greater than 25 diameters. Fully developed turbulent flow was attained above an orifice length of 30 diameters for both entrance types.

The objectives of the atomization studies were to determine the influence of a number of hydraulic, geometric and free jet parameters on dropsize and, where possible, to obtain empirical correlations relating the mass median dropsize to those parameters. The parameters that were investigated in the dropsize studies can be divided into three categories: (1) those pertaining to the characteristics of the individual jets, including injection velocity, orifice diameter, velocity profile and turbulence intensity, (2) those which are characteristic of the opposing jets such as dynamic pressure ratio, diameter ratio and propellant miscibility and (3) injector design parameters such as entrance type (parallel-feed manifolds only) impingement angle and free jet length. In these studies four element types were utilized. namely; like-doublets, unlike-doublets, triplet and pentad.

The injection velocity range of the like-doublet experiments was sufficiently large so that atomization data was obtained in both the laminar and turbulent flow regimes. In those cases where the free jets were laminar, the dropsize was found to be a strong function of the velocity profile which, in turn, depends upon the jet Reynolds number and the orifice length. A substantially smaller velocity profile dependence was obtained when the jets were turbulent. Although the existence of turbulence influenced the dropsize-velocity relation, the level of turbulence was found to be immaterial to the mean droplet size.

For like-doublet elements, the following empirical correlations were obtained (60^{o} impingement angle only):

Laminar Jet

$$\bar{D} = 4.85 \times 10^{4} \; V_j^{-0.75} \left(\frac{p_c}{p_j}\right)^{-0.52} d_j^{\;0.57}$$

and

Turbulent Jet

$$\bar{D} = 15.9 \times 10^{4} \; V_j^{-1.0} \left(\frac{p_c}{p_j}\right)^{-0.10} d_j^{\;0.57}$$

where

$\bar{D}$ = mass median droplet size, microns

V_j = mean injection velocity, ft/sec

d_j = orifice diameter, inches

and

$\frac{p_c}{p_j}$ = velocity profile parameter defined as the ratio of the centerline dynamic pressure to the mean dynamic pressure

Additional like-doublet experiments indicated that the dropsize depended upon the impingement angle according to the expression

$$\bar{D}_{\gamma} = (1.42 - 0.0073\,\gamma)\;\bar{D}_{60}$$

where $\bar{D}_{\gamma}$ is the dropsize (in microns) obtained at an impingement angle of γ degrees and $\bar{D}_{60}$ is the dropsize produced at an impingement angle of 60 degrees.

The influence of jet misalignment on dropsize was found to be

$$\bar{D}_{\Delta} = \bar{D}_{\Delta = 0} \left(1 - \frac{\Delta}{d_j} \right)^{-0.19}$$

where Δ is the distance (in inches) between parallel planes passing through the jet axis.

Sharp entrance orifices were found to effect dropsize indirectly through the occurrence of jet separation. It is shown that, by properly accounting for changes in the free jet velocity and diameter resulting from separation, the dropsizes obtained with sharp entrance orifices can be correlated with the above laminar jet correlation.

Finally, the occurrence of free jet disintegration prior to jet impingement can increase the median dropsize by as much as 40%. This result could be especially important when short ($L_o/d_j \leq 6$) orifices are used in conjunction with cross-feed manifolds. As previously noted, the high turbulence level (presumably due to jet disintegration) that is encountered with this orifice/manifold combination would have an adverse effect on atomization.

The primary independent parameters in the unlike-doublet experiments were the injection velocity, dynamic pressure ratio, orifice diameter, and propellant miscibility. For this element type, the following correlations were obtained (60° impingement angle only):

$$\bar{D}_f = 2.9 \times 10^4 \, V_f^{-0.766} \left[\frac{p_c}{p_j} \right]_f^{-0.65} d_f^{0.293} \, P_D^{0.165} \left[\frac{d_o}{d_f} \right]^{0.023}$$

and

$$\bar{D}_o = 2.72 \times 10^4 \, V_o^{-0.57} \left[\frac{p_c}{p_j} \right]^{-0.30} d_o^{0.65} \, P_D^{-0.25} \left[\frac{d_o}{d_f} \right]^{-0.17}$$

where

$\bar{D}$ = mass median droplet size, microns

V = Injection velocity, ft/sec

$\frac{p_c}{p_j}$ = velocity profile parameter

d = orifice diameter, inches

and

P_D = dynamic pressure ratio, $(\rho V^2)_f / (\rho V^2)_o$

while the subscrips f and o refer to the fuel (smaller diameter) orifice and oxidizer (larger diameter) orifice, respectively. In cases of equal diameter doublets, the fuel dropsize correlation should be used for both propellants.

The injection velocities of the unlike doublet experiments were primarily in the laminar flow regime (i.e., corresponding to Reynolds numbers less than 10,000). Consequently, application of the above correlations must be limited to this flow regime.

Propellant miscibility was found to influence the median dropsize. The extent of the influence of miscibility will depend upon the specific injector hydraulic and geometric operating conditions, propellant combination and the free jet characteristics. For example, with short ($L_o/d_j = 1.5$) orifice elements, larger drops were obtained when wax and an aqueous solution of diethanolamine were used as propellant simulants as opposed to a wax/wax combination. With longer elements ($L_o/d_j = 10$), and hence greater velocity profile development, the two simulant combinations yielded the same dropsize.

The atomization characteristics of the triplet and pentad elements were examined as a function of injection veolocity only. For the triplet element, it was found that the empirical correlation

$$\bar{D} = 4250\ \bar{V}_j^{-0.575} \qquad (d_o = d_f = 0.067 \text{ inches}, \quad \gamma = 60 \text{ degrees})$$

could be used to calculate both the fuel and oxidizer dropsizes for this particular element.

The results obtained with the pentad element were, for the most part, in agreement with the results of Dickerson, et.al., Ref. 14. Differences were obtained, however, at lower injection velocities ($V \leq 80$ ft/sec) which may be attributed to velocity profile effects. Because of an insufficient quantity of data, this could not be verified.

The objective of the emulsification study was to evaluate the possible occurrence of emulsification by an examination of the droplets produced by impinging immiscible jets. These studies were performed with both unlike-doublet and pentad elements over a wide range total stream momentum. It was found that a nominal level of about a 1% emulsion was formed regardless of the momentum level. This result was obtained for both element types.

3.0 EXPERIMENTAL APPARATUS AND TECHNIQUES

3.1 INJECTION ELEMENTS

An important consideration in the design of the orifice was the method of fabrication. Several techniques were considered, including drilling and reaming, electrical discharge machining, and the use of tubing. The latter method, chosen on the basis of economy and quality control, was used when the orifice length to diameter ratio was greater than 50. For orifice lengths equal to or less than 10 diameters each orifice was first drilled and then reamed.

3.1.1 Single-Orifice Elements

A total of 22 single-orifice elements ranging in orifice length from 1.5 to 200 diameters, were utilized in the program. Of the 22, 5 have a sharp (square) entrance while the remainder have a contoured inlet with a radius equal to 1.5 orifice diameters. The fixture used to form impinging stream injectors from these elements is described in Section 3.1.3. For identification the elements are assigned a code number which also specifies the pertinent geometric dimensions as described below:

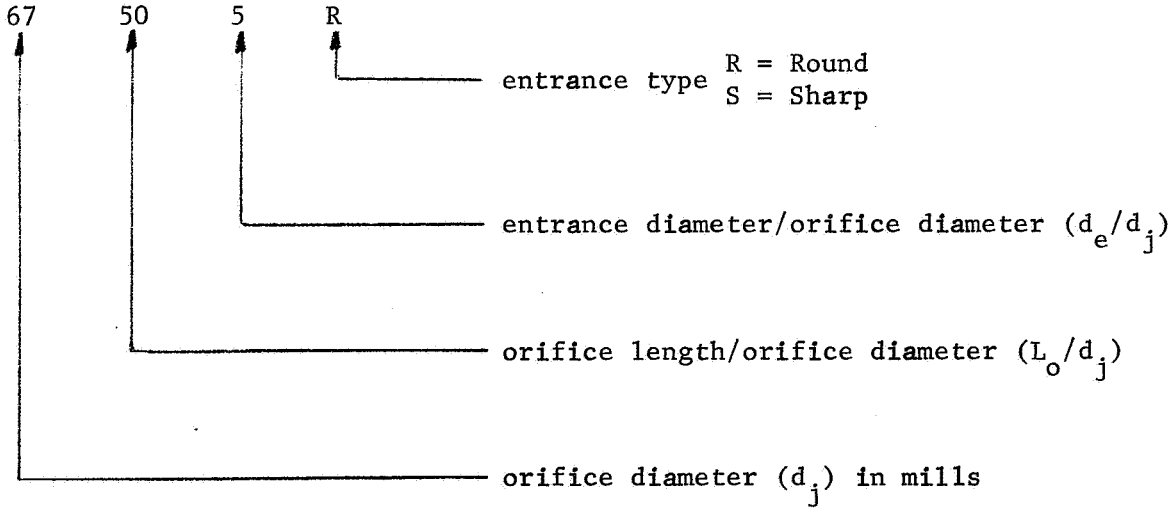

Long ($L_o/d_j \leq 50$) Orifice Design. Typical geometry of the long elements is shown on Fig. 1. The elements are fabricated from tubing, with the outer tubes swaged over the inner tube which comprises the orifice. The inner tubes are reamed to the final diameter after the swaging process. A total of six elements

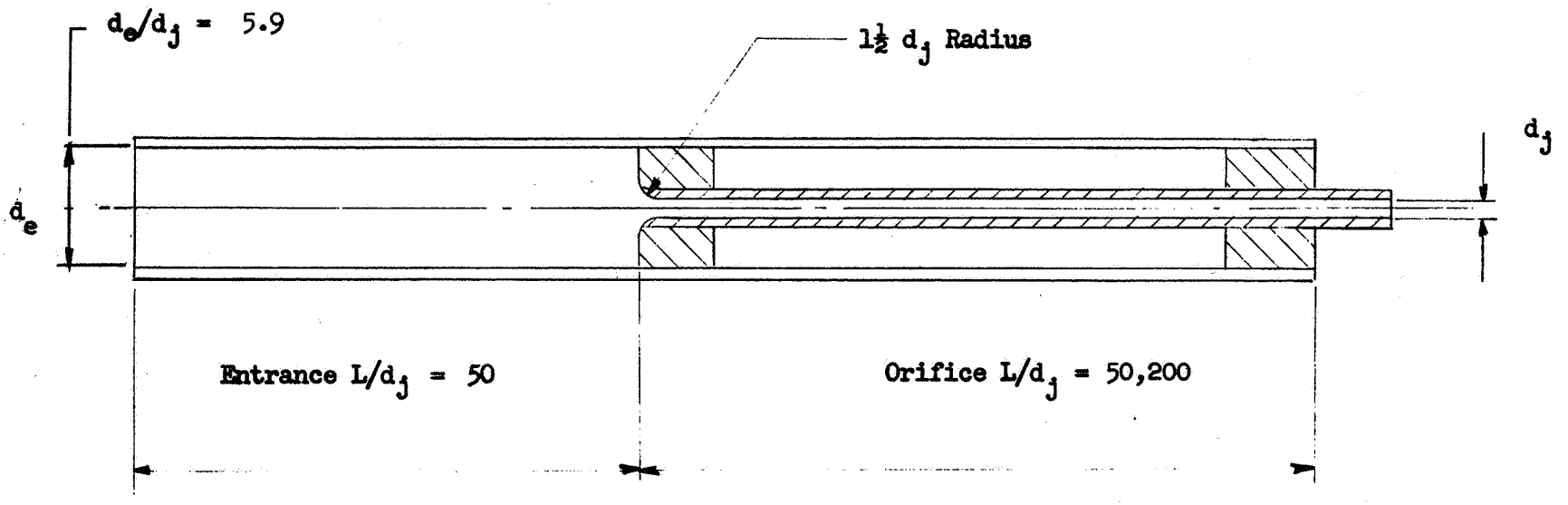

Figure 1. Typical Geometry for Long Single-Orifice Elements (d_j = 0.067, 0.069, 0.086, 0.128)

of this type were used in the program. The code numbers of the elements (specifying the physical dimensions of the orifices) and their discharge coefficients at an injection velocity of 50 ft/sec are summarized in Table 2.

TABLE 2 SUMMARY OF LONG L/d_j ELEMENTS

Code Number	C_D	No. Fabricated
67-50-5R	0.73	2
86-50-5R	0.73	1
128-50-5R	0.73	1
69-200-9R	0.65	2

Short ($L_o/d_j \leq 10$ Orifice Design. The configuration of the short elements is shown on Fig. 2. The orifice hole is drilled and reamed in a stainless steel plate. Tool marks and burrs are removed by polishing. The orifice plate is then silver soldered to a large diameter tube which also acts as a calming section to provide quiescent orifice entry conditions. A total of 12 elements of this type were fabricated; 6 with a sharp-edged orifice entrance and 6 with a rounded entrance.

The geometry of the remaining short orifices, designated by the code number 60-1.5-10R is shown on Fig. 3. These elements were fabricated using the above techniques but differ from the other short orifices in that, because of space limitations imposed by program requirements of short orifice and free jet lengths and large diameter upstream section, it was necessary to place the orifice off the centerline of the upstream calming section.*

The code numbers of the short orifice elements and their discharge coefficients are summarized below in Table 3.

*Velocity profile measurements of the free jet indicated that the influence of the non-symmetrical orifice inlet conditions was minimal for orifice length-diameter radius = 1.5.

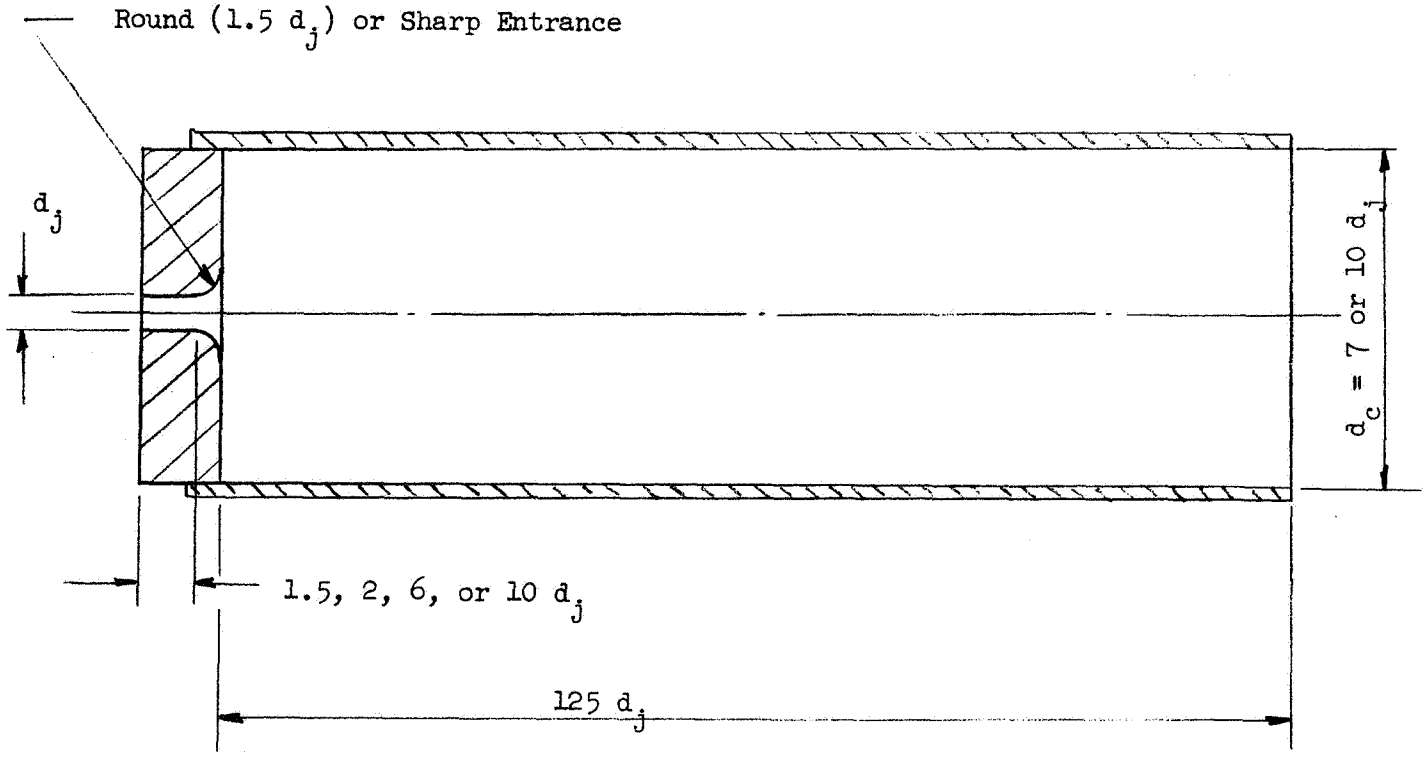

Figure 2. Typical Geometry for Short Single-Orifice Elements (d_j = 0.060, 0.061, 0.063, 0.090, or 0.120)

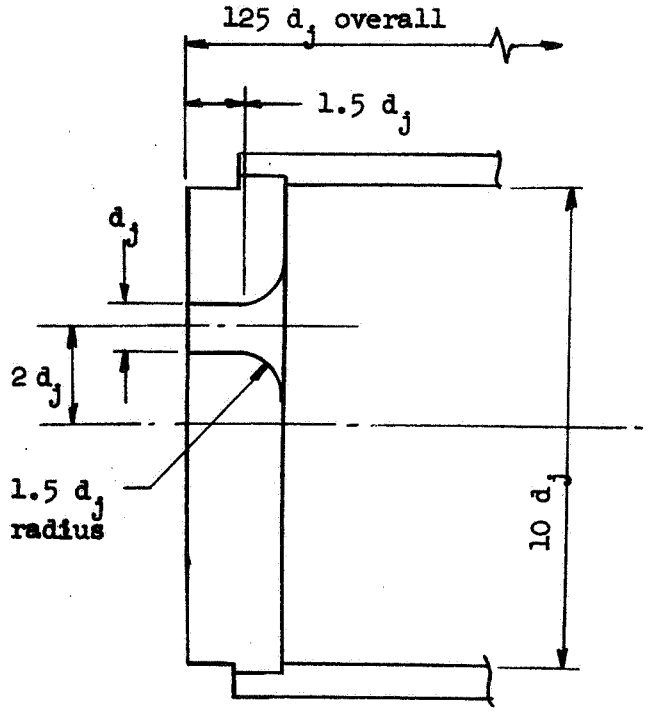

Figure 3. Schematic of Orifice Used in Laminar Jet Studies

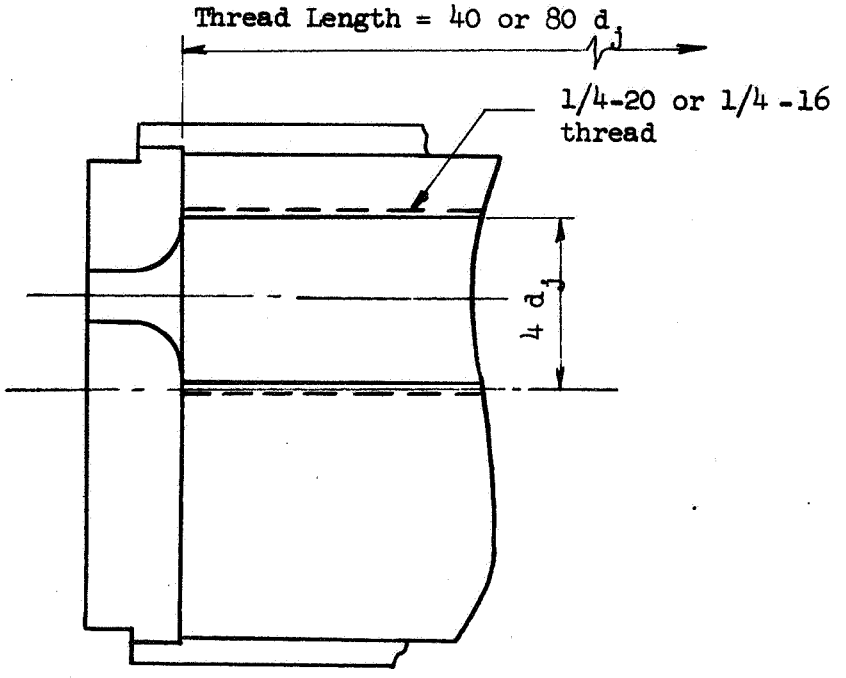

Figure 4. Schematic of Orifice Used in Turbulent Jet Studies

TABLE 3. SUMMARY OF SHORT L/d_j ELEMENTS

Code Number	C_D	No. Fabricated
60-1.5-10R	0.92	2
61-6-7R	0.87	2
63-10-7R	0.82	2
61-2-7S	0.60	2
61-6-7S	0.60	2
61-10-7S	0.60	2
90-1.5-10R	0.93	1
120-1.5-10R	0.94	1

Turbulence Generator. A specific objective of the program was the evaluation of the influence of internal jet turbulence on dropsize formation. This objective required the design of an injection system which produced liquid jets having both very low (nearly laminar) and very high internal turbulence levels. In order to minimize velocity profile effects the orifice element used to obtain the turbulent jets is the 60-1.5-10R element desribed above.

In order to generate turbulence in the jets, threaded plugs were inserted into the large diameter reservoir preceding the orifice as shown on Fig. 4. By varying the thread pitch and the length of the threaded section, the turbulence intensity within the jets could be varied. To provide a smooth transition between the turbulence generator and the orifice entrance, the thread diameter was taken to be approximately that of the maximum diameter of the orifice contour (i.e., 4 d_j).

No attempt was made to characterize the turbulence levels obtained from the various pitch threads or threaded section lengths. The object was simply to achieve turbulence levels equivalent to pressure fluctuations from about 1 to 10% of the mean pressure, and, at the same time, to maintain jet coherence up to free jet lengths of about 10 d_j. However, several general observations can be made. (1) Below a threaded section length of around 2 thread diameters, extremely turbulent, unstable jets were produced. This was probably a result

of fluid sepearation at the sharp edged entrance to the threaded plugs. With a short plug length, flow re-attachment occurs near the mouth of the contoured orifice. Since the orifice is of insufficient length to stabilize the flow before exiting, jet disintegration occurred within free jet lengths of 5 d_j. (2) Above a plug length of about 4 d_j, the turbulence level increased slowly with plug length. (3) Higher turbulence levels were obtained with a larger pitch thread, i.e., 1/4 - 16 thread generatred more turbulence than the 1/4-20 thread.

After an experimental trial and error procedure, two configurations of threaded plugs were adopted. For jet velocities equal to or greater than 80 ft/sec (entrance Reynolds number of about 2000), the orifice was preceded by a 40 d_j (10 d_e) length plug containing a 1/4 - 20 thread. When the injection velocity was less than 80 ft/sec, a configuration consisting of a 20 d_j length of 1/4 - 20 thread preceded by a 50 d_j length of 1/4 - 6 thread was utilized.

Cross-Velocity Manifold and Orifice. The primary objective of the cross-velocity studies was to determine the minimum orifice length at which orifice entrance conditions cease to significantly influence the free jet. To satisfy this requirement the orifice elements were designed such that they could be easily incorporated into a cross-velocity manifold block. The geometry of the elements, which are designated by the code numbers 61-100-OR and 61-10C 05, is shown on Fig. 5. Two orifice elements were fabricated, one with a contoured inlet and one having a square entry. Both have an orifice diameter of 0.061 inches and were initially 100 orifice diameters in length. The orifice length was varied by cutting off a section at the orifice exit after testing at a specific L_o/d_j was completed. The exit face was then polished to remove burrs.

Stainless steel tubing was used in the fabrication of the orifice elements. As shown on Fig. 5, the tube comprising the orifice was swaged into a 2-inch diameter plate. An outer tube was then silver soldered to the plate to provide support for the orifice.

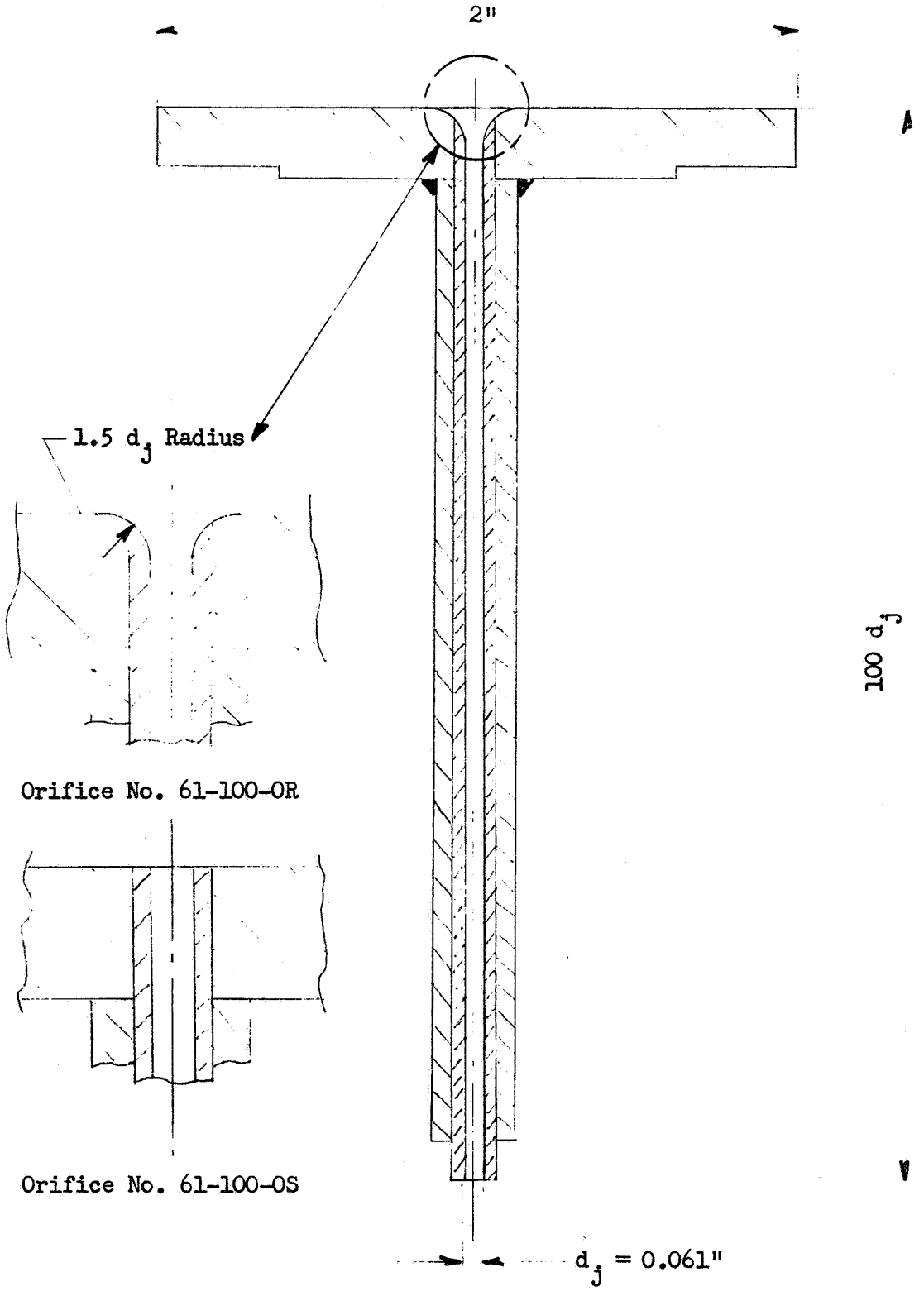

Figure 5. Configuration of Orifice Used in Cross-Velocity Studies

The manifold block that housed the elements, shown on Fig. 6, was identical to the one used in a recent Rocketdyne study of non-circular orifice holes, Ref. 10. The cross-Section of the passage behind the orifice is 0.34 by 0.34 in. (0.0115 $in.^2$).

3.1.2 Multiple-Orifice Elements

The configuration of the 10 L_o/d_j orifices are shown schematically on Fig. 7. These orifices are identical to thos of the Ref. 14 program. A total of five elements were used; two like-doublets, two unlike doublets and one pentad. The nominal free jet length for each element is five diameters (based on the average orifice diameter) with an impingement angle of 60 degrees.

For the like- and unlike-doublet elements, the entrance geometry consisted of a straight tube having a cross-section of three orifice diameters and a length of approximately 17 diameters. This entry length-to-diameter ratio is relatively short in that it does not permit the establishment of fully developed flow (either laminar or turbulent) at the orifice entrance. Combined with the relatively short orifice length of 10 jet diameters, the orifice flow at the exit is therefore not independent of the entry flow.

The inlet geometry for the pentad element was somewhat different as shown on Fig. 7. The outer four orifices (oxidizer) were fed from an annular manifold. The central fuel orifice was fed from a straight tube having a cross section of three jet diameters and a length of approximately 17 x the entrance diameter.

To aid identification, these orifices were also assigned a code number which specifies the geometric dimensions and the element type. The code is defined as follows:

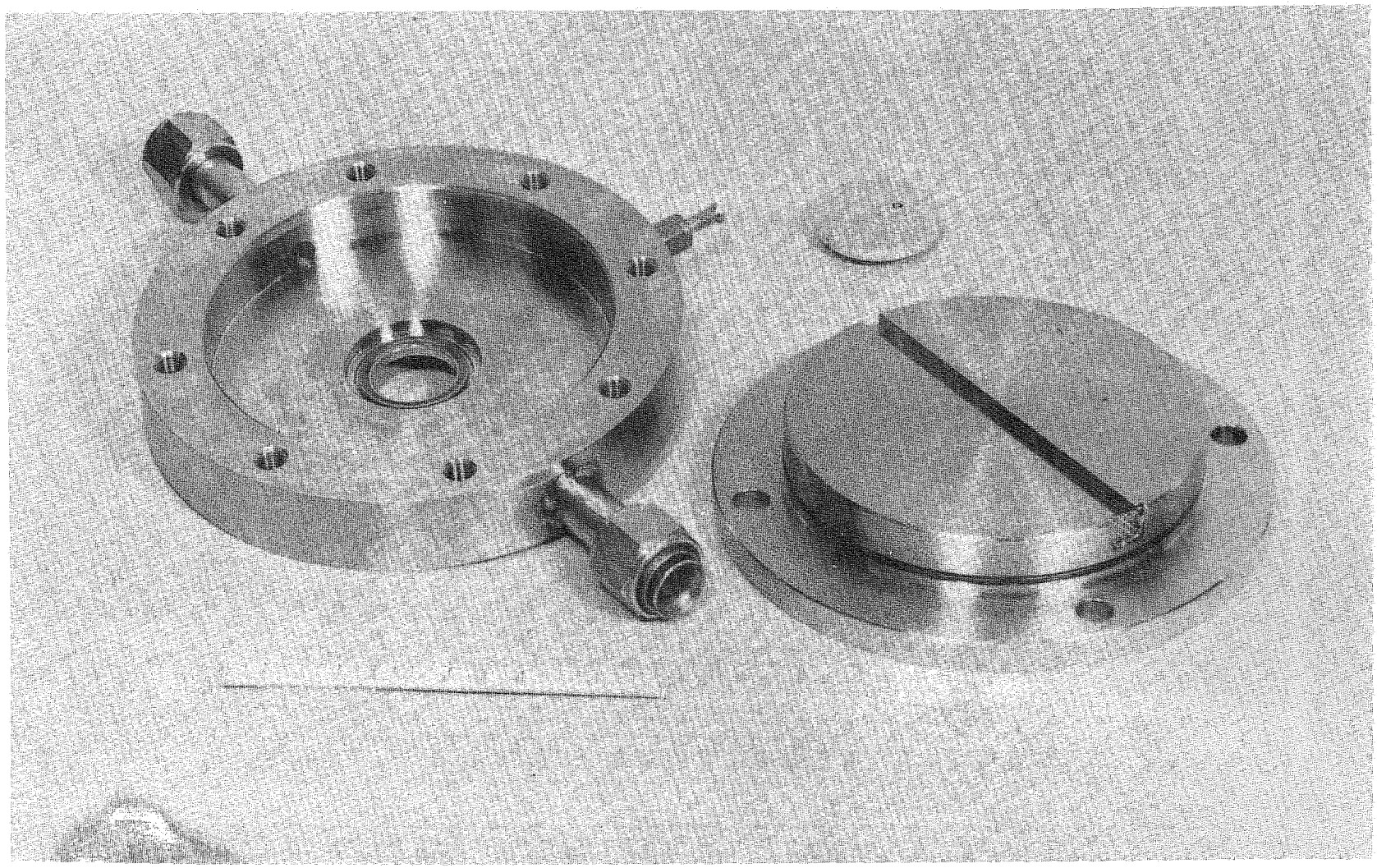

5AJ21-7/31/69-S1A

Figure 6 . Orifice and Manifold Block for Single Orifice Study

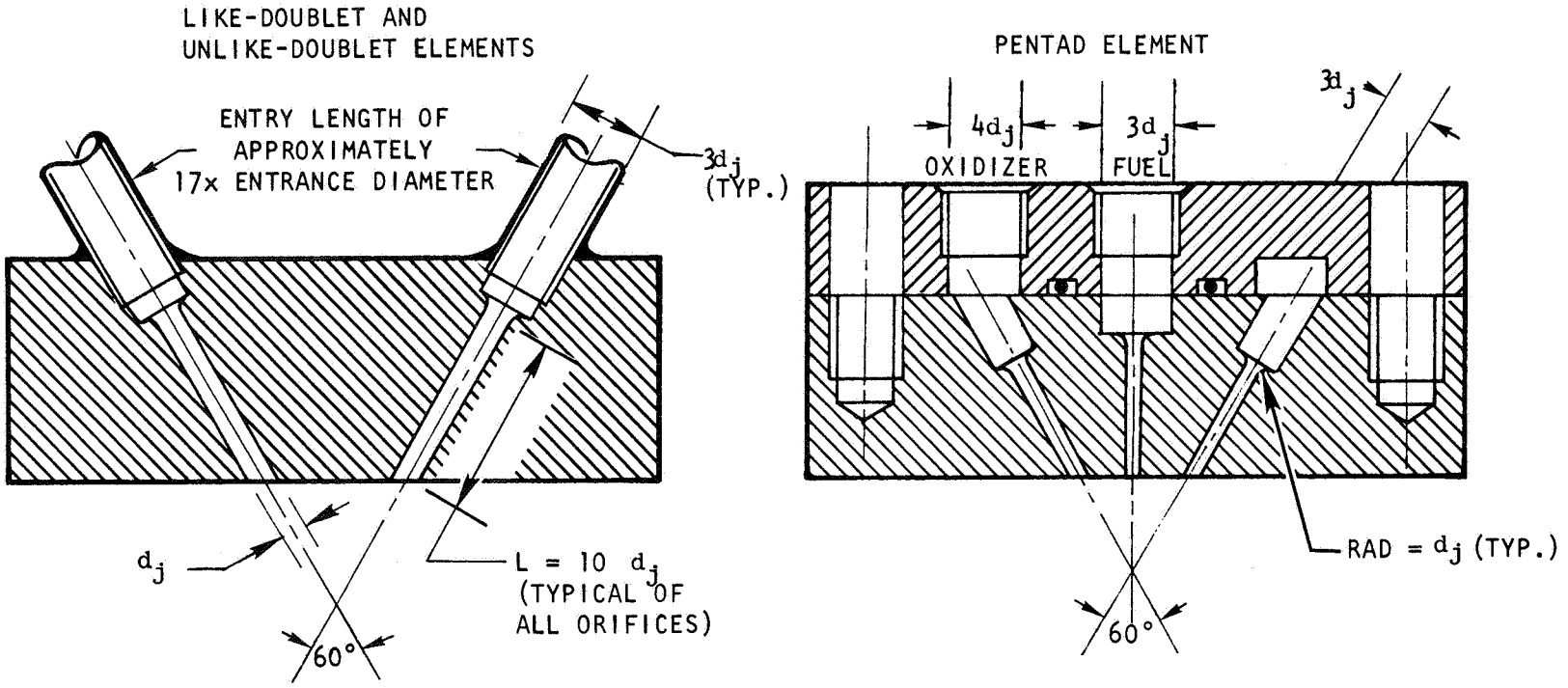

Figure 7. Schematics of Short (10:1) L_o/d_j Elements Used in Low Injection Velocity Studies

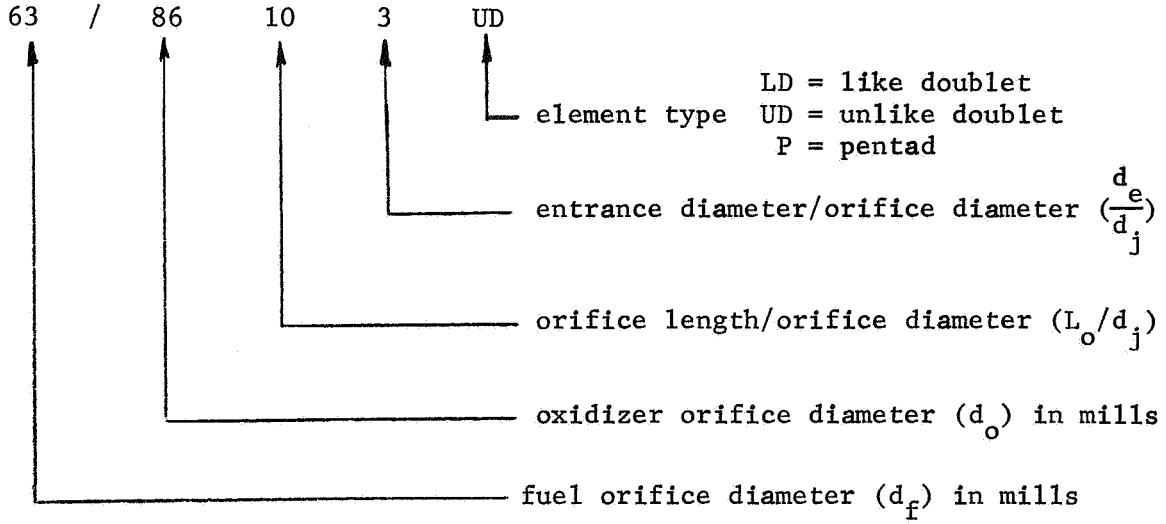

The orifice geometry for each element is summarized in Table 4.

TABLE 4. SUMMARY OF MULTIPLE-ORIFICE ELEMENTS

Element Type	Orifice No
Like-Doublet	63/63-10-3LD
Like-Doublet	81/81-10-3LD
Unlike-Doublet	63/86-10-3UD
Unlike-Doublet	63/128-10-3UD
Pentad (Four Oxidizers Impinging on Central Fuel)	86/63-10-3P

3.1.3 Adjustable Injector

The program requirements of various injector types (like-doublets, unlike doublet, triplet and pentad), and variations of impingement angle and free jet length (like-doublet only) suggested the desirability of an adjustable injector to minimize fabrication costs. Consequently, a single-element injector was designed and fabricated to incorporate the single-orifice elements. A schematic of this injector is shown on Fig. 8. The basic assembly consisted of a base plate, tube clamps, tube holders, and the orifices. With these components, various combinations of like-doublet, unlike-doublet, and coplanar triplet injectors could be assembled. Adjustment features of this assembly

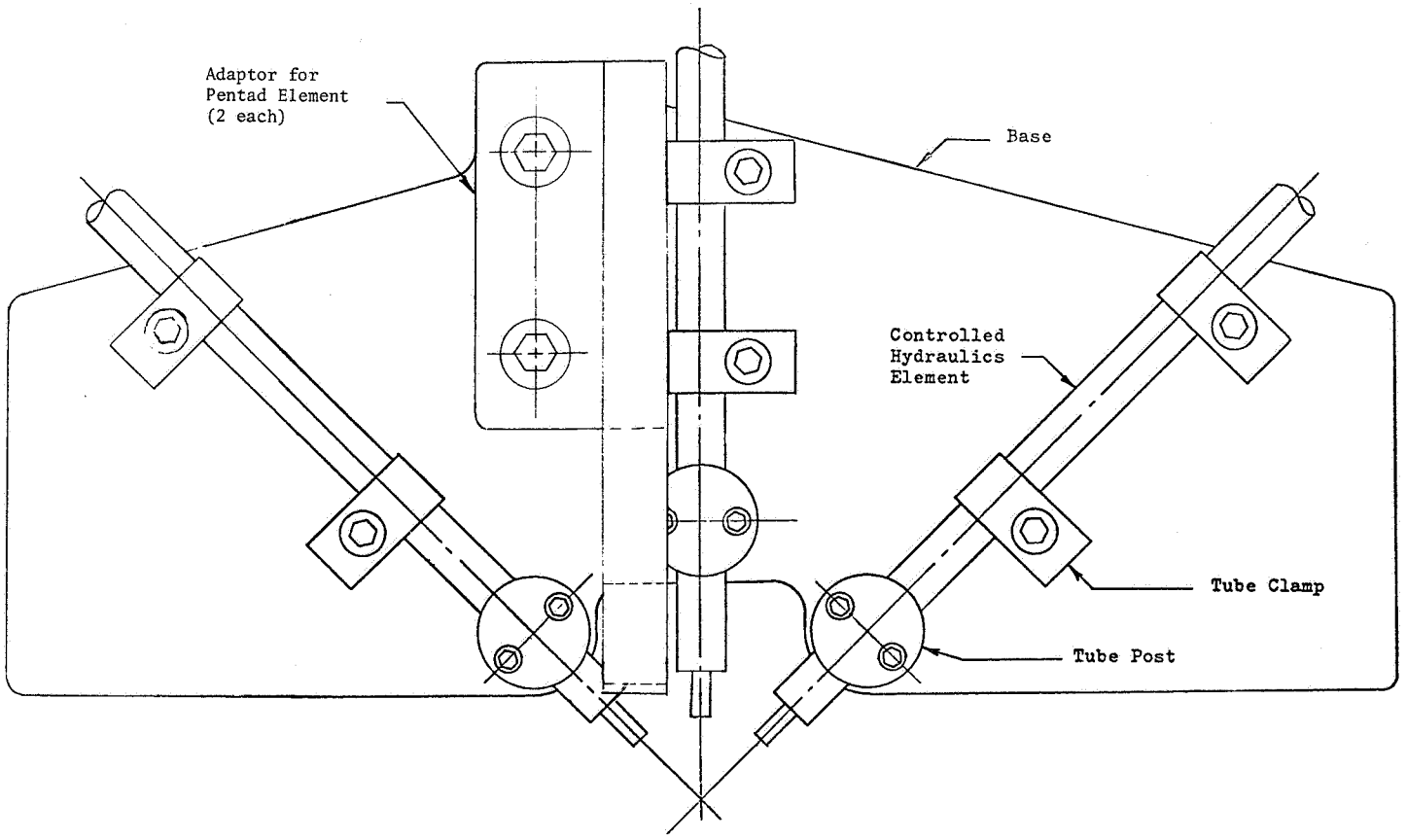

Figure 8 Adjustable Injector Design Incorporating L_o/D_j = 50 Elements (Triplet Configuration Shown)

included variations of included impingement angle from 45 to 90 degrees, free jet length from 1 to 10 d_j, and orifice diameter from 0.063 to 0.128 inch. The pentad (4-on-1) configuration required the addition of two side plates, and the associated clamps, posts, and orifices. Adjustment features of the pentad injector were the same as those listed above.

Photographs of the injector assembly are illustrated on Fig. 9. A pentad element having a free jet length of 5 and an impingement angle of 60 degrees is shown.

3.2 PROPELLANT SIMULANTS

Three propellant simulants were used during this study: (1) Shell Type 270 paraffin wax, (2) water, and (3) aqueous solutions of diethanolamine. Because of its desirable sieving characteristics, Shell type 270 wax was selected for use as a propellant simulant in the dropsize studies. However, utilizing the Shell 270 molten wax can present some problems in data reduction. Specifically, when the wax droplets freeze, they first form a solid outer shell which remains rigid. When further freezing of the remaining core takes place, a hollow core is formed because the wax specific gravity changes from 0.76 to 0.92. Visual observation of the droplets under a microscope has substantiated that this phenomena occurs.

Since the outer shell freezes before the core, the final frozen dropsize will be near that of the initial molten droplet. However, if it is desired to convert the mass data to the number of droplets, it would be necessary to accurately determine the droplet density. This density will be different from that quoted for Shell 270 because of the hollow core.

If it is assumed that the outer diameter of the liquid drop remains fixed upon freezing, the diameter of the hollow core can be computed as follows. The mass contained in a liquid drop of diameter D_o is

$$m = \frac{\pi}{6} D_o^3 \rho_L$$

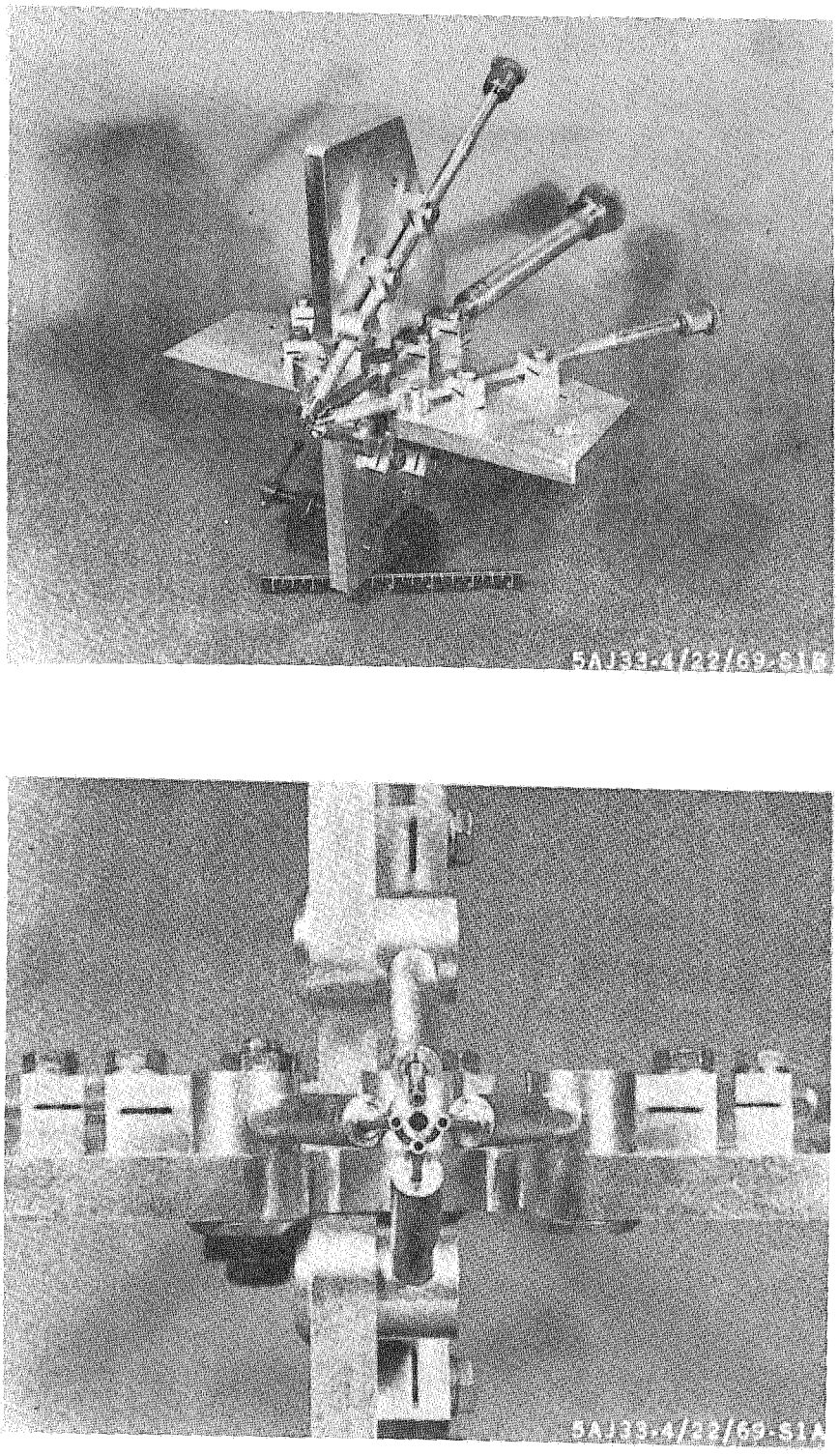

Figure 9. Adjustable Tube Injector Incorporating 50 L_o/d_j Elements (Pentad Element Shown)

Because of the change in density between the liquid and solid states, the frozen drop will occupy a volume given by

$$\frac{\pi}{6}\left(D_o^3 - D_i^3\right) = \frac{}{6} D_o^3 \frac{\rho_L}{\rho_S} = \left(\frac{0.76}{0.92}\right) \frac{\pi}{6} D_o^3$$

Solving for D_i yields

$$D_i = 0.56 \; D_o$$

which corresponds to a core volume of about 18% of the total drop volume.

Two of the more important physical properties in droplet studies are the viscosity and surface tension. At the nominal injection temperature of 200 F, the magnitude of these properties are 4 centipoise (2.69×10^{-3} lbm/ft-sec) and 17 dynes/cm (3.74×10^{-2} lbm/sec^2) respectively. The temperature variation of the viscosity and surface tension, obtained from the Shell Chemical Co. (Ref. 20), are presented on Figs. 10 and 11.

One of the objectives of the program was to determine the effect of propellant miscibility on dropsize. Consequently a literature search was made to determine suitable liquids for use in the miscibility studies. It was considered desirable to use a wax immiscible liquid which possessed the same density, viscosity, and surface tension. This allows a direct comparison of the effects of propellant miscibility on dropsize distribution. Several candidate liquids were evaluated, including water, glycols, ethanolamines, and various other amine compounds. However, no one compound or blend could meet all of the criteria. Assuming solubility and viscosity to be two of the more important factors, an aqueous solution containing diethanolamine appeared to be the best candidate. (For brevity, the diethanolamine-water mixture is henceforth referred to as DEW.) This mixture was found to be insoluble in the wax, and has a density of about 1.0 gm/cc as compared to wax which is 0.76 gm/cc. In addition, diethanolamine has the advantage of being non-toxic, compatible with aluminum and stainless steel, and inexpensive. An alternate liquid that was considered was water thickened to increase the viscosity.

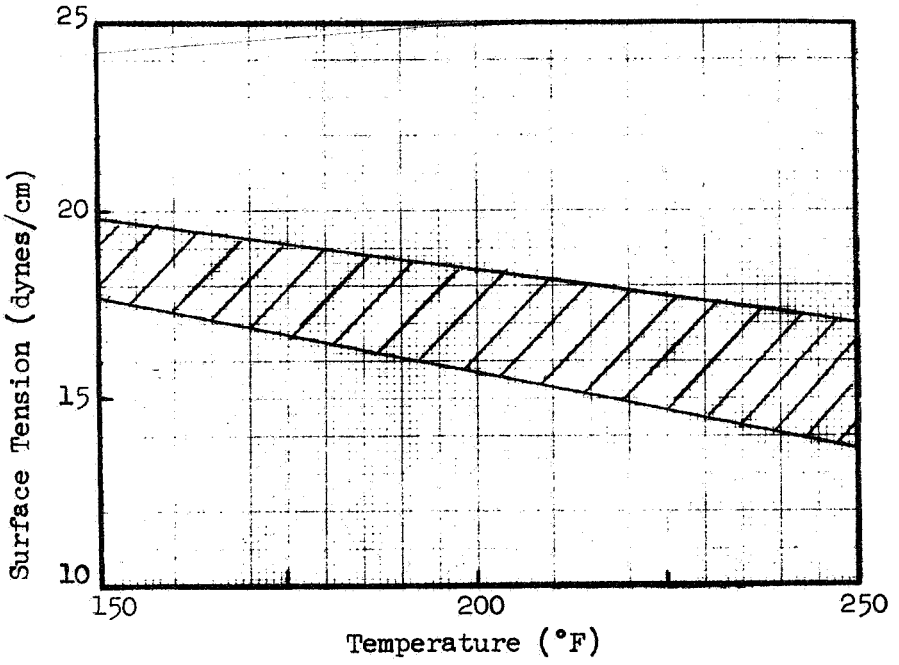

Figure 10. Surface Tension of Shell 270 Wax

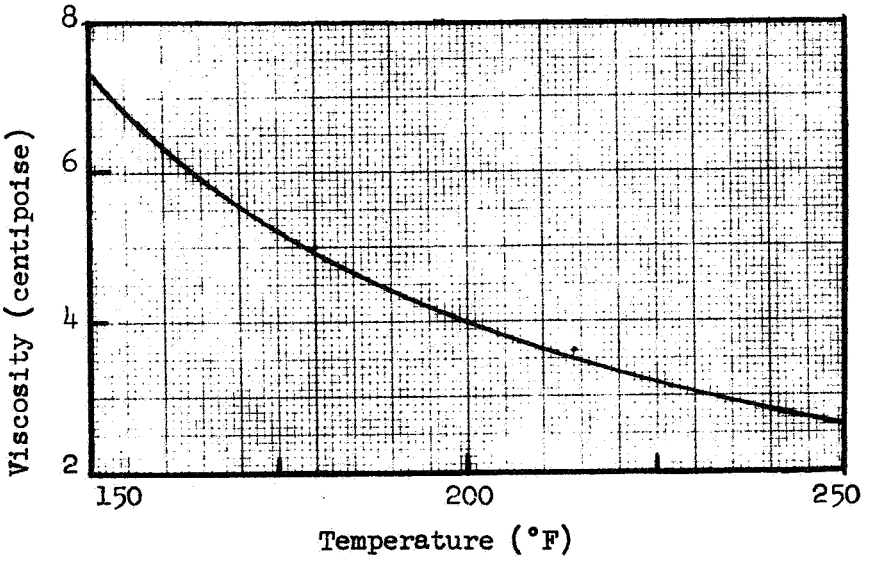

Figure 11. Viscosity of Shell 270 Wax

For the study of the internal characteristics of the free jets, a fluid was required that would behave dynamically (i.e., have the same Reynolds No.) in a manner identical to the molten wax at the same injection velocities. This, of course, is readily accomplished by selecting a liquid which has a kinematic viscosity at ambient temperatures equivalent to that of 200 F paraffin wax. Because of its above stated advantages, an aqueous solution of diethanolamine was also used here. In this case, the solution contained 65% (by volume) of water.*

In the dynamic pressure ratio studies of Task V, diethanalamine was again used as a propellant simulant in conjunction with the molten wax. The composition of the solutiion in these tests was 17% water and 83% diethanolamine. At 200 F this mixture has a kinematic viscosity equivalent to the molten wax.

The pertinent physical properties of all propellant simulants used in the program are summarized below.

TABLE 5. PHYSICAL PROPERTIES OF PROPELLANT SIMULANTS

Fluid	Temp. F	Density lbm/ft^3	Viscosity lbm/ft-sec	Kinematic Viscosity ft^2/sec	Surface Tension dynes/cm
Shell 270 Wax	200	47.7	2.69×10^{-3}	5.63×10^{-5}	17
Water	200	60.1	2.05×10^{-4}	3.41×10^{-6}	60
75% DEA** 25% H_2O	200	63.9	2.0×10^{-3}	3.13×10^{-5}	NA
35% DEA 65% H_2O	70	64.0	3.6×10^{-3}	5.63×10^{-5}	NA
83% DEA 17% H_2O	200	64.4	3.6×10^{-3}	5.63×10^{-5}	NA

*At the initiation of the program, the best information available on the viscosity of the Shell 270 paraffin indicated that, at a temperature of 200 F, the viscosity was 3 centipoise (2.02×10^{-3} lbm/ft-sec). The 75% diethanolamine solution used in Tasks I and II was chosen on the basis of this information.

** diethanolamine

3.3 EVALUATION OF FREE JET CHARACTERISTICS

In order to gain a better understanding of the influence of the internal characteristics of free jets on the atomization process, a facility was constructed to evaluate the free jet turbulence and velocity profiles. A description of the facility and the detailed experimental procedure is presented in Appendix A.

Of central importance in the design of the facility was the experimental technique adapted to measure the free jet characteristics. An obvious approach is, of course, to insert a pitot tube directly into the free jet and measure the local stagnation pressure which can, in turn, be converted to a local fluid velocity. A similar approach, but one which measures the velocity components directly, is to use a hot film anemometer.

The pitot tube approach was examined by Rupe (Ref. 21) and found to be lacking for several reasons; one of which is that the probe was unable to measure pressures near the periphery of the jet. This was due to the fact that the surface of the jet is highly distorted (either by aerodynamic forces or the probe itself) and the probe actually senses an intermittant flow which is not indicative of the true fluid velocity. For similar reasons, and, in addition, the cost incurred by the short life-expectancy under the test conditions of this program, the use of a hot film anemometer was eliminated.

As an alternative to the pitot tube, Rupe developed a technique using a dynamic-head probe which he called the flat plate probe. This technique was adopted for use in this program. The development and theory of operation of the flat plate probe is thoroughly discussed in Ref. 21. Those aspects which are pertinent to the acquisition and interpretation of the data presented in this report are discussed below.

3.3.1 Flat Plat Pressure Probe

The basic configuration of the probe is simply a flat circular plate with a small diameter hole in the center. The hole opens into a cavity which is bounded by a pressure sensing device. The design of the probe used in this

program is shown on Fig. 12. In relation to the jet diameter, the probe hole is small (in this case less than 0.1 d_j) while the plate is large.

The method of operation is to place the probe perpendicular* to a liquid jet and, by traversing the probe across the jet, to measure the pressure distribution on the flat plate produced the impingement of the jet as shown schematically on Fig. 13. If a pressure sensing device that is capable of measuring instantaneous deviations from the mean pressure is used in conjunction with the probe, it is possible to measure simultaneously the fluctuating component of pressure as well as the mean.

In this program, a Kistler type 623A pressure transducer was used with the flat plate probe. This transducer has a range of 0 to 3000 psi and can detect and measure pressure fluctuations up to 10 kHz in frequency. Shock tube tests, to 200 psia, indicated that the transducer output was linear and repeatable, with a sensitivity of 0.29 pCb/psi.

Since both components of pressure are to be measured, the frequency response characteristics of the probe must be examined. The probe cavity behaves, in essence, much like an acoustic resonator. When a pressure fluctuation of a specific frequency is applied at the opening to the probe cavity, an acoustic wave is generated which travels through the cavity and reflects back and forth from the walls and the diaphragm of the transducer. If this frequency is equal to the resonant frequency of the cavity, the amplitude of the wave will be increased, rendering an erroneous measurement of the true amplitude of the pressure fluctuation.

The dynamic response characteristics of the probe were determined by filling the probe cavity with a water-diethanolamine solution and using a Panoramic wave analyzer to analyze the raw signal produced by the impingement of a fully developed turbulent jet upon the probe -transducer assembly. A spectrum analysis of the signal shown on Fig. 14a, indicates that the resonant frequency

---

* In general, this is not necessary

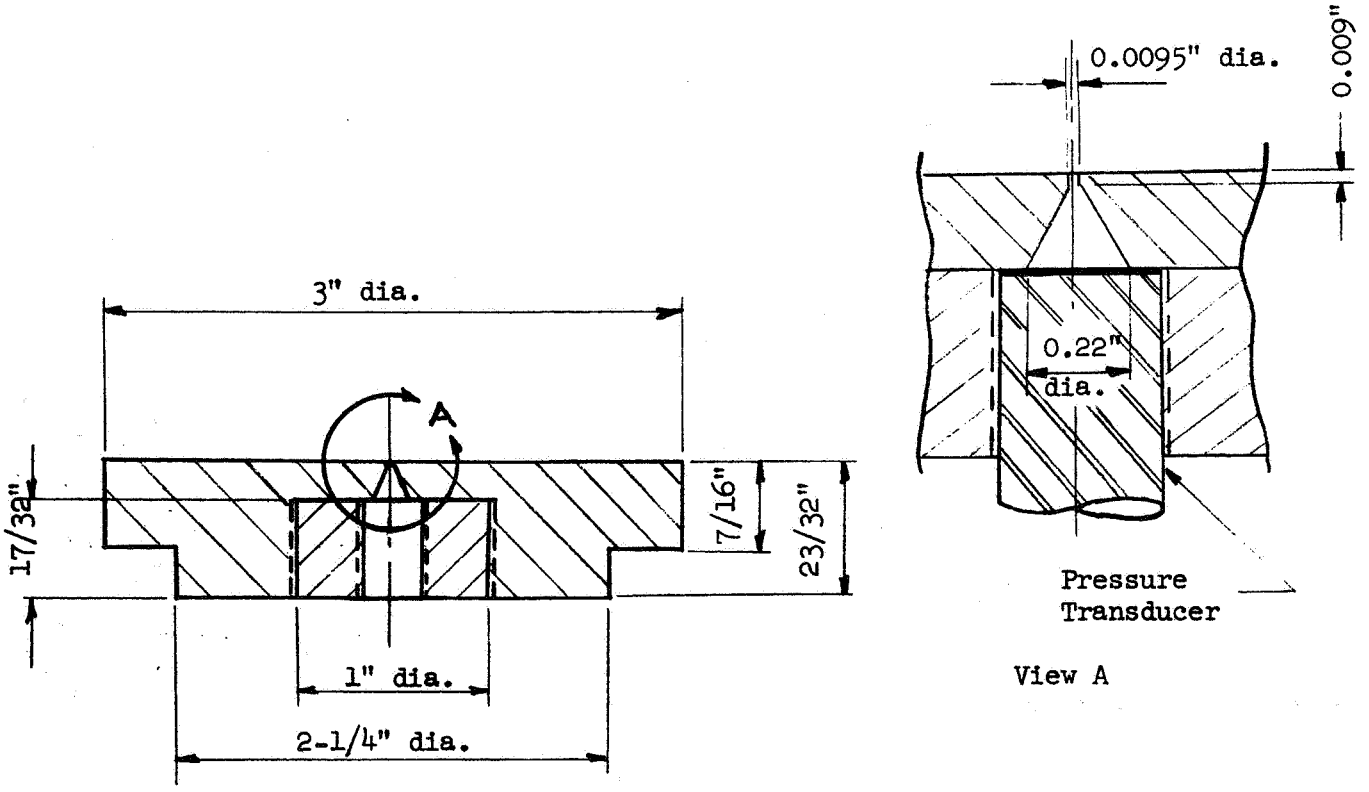

Figure 12. Flat Plate Pressure Probe

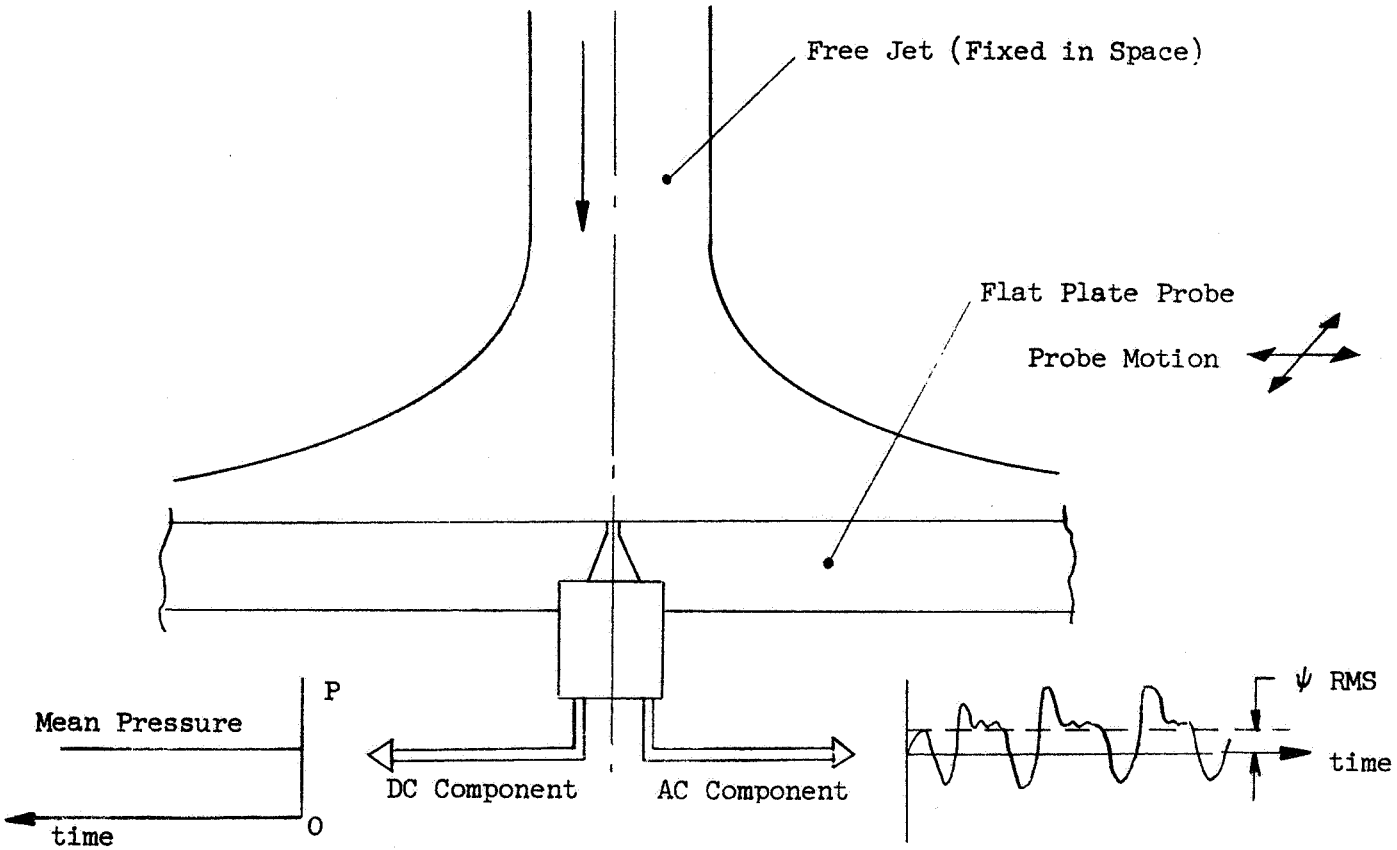

Figure 13. Schematic of Flat Plate Pressure Probe Technique

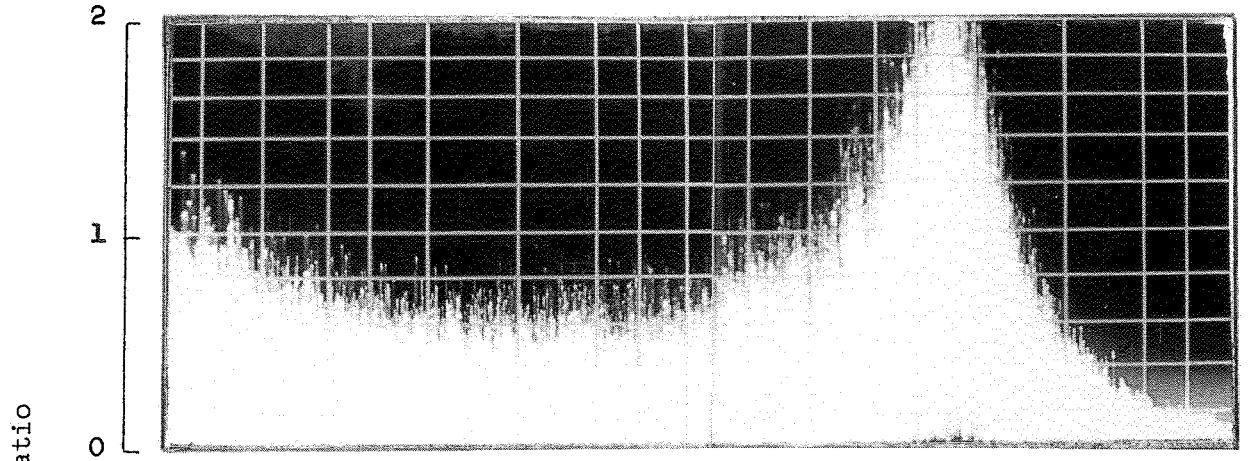

Figure 14a. Without Filter

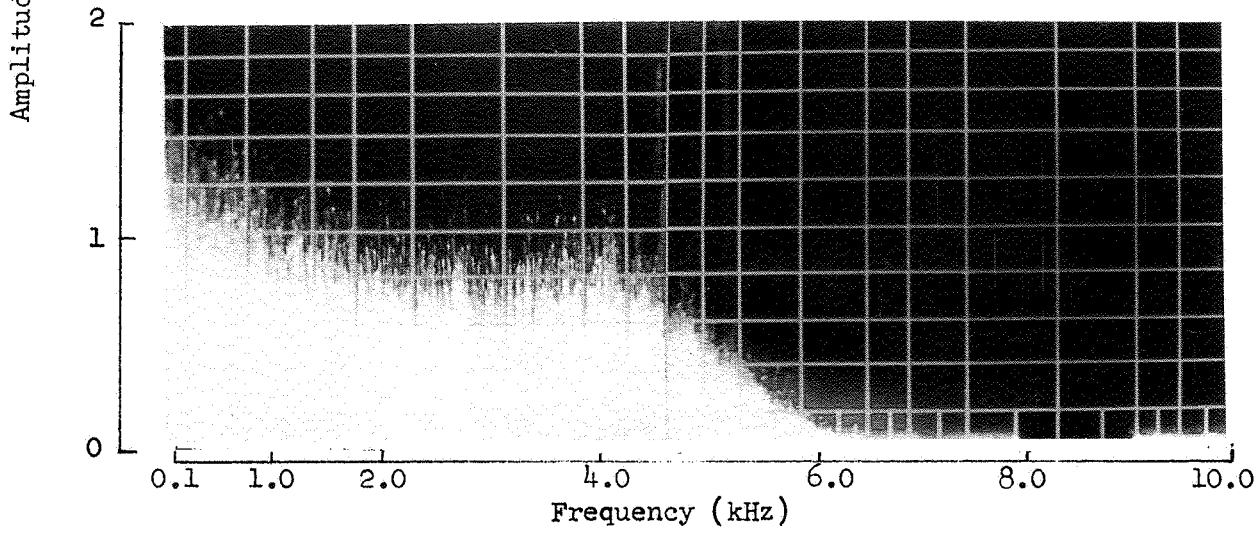

Figure 14b. With Filter

Figure 14. Frequency Response Characteristics of Flat Plate Pressure Probe

of the cavity is 7.4 kH_z, This frequency was eliminated from the output of the Kistler transducer by means of a filter set to initiate cutoff at 4.5 kHz. The resulting frequency distribution is shown on Fig. 14b. As a consequence, only frequencies in the range of 0 to approximately 4 kHz are accurately measured by the probe-transducer assembly. The amplitudes of fluctuations with frequencies above 4 kHz are either attenuated or eliminated from the measurements.

Since the presence of the flat plate probe distorts the jet, the measurements obtained by this technique do not directly yield the turbulence and velocity profiles. How they are inferred from the experimental data is described below.

3.3.2 Velocity Profile Measurements

The basic hypothesis in the flat plate probe technique is that a liquid jet with a given velocity profile will produce a unique pressure distribution when impinged upon a flat plate. This was suggested by a numerical solution obtained by LeClerc, Ref. 22, which demonstrated that a uniform velocity profile jet will produce a discrete pressure distribution.

Although the technique does not yield a quantitative measurement of the velocity profile, it does afford a method of qualitatively evaluating an unknown velocity profile by comparing the measured pressure distribution to that produced by a jet with a known velocity distribution. To provide pressure distributions that would serve as a basis of comparison, Rupe, Ref. 23, measured the pressure profiles produced by fully developed laminar jet and a fully developed turbulent jet. A third reference pressure distribution is provided by the LeClerc solutuion for a uniform velocity jet.*

* Measurement of the pressure distributions produced by a nearly uniform velocity jet were also obtained by Rupe, Ref. 23.

In the current study, the velocity profiles of the jets produced by the various orifices used in the atomization measurements are categorized according to their agreement with the above three reference profiles.

3.3.3 Turbulence Intensity Measurements

In the study of turbulent flow, the velocity of a fluid particle is frequently defined as the time averaged sum of two terms: (1) the mean velocity of the fluid V_j, and (2) the instantaneous deviation from the mean velcoity, v'.

The latter is generally used to define the intensity of turbulence within the fluid according to the relation (see e.g., Schlichting, Ref. 24).

$$T = 1/3 \sqrt{(v'^2_x + v'^2_y + v'^2_z)} / V_j$$

where v'_x, v'_y and v'_z are the fluctuating velocity components in the x, y and z directions respectively. Turbulence intensity is thus defined as the non-dimensional RMS value of the fluctuating velocity components. When $v'_x = v'_y = v'_z$, the turbulence intensity is characterized as isotropic. Obviously, when v' = 0, the fluid motion is laminar.

It was noted above that the mean pressure distribution produced by the impingement of a free jet upon the flat plate probe is associated with a unique free jet velocity distribution. Similarly, the instantaneous deviation from the mean pressure at a specific point in the pressure distribution is associated with a velocity fluctuation at a unique point within the free jet Consequently, the distribution of instantaneous pressure deviations is produced by a unique distribution of free jet velocity fluctuations, or equivalently, turbulence intensity profile. However, in the interpretation of the flat plate probe turbulence measurements, several factors must be considered before an inference can be made on the turbulence intensity existing within the jet.

1. The flat plate probe measures dynamic pressure fluctuations that are normal to the plate. Consequently, this would be a true measure of the intensity only when the turbulence is isotropic (i.e., equal in all spatial directions).

2. Large scale disturbances at the entrance to short orifices, aerodynamic forces at the jet boundary, and the relaxation of the velocity profile in the free jet cause gross oscillations of the jet. Thus, the fluctuations sensed by the probe are a composite of large and small scale disturbances caused by jet instabilities and flow generated turbulence, respectively.*

3. The physical presence of the flat plate probe may distort the intensity level.

4. Since the output of the transducers is filtered, turbulent frequencies are measured only over a finite bandwidth.

In view of the above qualifications, statements regarding the turbulence measurements obtained in this study are limited to gross comparisons of the overall apparent turbulence levels and profiles within the various free jets.

3.4 DROPSIZE AND DROPSIZE DISTRIBUTION MEASUREMENTS

The experimental technique used to determine mean droplet size as well as the dropsize distribution was the method of molten wax. In this technique, molten wax is injected into the atmosphere through the orifices at a temperature of about 200° F (i.e., 40° F above the solidification point) and collected on an 18 by 50 ft. table. The wax droplets solidify during their trajectory from the orifice exit to the table and, during the experiment, are washed from the table into a collection tank with water. A representative sample of around 10 grams is then thoroughly washed, vacuum dried and sieved. Generally, thirteen sieves of various sizes are utilized and a cumulative mass/dropsize distribution is obtained. A more detailed description of the facility and data reduction procedures is presented in Appendix B.

---

*Another way to view the effect of the gross oscillations is to imagine that the streamlines remain perfectly normal to the flat plate probe. If the probe is then rapidly oscillated between a high pressure point (e.g., the centerline of the jet) and a point of lower pressure, it will appear as though a pressure fluctuation exists within the free jet.

The experimental approach was designed to determine variations in droplet size and droplet size distribution with changes in specific geometric and hydraulic parameters. The ability to distinguish between measured variations in the atomization characteristics is determined by the accuracy and repeatability of the experiment. Consequently, prior to the presentation of the experimental results the reproducibility of the dropsize measurements is examined.

To determine the limits of data reproducibility, two separate sets of experiments were conducted to measure dropsize over a range of injection velocity from 70 to 190 ft/sec employing a like doublet injector. The results of these tests are presented in Table 6. The mass median dropsize was repeated to within 5% as indicated on Fig. 15.

TABLE 6. FACILITY CHECKOUT AND DATA REPEATABILITY TESTS

Like Doublet Element
Orifice No. 63/63-10-3LD

Test No.	Wax Flowrate, lb/sec	Injection Velocity, ft/sec	Mass Median Dropsize, microns
41	0.150	72.5	413
42	0.162	78.1	415
43	0.207	100.1	337
44	0.227	110.0	303
45	0.268	129.9	256
46	0.309	149.7	223

Another aspect of the data quality is related to the size of the droplets. When the mass median dropsize is greater than 450-500 μ , the time the droplets spend in their trajectory between the injector and the collection table is not sufficient to freeze the larger drops in the distribution. Consequently, upon impact with the collection table these drops are crushed, resulting in "flakiness" of the data sample. This effect was minimized, but not eliminated,

by reducing the injection temperature of the molten wax to approximately 185°F. The error introduced in the mass median dropsize is within the experimental error stated above providing the mass percentage of flakes is less than about 20%. However, many of the dropsize distributions for the larger mass median dropsizes ($\leq 450\ \mu$) were invalidated and are not presented in this report.

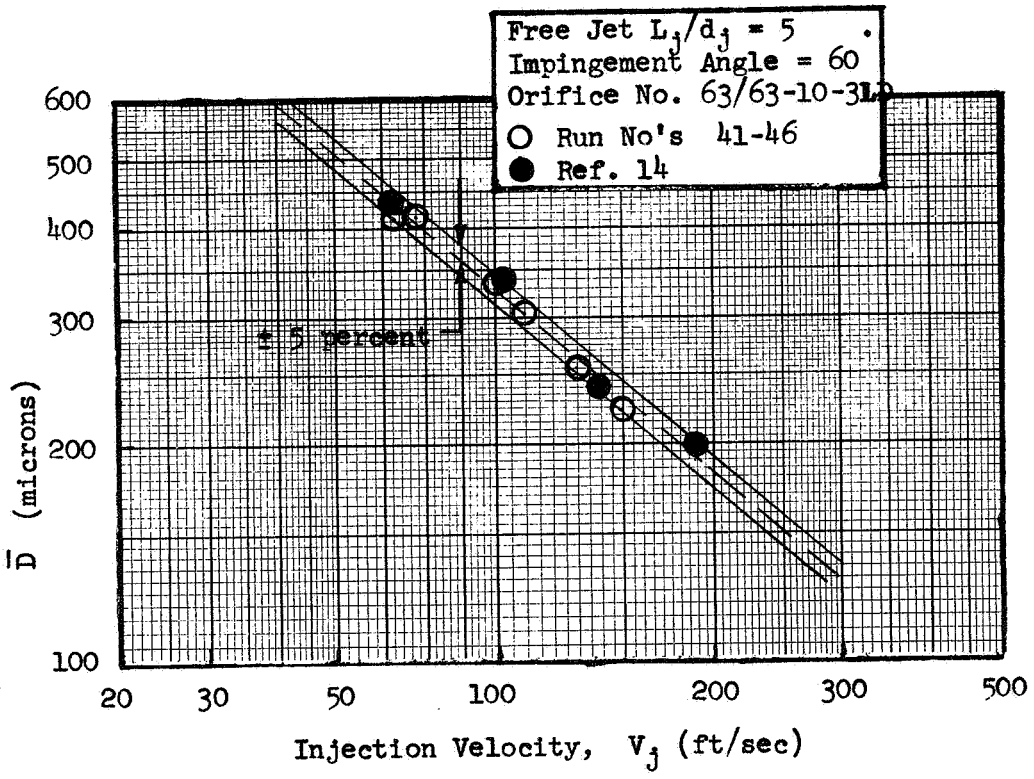

Figure 25. Results of Facility Checkout and Data Repeatability Tests

4.0 EXPERIMENTAL RESULTS

The overall objective of the program was to experimentally investigate the influence of various injector and free jet parameters on the atomization process resulting from the impingement of liquid jets. In some cases it was possible to isolate one specific parameter and examine its influence on droplet formation alone. More often, the experimental results exhibit the effect of two (or more) parameters and must be interpreted accordingly.

Because of the large number of parameters that were examined in the course of the program and their inter-relationship in the atomization phenomena, it seems appropriate to first present the experimental results with a minimum discussion. The influence of the individual parameters on the experimental results is then interpreted and discussed in Section 5.0.

The experimental portion of the program can be divided into three distinct parts: (1) an examination of the internal characteristics of free jets formed by various orifice and flow conditions, (2) a study of the dropsizes and dropsize distributions produced by the impingement of free jets, and (3) a determination of the occurrence of emulsification. The results of this study are presented in the above order and are further sub-divided according to the parameters investigated.

Throughout this section and Section 5, the terms "laminar", "turbulent" and "velocity profile" are used repeatedly. The distinction between "turbulent" and "laminar" flow is based on the existance or absence of random velocity fluctuations within the flow field. If these fluctuations exist, the flow is classified as turbulent while their absence implies laminar flow. The term "velocity profile" refers to the distributions of mean velocity within the flow only and places no restriction on the type of flow which may be either laminar or turbulent.

4.1 FREE JET CHARACTERISTICS

The specific free jet characteristics of interest are the velocity profile and the distribution and magnitude of velocity fluctuations within the free jet. The primary reasons for obtaining these measurements are: (1) to determine the characteristics of the jets produced by the orifices used in the atomization experiments and (2) to evaluate the effect of various hydraulic and orifice design parameters on the free jet. The parameters examined include: the injection velocity, V_j, manifold cross velocity, V_c, orifice entrance configuration, orifice diameter, d_j, orifice length, L_o/d_j, and free jet length, L_j/d_j.

The experimental technique used to measure the internal characteristics of the jets is described in Section 3.3. The experimental results are presented in terms of the non-dimensional mean pressure, p/p_j, and the time average deviation from the mean ψ/p_j (see Fig. 13). The quantity, ψ, is the RMS value of $(p(t)-p)$, where $p(t)$ is the instantaneous pressure while p is the mean pressure at the radial position, r, measured from the centerline of the jet. The normalizing pressure, p_j, is defined as the dynamic pressure of a uniform velocity jet (i.e., $1/2\,\rho V_j^2$).

The property of the jet that is most indicative of the extent of velocity profile development is the pressure ratio at the centerline, p_c/p_j. For example, a uniform velocity jet will have a centerline pressure ratio of unity while, for a fully developed laminar jet, $p_c/p_j = 4$. Similarly, the quantity that provides a direct measure of the level of turbulence within the jet is the time averaged pressure fluctuation at the jet center, ψ_c/p_j. The majority of the experimental results are presented in terms of these two parameters. In addition, radial distributions of the mean and fluctuating pressure components, at constant injection velocity, were also measured for most of the orifice elements examined. These measurements were obtained along two orthogonal lines intersecting at and lying in a plane perpendicular to the jet centerline. Unless otherwise stated, the jets were symmetrical and these data are presented along a ray originating at the centerline of the jet.

The results presented in the following paragraphs are divided into two categories. In the first, the characteristics of the jet produced by a particular orifice configuration were examined as a function of the injection velocity. The direction of flow in the entrance manifold was parallel to the axis of the orifice as shown on Fig. 16a. Furthermore, the orifices used in these tests were subsequently utilized in the atomization experiments and the ranges of injection velocities and free jet lengths at which the jet characteristics were measured are comparable to those of the droplet studies.

In the second set of experiments, the manifold cross velocity was varied while the injection velocity was held constant. For these tests, the direction of flow in the entrance manifold was orthogonal to the orifice axis as shown on Figs. 16b and 16c. These orifices were not used in the atomization experiments.

4.1.1 Effect of Injection Velocity on Jet Characteristics

The internal characteristics of the jets produced by 11 orifice element configurations, selected from the 22 fabricated for use in the atomization tests, were examined. For each orifice, the centerline pressure, p_c, and the turbulence intensity parameter, ψ_c, were measured over an injection velocity range of from 30 to 160 ft/sec. The code numbers of the 11 orifice elements, specifying the orifice diameter, length/diameter ratio and entrance configurations, are listed in Table 7 together with the free jet length at which measurements were taken. The injection velocities at which radial distributions of pressure and turbulence were obtained are also listed in Table 7.

Round Entrance Orifices. The variation of the centerline pressure ratios obtained with the 1.5 L_o/d_j orifices are shown on Fig. 17 as a function of injection velocity. For the smallest diameter orifice, the measurements were obtained at free jet lengths up to 10 d_j. As shown on Fig. 17, the pressure ratio decreases monotonically with increasing jet velocity but was found to be invariant with free jet length in the case examined.

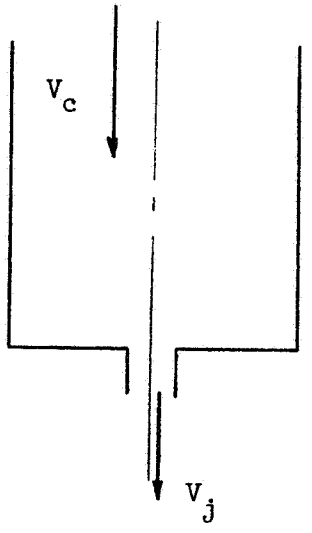

Figure 16a

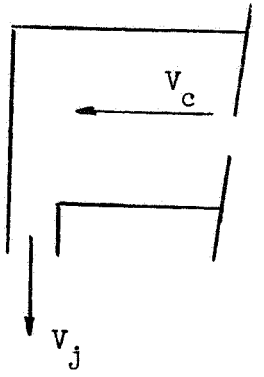

Figure 16b

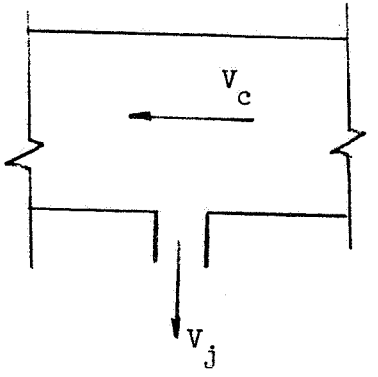

Figure 16c

Figure 16. Orifice Entry Configurations

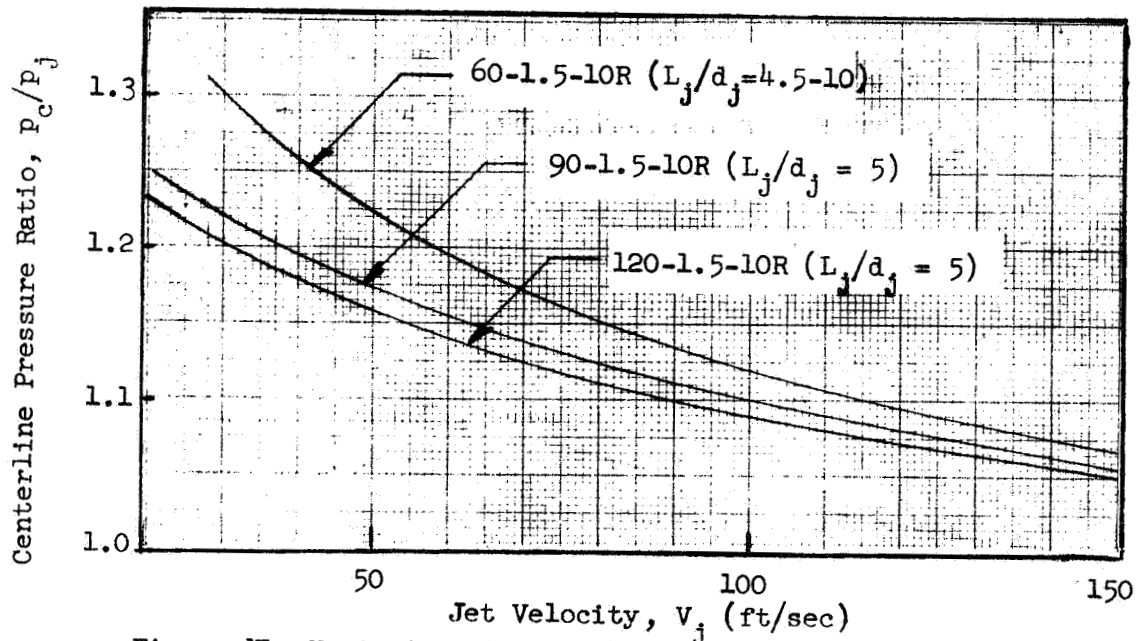

Figure 17. Variation of Centerline Pressure with Injection Velocity (L_o/d_j = 1.5)

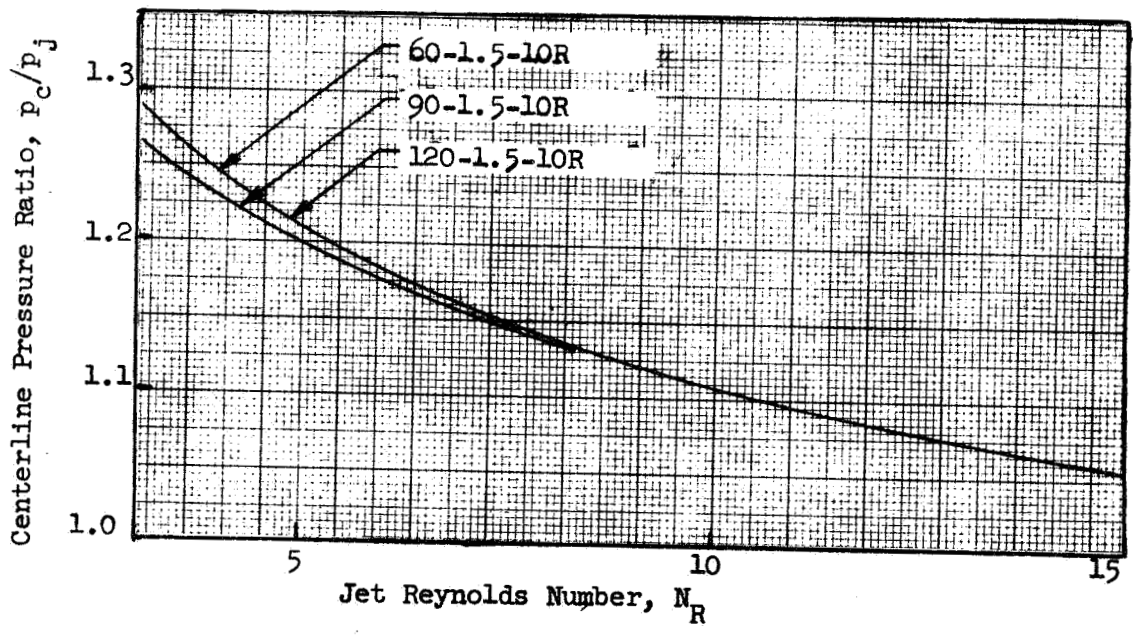

Figure 18. Variation of Centerline Pressure Ratio with Reynolds Number

Since the three elements are geometrically similar, it is to be expected that the jets are also dynamically similar when their Reynolds numbers are equal. This is shown on Fig. 18 where the pressure ratios are compared at constant Reynolds numbers and this is also illustrated on Fig. 19 by the similarity of the radial distributions of pressure, produced by the 0.120 and 0.060-inch-diameter orifices at identical Reynolds numbers but injection velocities of 40 and 80 ft/sec respectively.

TABLE 7. SUMMARY OF ORIFICE ELEMENTS SELECTED FOR JET CHARACTERISTICS STUDY

Orifice No.*	L_j/d_j	Radial Distributions V_j (ft/sec)
120 - 1.5 - 10R	5.0	40
90 - 1.5 - 10R	5.0	-
60 - 1.5 - 10R	4.5, 7, 10	40, 80, 120, 160
61 - 6 - 7R	5.0	-
63 - 10 - 7R	5.0	37, 120
63/63 - 10 - 3LD	5.0	40, 120
67 - 50 - 5R	2 to 15	40, 120
69 - 200 - 9R	5.0	37
61 - 2 - 7S	5.0	-
61 - 6 - 7S	5.0	-
61 - 10 - 7S	5.0	36, 100

*See Section 3.1 for definition of orifice number.

The combination of short orifice length and quiescent inlet conditions (inlet velocity on the order of 0.01 V_j) result in a nearly turbulence-free jet. At free jet lengths up to 5 d_j, the maximum pressure fluctuation measured with all three orifices was about 0.005 p_j.

The radial distributions of pressure obtained with the 0.060-inch diameter orifice at injection velocities of 40, 80, 120, and 160 ft/sec are shown on Fig. 20. Also shown is the analog solution, obtained by LeClerc, Ref. 22,

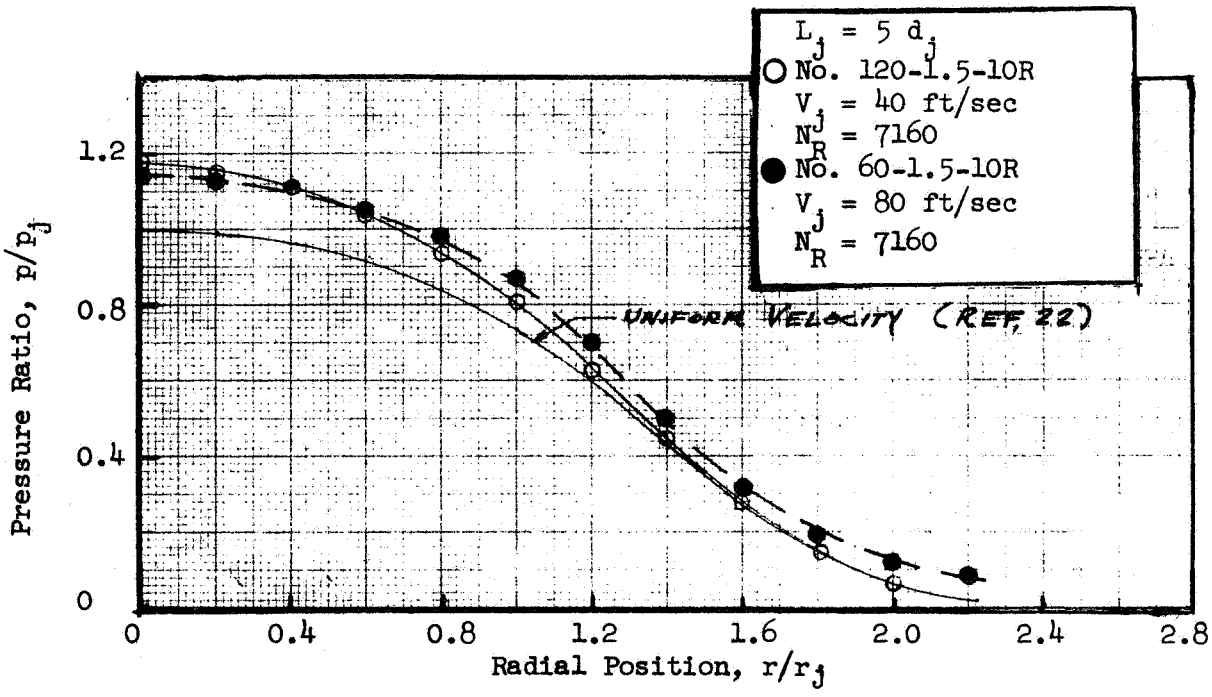

Figure 19. Pressure Distributions Obtained with Short (L_o/d_j = 1.5) Orifices

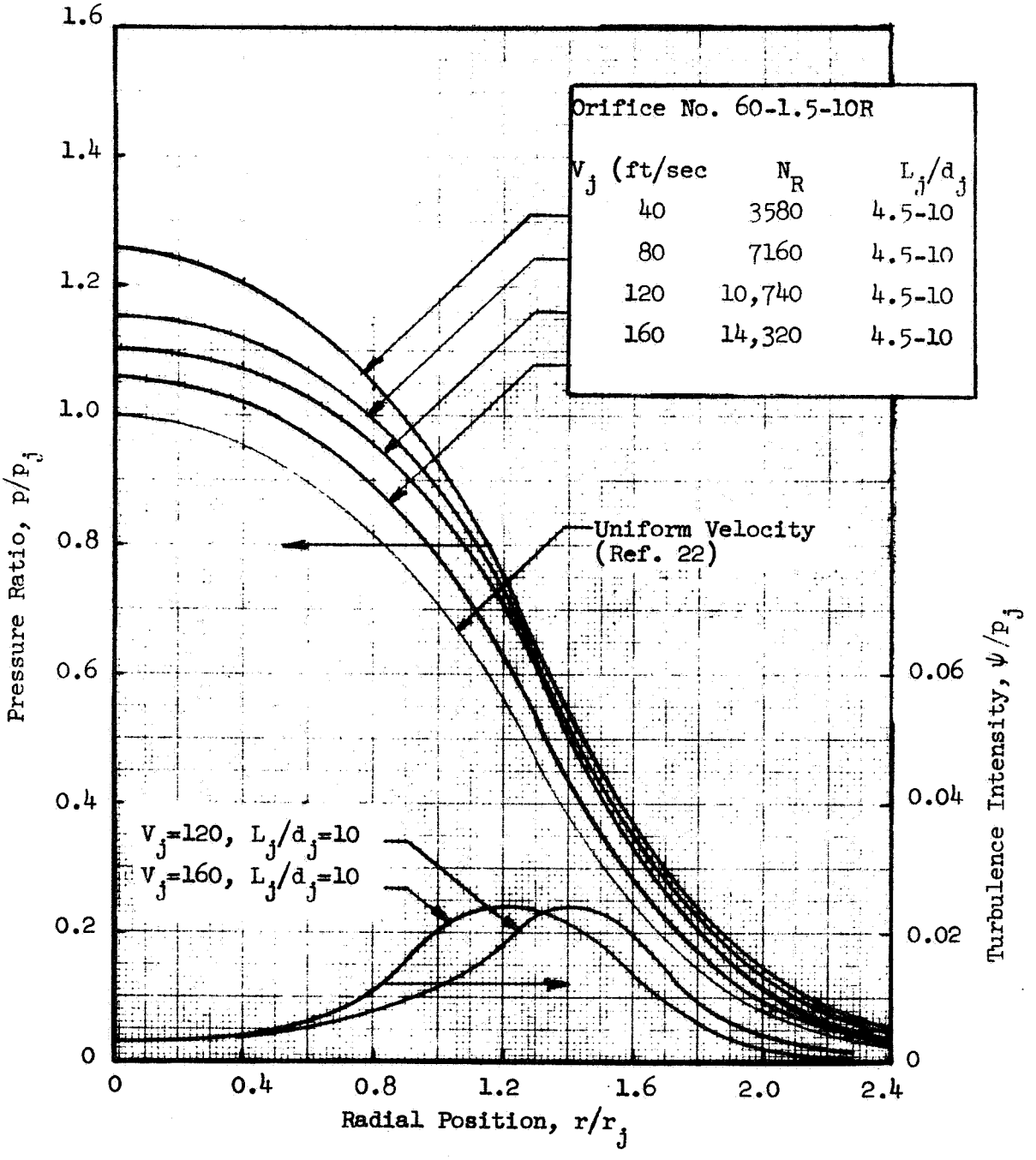

Figure 20. Pressure and Turbulence Intensity Profiles Produced by Laminar Jet (Orifice L_o/d_j = 1.5)

for the pressure distribution produced by a uniform velocity jet (i.e., $p_c/p_j = 1$). A comparison of the analytical and experimental pressure distributions indicates that this orifice produces a jet that is nearly uniform in velocity. It is also seen that the pressure distributions still more closely approach that of a uniform velocity jet as the injection velocity is increased.

Although the mean pressure did not vary, the pressure fluctuations were found to increase when the free jet length was greater than 5 d_j. The distributions of ψ/p_j measured at a free jet length of 10 d_j and injection velocities of 120 and 160 ft/sec are also shown on Fig. 20. It is seen that the maximum pressure fluctuation has increased to about 2% of the mean dynamic pressure in the case where the injection velocity is 120 ft/sec or greater. At free jet lengths of 7 d_j, a maximum fluctuation of about 1% (not shown on Fig. 20) was observed at a velocity of 160 ft/sec which decreased to nearly zero at 80 ft/sec. As previously noted, the maximum value of ψ/p_c was about 0.5% when L_j/d_j was less than 5.

The jets used in the study of turbulence effects on atomization were produced by the same 0.060-inch diameter orifices. In order to generate turbulence in the jets, threaded plugs, described in Section 3.1, were inserted into the large diameter reservoir preceding the orifice. However, the threads generate a substantial amount of large scale radial as well as longitudinal turbulence. Since the orifice length is small, the radial turbulence is not damped and disintegration of the jet occurs within a short distance from the orifice exit. Nevertheless, this technique did produce jets that were highly turbulent, relatively stable within the free jet lengths required and with a nearly-uniform velocity profile.

The variations of the turbulent jet centerline pressure ratio with injection velocity, measured at free jet lengths of 4.5, 7, and 10 d_j, are compared to analogous data for the laminar jet on Fig. 21. The pressure fluctuation, ψ, also shown on Fig. 21, exhibits a substantial increase with free jet length.

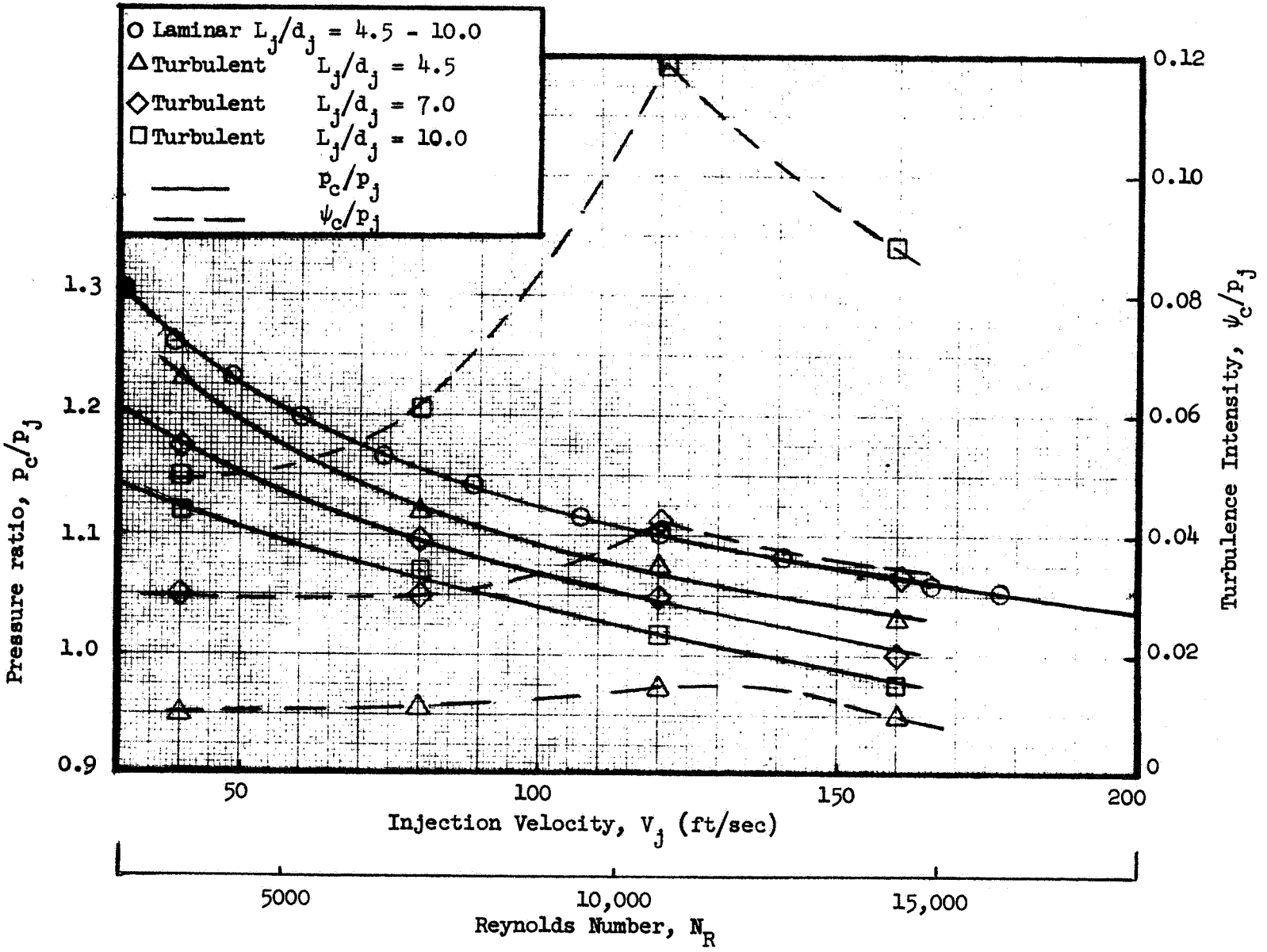

Figure 21. Variation of Jet Characteristics with Injection Velocity (L_o/d_j = 1.5)

Except at the longest free jet length, the pressure fluctuation ratio, ψ/P_j, did not significantly vary with the injection velocity. The reason for the maximum turbulence levels at the injection velocity of 120 ft/sec was not ascertained. However, since this velocity corresponds to a Reynolds number in the threaded section of about 3000 (note that the critical Reynolds number is 2700), much of the turbulence generated at lower N_R may be damped out before the fluid enters the orifice.

The mean and fluctuating (radial) pressure distributions produced by the turbulent jets at injection velocities of 40, 80, 120, and 160 ft/sec are shown on Figs. 22 to 25. Each figure illustrates the measured distributions at free jet lengths of 4.5, 7, and 10 orifice diameters. Also shown is LeClerc's analog solution for a uniform jet. At a free jet length of 4.5 d_j, the pressure distributions are similar to those produced by the laminar jets and indicate a nearly uniform velocity profile. However, as the free jet length is increased, there is a significant "widening" of the profile, particularly at injection velocites of 80 ft/sec or more.

In the experimental results presented above, it was shown that the measured turbulence intensity for both the laminar and turbulent jets increased with free jet length. Since there is no mechanism for generating internal turbulence once the jet leaves the orifice, the measured pressure fluctuations are attributed to oscillations of the jet itself. These oscillations, generated by the action of aerodynamic forces on the surface of the jet, are clearly seen in the photographs* of the laminar and turbulent jets shown on Fig. 26. In the case of the laminar jet at a velocity of 40 ft/sec, Fig. 26a, the appearance of surface disturbances occurs at a free jet length of approximately 12. This is consistent with the low level pressure fluctuations measured at free jet lengths less than 10 d_j. At higher injection velocities both the laminar and turbulent jets exhibit surface disturbances at free jet lengths of 10 d_j. This again is consistent with the measurement of high pressure fluctuations at the longer free jet lengths. In addition,

*The photographs were obtained with a Fastax camera at a film speed of 3000 frames/sec.

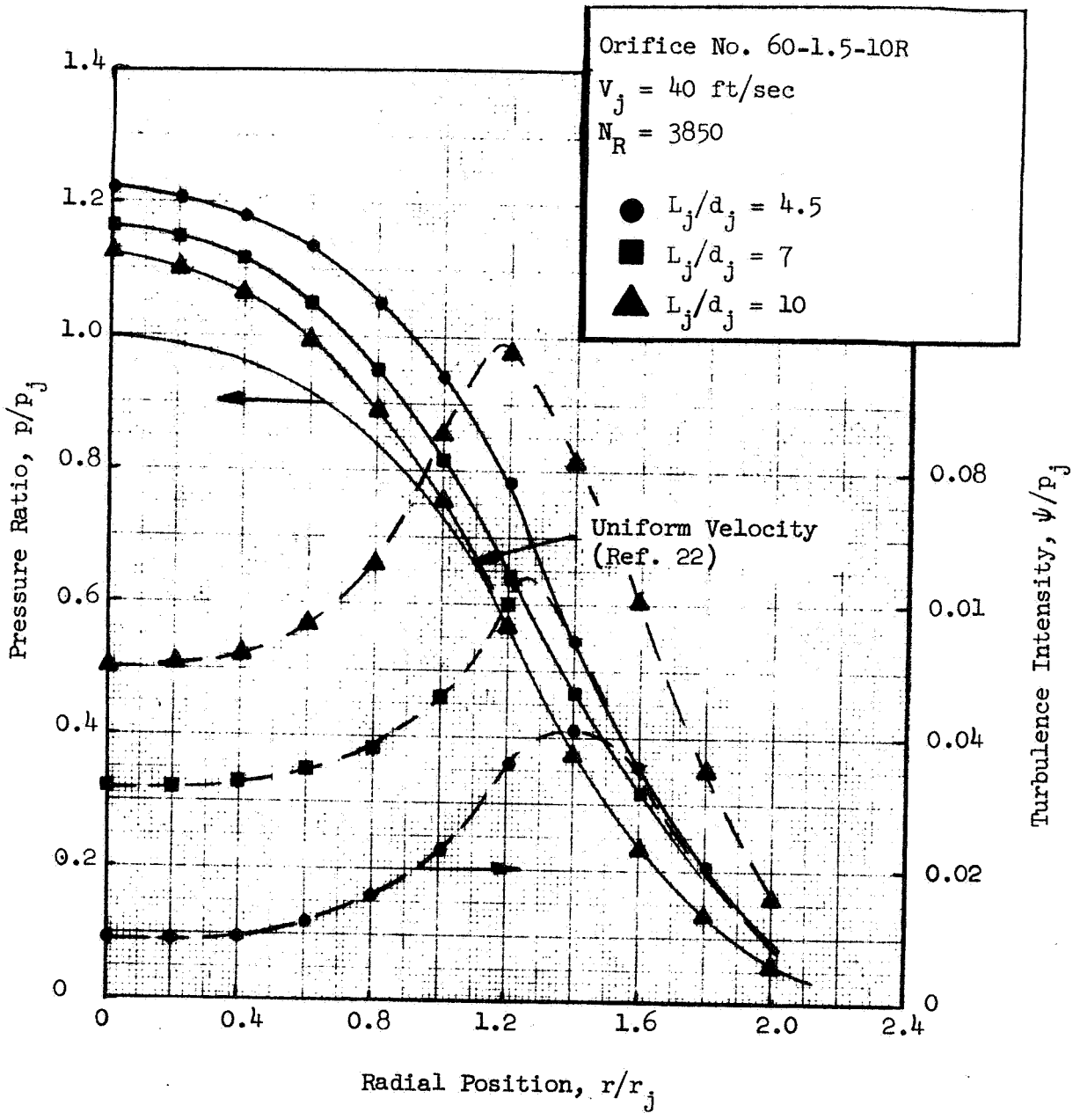

Figure 22. Pressure and Turbulence Intensity Profiles Produced by Turbulent Jet (V_j = 40 ft/sec)

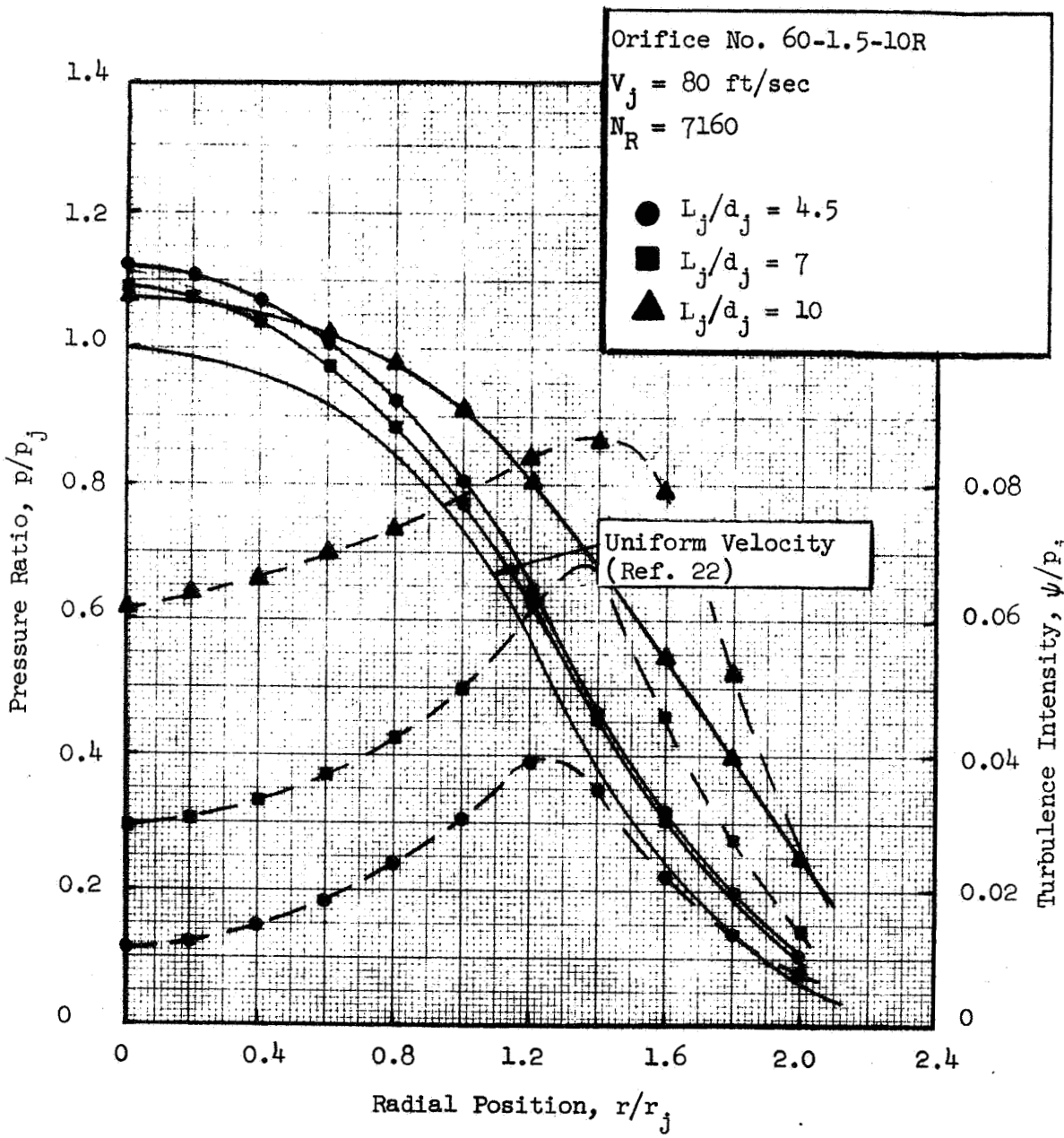

Figure 23. Pressure and Turbulence Intensity Profiles Produced by Turbulent Jet (V_j = 80 ft/sec)

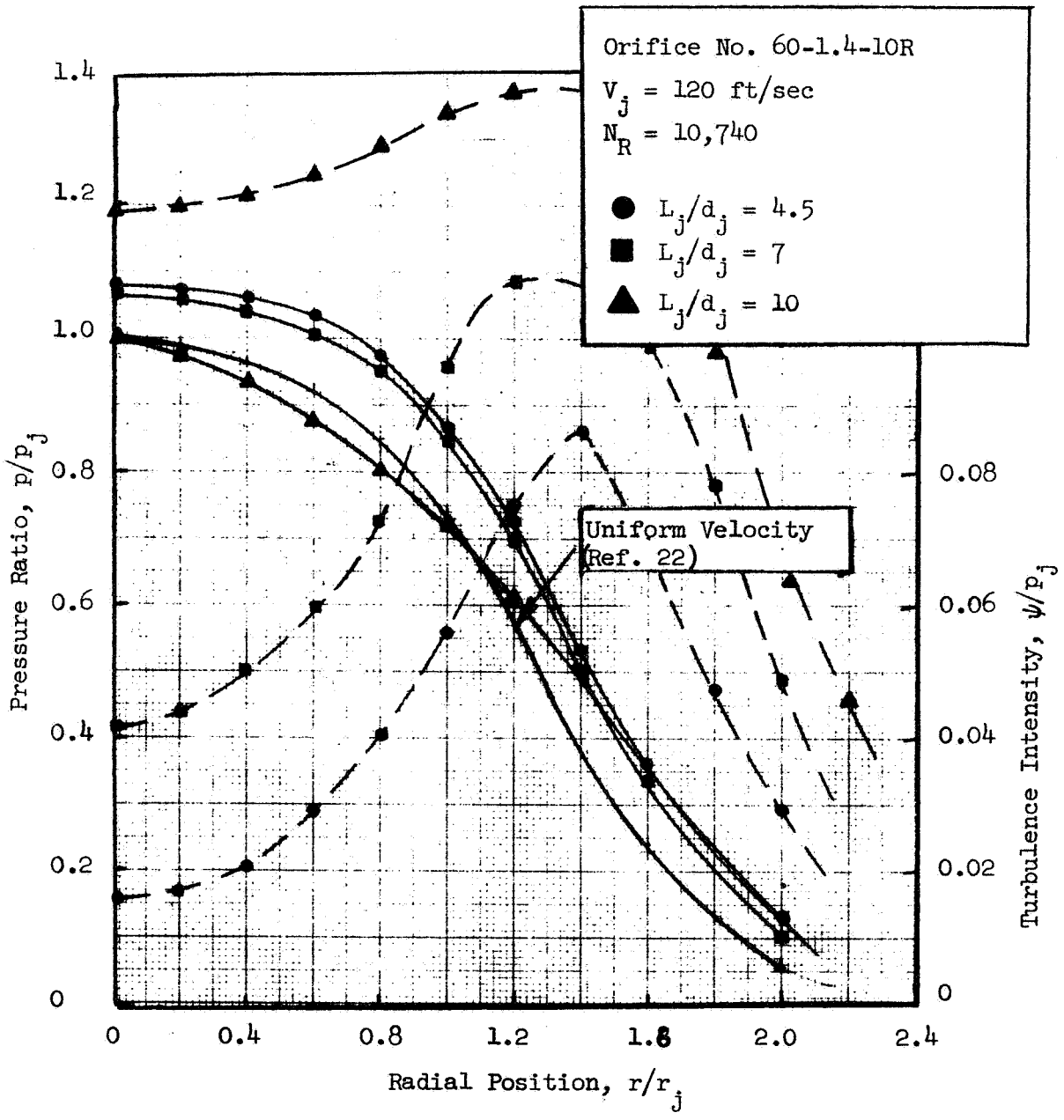

Figure 24. Pressure and Turbulence Intensity Profiles Produced by Turbulent Jet (V_j = 120 ft/sec)

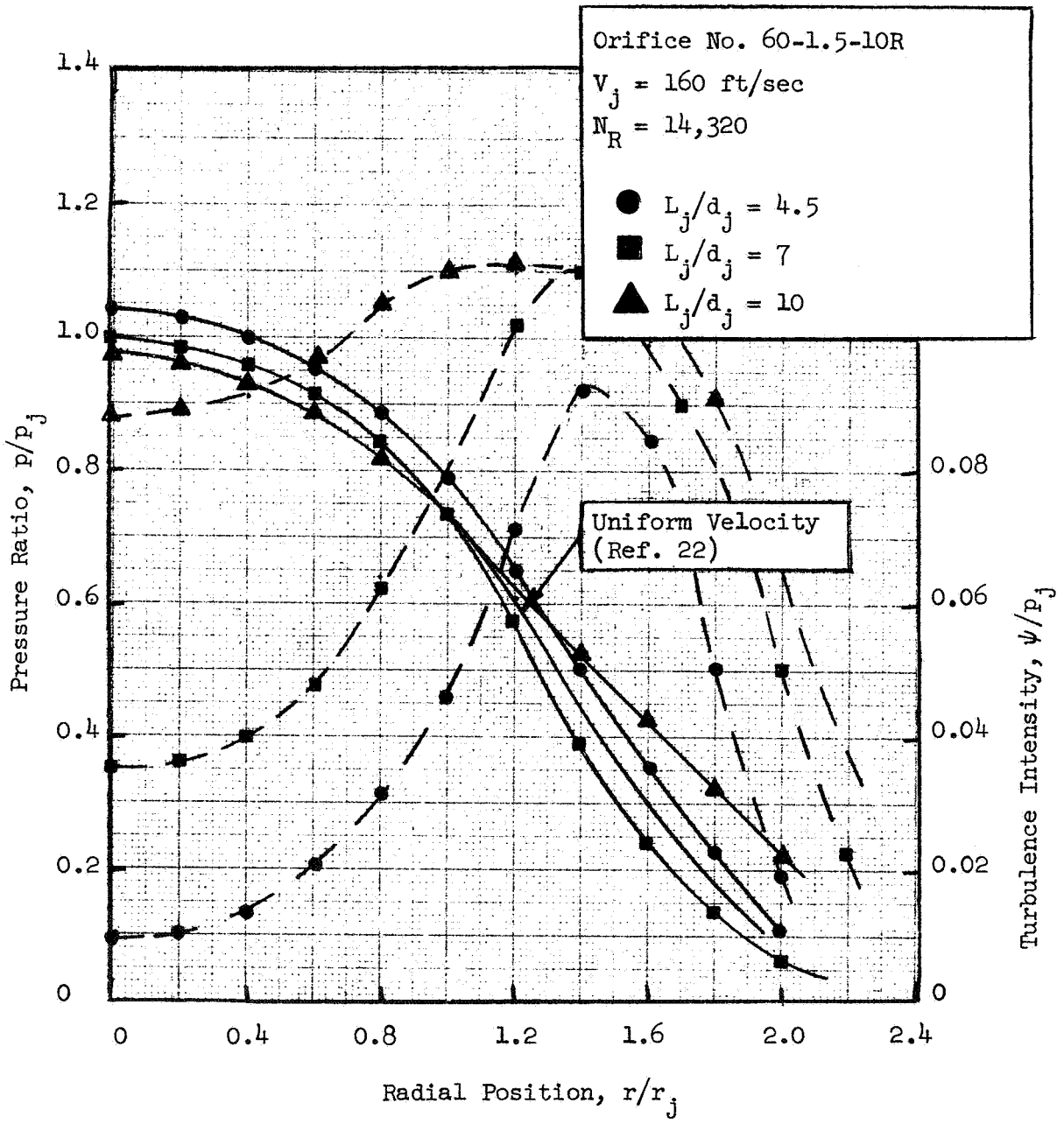

Figure 25. Pressure and Turbulence Intensity Profiles Produced by Turbulent Jet (V_j = 160 ft/sec)

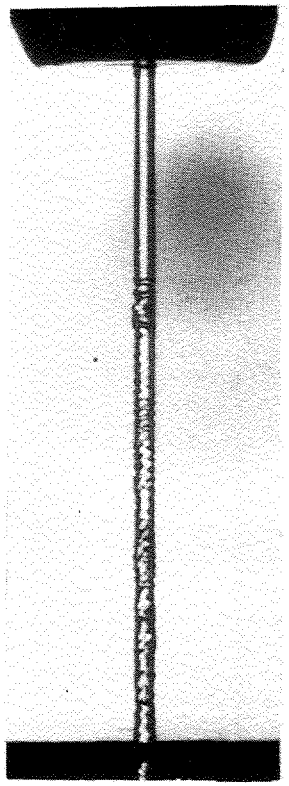

Laminar Jet
V_j = 40 ft/sec
N_R = 3580

Figure 26a

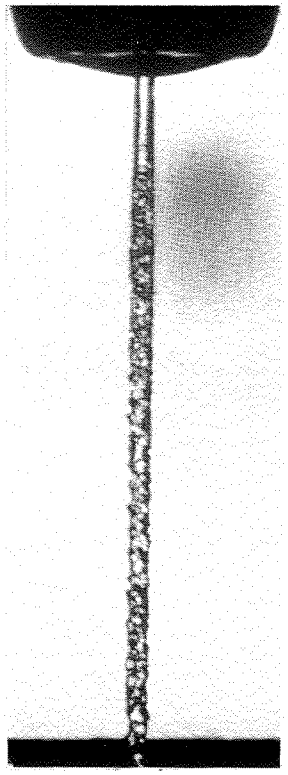

Laminar Jet
V_j = 80 ft/sec
N_R = 7160

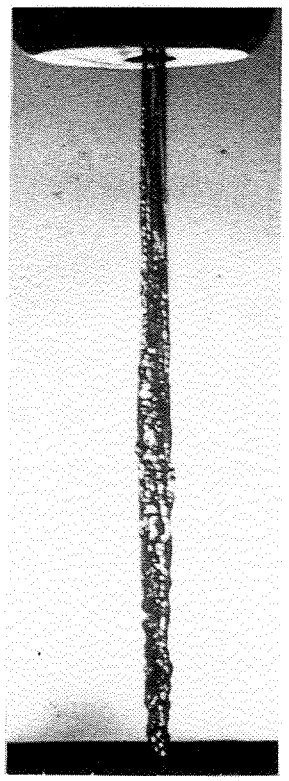

Turbulent Jet
V_j = 80 ft/sec
N_R = 7160

Figure 26b

Figure 26. Visual Comparison of Uniform Velocity Profile, Laminar and Turbulent Jets

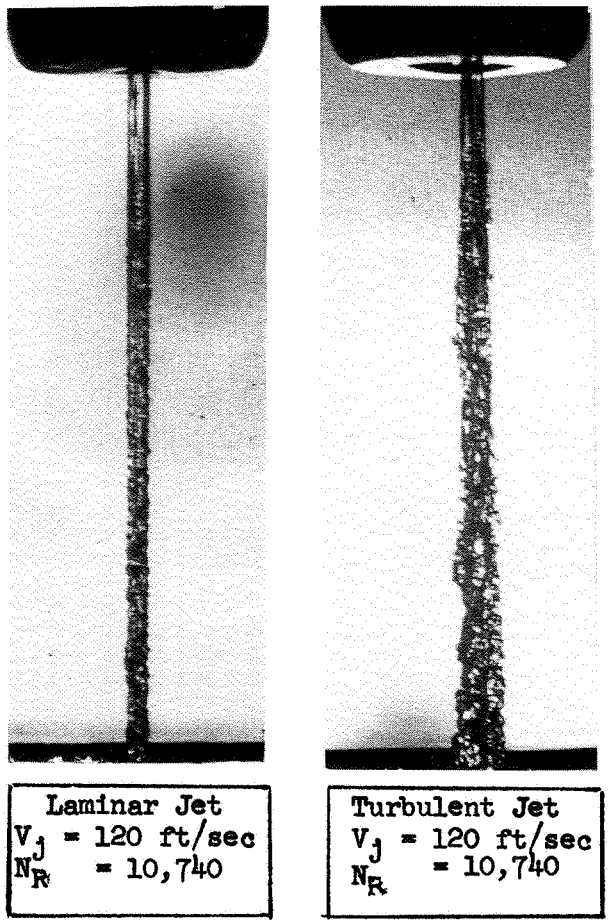

Figure 26c

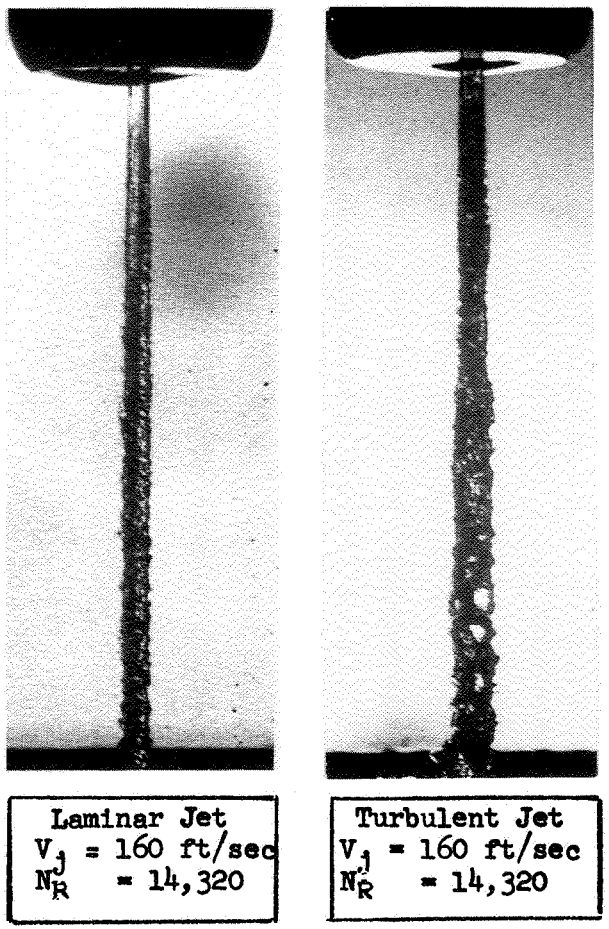

Figure 26d

Figure 26 (Continued) Visual Comparison of Uniform Velocity Profile, Laminar and Turbulent Jets

the noticeable widening of the pressure distribution measured with the turbulent jets (see e.g., Fig. 25) is in agreement with the spreading of the turbulent jet clearly seen, for example, on Fig. 26d.

The five remaining round entrance orifices that were examined differ primarily in their length, which ranged from 6 to 200 diameters. The measurements of the characteristics of jets produced by these orifices provided information regarding the extent of profile development and the variation of the turbulence level with orifice length. Unless otherwise noted, the measurements were performed at a free jet length of 5 orifice diameters.

The centerline pressure ratios and turbulence levels for the $6\ L_o/d_j$ orifice and the two $10\ L_o/d_j$ orifices are shown on Fig. 27 as a function of the injection velocity. For comparison, the pressure ratio variation obtained with orifice No. 60-1.5-10R is also shown. At low injection velocities, the centerline pressure obtained with the two 10 L_o/d_j elements are quite similar. However, at an injection velocity of about 90 ft/sec, the jet produced by orifice No. 63/63-10-3LD exhibited a discontinuous change in the turbulence intensity and pressure variation with injection velocity as shown on Fig. 27. (A possible reason for this discrepancy is presented in Section 5.1.2.) Both the pressure and turbulence intensity within the jets produced by the remaining 10 L_o/d_j and the 6 L_o/d_j orifices varied monotonically with injection velocity.

The radial distributions of pressure and turbulence produced by the jets issuing from the 10 L_o/d_j orifice elements at nominal injection velocities of 40 and 120 ft/sec are compared on Figs. 28a and 28b respectively. It is seen that the two elements produce jets with very similar velocity profiles but which differ significantly in the level of turbulence intensity at the higher injection velocity. A comparison of the measured pressure distributions to LeClerc's solution, also shown on Fig. 28, indicates that the distribution of velocity within the jets is non-uniform.

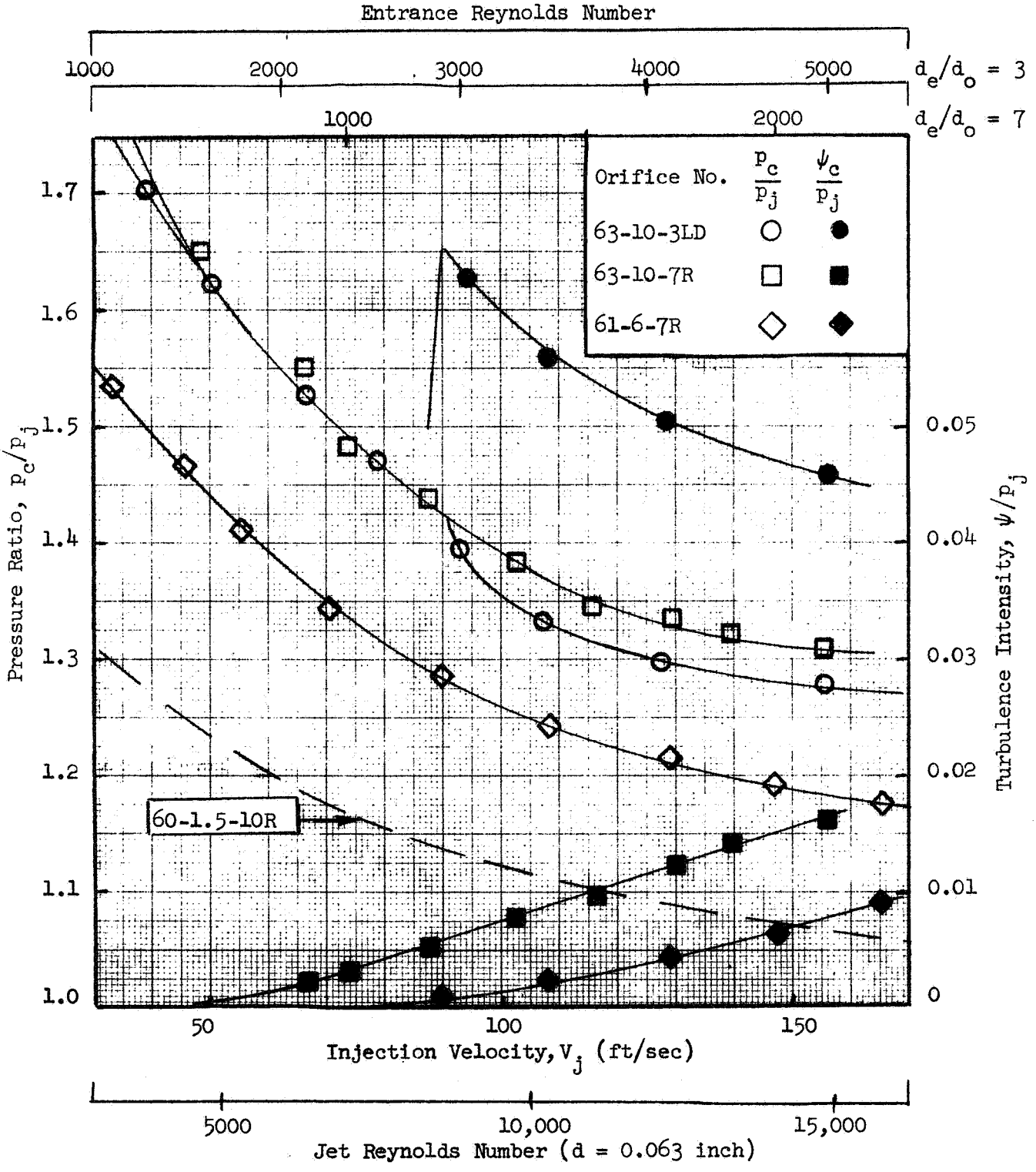

Figure 27. Variation of Centerline Pressure Ratio and Turbulence Intensity with Injection Velocity (L_o/d_j = 6 and 10)

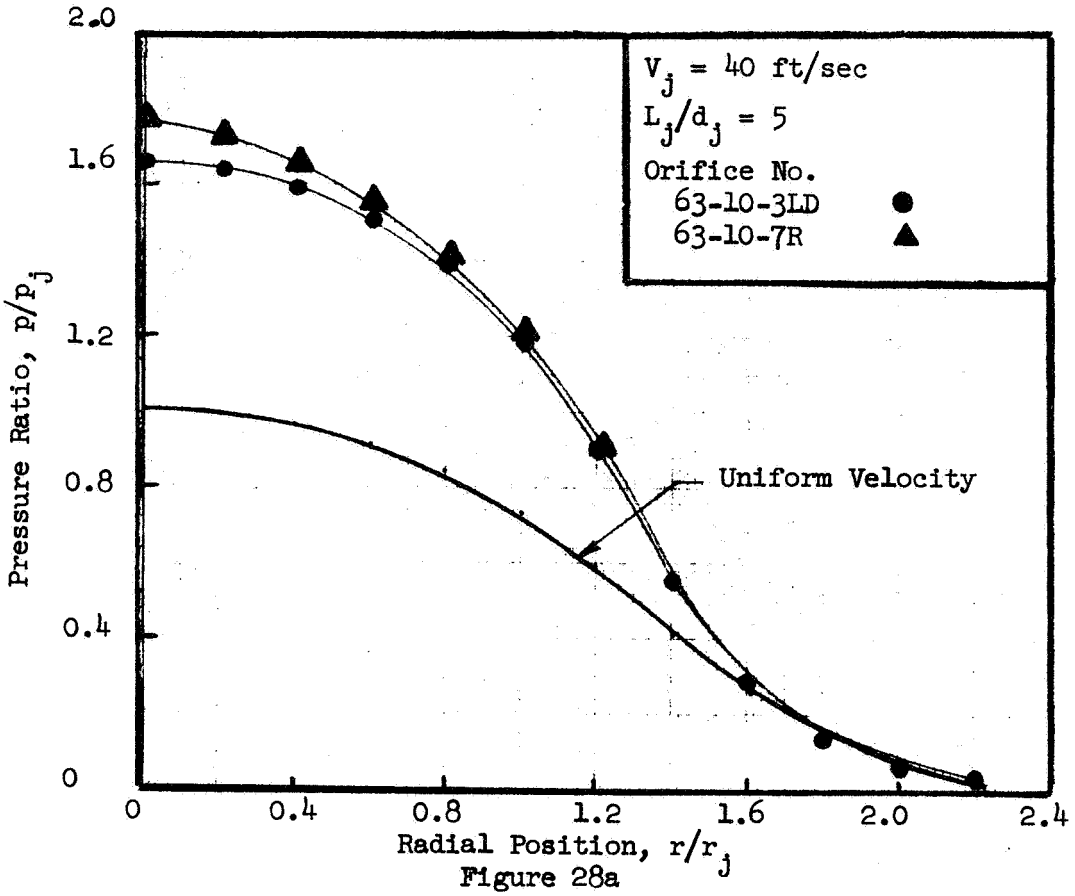

Figure 28a

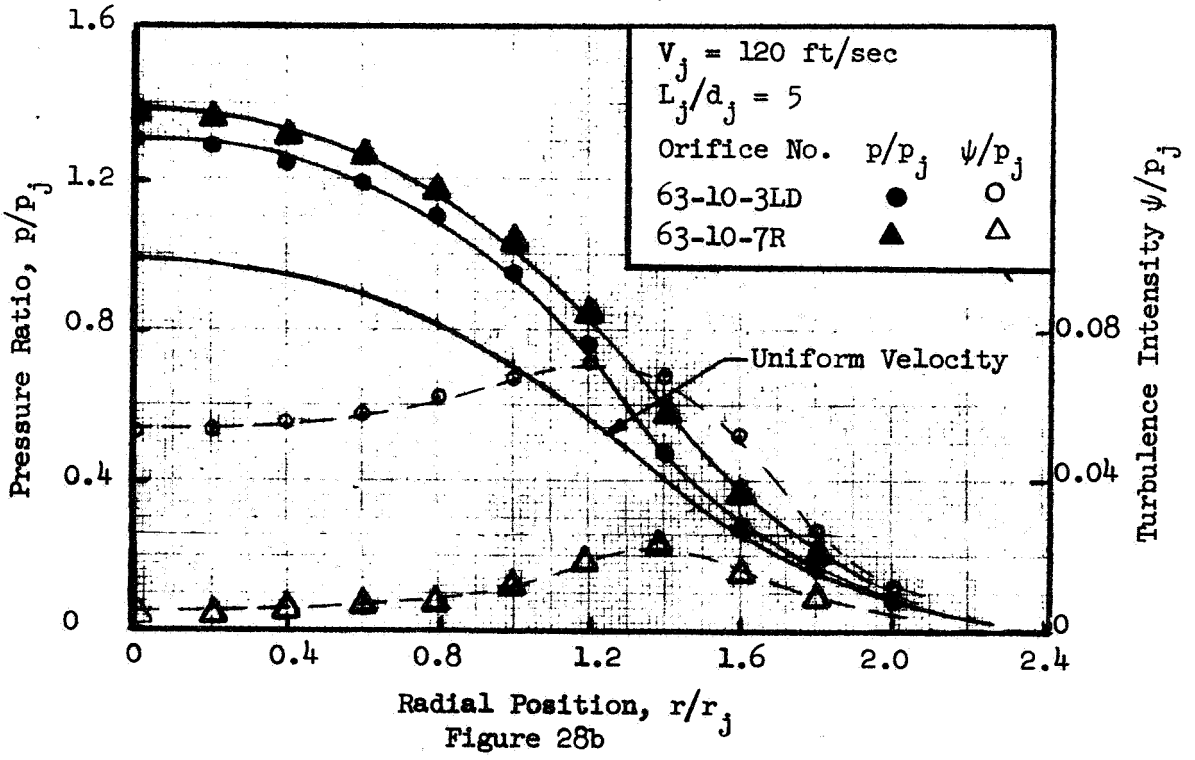

Figure 28b

Figure 28. Pressure and Turbulence Intensity Profiles Obtained with 10 L_o/d_j Orifice

The variation of the centerline pressure ratios and turbulence levels with injection velocity for the 50 and 200 L_o/d_j elements are shown on Fig. 29. At low injection velocities, the free jets produced by both orifices are laminar. As is to be expected, the centerline pressure ratio of the 200 L_o/d_j orifice approaches that of a fully developed laminar jet at the lower injection velocities.

A characteristic of both orifice configurations is that the jets they produce become turbulent at an injection velocity on the order of 100 ft/sec. This transition to a turbulent jet is accompanied by a rapid increase in the turbulence intensity level similar to that observed with the 10 L_o/d_j element No. 63/63-10-3LD. Above an injection velocity of 100 ft/sec, the centerline pressures for the 50 and 200 L_o/d_j orifices attain a constant value indicating the establishment of fully developed turbulent flow. It is seen that there is a slight difference in the level of centerline pressure for the two orifices. However, this is to be expected since the centerline velocity of a fully developed turbulent jet is a function of both Reynolds number and surface roughness (see e.g., Schlichting, Ref. 24).

The non-dimensional turbulence intensity, ψ_c/p_j, also shown on Fig. 29 is seen to diminish with increasing injection velocity once turbulent flow is established. However, when compared on the basis of absolute magnitude, ψ_c increases with velocity. This trend is consistent with measurements of turbulent jets obtained by Rupe, Ref. 23.

The pressure and turbulence (radial) profiles obtained with the 50 L_o/d_j orifice at injection velocities of 40 and 120 ft/sec are shown on Fig. 30. The pressure profile produced by the low velocity jet is compared to LeClerc's solution on Fig. 30a. As is readily seen, the pressure distribution exhibits a significant deviation from that produced by a uniform velocity jet.

The high velocity profiles for the 50 L_o/d_j element, Fig. 30b, are compared to those produced by a fully developed turbulent jet (Reynolds number of

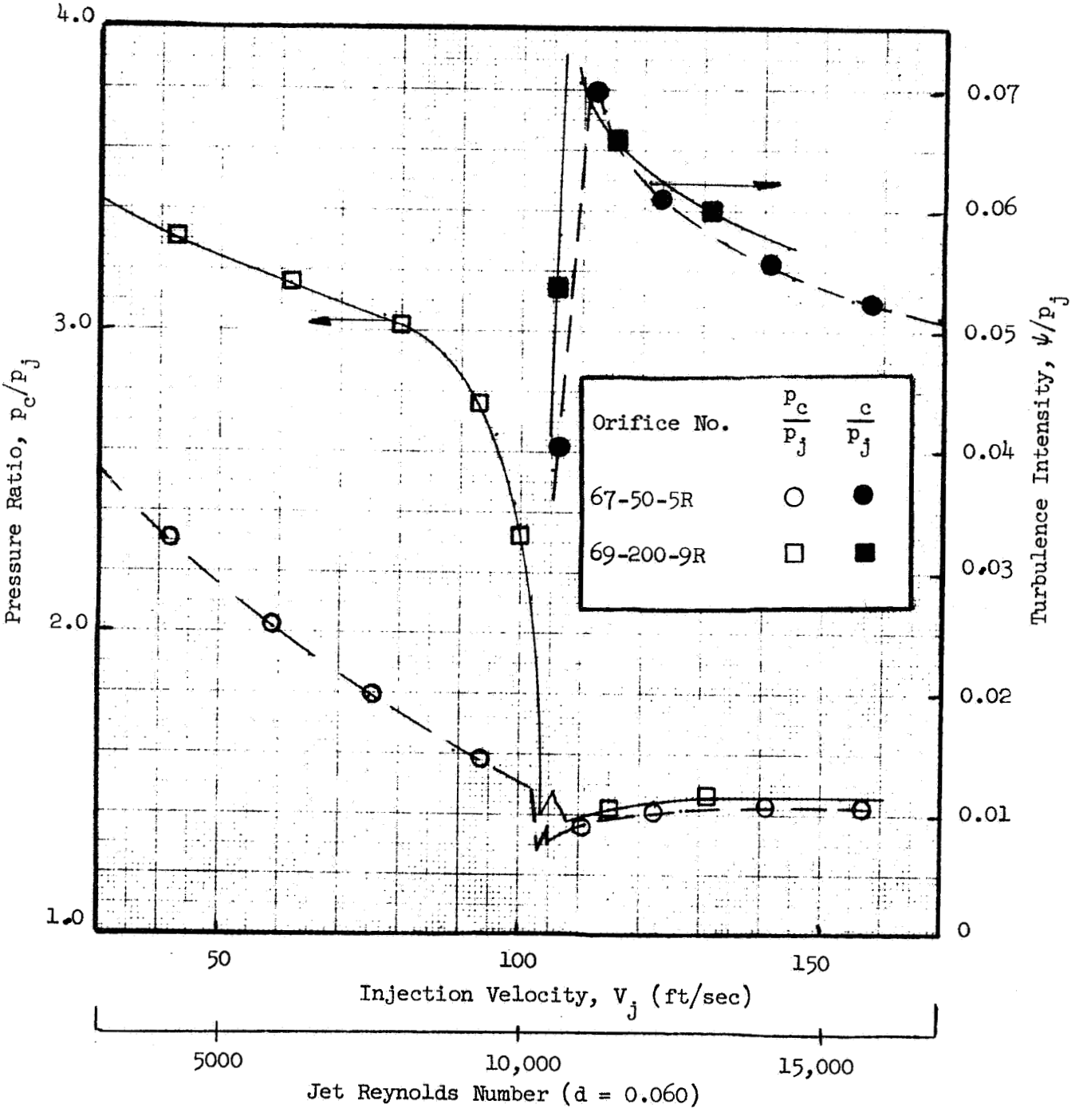

Figure 29. Variation of Centerline Pressure Ratio and Turbulence Intensity with Injection Velocity (L_o/d_j = 50 and 200)

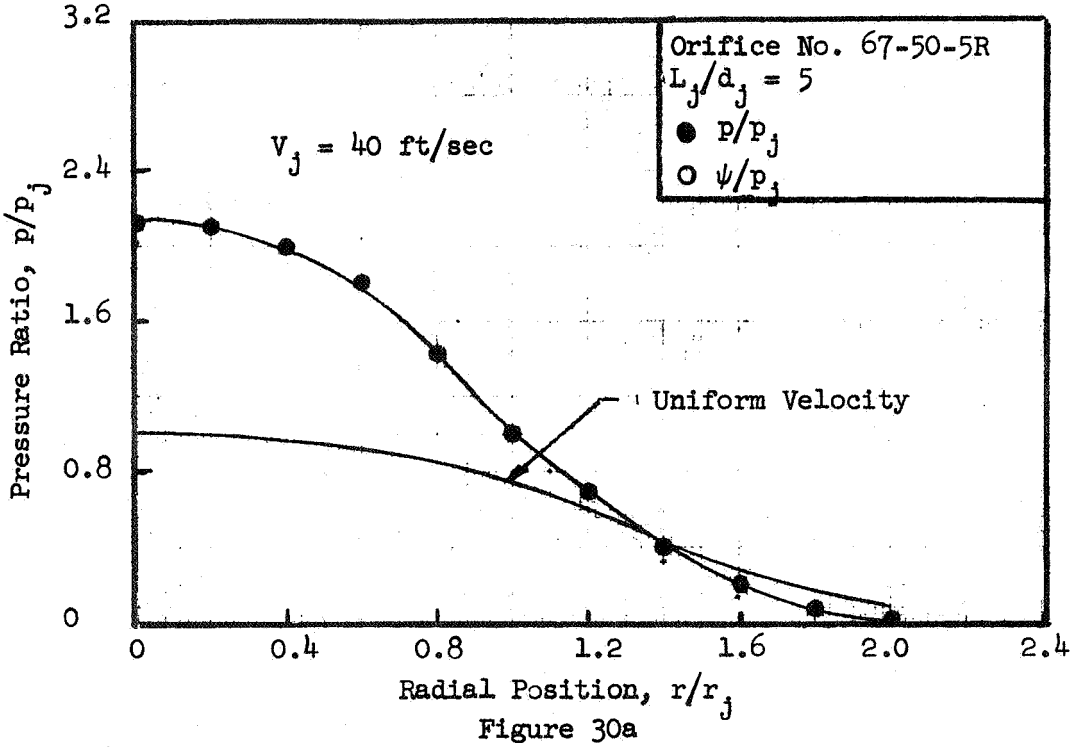

Figure 30a

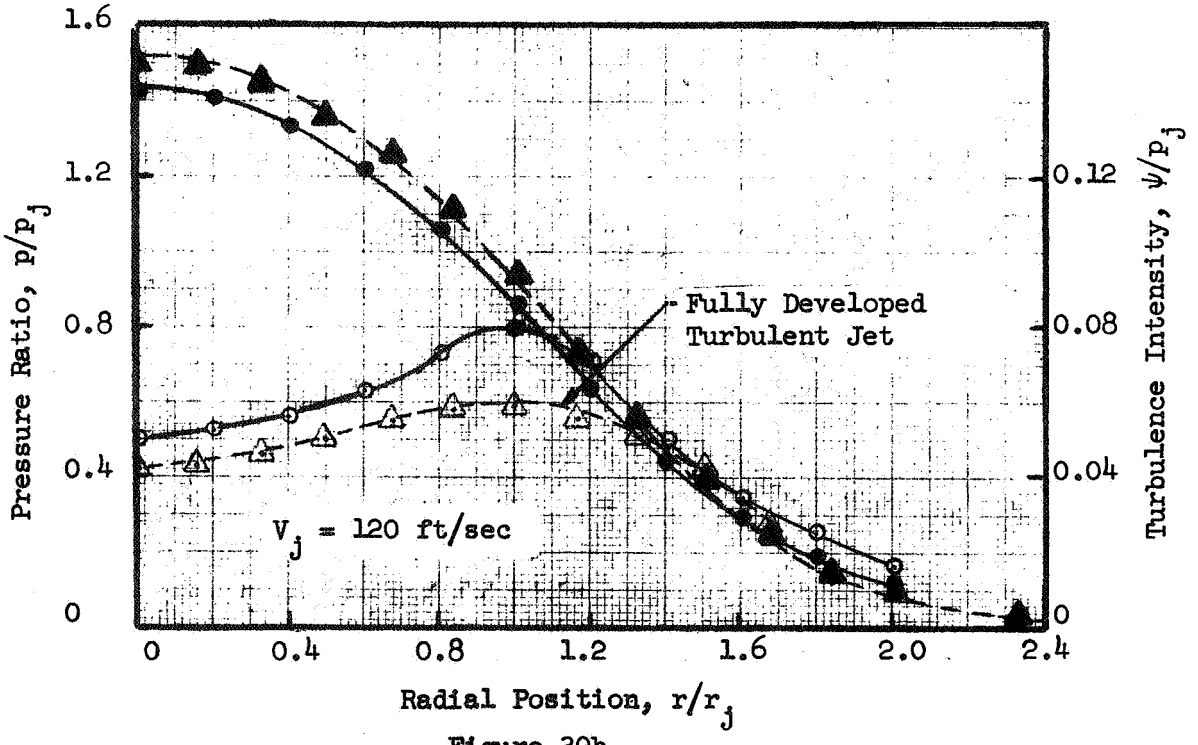

Figure 30b

Figure 30. Pressure and Turbulence Intensity Profiles Obtained with 50 L_o/d_j Orifice

46,300) measured by Rupe. Allowing for the influence of Reynolds number on the distribution of velocity and turbulence, the profiles are seen to be quite similar; verifying that fully developed turbulent flow has been established.

The turbulence levels for the fully developed turbulent jets, Fig. 30b, are seen to reach a maximum at a position approximately equal to the jet radius. This is a result of the high levels of turbulence generated at the walls of the orifice and persisting in the free jet. It is interesting to note that for a less than fully developed jet, this maxima is measured at a greater radial distance as shown on Fig. 28b for the 10 L_o/d_j elements.

The pressure distribution obtained at an injection velocity of 37 ft/sec with the 200 L_o/d_j orifice is shown on Fig. 31. The measured profile is compared to that produced by a fully developed laminar jet. The latter, measured by Rupe, was produced by a 200 L_o/d_j orifice at a Reynolds number of 1471. The centerline pressure ratio for a fully developed laminar jet is, of course, 4. That this level was not reached is due to two factors. The first is that some velocity profile decay will occur over the free jet length. In addition, the Reynolds number for the profile obtained in the current study is too high for fully developed laminar flow to be attained in a 200 L_o/d_j orifice.

In the study of the influence of free jet length on atomization, the majority of the experiments were conducted with the 50 L_o/d_j orifices. Consequently the characteristics of the jet produced by this orifice were examined as a function of free jet length. The variation of the centerline pressure ratio and turbulence intensity at an injection velocity of 100 ft/sec are shown on Figs. 32 and 33 respectively. Oscilloscope traces produced by the pressure fluctuations are shown as inserts on Fig. 33. An examination of the variation of the two pressure components with L_j/d_j reveals that both experience a discontinuous change at a jet length of about 5 d_j. This rapid change is attributed to jet disintegration.

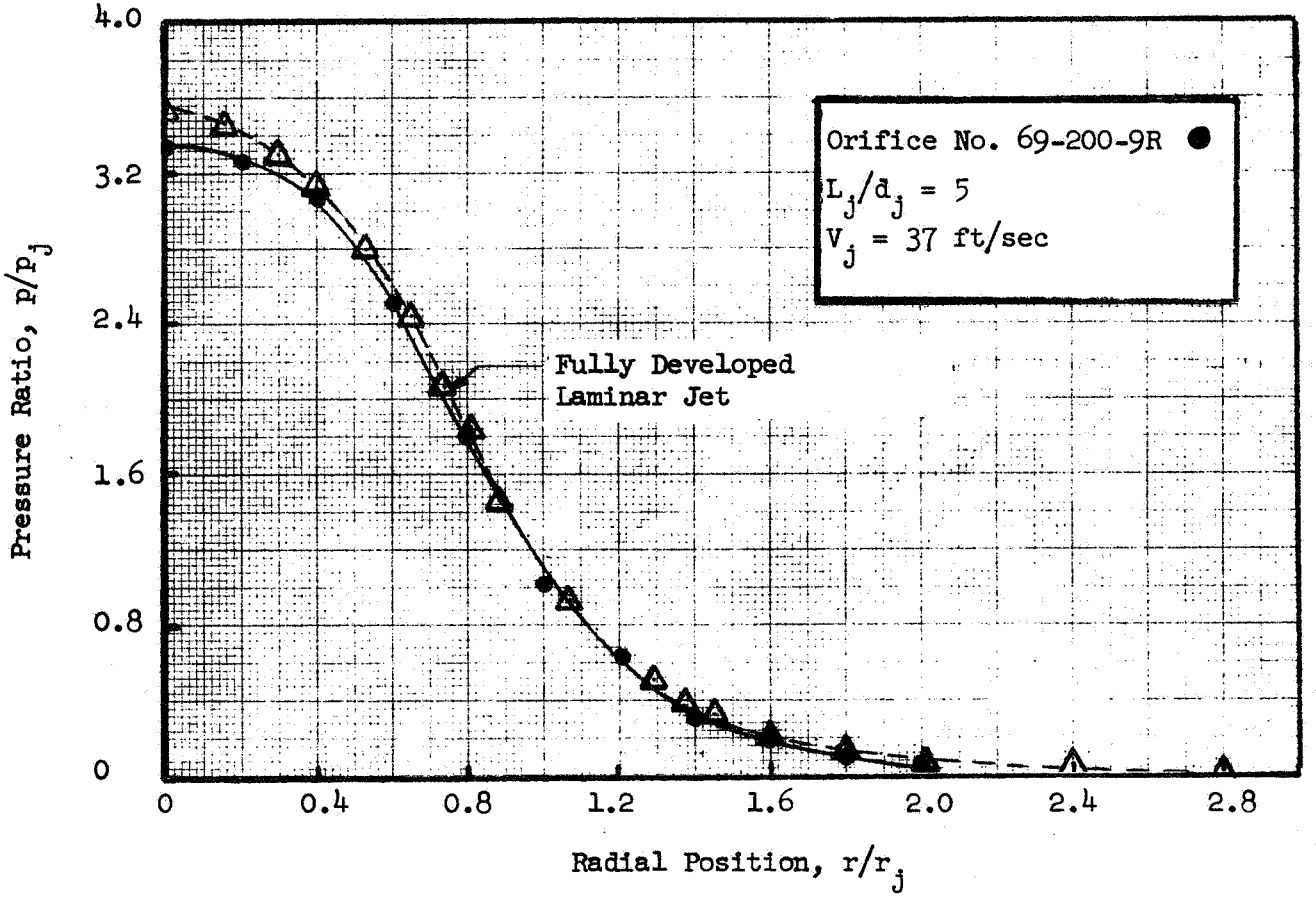

Figure 31. Pressure Profile Obtained with 200 L_o/d_j Orifice

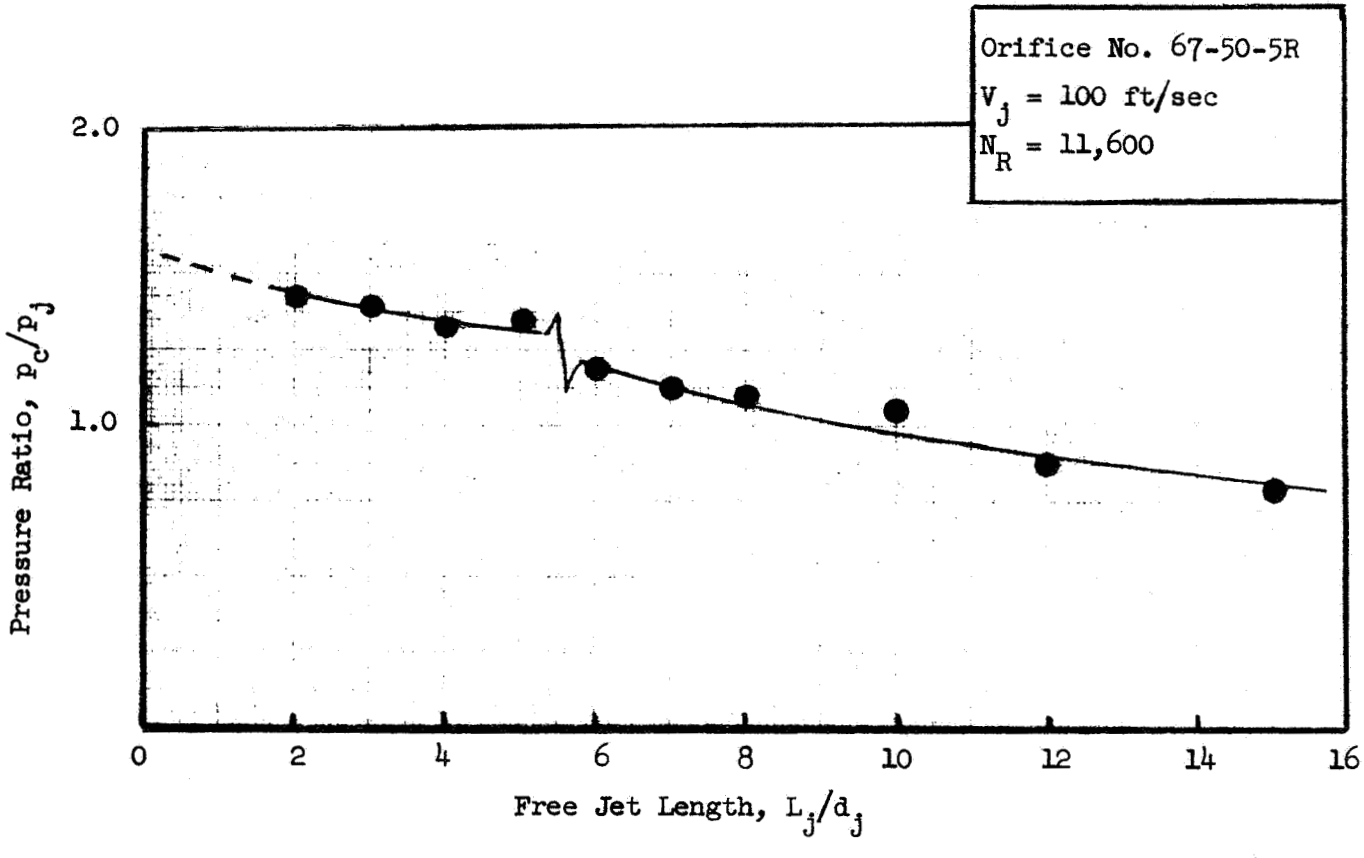

Figure 32. Variation of Centerline Pressure Ratio with Free Jet Length (L_o/d_j = 50)

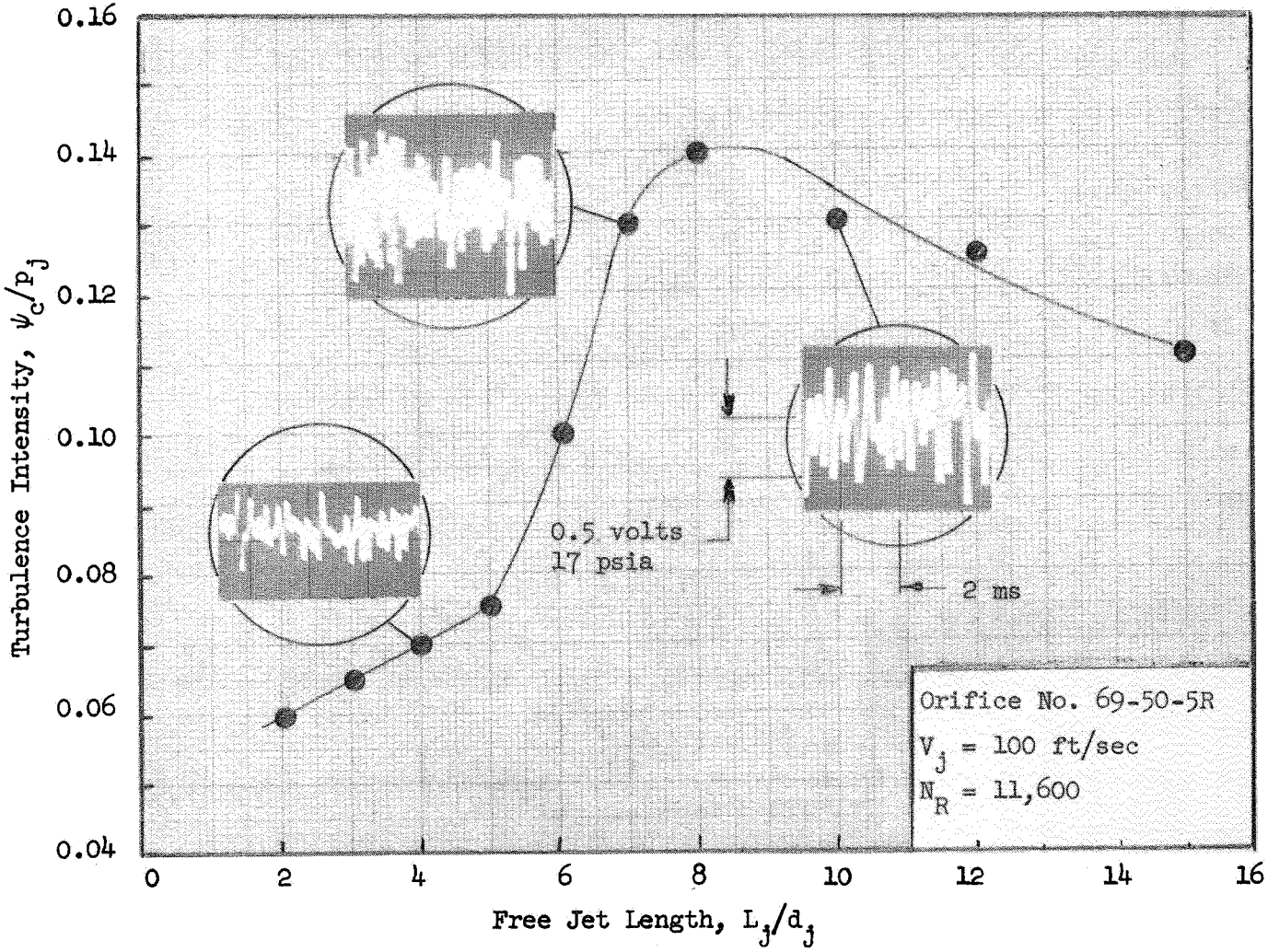

Figure 33. Variation of Centerline Turbulence Intensity with Free Jet Length (L_o/d_j = 50)

Sharp Entrance Orifices. The internal characteristics of the jets produced by the sharp entrance orifices were found to be significantly different from those measured within jets produced by round entrance orifices of comparable geometric dimensions. Shown on Fig. 34 are the centerline pressure ratio versus injection velocity data obtained with the 2, 6 and 10 L_o/d_j sharp entrance orifices. Up to a velocity of about 35 ft/sec the jets produced by all three orifices were highly turbulent and had near the same centerline pressure ratio. Between 35 and 50 ft/sec the jets completely separated from the walls of the orifice. Visual observation of the jets confirmed that separation had indeed occurred. At higher velocities, the jets issuing from the three orifices again attained nearly the same centerline pressure ratio but with no measurable turbulence intensity.

The pressure and turbulence profiles produced by the orifices were essentially identical. Shown on Fig. 35 are radial p/p_j and ψ/p_j distributions obtained with the 10 L_o/d_j element at injection velocities of 36 and 108 ft/sec. As would be expected from the centerline pressure ratio, the velocity profile at an injection velocity of 36 ft/sec, Fig. 35a, is non-uniform. What is unusual however, is the distribution of turbulence within the free jet. Unlike the previous measurements of turbulent jets the intensity is at a maximum in the center.

The pressure distribution obtained with this jet at the higher injection velocity, Fig. 35b, must be interpreted in view of the fact that complete separation of the jet has occurred. In this case, the pressure profile should be very similar to that produced by a sharp edge orifice. In order to make this comparison, the scale of the coordinates of Fig. 35b must be adjusted because of the now smaller jet radius and higher jet velocity. If it is assumed that the jet is uniform in velocity profile, continuity of the mass flowrate requires that r_j/r_s, where r_s is the radius of the separated jet, be equal to $(p_c/p_j)^{1/4}$. Since the magnitude of (p_c/p_j) is equal to 2.29 at an injection velocity of 108 ft/sec, r_j/r_s is 1.23.

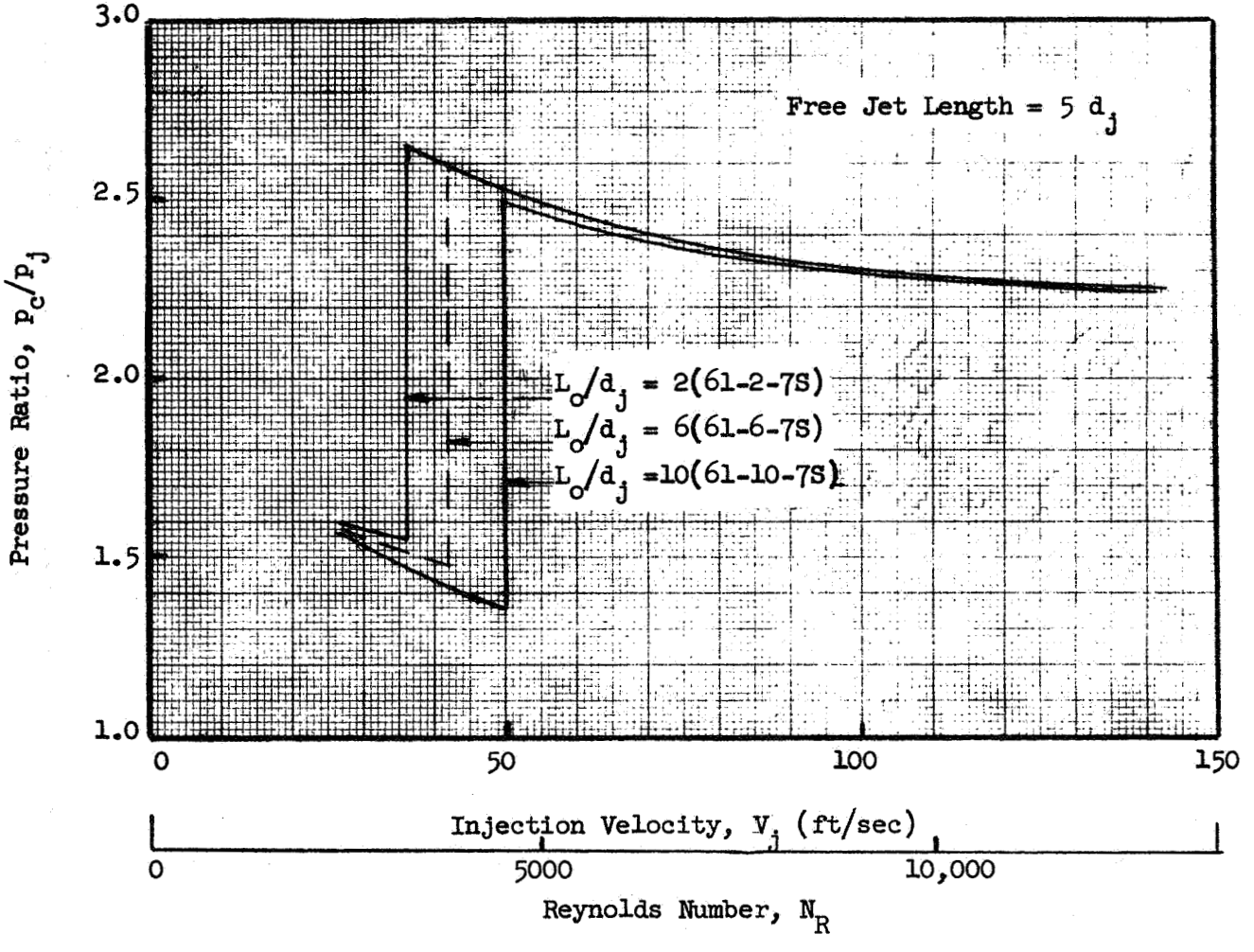

Figure 34. Variation of Centerline Pressure Ratio with Injection Velocity (sharp entrance)

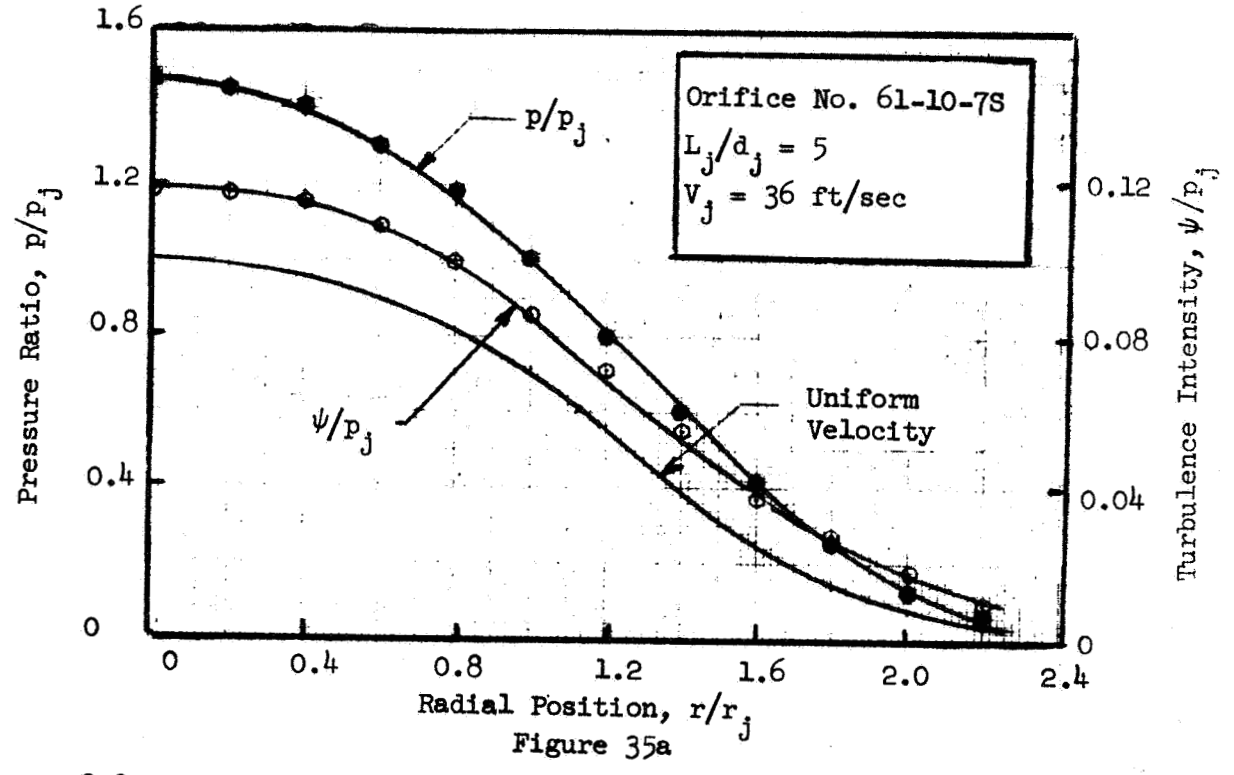

Figure 35a

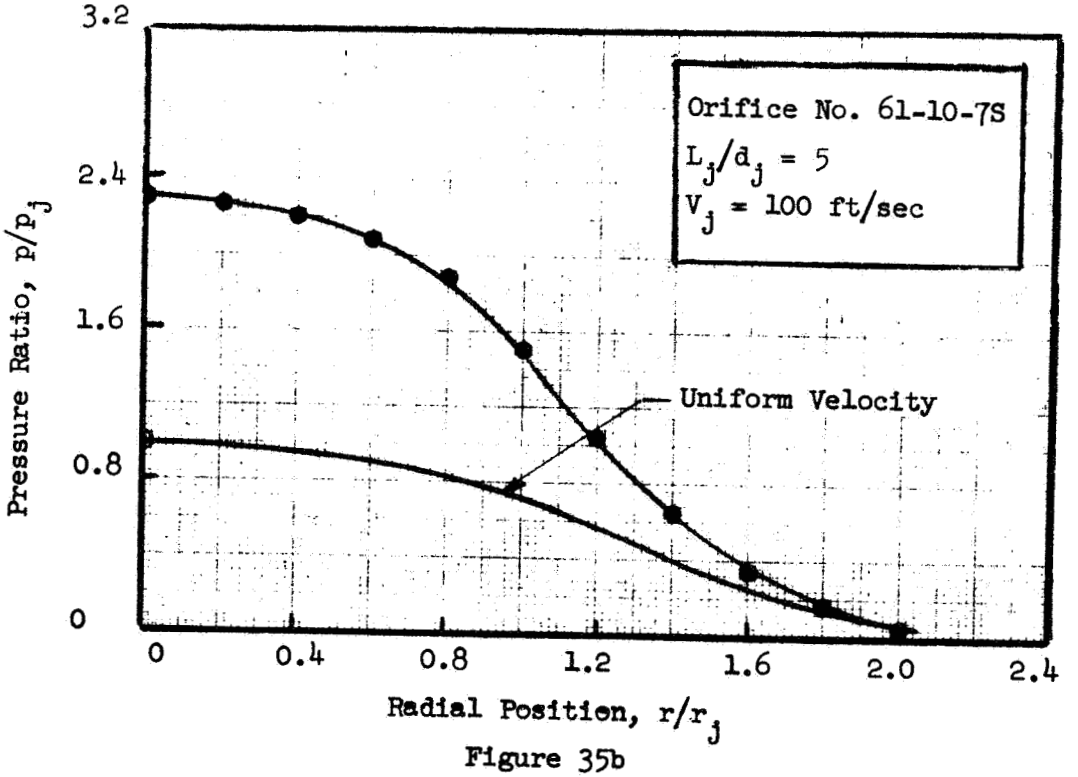

Figure 35b

Figure 35. Pressure and Turbulence Intensity Profiles Obtained with Sharp Entrance Orifice

The data presented on Fig. 35b are replotted on Fig. 36. The change of scale of the coordinates was accomplished by normalizing the radial position by the radius of the separated jet, r_s, while the pressure ratio was forced to pass through unity at r = 0 by dividing each point of the distribution shown on Fig. 35b by its centerline value. Also shown on Fig. 36 are Rupe's measurements of the pressure distribution produced by a jet issuing from a sharp-edged orifice and LeClerc's analog solution. It is seen that the profile produced by the separated jet agrees quite well with Rupe's measurements and that both are similar to the analog solution for the uniform velocity jet.

4.1.2 Effect of Cross Velocity on Jet Characteristics

The second series of tests performed in this study was directed to an evaluation of the influence of the orifice entry conditions on the internal jet characteristics when a manifold cross velocity was imposed. Two orifices were used to obtain the measurements; the round entrance (60 - 100 - OR) and the sharp entrance orifice (60 - 100 - OS).

A specific objective of the study was to determine the orifice length at which the cross velocity ceases to exert a significant influence on the free jet. The tests were performed at L_o/d_j ratios of 100, 75, 50, 25, 20, 15, 10, and 6, while the manifold cross velocities* were 0, 5, 10, and 20 ft/sec. The velocity of flow through the orifice was maintained constant at 120 ft/sec.

After the completion of testing at each value of L_o/d_j, the orifice length was shortened by cutting off a section at the orifice exit. In this manner, the identity of the entrance conditions for each test was assured.

Before proceeding to examine the effect of cross velocity per se, it is necessary to define the influence of variable orifice inlet conditions at zero cross velocity.

*The "cross velocity" is defined as the velocity within the manifold downstream of the orifice entrance.

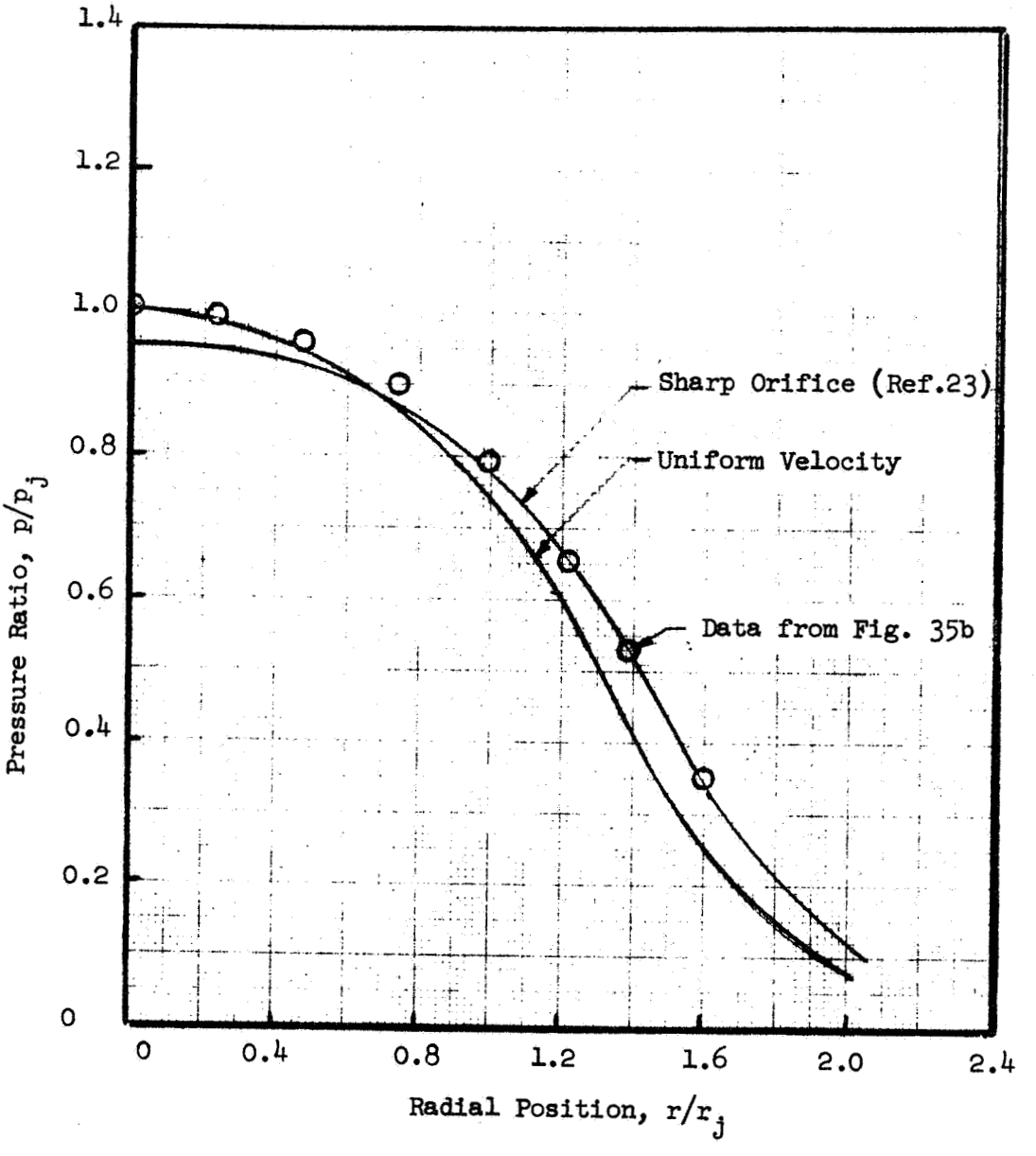

Figure 36. Comparison of Pressure Profiles Produced by Separated Jet and Uniform Velocity Jet

The variation of the centerline pressure ratios and turbulence intensity levels at zero cross velocity are presented in Fig. 37 as a function of orifice L_o/d_j for both orifices. It was previously noted that the orifice was fed from the manifold in a direction perpendicular to the axis of the orifice as shown on Figs. 16b and 16c. This constituted an entrance condition different from that of the previous experiments. The influence of the direction at which fluid enters the orifice is illustrated by a comparison of the rounded entrance orifice measurements with the results obtained with the 6 to 50 L_o/d_j, round entrance orifices presented previously on Fig. 27 and also shown on Fig. 37. As can be seen on Fig. 37a, one effect of the orthogonal feed is a reduction in the centerline pressure ratio. The large amount of turbulence generated by feeding the orifice in this manner is illustrated on Fig. 37b, where it is seen that an increase in free jet turbulence occurs when the orifice length is shortened. The converse was true when the orifice was fed from an essentially quiescent reservoir. In addition, it should be noted that the flow through the sharp entrance orifice did not separate in this case. This entrance type also exhibited a greater increase in the free jet turbulence level at small L_o/d_j's than did the rounded entrance orifice but produced a similar centerline pressure ratio.

When the orifice L_o/d_j was greater than 25, the characteristics of the jets produced by both the round and sharp entrance orifices were indistinguishable. The level of the centerline pressure ratio and turbulence intensity indicates the establishment of fully developed turbulent flow at about an L_o/d_j of 30.

The influence of cross velocity is best illustrated by normalizing the pressure and turbulence levels by their values measured at zero cross velocity and the same L_o/d_j. Figure 38 shows the normalized pressure and turbulence levels for the sharp entrance orifice as a function of manifold cross velocity. For orifice lengths greater than 15 d_j, the cross velocity had no effect on the centerline pressure. Below that value a noticeable drop in the pressure occurred as can be seen on Fig. 38a. The centerline turbulence levels were affected by cross velocity up to an orifice length of 25 d_j as shown on Fig. 38b.

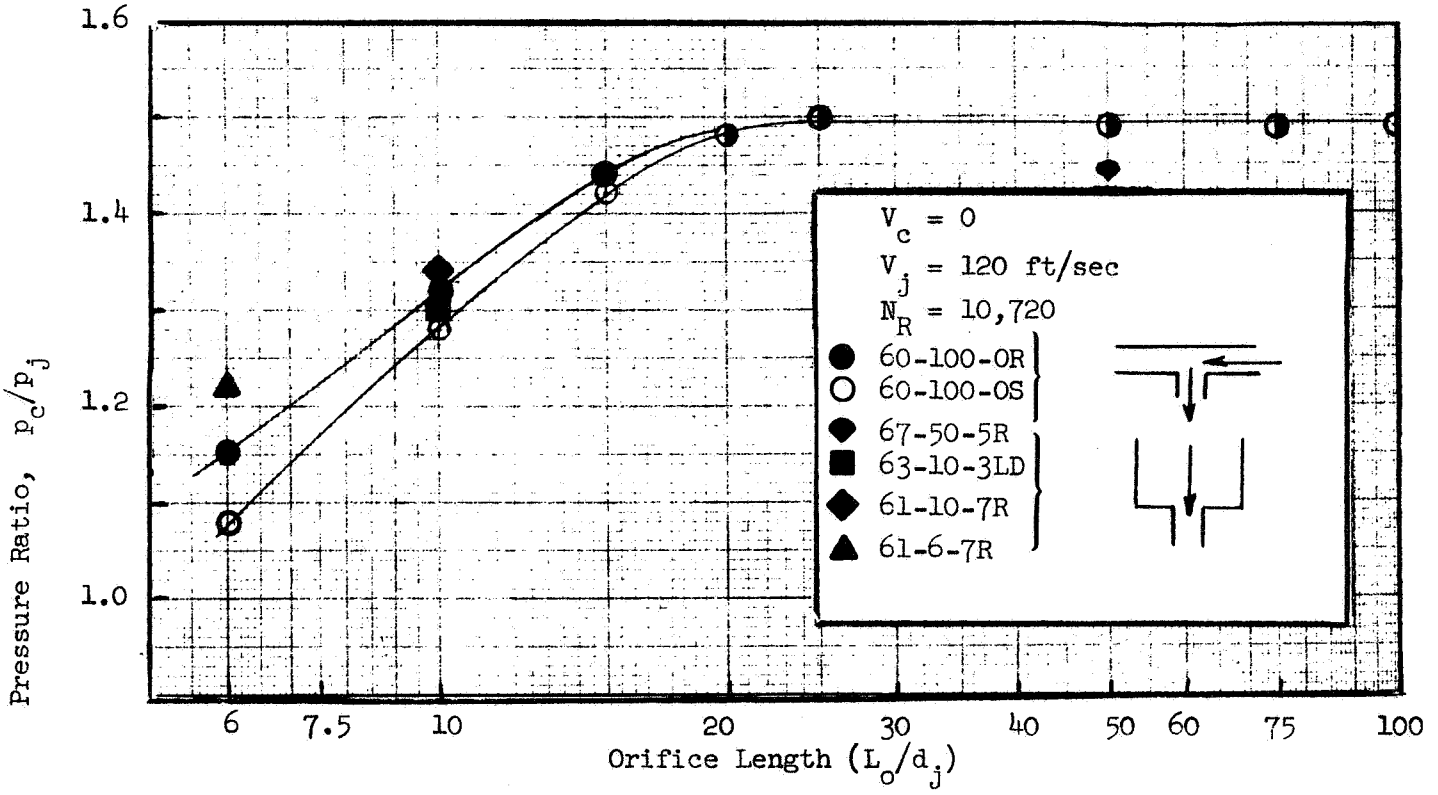

Figure 37a

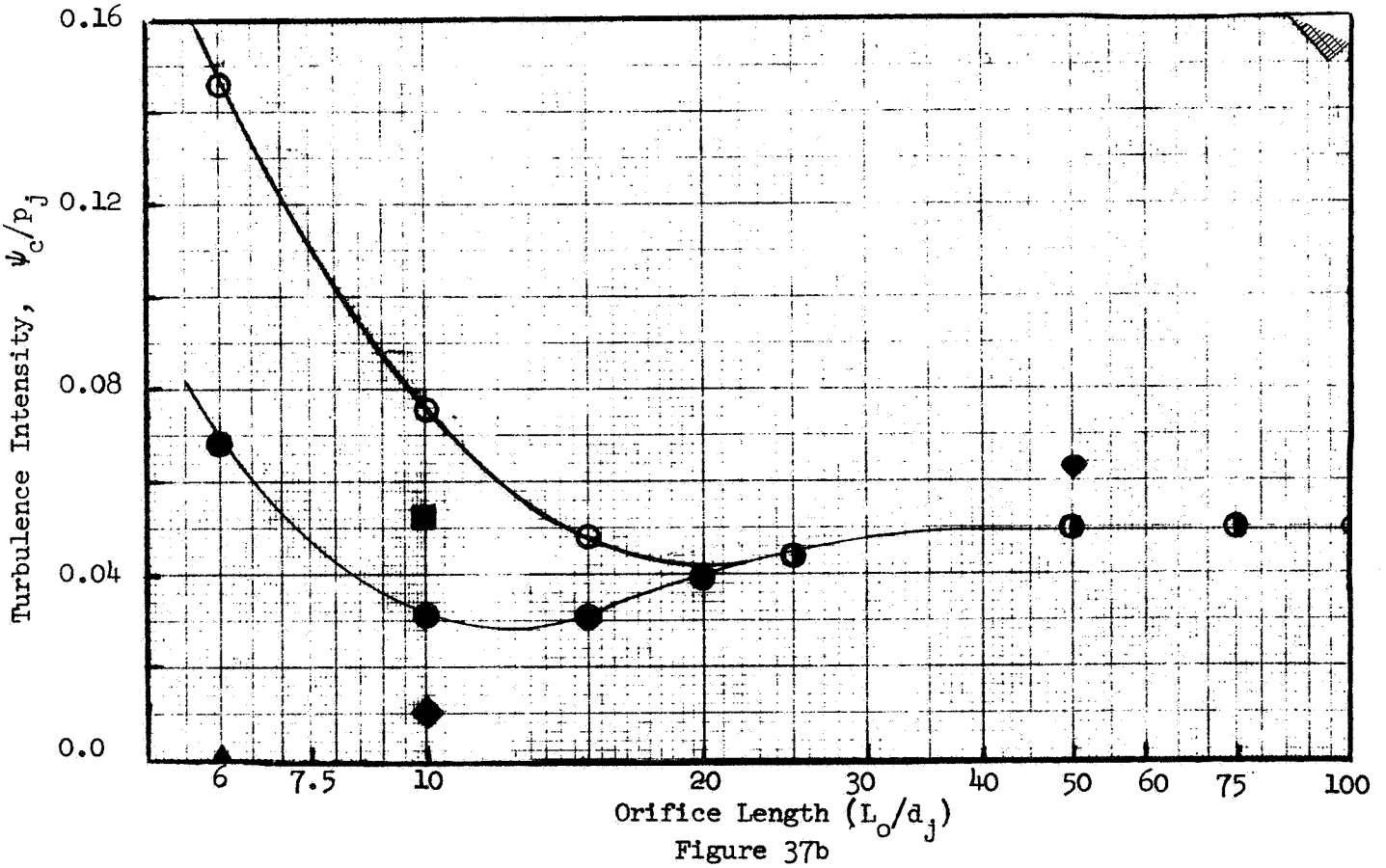

Figure 37b

Figure 37. Influence of Manifold Type on Jet Characteristics

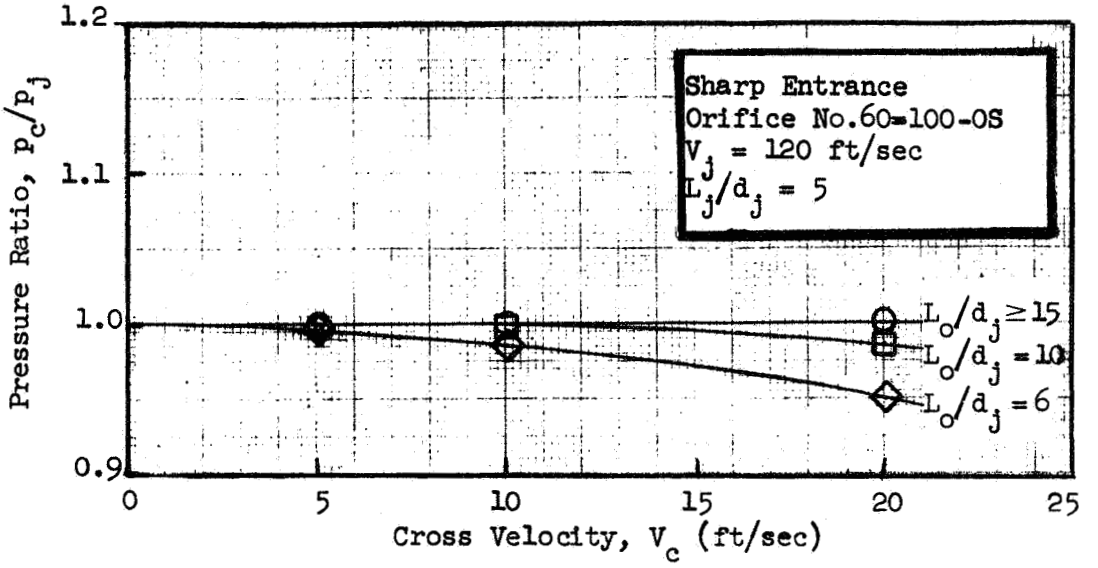

Figure 38a

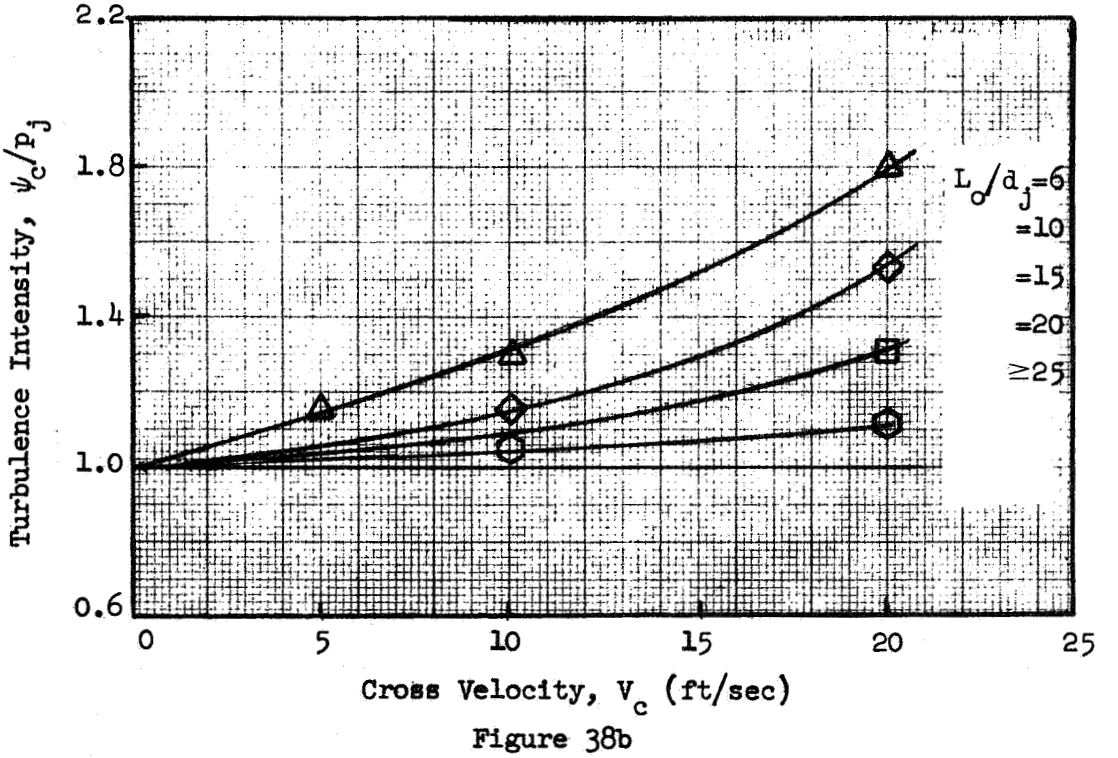

Figure 38b

Figure 38. Influence of Cross Velocity on Jet Characteristics (sharp orifice)

The results are presented in the same manner for the rounded entrance orifice on Fig. 39. In this case, the centerline pressure was also affected by the highest cross velocity at an L_o/d_j of 10 but to a lesser extent. An influence on the turbulence level was first observed at an L_o/d_j of 15.

Measurements of the pressure and turbulence intensity distributions (with distance from the jet centerline) produced by both jets are shown on Fig. 40 for an orifice L_o/d_j of 20. The profiles are shown for the conditions of a 0 and 20 ft/sec cross velocity. At an L_o/d_j of 20, the pressure profiles produced by both orifices were identical and no variation was observed with increased cross velocity. The level of the turbulence intensity profile produced by the round entrance orifice was less than that of the sharp entrance orifice and was also unaltered by cross velocity. In the case of a sharp entrance, a change in the turbulence distribution, as well as the level was observed at the maximum cross velocity.

When the orifice L_o/d_j was decreased to 10, the cross velocity produced very noticeable changes in both the pressure and turbulence profiles for each orifice as shown on Figs. 41 and 42. As previously noted, the centerline pressure ratio was found to decrease for both orifice entrance types when a cross velocity was imposed suggesting that less velocity profile development had occurred. In addition a slight distortion of the pressure distribution in the direction of the cross flow was measured for the sharp entrance orifice as shown on Fig. 41.

The level of turbulence within the jet was reduced by rounding the orifice inlet as can be seen from a comparison of Figs. 41 and 42. There was, however, an increase in the level of, and a slight non-symmetry in the distribution of turbulence when cross flow was imposed with both entrance types.

4.2 ATOMIZATION CHARACTERISTICS OF IMPINGING JETS

The experimental technique used to determine the droplet size and size distribution was the method of frozen wax described in Section 3.4 and Appendix B.

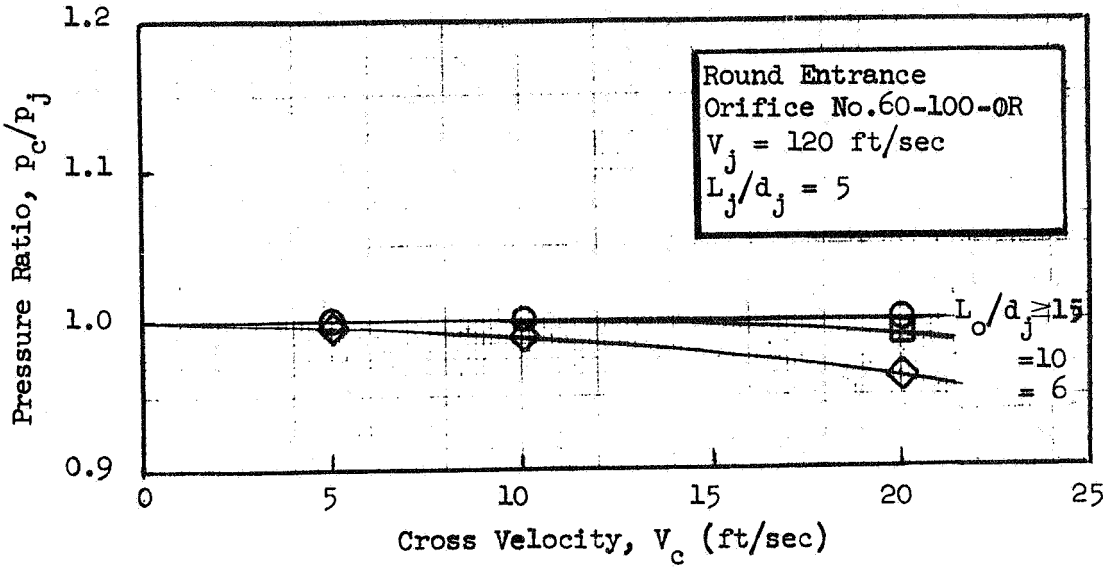

Figure 39a

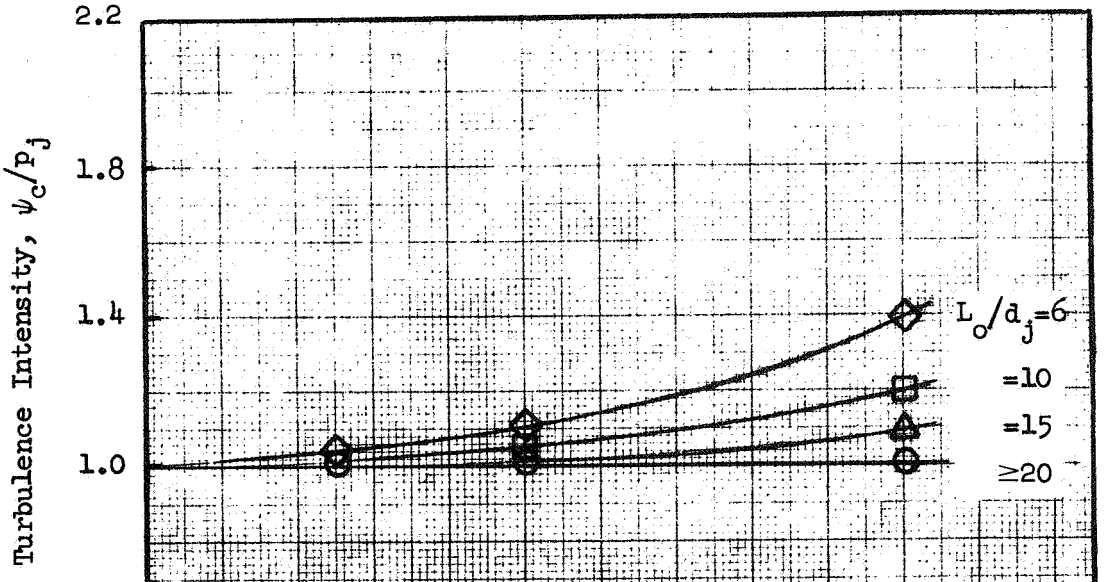

Figure 39b

Figure 39. Influence of Cross Velocity on Jet Characteristics (round entrance)

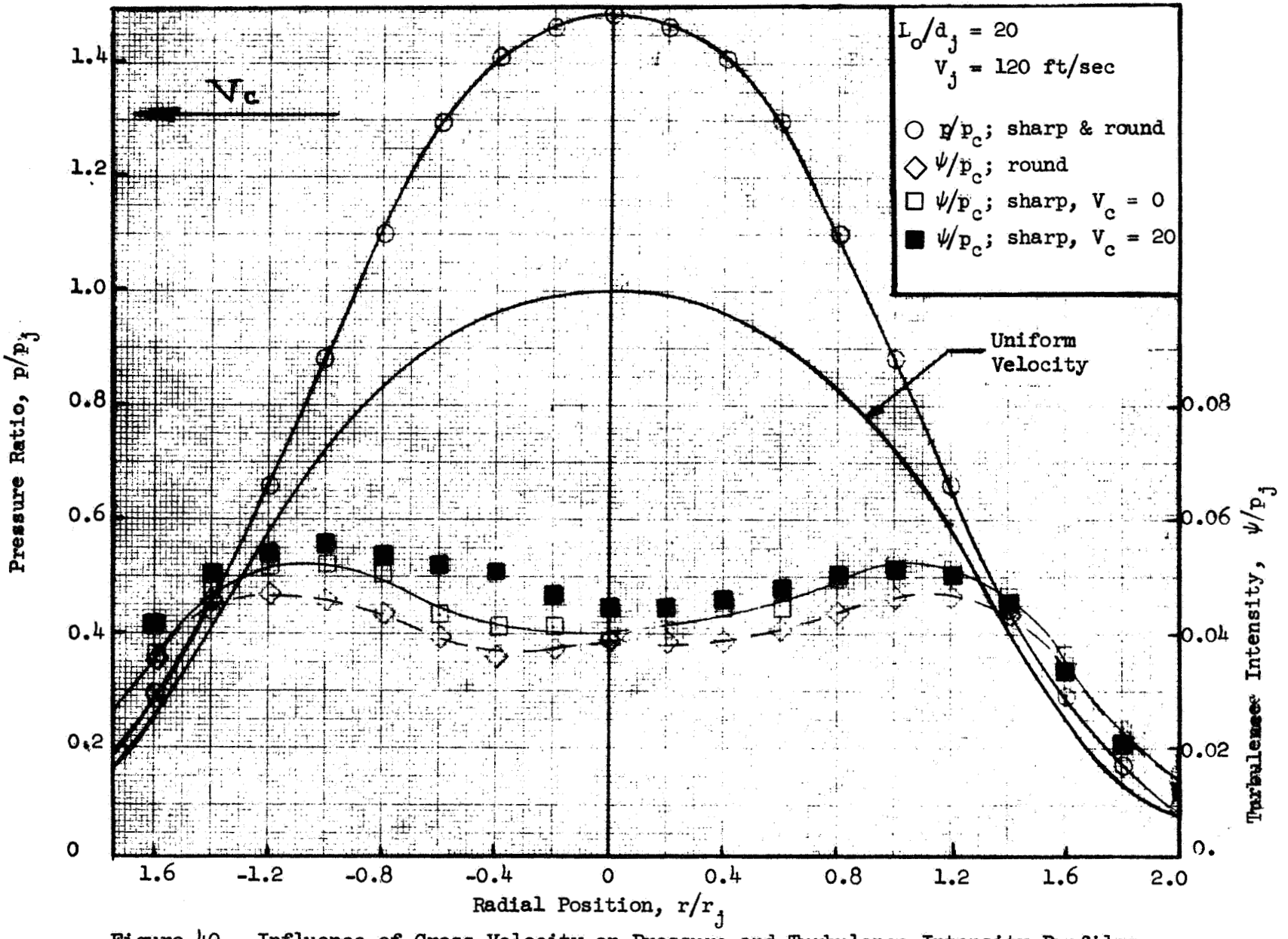

Figure 40. Influence of Cross Velocity on Pressure and Turbulence Intensity Profiles

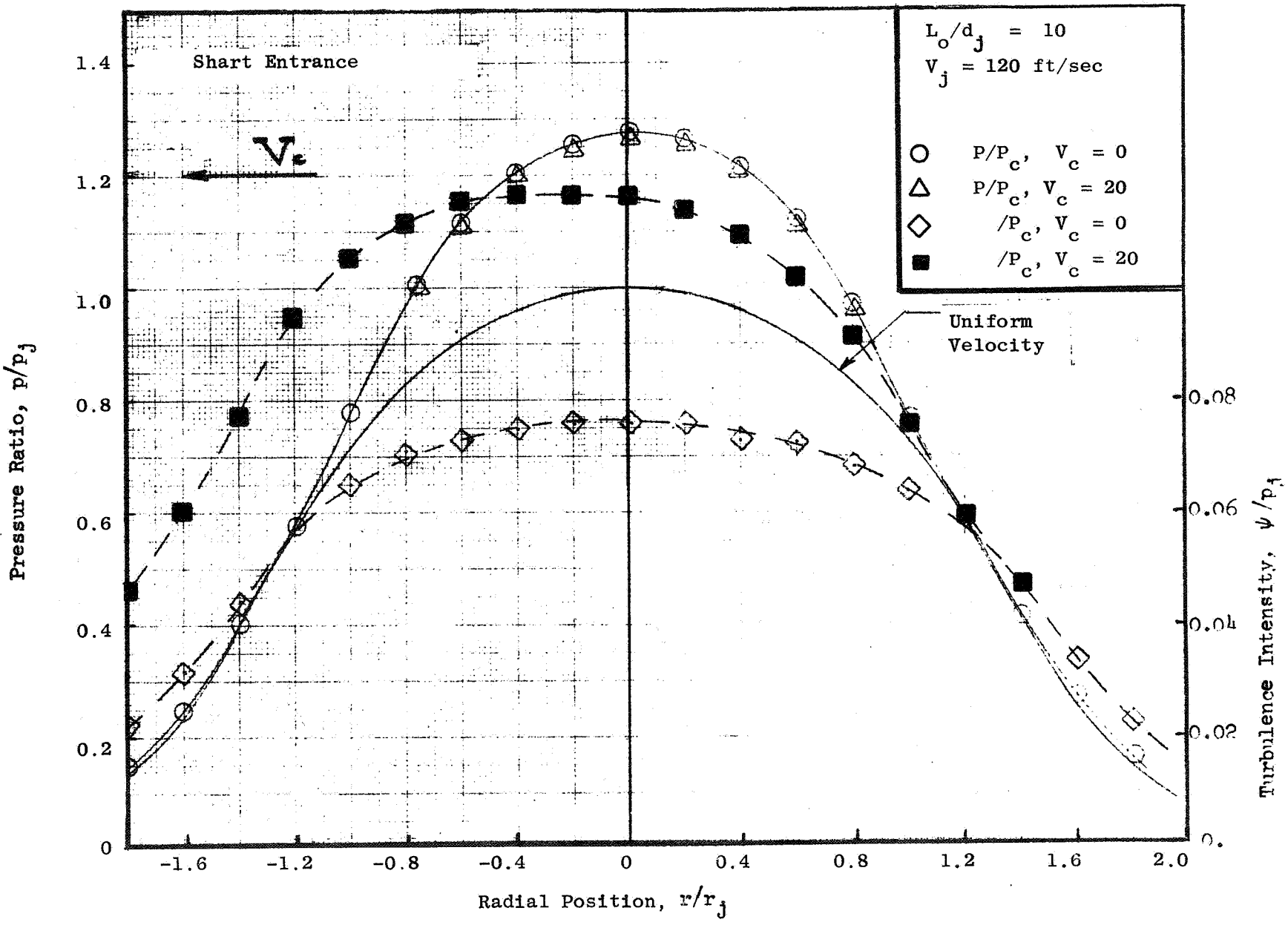

Figure 41. Influence of Mass Velocity on Pressure and Turbulence Intensity Profiles

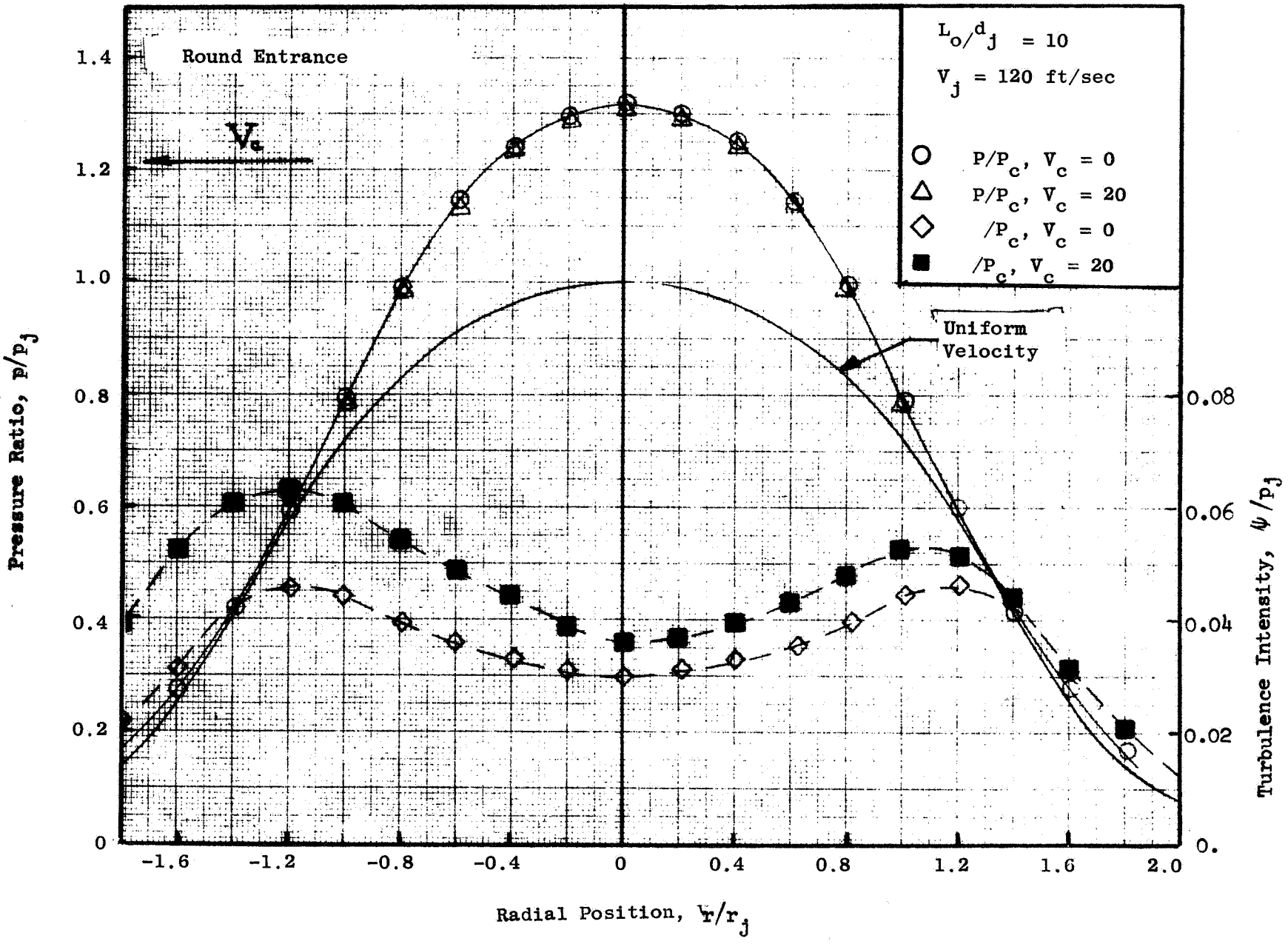

Figure 42. Influence of Cross Velocity on Pressure and Turbulence Intensity Profiles

The parameters affecting atomization that were directly examined include: (1) those parameters pertaining to the individual jets before impingement;

V_j, the injection velocity ($\dot{w}/A_o \rho$)

p_c/p_j, a characteristic of the extent of velocity profile development (a function of both the jet Reynolds number and orifice length)

ψ_c/p_j, a characteristic of the turbulence intensity level and which designates the flow regime (i.e., laminar or turbulent)

and

d_j, the orifice diameter

(2) the parameters describing the relative dynamic and physical characteristics of the opposing jets;

P_D, the dynamic pressure ratio, $(\rho V_j^2)_f/(\rho V_j^2)_o$

d_o/d_f, the diameter ratio

and (ξ), propellant miscibility, using both miscible and immiscible propellant combinations

and (3) the orifice design parameters;

orifice entrance configuration (sharp versus round)

Δ, misimpingement

L_j/d_j, the free jet length

γ, the impingement angle

and

n, the number of impinging jets (element type)

Influences of the orifice length/diameter ratio, L_o/d_j, on atomization appear through its effects on the character of the individual jets before impingement (principally the free jet velocity profile). Therefore, it will not be considered here as an independent geometric parameter.

The atomization characteristics of four element types were examined: the like-doublet, unlike-doublet, triplet (2 on 1) and pentad (4 on 1). The like-doublet was the most thoroughly examined element. The parameters investigated with this element included all of the above excepting those obviously pertaining only to unlike-impinging elements such as P_D and propellant miscibility. The parameters believed to effect the atomization of jets issuing from unlike-doublet elements that were studied are V_j, P_D, ψ_c/p_c, diameter ratio and propellant miscibility. The atomization characteristics of the triplet and pentad were examined as a function of V_j only.

The dropsize results presented below are in terms of (1) the mass median diameter of the spray, $\bar{D}$, and (2) dropsize distributions presented as a cumulative mass fraction versus the normalized dropsize, $D/\bar{D}$.

4.2.1 Like-Doublet Atomization Results

A total of 104 atomization tests were performed using 10 geometrically different like-doublet elements. In these tests, molten wax was used exclusively as the propellant simulant.

The parameters that were examined and the number of tests performed with each element are listed below in Table 8. The results of the tests and all pertinent hydraulic and dynamic parameters are summarized in Table C1 of Appendix C. Unless otherwise noted, these tests were performed at unity dynamic pressure ratio, a free jet length of 5 d_j, an impingement angle of 60° and at a condition corresponding to optimum mixing (i.e. $(\rho V_j^2 d_j)_{ox}/(\rho V_j^2 d_j)_f = 1$, Ref. 25).

Injection Velocity, V_j. In order to isolate the effect of injection velocity on the atomization process, the orifices should produce jets which exhibit minimal velocity profile and turbulence intensity variations over the range of velocities examined. From the results of the studies of free jet characteristics presented in Section 4.1.1, it is known that the jets

TABLE 8. SUMMARY OF LIKE-DOUBLET ATOMIZATION TESTS

Orifice Number	Parameters Investigated (Run Numbers)								Number of Tests
	Injection Velocity	Velocity Profile	Turbulence Intensity	Diameter	Orifice Entrance	Mis-impingement	Free Jet Length	Impingement Angle	
60-1.5-10R	(1-14)		(20-30)			(15-19)	(1-14) (20-30)		30
61-6-7R		(31-33)			(31-33)				3
63-10-7R		(34-37)			(34-37)				4
63/63-10-3LD		(38-46)							9
81/81-10-3LD				(47-49)					3
67-50-5R		(50-57)					(58-85)	(58-85)	36
69-200-9R		(86-90)							5
61-2-75					(91-96)	(97)			7
61-6-75					(98-100)				3
61-10-75					(101-104)				4

produced by the 60-1.5-10R orifice are essentially laminar ($\psi_c/p_j \cong 0$) and possess a nearly uniform-velocity profile ($1 \leq p_c/p_j \leq 1.28$) within the injection velocity range of from 30 to 220 ft/sec.

Since these jets satisfy the above requirements, the injector element used in this set of experiments was formed from two 60-1.5-10R orifices and had an impingement angle of 60 degrees. The free jet length was varied from 4.5 to 10 orifice diameters. The dynamic pressure ratio was maintained constant at a nominal value of 1.1.

A total of 14 molten wax tests were performed. The measured mass median dropsizes and all pertinent hydraulic and dynamic parameters of the atomization tests, designated by run numbers 1 to 14, are summarized in Table C1 of Appendix C. The variation of the mass median dropsize with mean injection velocity, defined as the average velocity of the two jets, is shown on Fig. 43. (Equation 6 refers to an empirical correlation developed in Section 5.2.1.) Since the measurements of the internal characteristics of the laminar jets have shown that the velocity profile does not change with free jet length, it is to be expected that dropsize is invariant with respect to the free jet L_j/d_j ratio. This is demonstrated on Fig. 43 where it is seen that the mass median dropsizes obtained at free jet lengths of 7 and 10 orifice diameters agree quite well with dropsize measurements at an L_j/d_j ratio of 4.5.

The dropsize distributions obtained at nominal injection velocities of 80 and 160 ft/sec are compared on Fig. 44. These results indicate that a slightly more monodisperse spray field is achieved at higher injection velocities with the difference between the distributions occurring primarily in the number of smaller droplets in the spray.

Velocity Profile, p_c/p_j

The distribution of velocity within a free jet can be varied by changing either the injection velocity or the orifice length. In this study, both

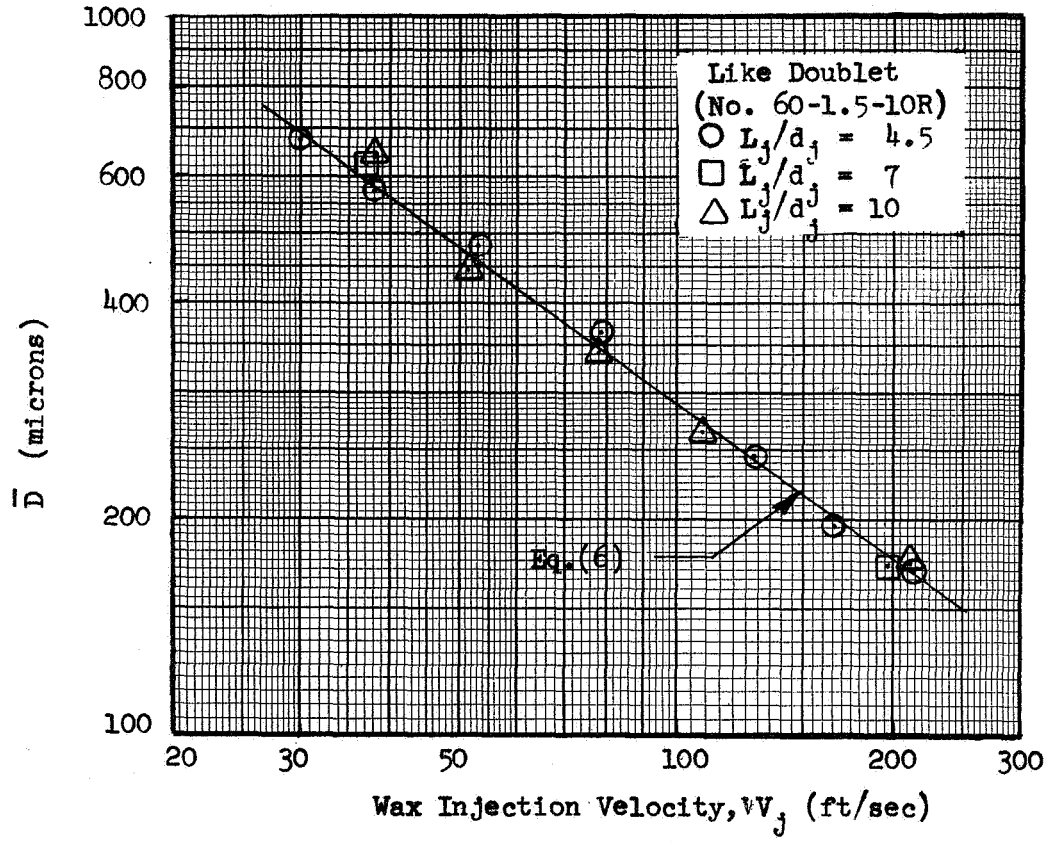

Figure 43. Mass Median Dropsize versus Injection Velocity for a Like-Doublet ($\bar{L}_o/d_j$ = 1.5)

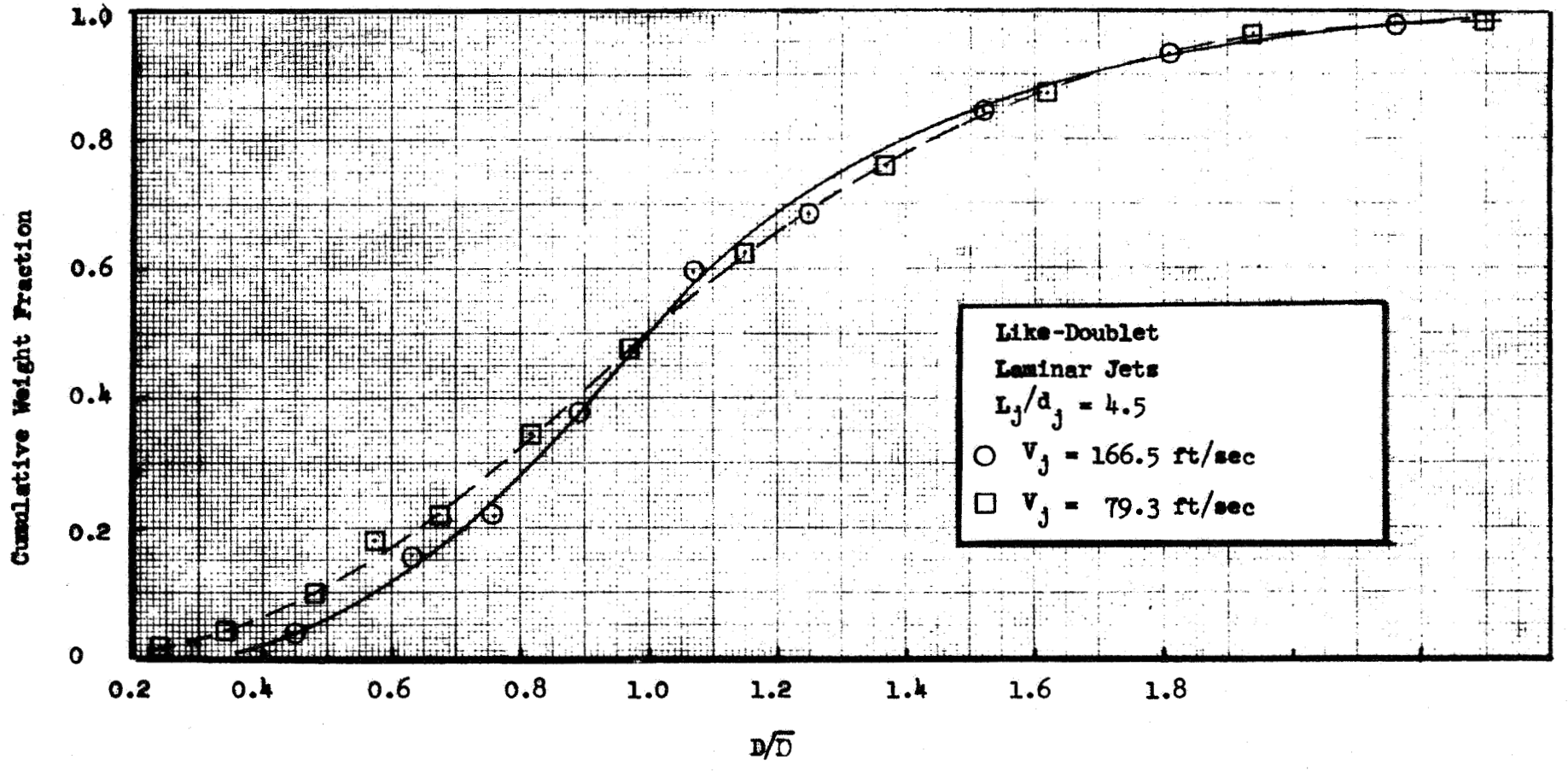

Figure 44. Influence of Injection Velocity on Dropsize Distribution (L_o/d_j = 1.5)

methods were employed to produce velocity profiles ranging from nearly uniform to nearly fully developed laminar (FDL) and fully developed turbulent (FDT).

Qualitative measurements of the velocity profiles existing within the free jets produced by the 6, 10, 50 and 200 L_o/d_j orifices were obtained in order to evaluate the extent of velocity profile development as a function of the injection velocity. The results of these experiments were presented in Section 4.1.1. It should be recalled that the measurements were obtained using a fluid which, at ambient temperatures, is dynamically similar to the molten wax at the injection temperature of 200°F.

The results of these atomization experiments, run numbers 31 to 46, 50 to 57, and 86 to 90, are presented in Table C1 of Appendix C. The mass median dropsizes obtained with the 6 to 200 L_o/d_j like-doublet elements are summarized on Fig. 45. Also shown are the data obtained with the 1.5 L_o/d_j element, runs 1 to 7 in Table C1, which provide dropsize measurements resulting from the impingement of nearly uniform velocity profile jets.

In order to correlate the dropsizes with the extent of profile development, the dropsize data were plotted as a function of the centerline pressure ratio of the free jet. The magnitude of the centerline pressure ratio, at the injection velocity of the wax, is obtained from Fig's 21, 27, or 29. The broken lines on Fig. 45 are lines of constant L_o/d_j while the solid lines represent the variation of $\overline{D}$ with the centerline pressure ratio at constant injection velocity.

Up to an injection velocity of about 100 ft/sec, the jet characteristic measurements indicated that the jets produced by all the orifices were laminar. Above this velocity the jets obtained with the 50 and 200 L_o/d_j orifices were fully developed turbulent while the 10 L_o/d_j orifices produced turbulent, but not fully developed jets. From Fig. 45 it is seen that the bulk of the dropsize data were obtained with laminar jets. Although

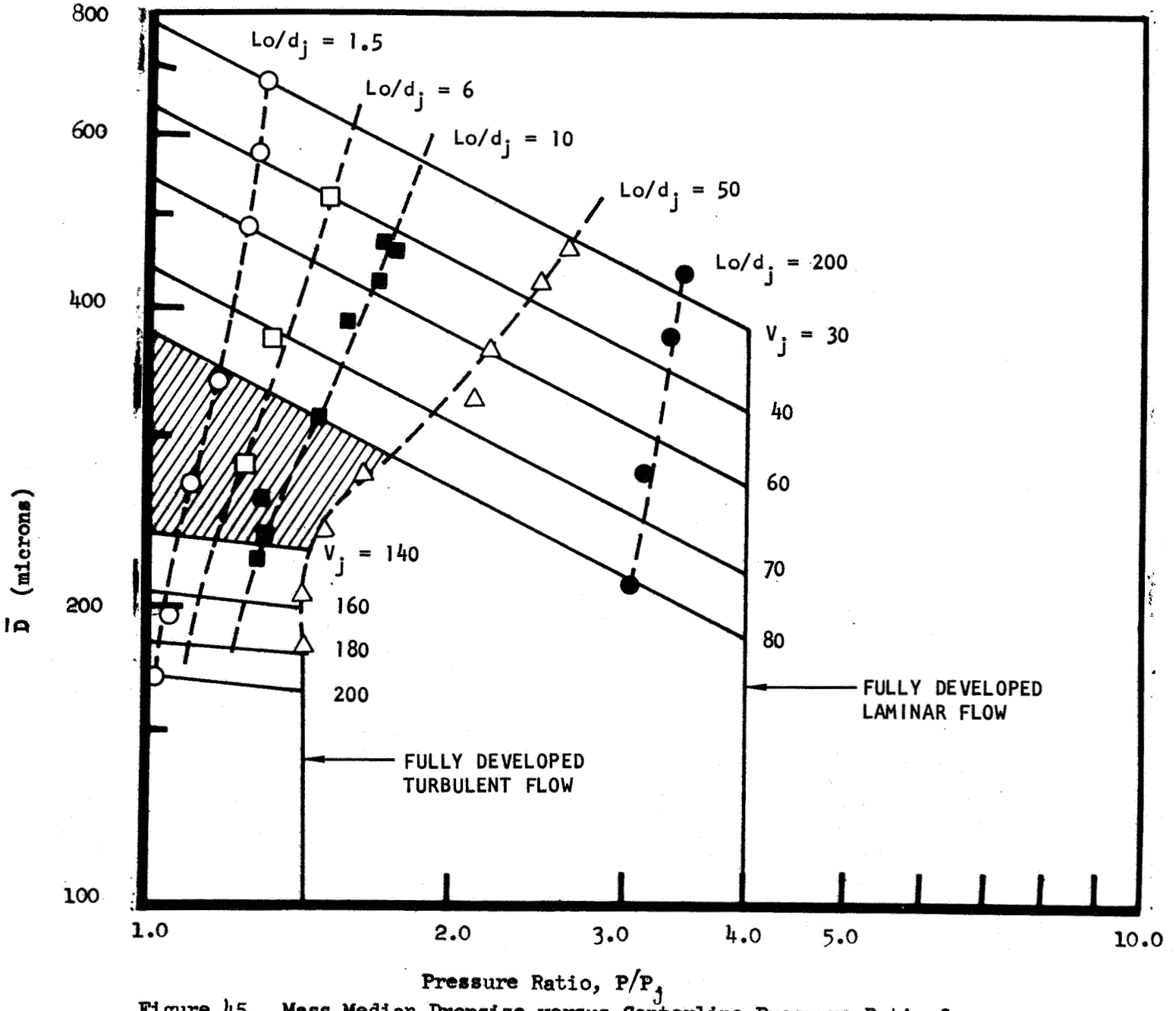

Figure 45. Mass Median Dropsize versus Centerline Pressure Ratio for Like-Doublet Elements

only a few turbulent jet data points were obtained, a comparison of the slopes of the constant velocity lines above and below 100 ft/sec suggests that the velocity profile exerts a greater influence on the mass median dropsize when the jets are laminar. For example, a fully developed turbulent jet with a centerline pressure ratio of 1.43 will produce a dropsize only approximately 5 percent smaller than a uniform velocity jet. On the other hand, a laminar jet at the same stage of profile development, i.e., $p_c/p_j = 1.43$) will result in a dropsize about 18 percent smaller.

The influence of the laminar velocity profile is especially evident on Fig. 46 when the dropsizes produced by the various L_o/d_j like-doublet elements are compared with the data obtained with the 1.5 L_o/d_j element on the more familiar basis of injection velocity. (The equation numbers refer to empirical correlations developed in Section 5.2.1.) As shown there, an increase in the orifice length and hence a greater profile development results in a significant decrease in the dropsize. In the case of the 200 L_o/d_j orifice, associated with a nearly fully developed laminar profile, the dropsize is about 40 percent smaller than that obtained with the 1.5 L_o/d_j element (e.g., at V_j = 50 ft/sec).

The dropsize distributions obtained with the 1.5 and 200 L_o/d_j orifices at an injection velocity of 80 ft/sec are compared on Fig. 47. It is apparent that the effect of the velocity profile on the normalized distribution about $\bar{D}$ is small.

Turbulence Intensity, ψ_c/p_j

In order to eliminate the possibility of introducing velocity profile effects, the study of the influence of turbulence on droplet formation was performed with nearly-uniform velocity jets. Since these jets are necessarily produced by short orifices, turbulence must be artificially generated in place of the turbulence normally produced at the orifice walls. For this purpose, a turbulence generator was placed at the entrance to the 60-1.5-10R orifice. Descriptions of the turbulence generator and the levels of turbulence obtained in this manner were presented in Sections 3.1.1 and 4.1.1, respectively.

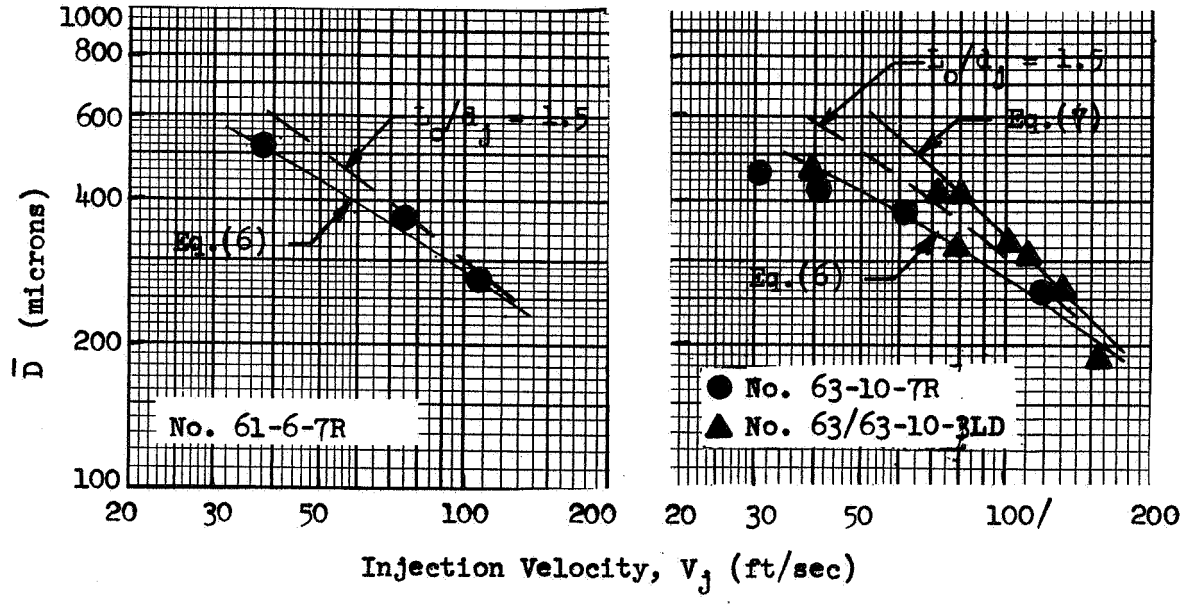

Figure 46a.

Figure 46b.

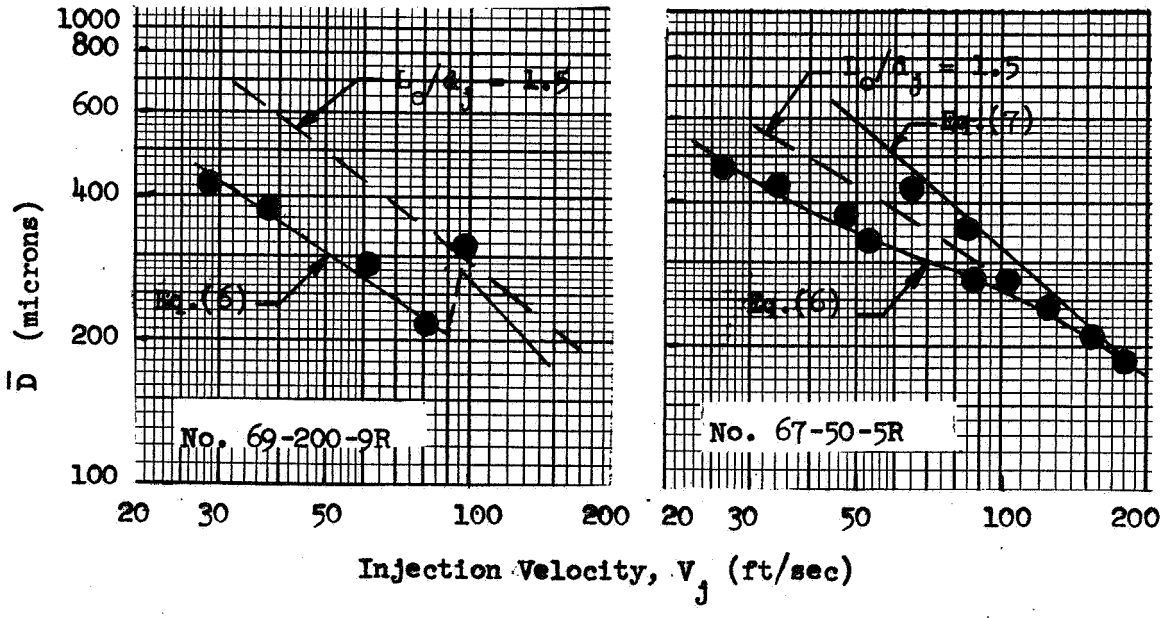

Figure 46c.

Figure 46d.

Figure 46. Mass Median Dropsize versus Injection Velocity for Like Doublets (L_o/d_j = 6,10,50, and 200)

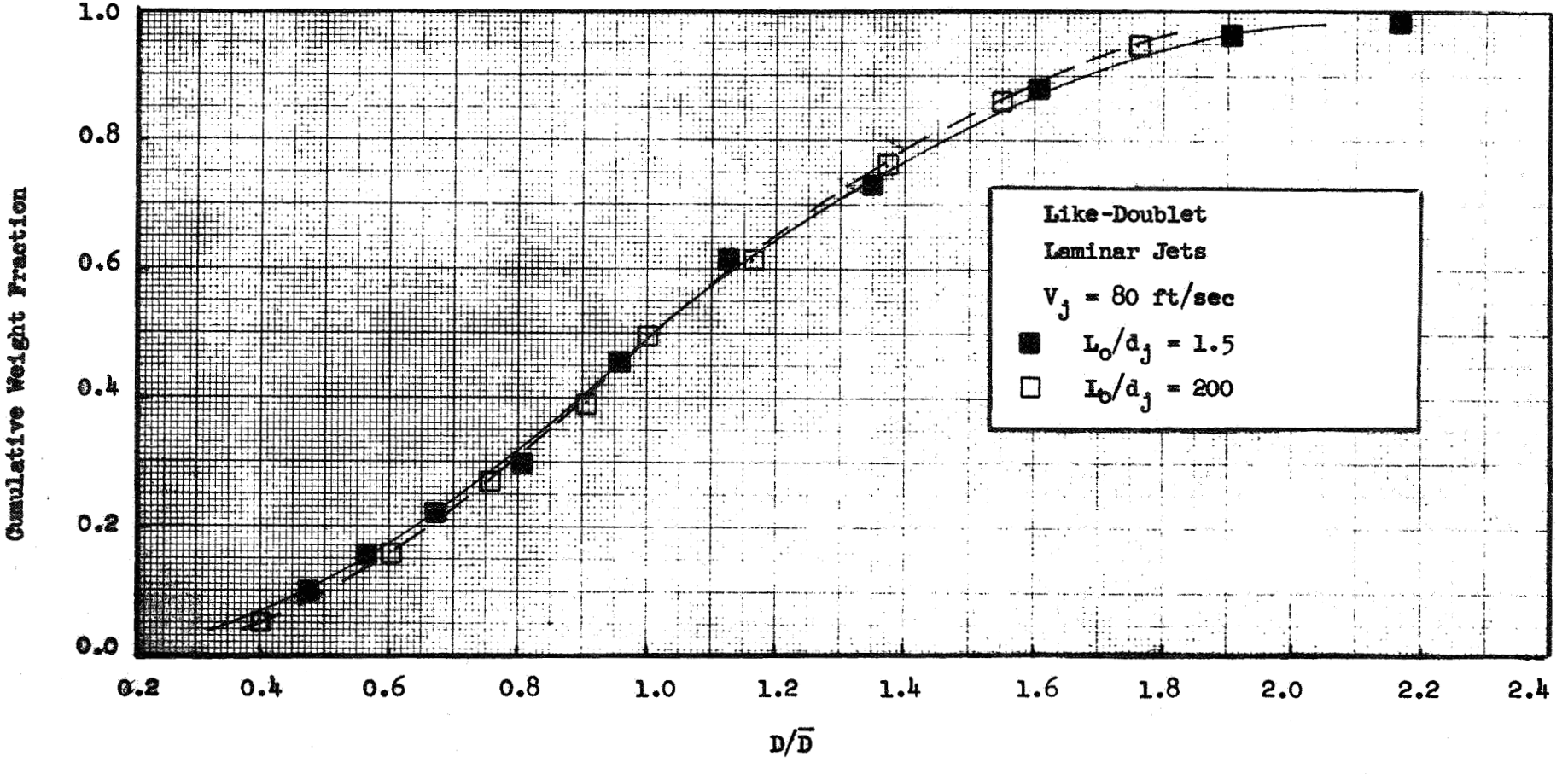

Figure 47. Influence of Velocity Profile on Dropsize Distribution

The atomization experiments were performed at the nominal injection velocities of 40, 80, 120, and 160 ft/sec. The nominal dynamic pressure ratio was 1.1. At a constant injection velocity, the level of turbulence at the impingement point was changed by a variation of the free jet length. The latter ranged from 4.5 to 10 orifice diameters.

The results of the experiments and the test conditions, run numbers 20 to 30, are presented in Table C1 of Appendix C. The mass median dropsize is shown on Fig. 48 as a function of the turbulence level at the jet centerline, characterized by the parameter ψ_c/p_j, for each of the nominal injection velocities. From the study of the internal characteristics of the turbulent jets, it was found that the level of turbulence, (ψ_c/p_j) within a fully developed turbulent jet is on the order of 0.05 at an injection velocity of 120 ft/sec (see e.g., Fig. 27). As is evident from Fig. 48, the turbulence level of the jets used in the atomization studies exceeded the above value at the longer free jet lengths. However, allowing for slight differences in the injection velocities, no significant variation in dropsize was observed as the turbulence level at the impingement point was changed from a value of about 0.01 to a level greater than would be expected with a fully developed turbulent jet.

The dropsize distributions produced by the turbulent jets are compared to dropsize distributions produced by impinging laminar jets on Figs. 49 and 50. At an injection velocity of 80 ft/sec, the existence of turbulence does not effect the distribution as shown on Fig. 49. An identical observation is made from Fig. 50 where the distributions produced by both the laminar and turbulent jets at an injection velocity of 160 ft/sec are compared. As in the case of laminar jet impingement, an increase in the injection velocity of turbulent jets results in a slightly more monodisperse spray as shown in Fig. 51, which illustrates turbulent jet distributions obtained at nominal velocities of 80 and 160 ft/sec.

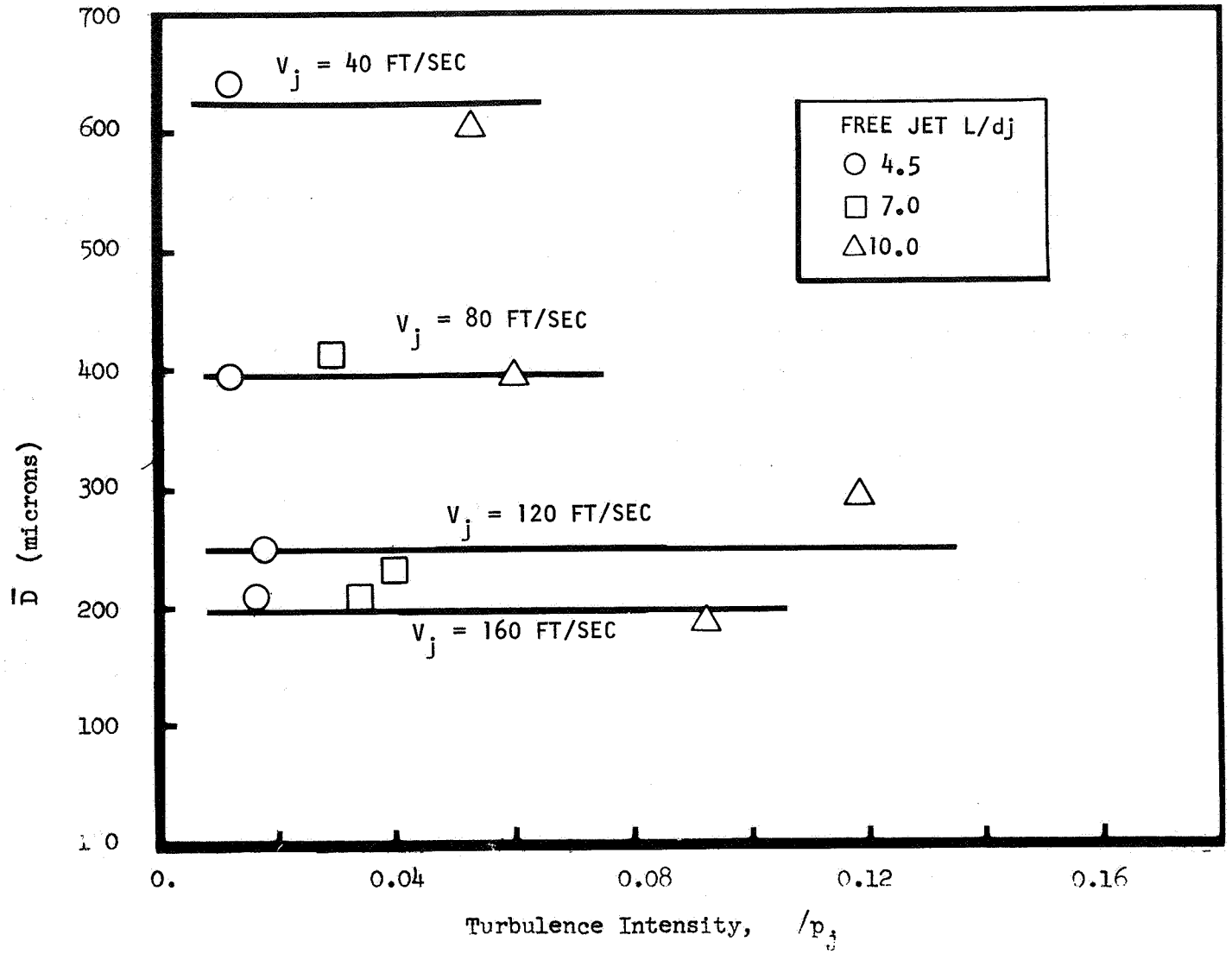

Figure 48. Mass Median Dropsize versus Turbulence Intensity for Like-Doublet (L_o/d_j = 1.5)

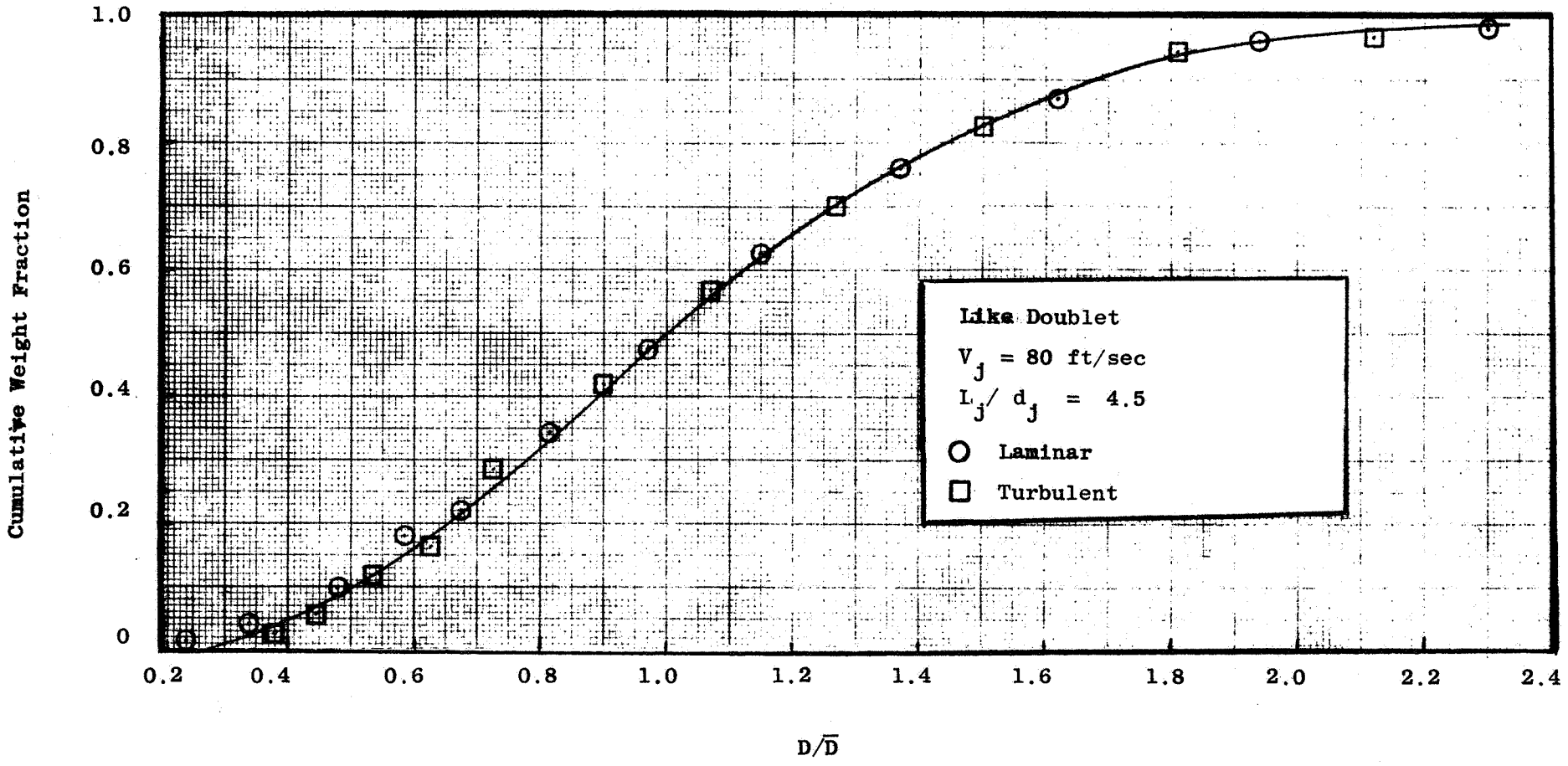

Figure 49. Influence of Turbulence on Dropsize Distribution ($L_o/d_j = 1.5$)

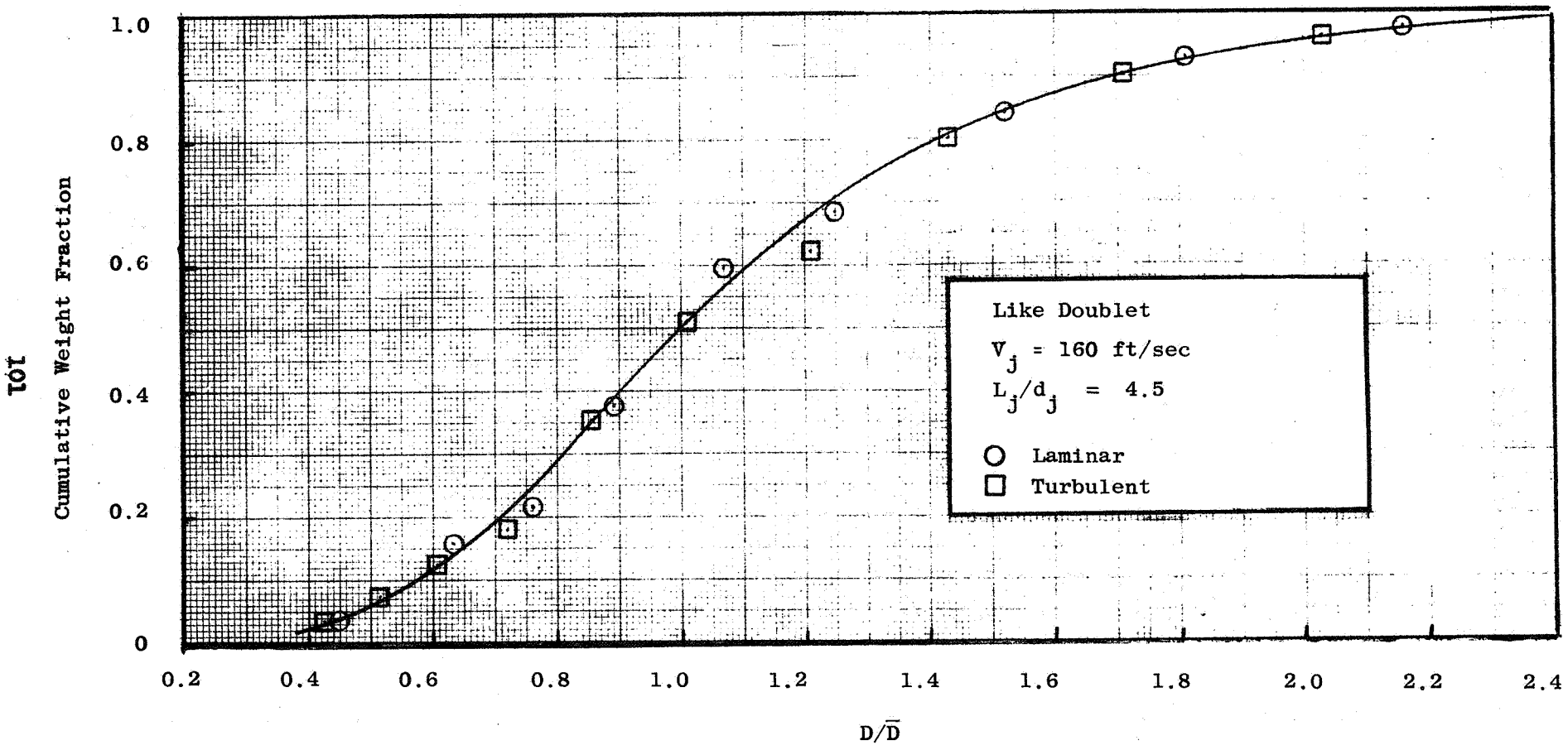

Figure 50. Influence of Turbulence on Dropsize Distribution (L_o/d_j = 1.5)

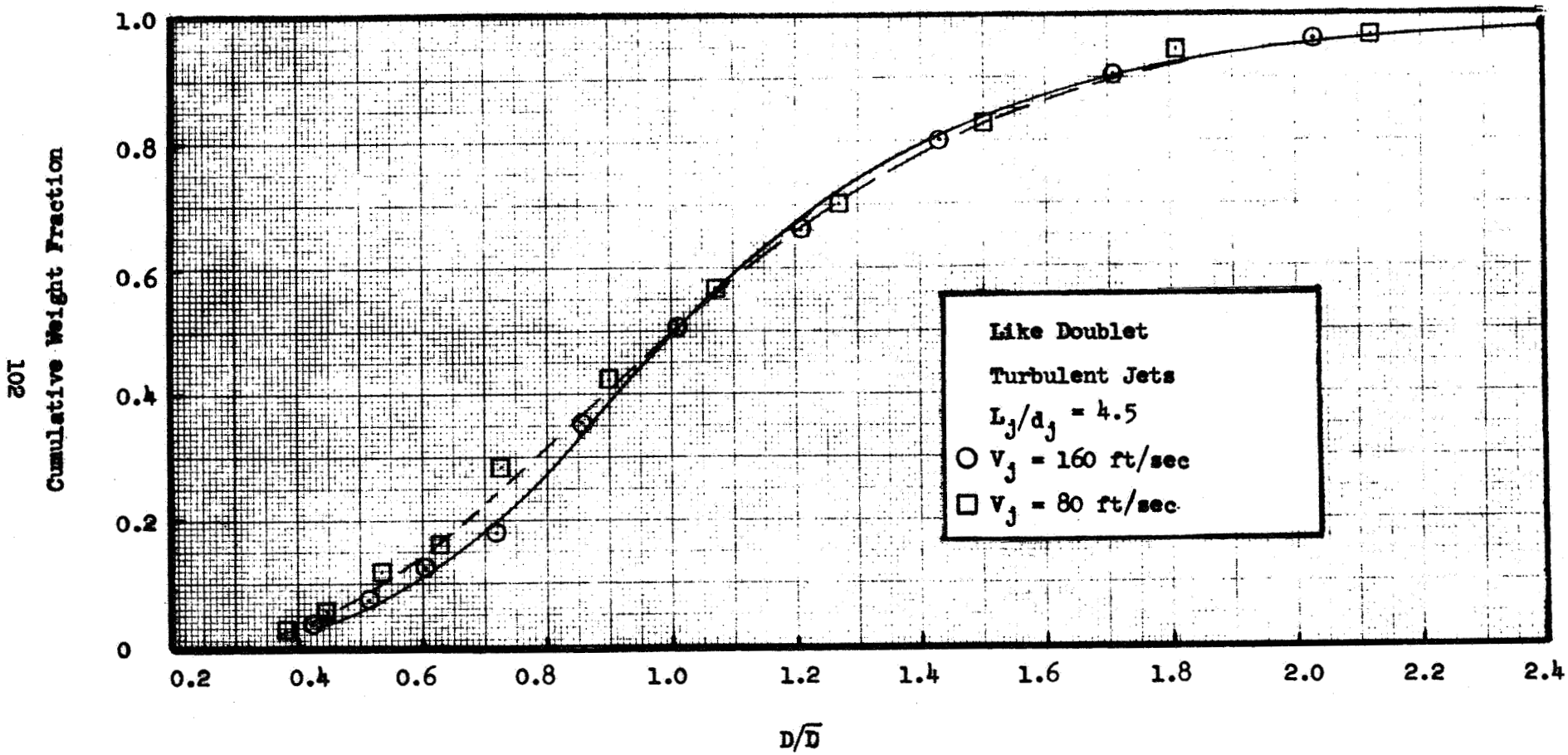

Figure 51. Influence of Injection Velocity on Dropsize Distribution (L_o/d_j = 1.5)

Orifice Diameter, d_j. In order to obtain data on the effect of orifice diameter on droplet size, three molten wax tests were performed with the 0.081-inch-diameter like-doublet element, No. 81-10-3LD. The nominal injection velocities were 30, 40 and 60 ft/sec.

The results from these tests, run numbers 47 to 49, and the pertinent test conditions are presented in Table C1 of Appendix C. The mass median dropsizes are compared to those obtained with the 0.063-inch-diameter element, number 63-10-3LD, on Fig. 52. Since these tests were conducted at injection velocities less than 100 ft/sec, the jets produced by both orifices were laminar. At a given injection velocity, the Reynolds numbers and hence the velocity profiles of the two jets were different. As a consequence, the influence of velocity profile on the results must be ascertained before an accurate assessment of orifice diameter effects can be determined. This is discussed further in Section 5.2.1.

As shown on Fig. 53, the distribution of dropsizes about the mean diameter is unaffected by a variation of orifice diameter. This result substantiates the work of Dickerson, et al., Ref. 14.

Orifice Entrance. In a rocket engine the length of the injector orifice is often on the order of 2 to 10 orifice diameters. With this short an orifice length, the dynamic characteristics of the free jets are critically dependent upon the orifice entrance conditions. Consequently, atomization tests were performed to evaluate the influence of entry configuration on the resulting dropsize and dropsize distributions.

In these tests, three like-doublet elements with sharp entrance orifices and L_o/d_j's of 2, 6, and 10 were used. The dynamic characteristics of the jet produced by the orifices used to form the doublets, numbers 61-2-7S, 61-6-7S, and 61-10-7S, were examined and the results previously presented in Section 4.1.1.

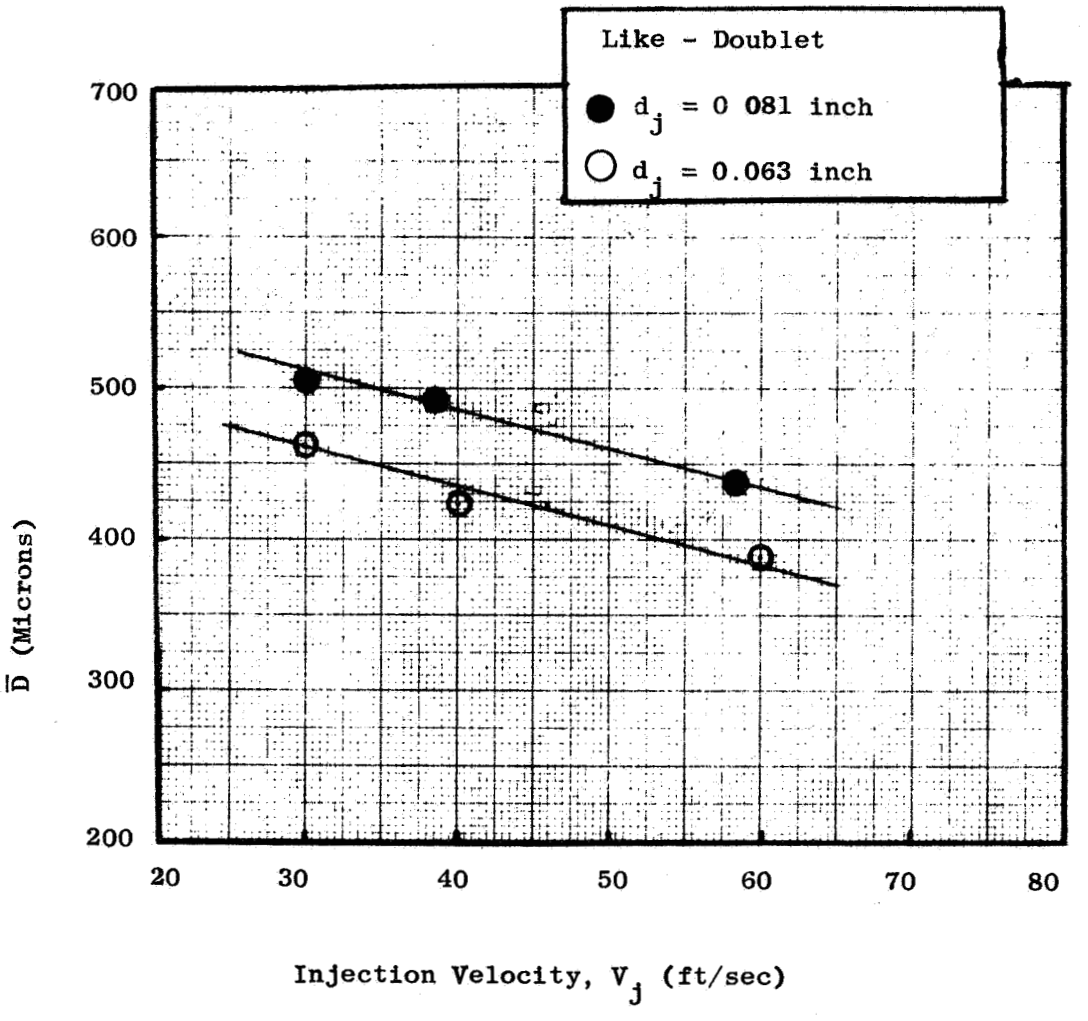

Figure 52. Influence of Orifice Diameter on Mass Median Dropsize

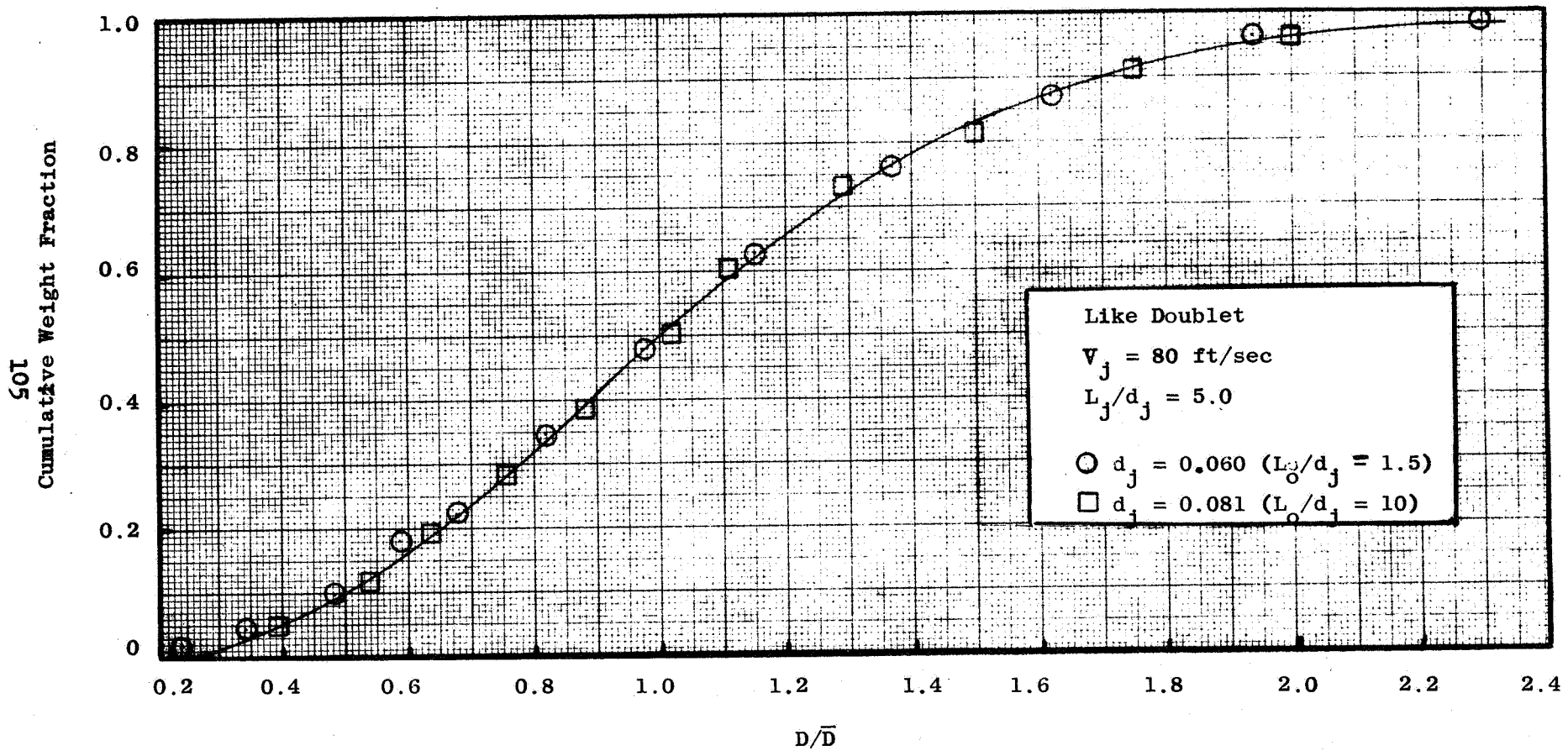

Figure 53. Influence of Orifice Diameter on Dropsize Distribution

A total of 13 tests, run numbers 91 to 104, were conducted. The test conditions and results are given in Table C1 of Appendix C. As shown there, the injection velocity ranged from 40 to 150 ft/sec. The mass median dropsizes of the sharp-edged orifice tests are compared to those obtained with the 6.0 and 10 L_o/d_j rounded entrance orifices on Fig. 54. It should be noted that V_j corresponds to the injection velocity of a "full" flowing jet (i.e., $w/\rho A_o$). From the study of the jets produced by the sharp orifices it was found that the jets completely separated from the orifice walls above an injection velocity of about 40 ft/sec. The associated higher jet velocity and smaller jet diameter resulted in a substantial decrease in the mass median dropsize as shown on Fig. 54. An exception to this was obtained with the 10 L_o/d_j orifice at the injection velocity of 40 ft/sec. In this case, the jet apparently re-attached within the orifice and resulted in a dropsize comparable to that obtained with the round-entrance orifice of the same length. As would be expected, the length of the orifice does not affect dropsize once separation has occurred.

The dropsize distribution obtained with the 2 L_o/d_j, sharp-edged orifice is shown on Fig. 55. Although jet separation resulted in a significant decrease in the median dropsize the distribution is quite similar to that obtained with a round entrance orifice at the same injection velocity.

Misimpingement, Δ . The influence of free jet misimpingement on atomization was examined using both round and sharp entrance orifices. The jets were caused to misimpinge by displacing the plane of one of the orifices a distance Δ as shown below.

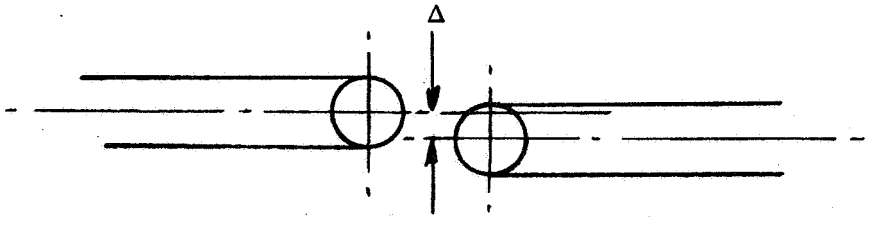

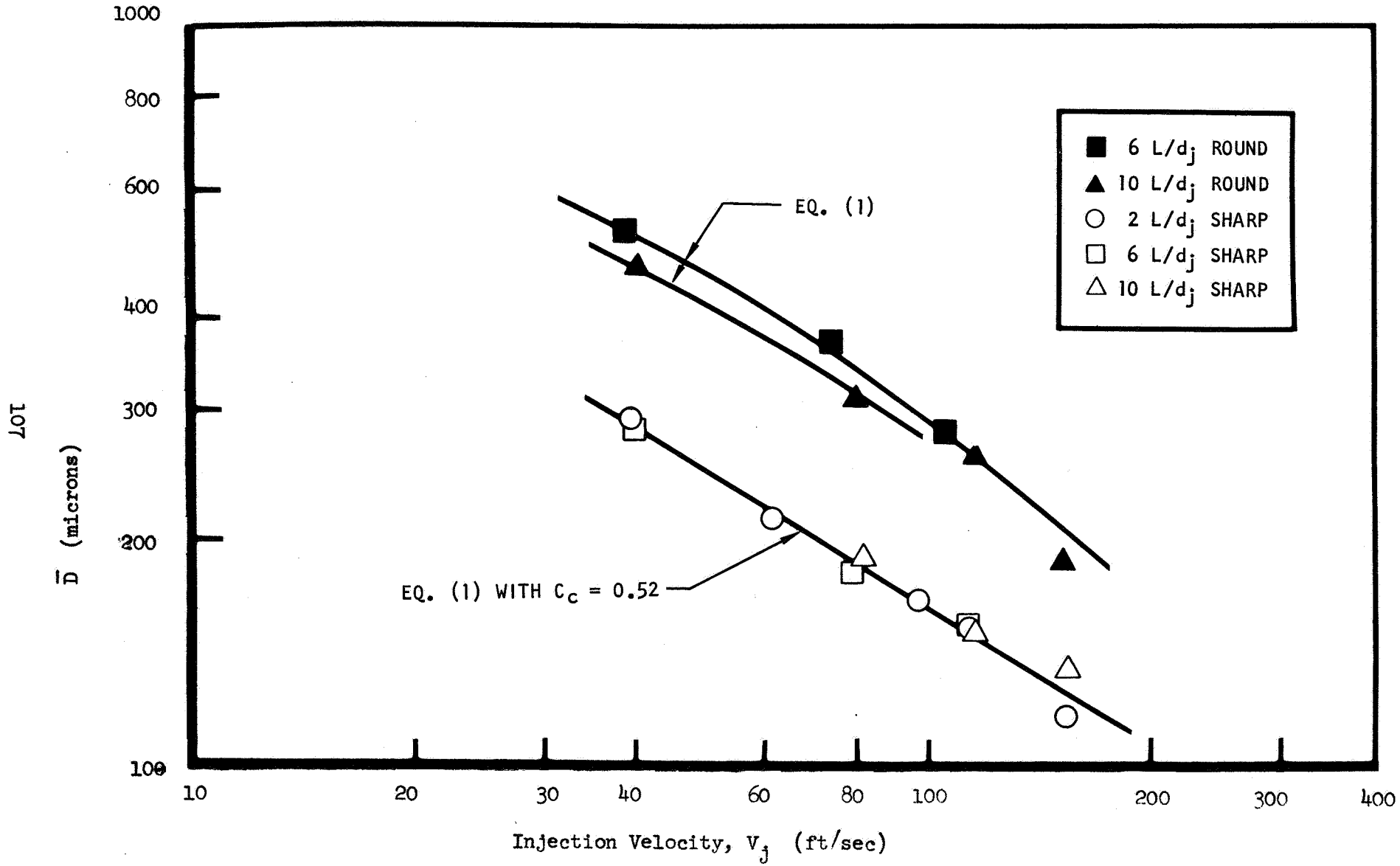

Figure 54. Influence of Orifice Entrance Type on Mass Median Dropsize (Like-Doublet)

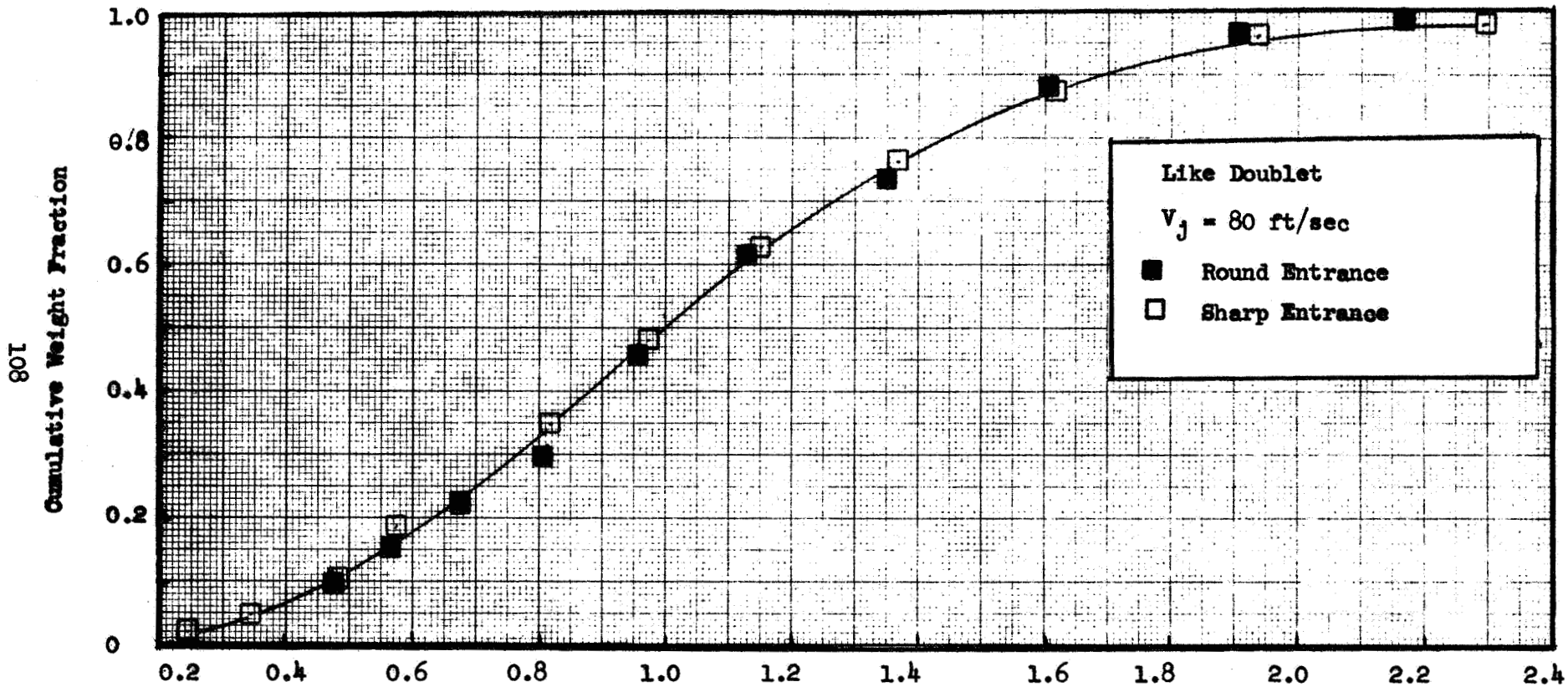

Figure 55. Influence of Orifice Entrance Type on Dropsize Distribution

Jet misalignment, defined as Δ/d_j, was varied from 25 to 75 percent. The tests were performed at injection velocities of 40 and 120 ft/sec with orifice number 60-1.5-10R and at 120 ft/sec with orifice number 61-2-7S.

The results of the atomization experiments, designated by run numbers 15 to 19 and 97, are presented in Table C1. The variation of the mass median dropsize with Δ/d_j is presented on Fig. 56, where it is evident that, for rounded orifices, an increase in the mean droplet size of approximately 20 percent occurred when the jets were misaligned by 0.75 d_j. The effect of misimpingement when sharp entrance orifices are used appears to be much larger. However, it should be recalled that Δ is based on the orifice diameter. Because of the jet separation that occurred with this orifice type, the percentage misimpingement, based on jet diameter, is actually closer to 70 percent (see Section 5.1.3).

Misimpingement of the jets was found to result in a significant variation in the dropsize distribution as shown on Figs. 57 and 58 for the round and sharp entrance orifices respectively. From a comparison of the distributions obtained when $\Delta = 0$ and $\Delta = 0.75\ d_j$, it is readily seen that misalignment affects the distribution of larger droplets in the spray field.

Free Jet Length, L_j/d_j. The influence of free jet length on dropsize was examined in a series of tests using like-doublets formed from the short orifices, number 60-1.5-10R, with and without the turbulence generating device, and the 50 L_o/d_j orifices, number 67-50-5R. The mass median dropsizes obtained with the laminar jets issuing from the short orifices, shown on Fig. 59, verify the anticipated result of no variation of dropsize with free jet length. Similarly, the turbulent jet dropsizes, previously shown on Fig. 48, remained essentially constant as the free jet length was varied.

Another series of 28 molten wax tests were conducted with the 50 L_j/d_j orifices at nominal injection velocities of 60, 85, and 105 ft/sec and impingement angles of 45, 60, and 90 degrees. In these tests, the free

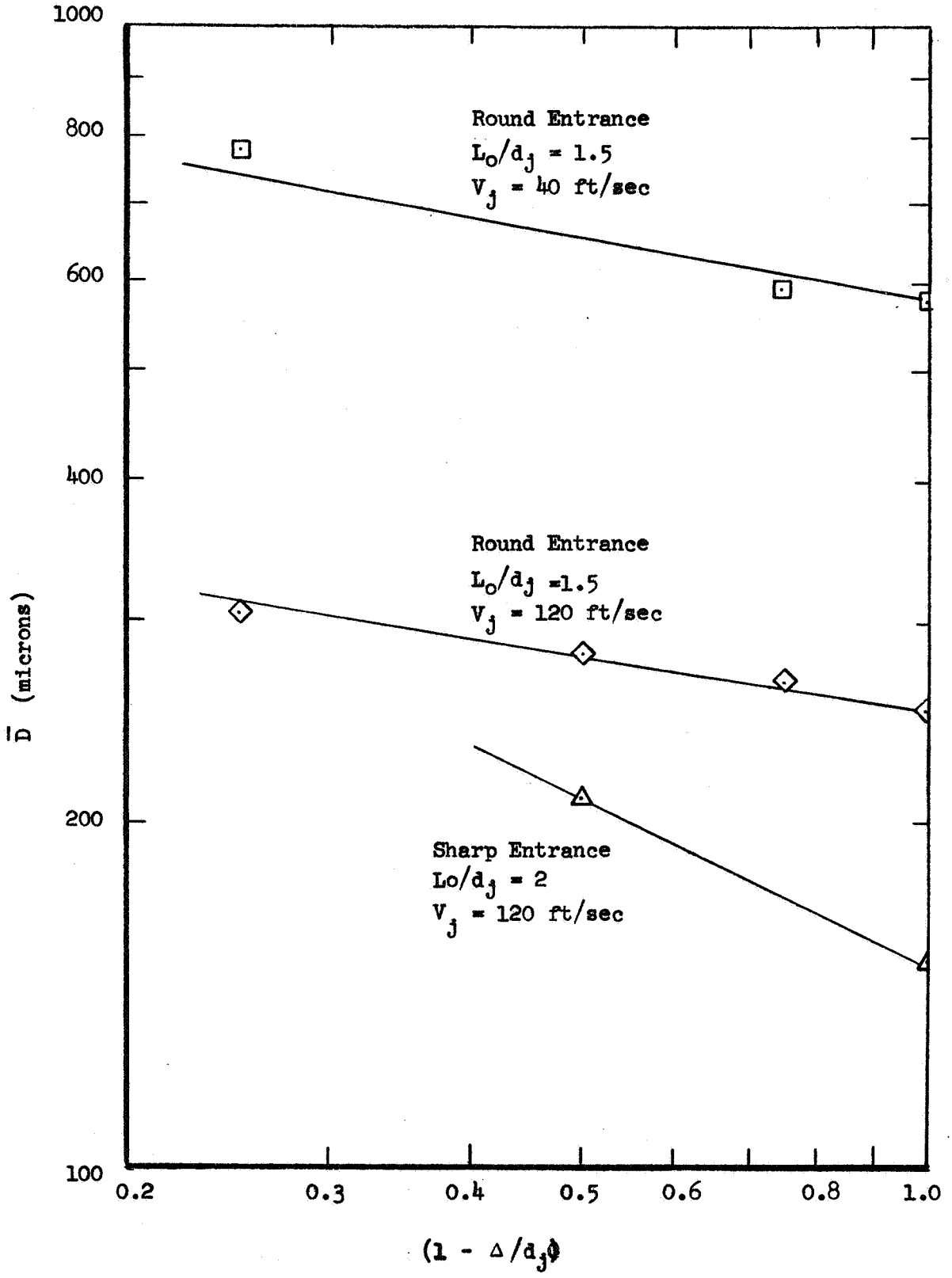

Figure 56. Influence of Jet Misalignment on Mass Median Dropsize (Like-Doublet)

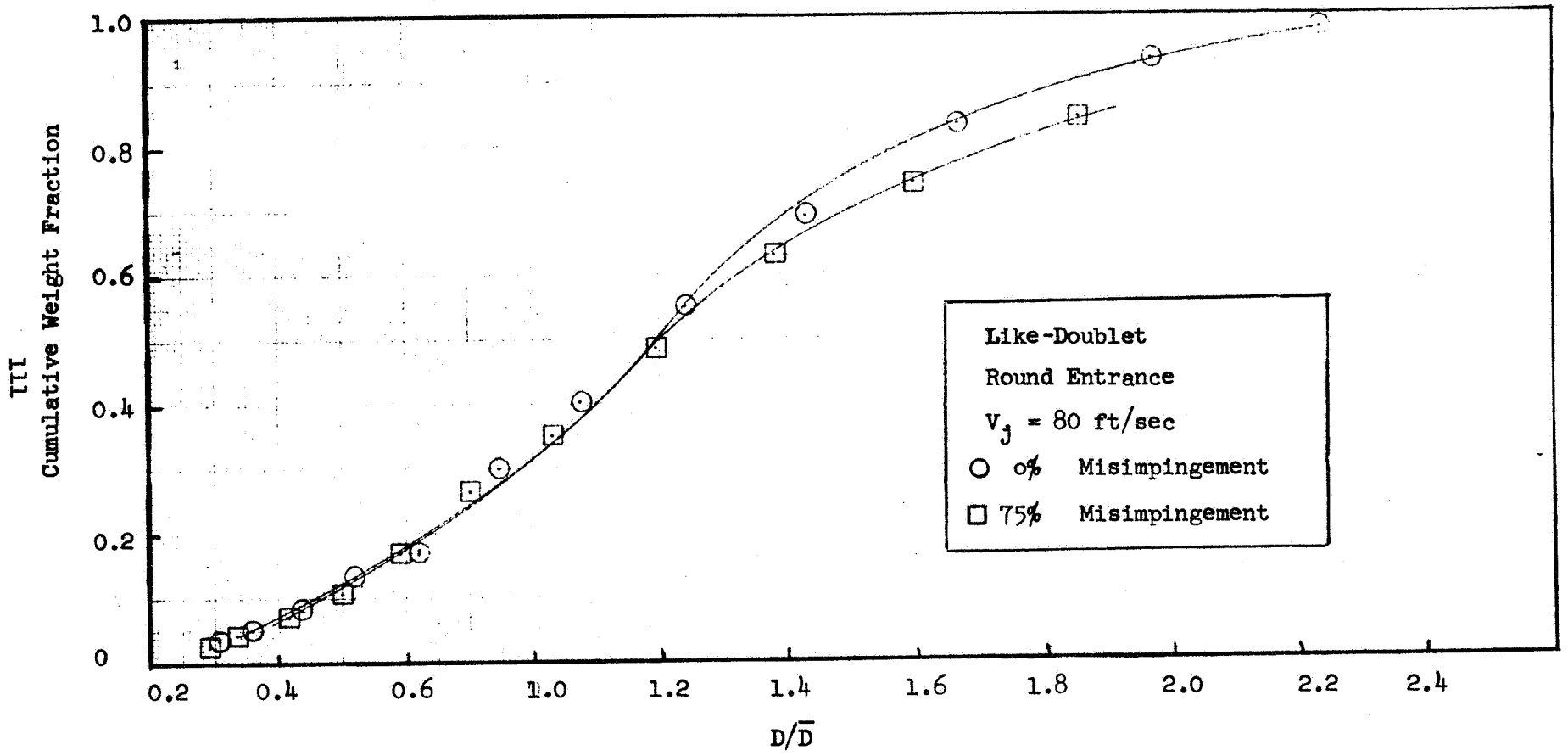

Figure 57. Influence of Misimpingement on Dropsize Distribution (L_o/d_j = 1.5)

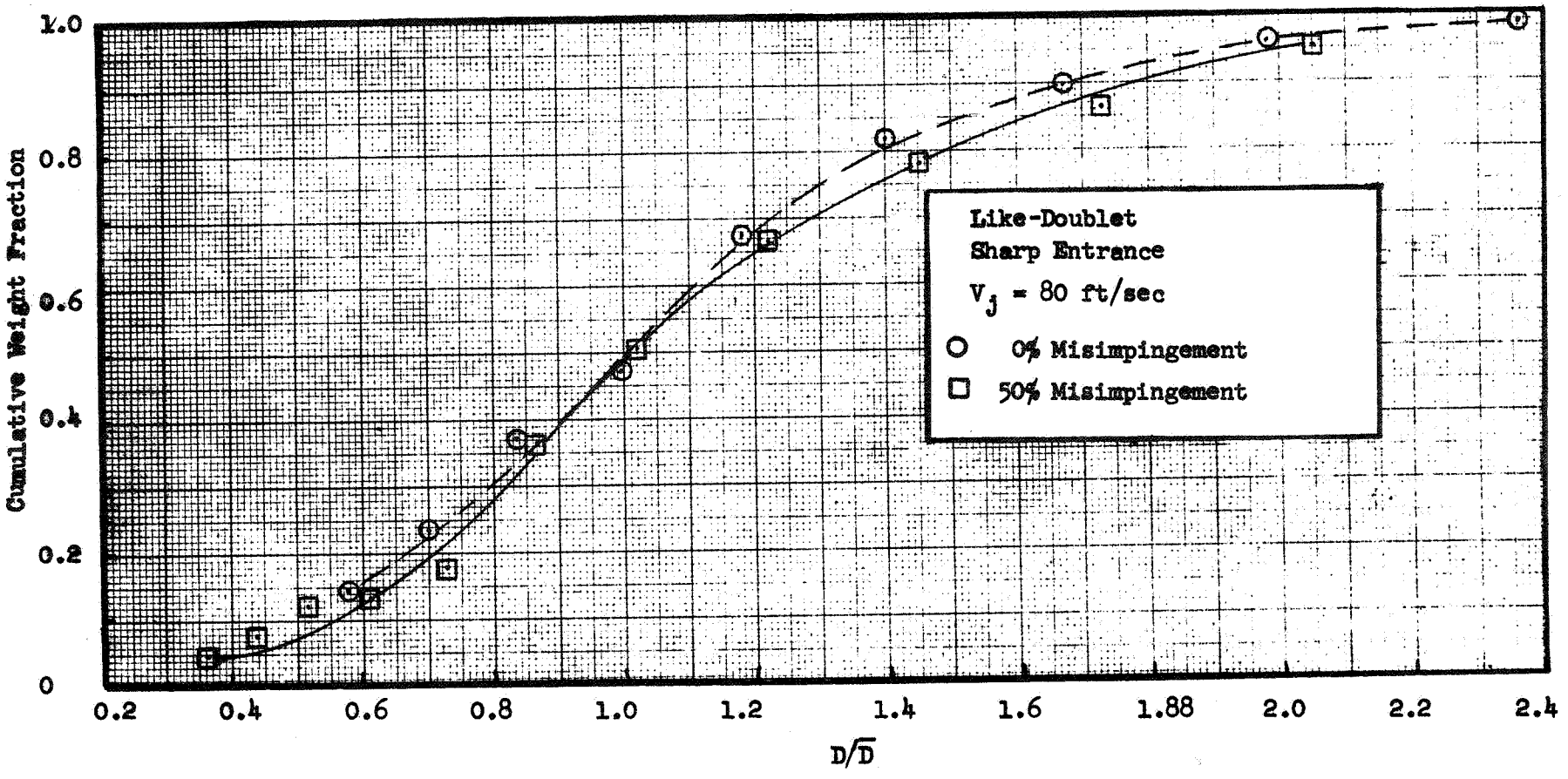

Figure 58. Influence of Misimpingement on Dropsize Distribution

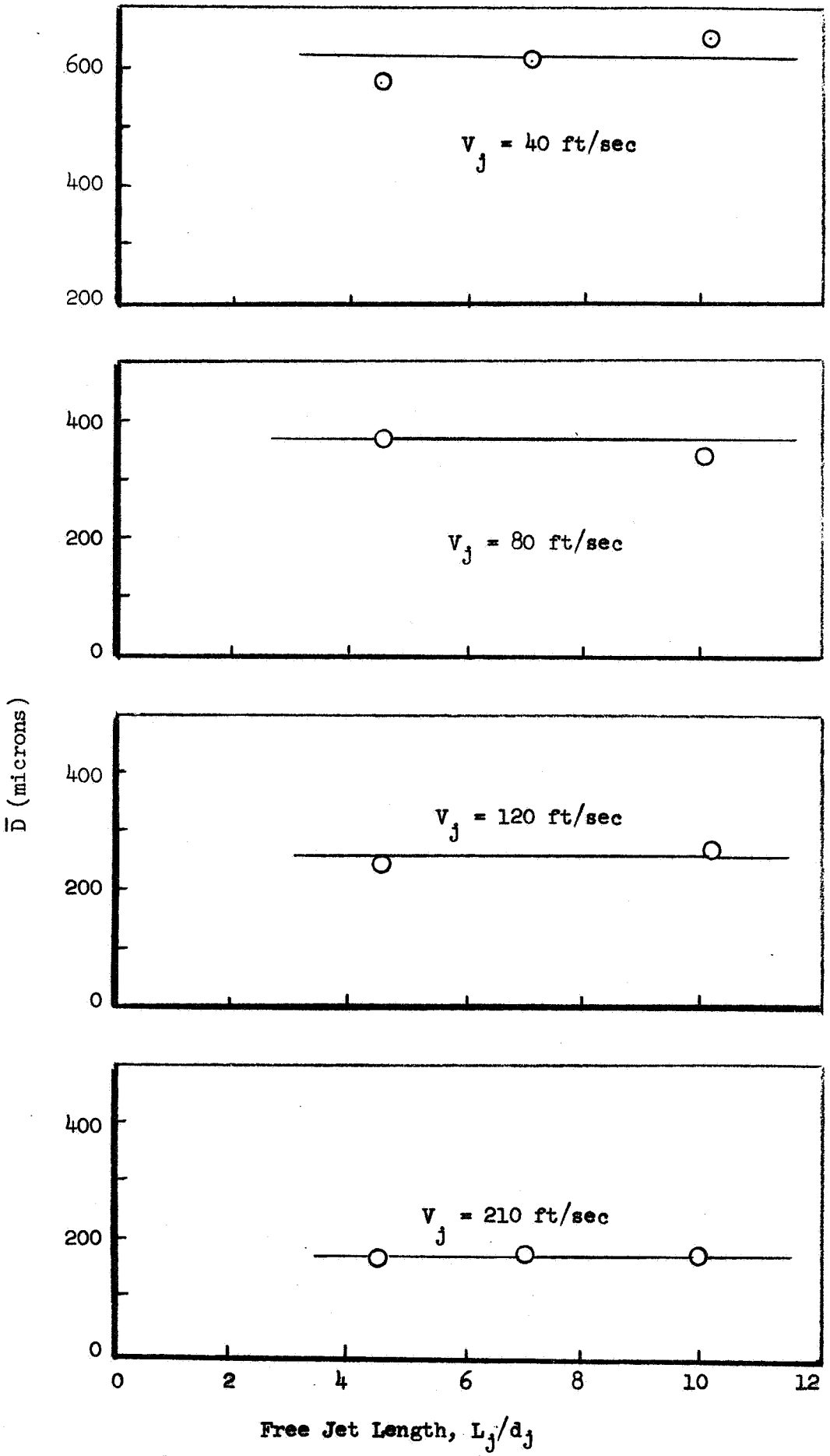

Figure 59. Influence of Free Jet Length on Mass Median Dropsize (Like-Doublet)

jet lengths were 1, 5, and 10 orifice diameters. The results and test conditions of the experiments, designated by run numbers 71 to 89, are presented in Table C1 of Appendix C. Unlike the previous results with short orifices, the general trend was an increase of the mass median dropsize with a corresponding increase of free jet length as shown on Fig. 60. The largest percentage increase (approximately 40 percent) was observed at the 90 degree impingement angle and nominal injection velocities of 85 and 105 ft/sec.

The dropsize distributions produced by laminar jets formed by the short orifices at the nominal injection velocity of 80 ft/sec and free jet lengths of 4.5 and 10 are compared with each other on Fig. 61 and to the turbulent jet distribution obtained at a free jet length of 10 d_j on Fig. 62. No variation in the distribution curves were observed with either the laminar or turbulent jet as the free jet length was increased. Although the mass median dropsize obtained with the 50 L_o/d_j orifices was found to increase with the free jet length, the same conclusion regarding the distribution can be drawn from Fig. 63 where the same dropsize distributions obtained at the free jet lengths of 1, 5, and 10 d_j, and impingement angles of 45, 60 and 90 degrees are compared.

Impingement Angle, γ. In the study of free jet length effects on dropsize, measurements were also obtained at various impingement angles. These tests were conducted at nominal injection velocities of 60, 85, and 105 ft/sec using a like-doublet element formed from the 67-50-5R orifices. The mass median dropsizes measured at a free jet length of 1 d_j and impingement angles of 45, 60, and 90 degrees are illustrated on Fig. 64. The data are presented as a non-dimensional dropsize, normalized by the mass median dropsize obtained at 60 degrees. Although some data scatter was observed, particularly at an impingement angle of 45 degrees, it is evident that an increase in the impingement angle produces smaller droplets.

The dropsize distribution was found to be unaffected by a variation of impingement angle as shown on Fig. 65.

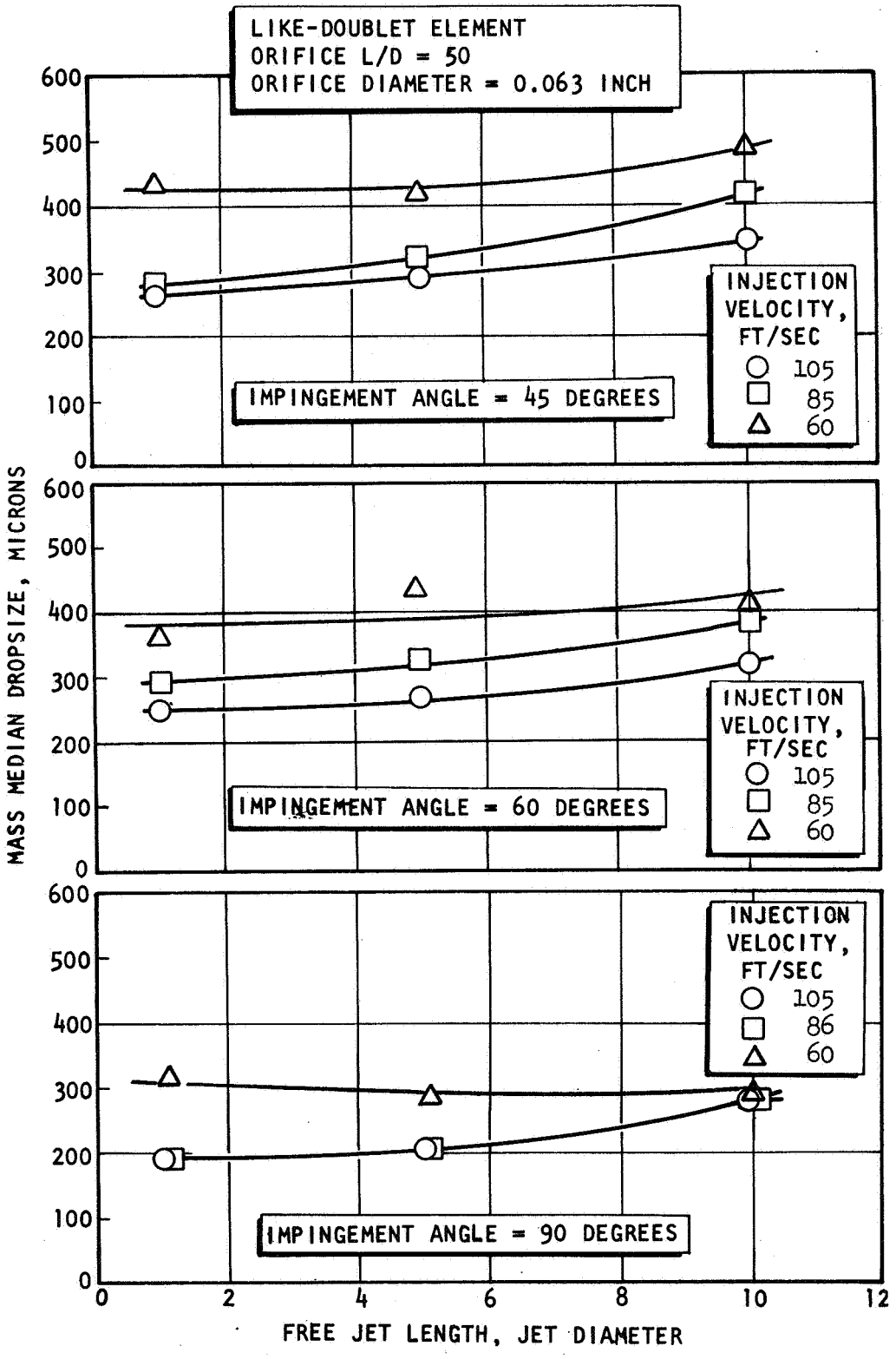

Figure 60. Influence of Free Jet Length on Mass Median Dropsize (Like-Doublet) $L_o/d_j = 50$)

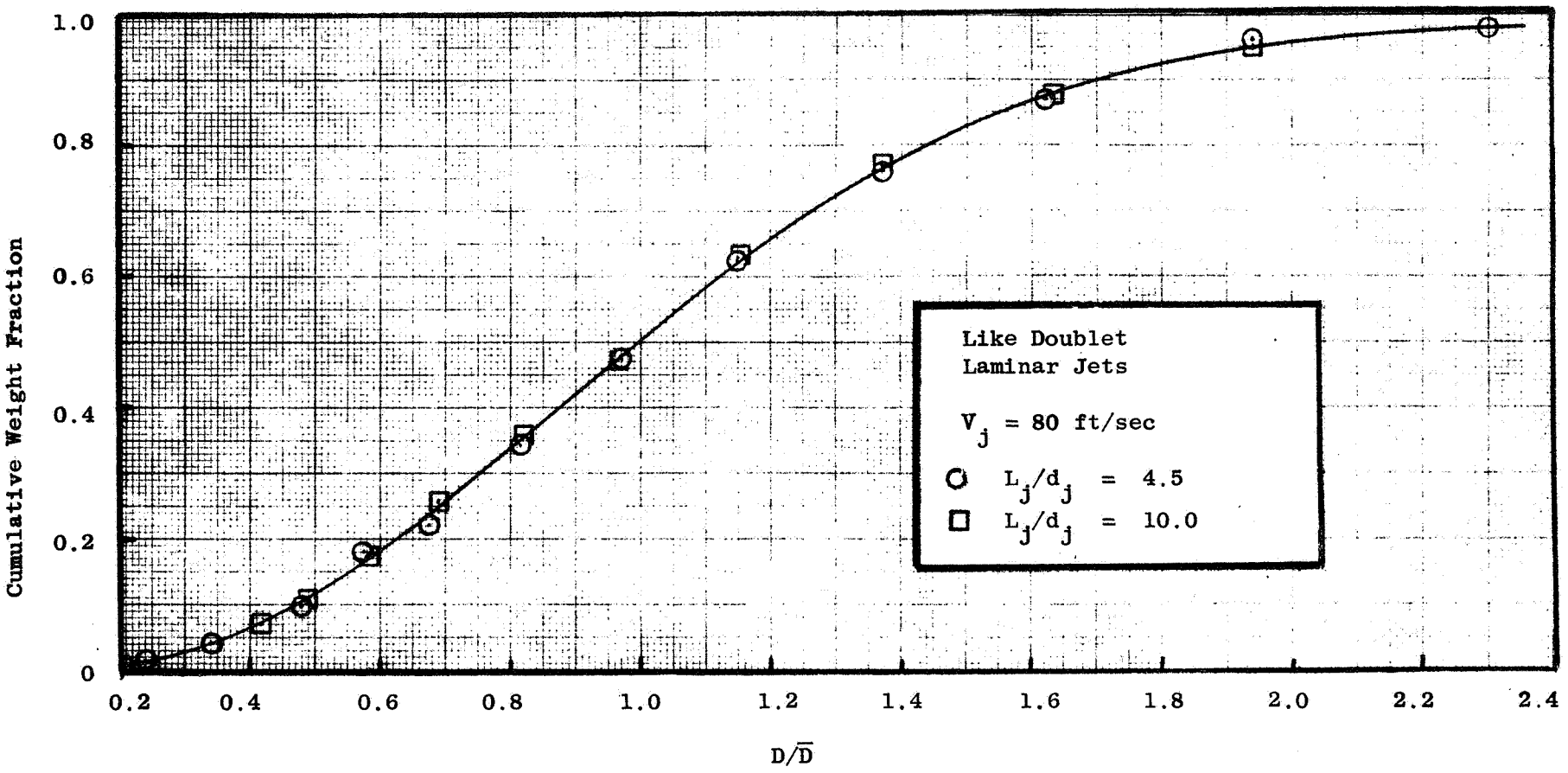

Figure 61. Influence of Free Jet Length on Dropsize Distribution (L_o/d_j = 1.5)

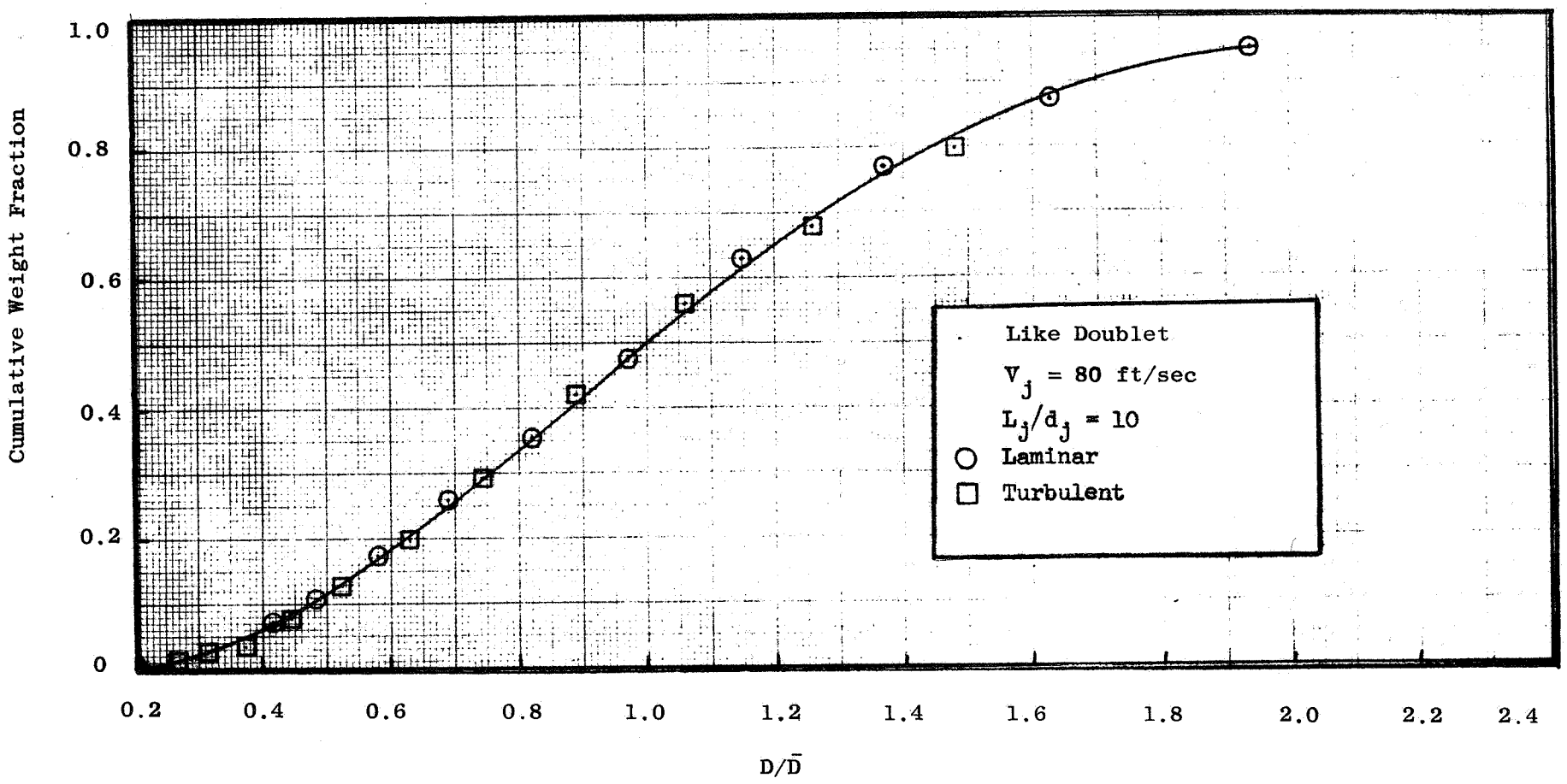

Figure 62. Influence of Turbulence on Dropsize Distribution (L_o/d_j = 1.5)

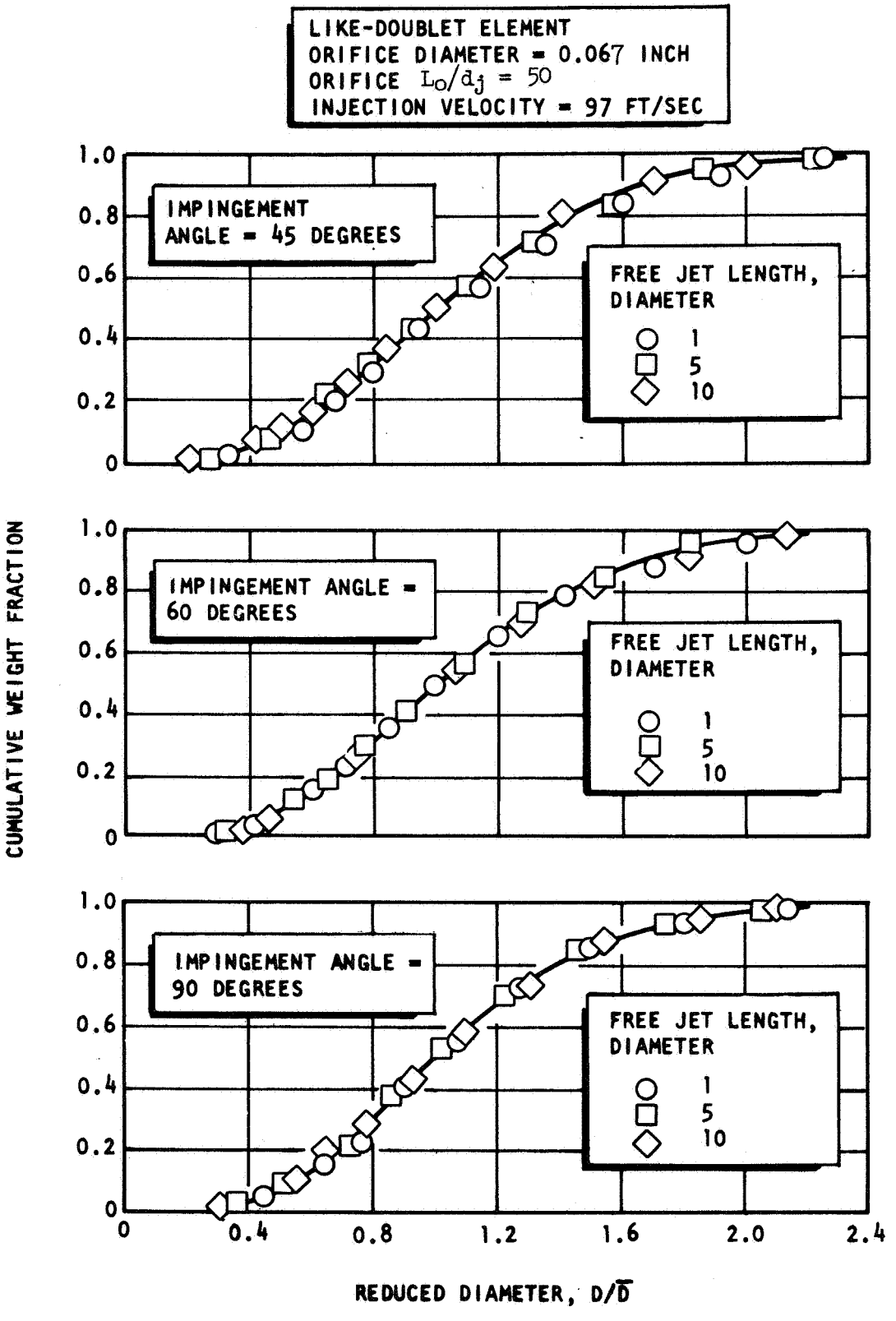

Figure 63. Normalized Distribution Curves for Unlike-Doublet Elements at Various Free Jet Lengths

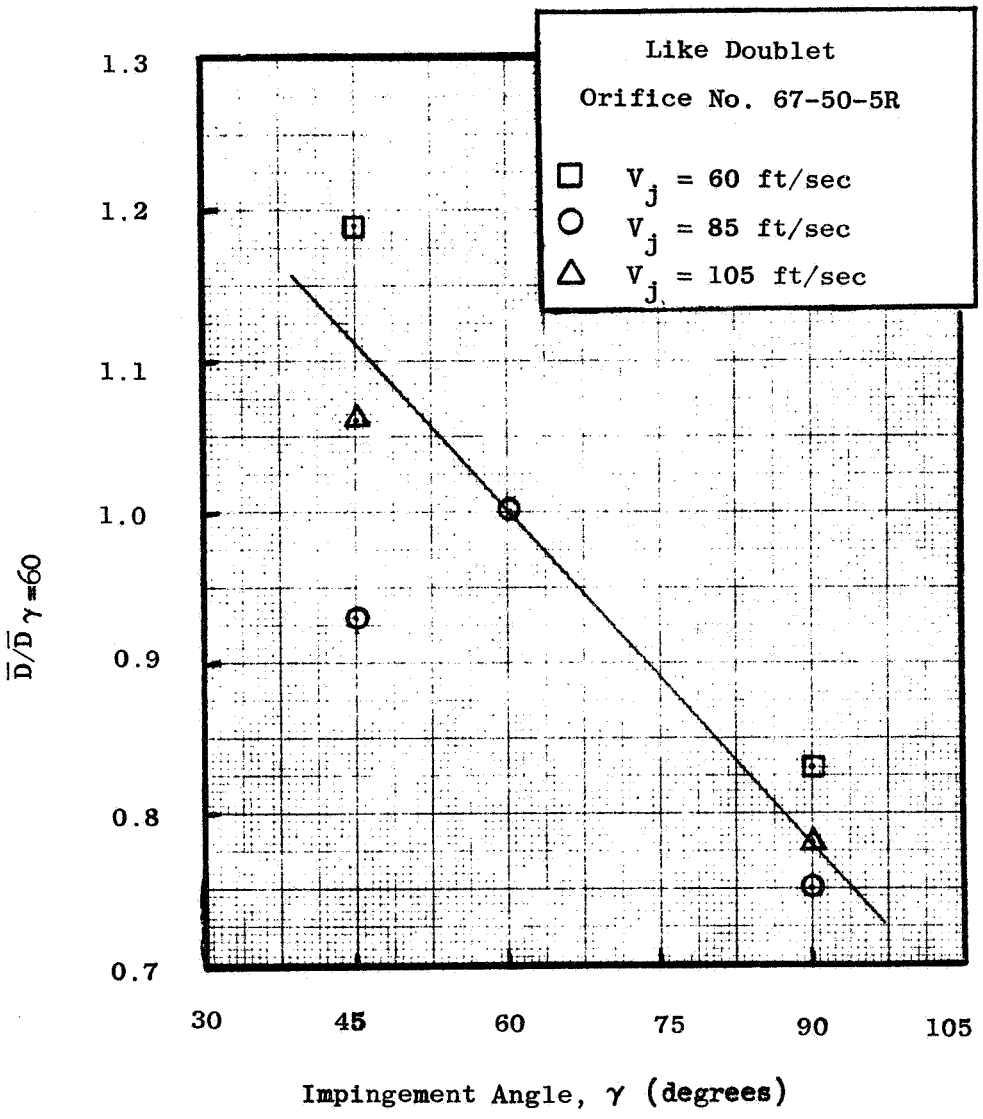

Figure 64. Influence of Impingement Angle on Mass Median Dropsize

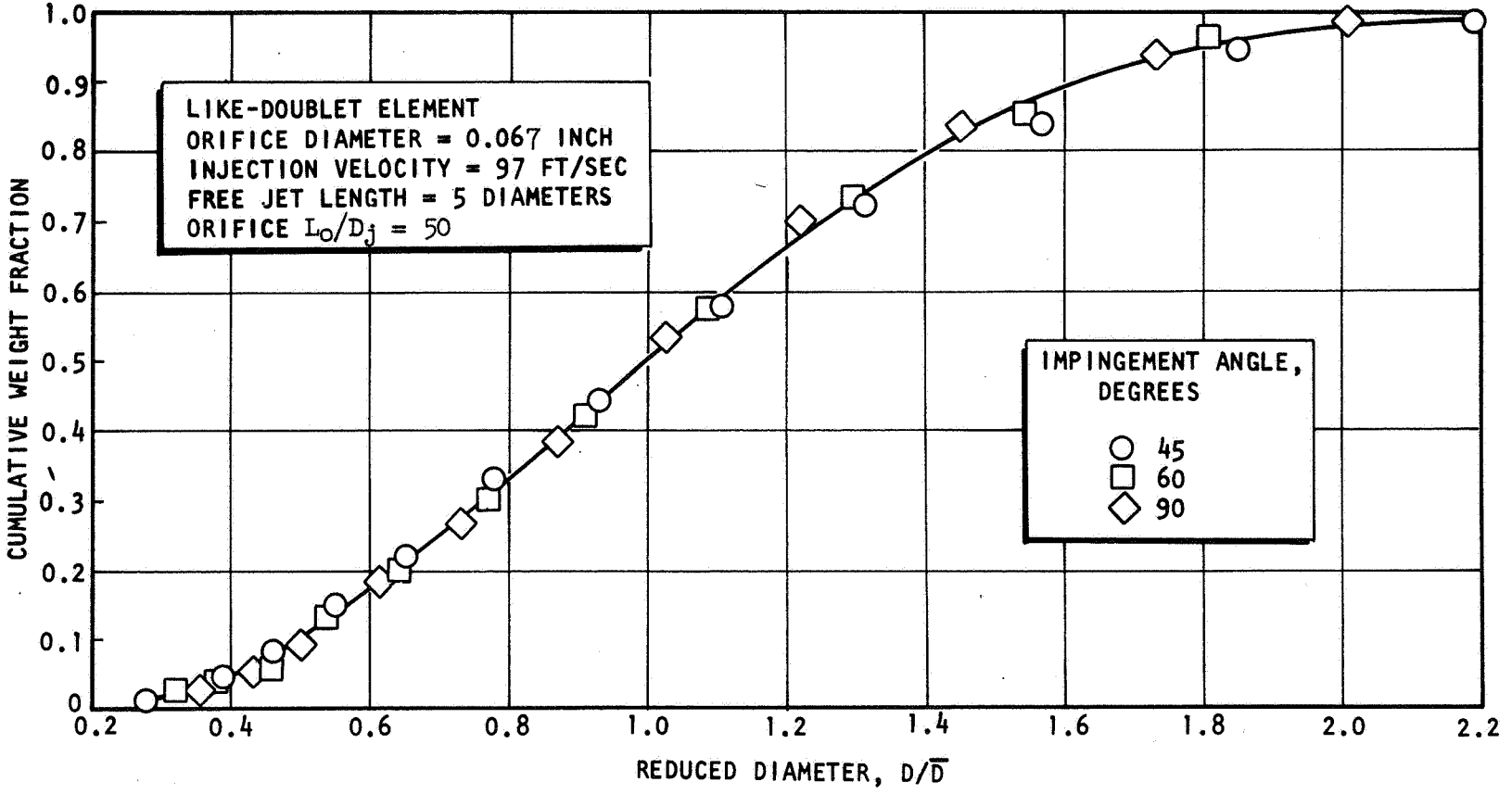

Figure 65. Normalized Distribution Curve for Like Doublet Element at Various Impingement Angles

4.2.2 Unlike-Doublet Atomization Results

A total of 80 experiments were performed in the investigation of the atomization characteristics of unlike-doublets. The tests were conducted with four propellant simulant combinations: (1) wax/wax, (2) wax/water, (3) wax/DEW1 (75 percent Diethanolamine, 25 percent water) and (4) wax/DEW2 (83 percent Diethanolamine, 17 percent water). Nine unlike-doublet elements were utilized. The orifices comprising these elements ranged in length from 1.5 to 50 d_j and had diameter ratios between 1 and 2.

The parameters that were examined and the number of tests performed with each element are listed below in Table 9. The results of the experiments and all pertinent hydraulic and dynamic parameters are summarized in Table C2 of Appendix C.

In the following paragraphs, the dynamic pressure ratio, P_D, is defined as

$$P_D = \frac{(\rho V_j^2)_{fuel}}{(\rho V_j^2)_{oxidizer}}$$

where V_j is the mean injection velocity ($\dot{w}/\rho A$). For consistency, the fuel orifice is taken to be the smaller of the two orifices. The diameter ratio is defined as, d_o/d_f, and, as a consequence, is always ≥ 1.

The optimum mixing criterion for a doublet element, as determined by Rupe, Ref. 25, requires that

$$\frac{(\rho V_j^2 d)_f}{(\rho V_j^2 d)_o} = 1$$

According to the above definition of dynamic pressure ratio, this condition reduces to

$$P_D = d_o/d_f$$

TABLE 9. SUMMARY OF UNLIKE-DOUBLET ATOMIZATION TESTS

Orifice Number(s)	Parameters Investigated (Run Numbers)					Number of Tests
	Injection Velocity	Turbulence Intensity	Dynamic Pressure Ratio	Diameter Ratio	Propellant Miscibility	
60-1.5-10R 60-1.5-10R		(105-112)	(105-116)		(113-116)	12
60-1.5-10R 90-1.5-10R			(117-128)			12
60-1.5-10R 120-1.5-10R			(129-140)			12
63/86-10-3LD	(141-146)			(141-146)		6
63-128-10-3UD				(147-149)		3
86-128-10-3UD				(150-152)		3
67-50-5R 67-50-5R					(153-155)	3
67-50-5R 86-50-5R	(156-161) (165-176)				(162-167) (174-176)	21
67-50-5R 128-50-5R					(177-184)	8

It should be noted that this criterion was, in general, not satisfied during the experiments.

Although several tests were performed using molten wax to simulate both propellants, the tests were, in general, conducted with wax as either the fuel or oxidizer simulant. In the former, an overall dropsize was measured, while the latter technique permitted separate measurements of the "fuel" or "oxidizer" dropsizes.

In obtaining all of the experimental results presented below, the impingement angle was held constant at 60 degrees and the free jet length was maintained a distance corresponding to five times the average of the two orifice diameters. Unless otherwise noted, the injection velocity refers to the wax propellant simulant.

Injection Velocity, V_j. The experimental investigation of the influence of injection velocity on the atomization characteristics of unlike-doublet elements was conducted with elements having a nominal diameter ratio of 1.3. The elements used were the multiple orifice element number 63/86-10-3UD and one formed from orifice numbers 67-50-5R and 86-50-5R. The tests were performed with both a wax/water propellant simulant combination (both elements) and a wax/DEW1 combination (50 L_o/d_j element only).

The results of these tests, assigned run numbers 141 to 146, 156 to 161 and 165 to 176, are presented in Table C2 of Appendix C. Figure 66 illustrates the mass median dropsizes obtained from the fuel and oxidizer orifices of both elements. The solid and dashed lines on both figures represent lines of constant dynamic pressure ratio. It should be noted that the slopes of these lines are approximate; their purpose being to "set-off" the fact that the tests were conducted at various dynamic pressure ratios.

Several observations can be made from the data presented on Fig. 66.
(1) An increase in the dynamic pressure results in a corresponding increase in the fuel dropsize, while the reverse is true for the oxidizer

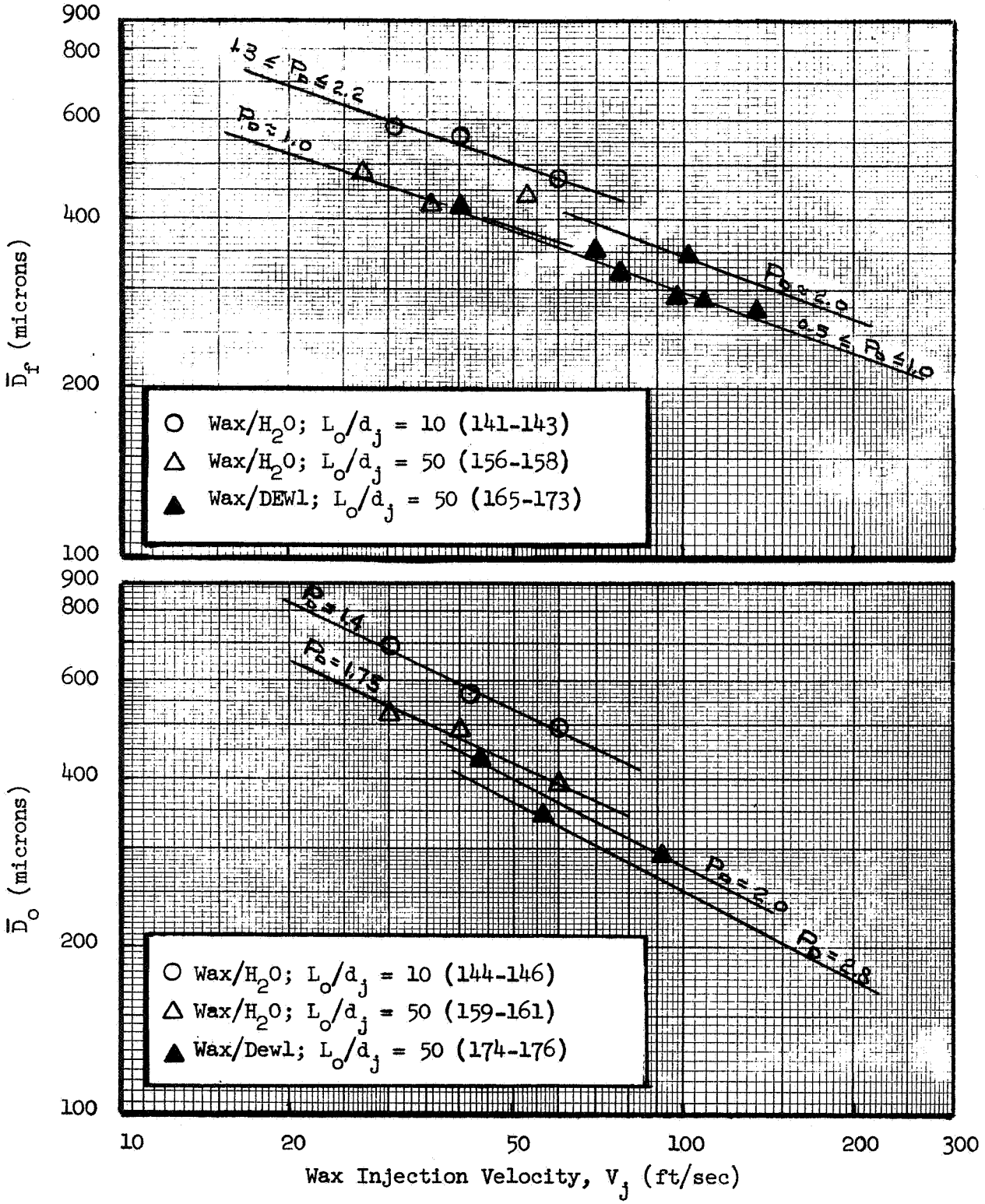

Figure 66. Mass Median Dropsize versus Injection Velocity for Like-Doublet

dropsize. This influence will be explored more fully in a later section. (2) The influence of the free jet velocity profile, as in the case of like-doublet elements, is apparent from a comparison of the dropsizes produced by the 10 and 50 L_o/d_j orifices.

Turbulence Intensity, ψ_c/p_j. An equal diameter element was used to evaluate free jet turbulence effects on unlike-doublet atomization. The element was formed from 60-1.5-10R orifices. A total of 8 tests were performed; four with and four without the turbulence generator. The experiments were conducted at a constant total momentum flux ($M_T = (\dot{w}V)_f + (\dot{w}V)_o$), of 9 ft-lbm-sec^2 and over a dynamic pressure ratio range of 0.45 to 2.0. The turbulence intensity level was on the order of 0.015.

The tests are designated by run numbers 105 to 112 in Table C2 of Appendix C. The variation of the mass median dropsize obtained from both the laminar and turbulent jets is shown on Fig. 67 as a function of dynamic pressure ratio. It is evident that there was no influence of turbulence on the mass median diameter under these conditions.

Dynamic Pressure Ratio, P_D. In the experimental investigation of the effects of dynamic pressure ratio on atomization, a total of 36 molten wax tests were performed using equal and unequal diameter elements. The doublet elements were formed from combinations of the single orifice element numbers 60-1.5-10R, 90-1.5-10R, and 120-1.5-10R yielding diameter ratios of 1.0, 1.5, and 2.0. The short orifice lengths were chosen to minimize velocity profile effects.

Twelve of the molten wax tests were performed with the equal diameter elements. Of the 12 tests, 8 were conducted using molten wax and DEW2 as propellant simulants. The remaining 4 experiments were conducted using only molten wax. The mass median dropsizes obtained from these experiments, run numbers 105 to 116, are presented on Fig. 68. Special emphasis was given to the case of unity dynamic pressure ratio. Five of the tests were conducted at or near this condition.

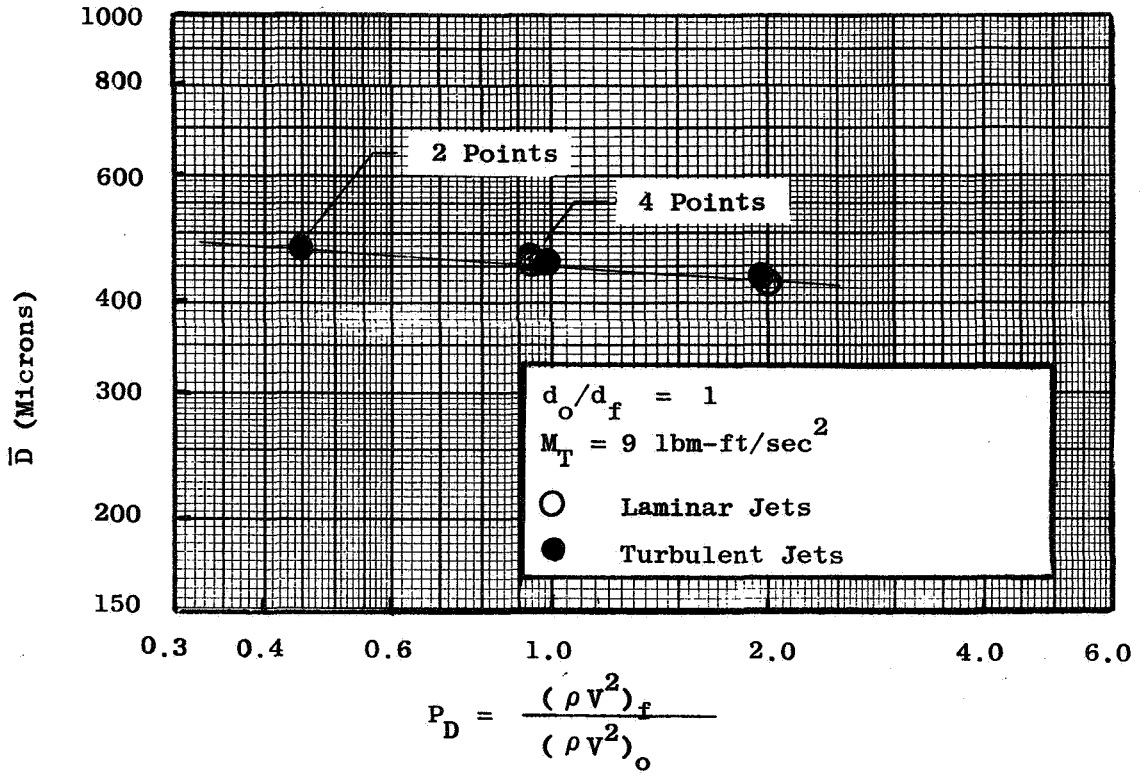

Figure 67. Comparison of Mass Median Dropsizes for Laminar and Turbulent Jet Impingement (Unlike-Doublet)

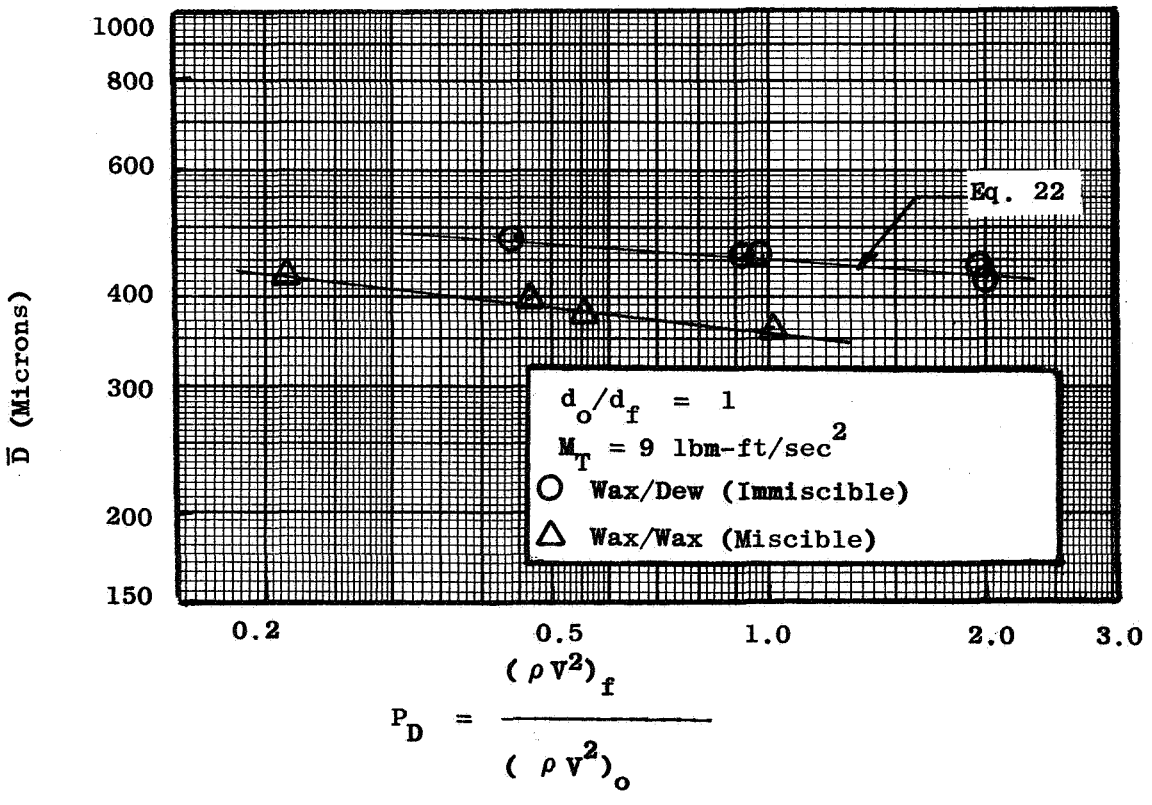

Figure 68. Comparison of Mass Median Dropsizes for Miscible and Immiscible Impingement

It was found that the wax/DEW (immiscible) propellant combination resulted in larger dropsizes than the wax/wax (miscible) combination. The trend with the wax/DEW combination is toward smaller mass median dropsizes as the dynamic pressure ratio is increased. Since (for the wax/wax tests) the results are symmetrical about $P_D = 1$, a minimum is attained at unity dynamic pressure ratio with miscible propellants. This condition also corresponds to optimum mixing.

The remainder of the tests were performed with unlike-doublet elements having diameter ratios of 1.5 and 2.0. Three tests each were conducted at a constant total momentum flux and a constant wax injection velocity. Wax and DEW were used as the propellant simulants. By interchanging the orifices flowing these simulants, the dropsizes produced by both the small diameter (fuel) and the large diameter (oxidizer) orifices were measured.

The mass median dropsizes and the test conditions at which they were obtained, run numbers 117 to 140, are presented in Table C2 of Appendix C. In the case of the 1.5 diameter ratio element, the dynamic pressure ratio was varied while maintaining a constant total momentum of 9 lbm-ft/sec^2. For the 2.0 diameter ratio element, the momentum level was 20 lbm-ft/sec^2. In addition, tests were performed at a constant wax injection velocity of 70 ft/sec while the total momentum level was changed. Both the fuel- and oxidizer-side dropsizes obtained with the 1.5 diameter ratio element are shown in Fig. 69. The results from the tests conducted with the 2.0 diameter ratio element are illustrated in Fig. 70. The equation numbers on the two figures refer to empirical correlations, presented in Section 5.2.2.

As in the case of equal diameter elements, the mass median dropsize of both the fuel and oxidizer decrease as the dynamic pressure ratio is increased while maintaining a constant total momentum. On the other hand, when the wax velocity (either fuel or oxidizer) is held constant, the dropsize decreases when the velocity of the opposing jet is raised.

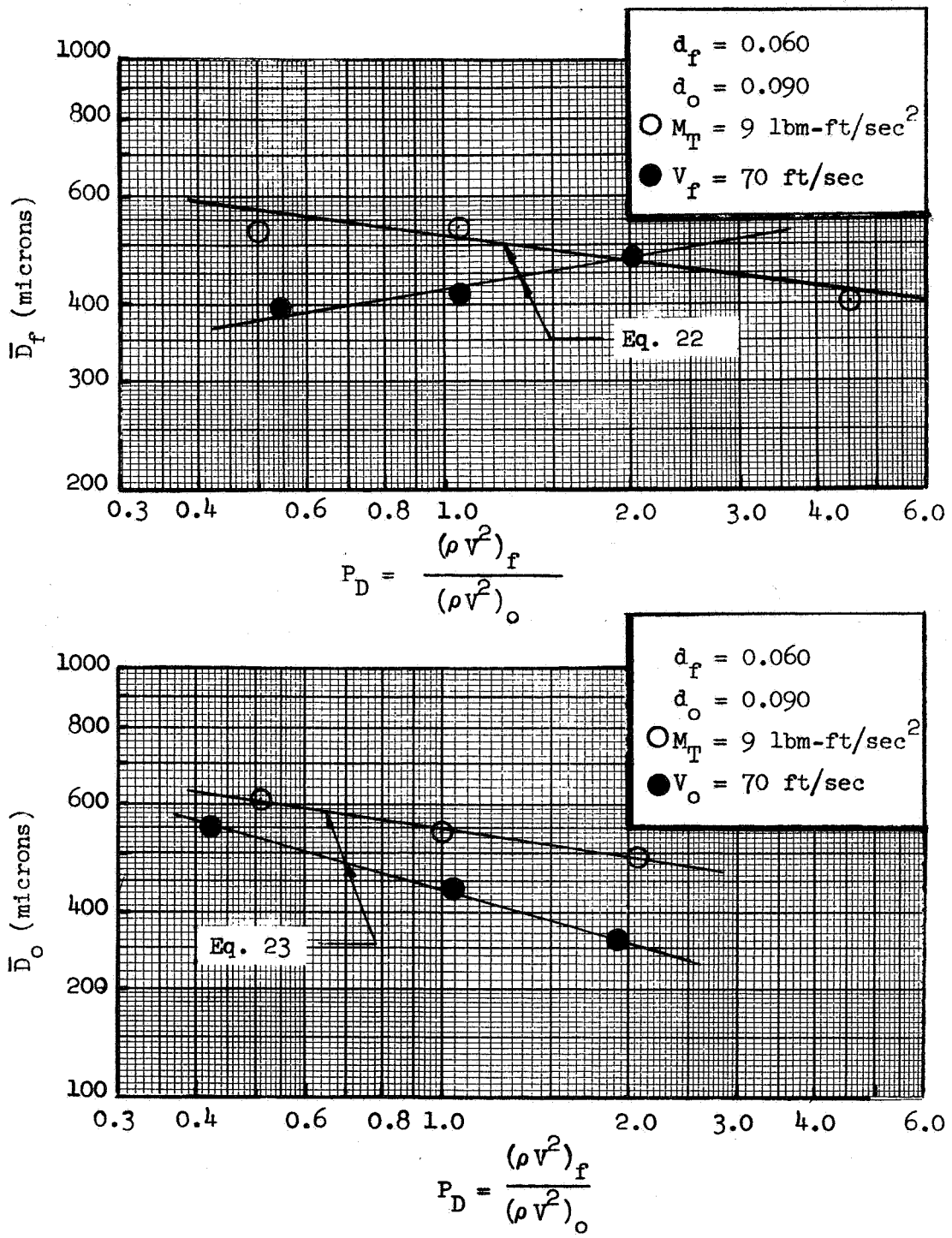

Figure 69. Mass Median Dropsize Versus Dynamic Pressure Ratio for 1.5 Diameter Ratio Doublet Element

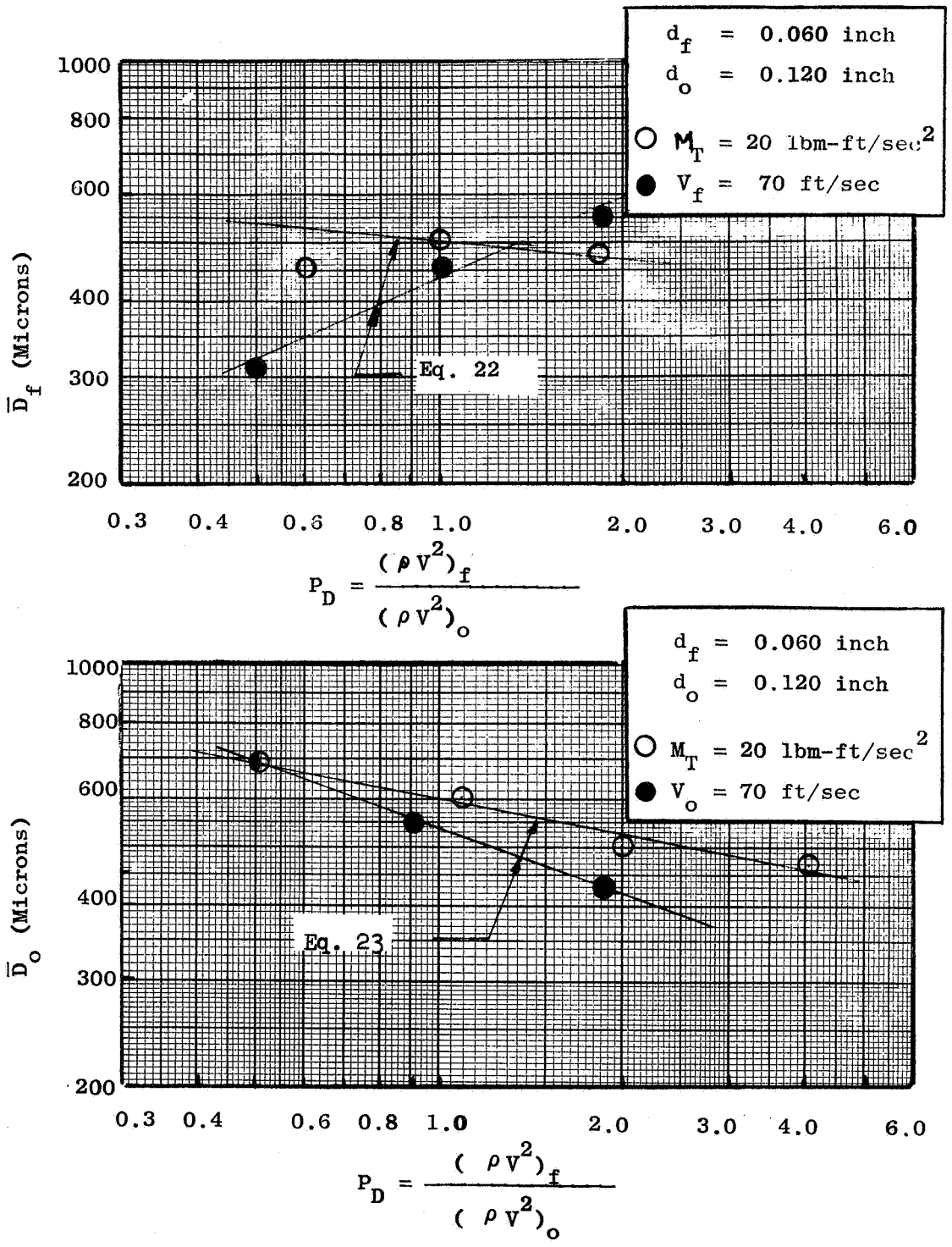

Figure 70. Mass Median Dropsize Versus Dynamic Pressure Ratio for 2.0 Diameter Ratio Element

Comparisons of the oxidizer and fuel dropsize distributions obtained with the 1.5 diameter ratio elements at nominal dynamic pressure ratios of 0.5 and 2.0 are presented on Figs. 71 and 72 respectively.

A comparison of the distributions obtained with the 1.0 diameter ratio element is shown on Fig. 73. It was noted above that the direction of change of the mass median dropsize with dynamic pressure ratio depended upon whether it was the fuel or oxidizer dropsize that was being examined. The variation of the dropsize distributions exhibits a similar dependence. In general, it can be stated that the dropsize distribution becomes more monodisperse when the variation of dynamic pressure ratio results in a decrease of the mass median dropsize.

Diameter Ratio, d_o/d_f. Although several tests were performed for the explicit purpose of examining diameter ratio effects on atomization, the majority of the data was indirectly obtained as a result of diameter perturbations in the miscibility and dynamic pressure ratio studies. The experiments that were performed in the diameter ratio studies utilized the 10 L_o/d_j unlike-doublet elements. Wax and water were used as propellant simulants.

The results of these tests, run numbers 141 to 152, are summarized in Table C2 of Appendix C. The mass median dropsizes for the fuel- and oxidizer-sides of the unlike doublets are shown on Fig. 74 as a function of injection velocity. The diameter ratios are indicated on the figure.

Considerable data scatter was observed in these tests because of the relatively large dropsizes. However, it can be observed that the fuel (smaller orifice) dropsize is not very sensitive to the diameter ratio. On the other hand, the oxidizer (larger orifice) dropsizes appear to vary inversely with the diameter ratio.

Additional results were obtained from the dynamic pressure ratio studies. Shown on Fig. 75 are the fuel and oxidizer dropsizes obtained at unity

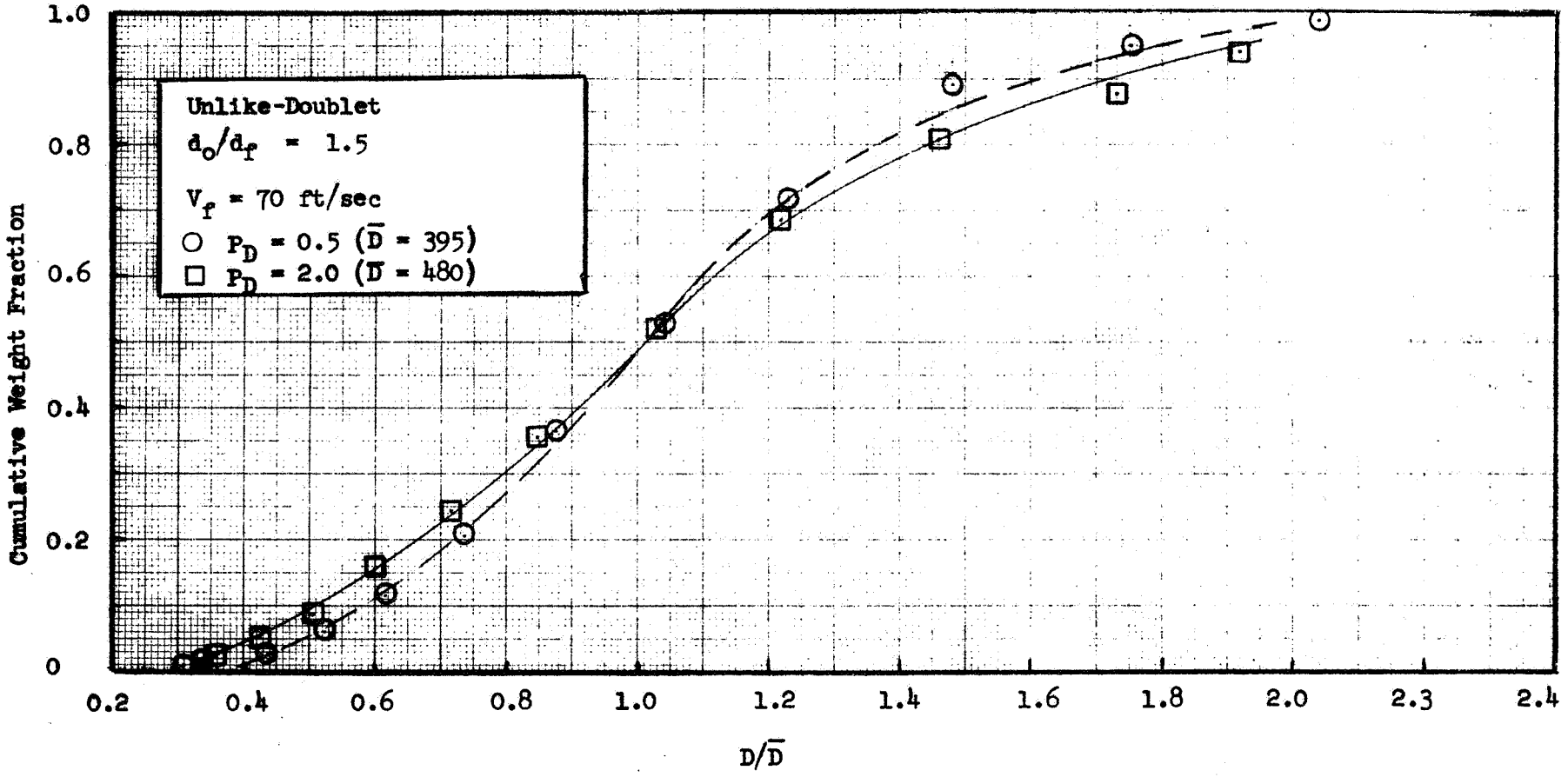

Figure 71. Influence of Dynamic Pressure Ratio on Fuel-Size Dropsize Distribution (L_o/d_j = 1.5)

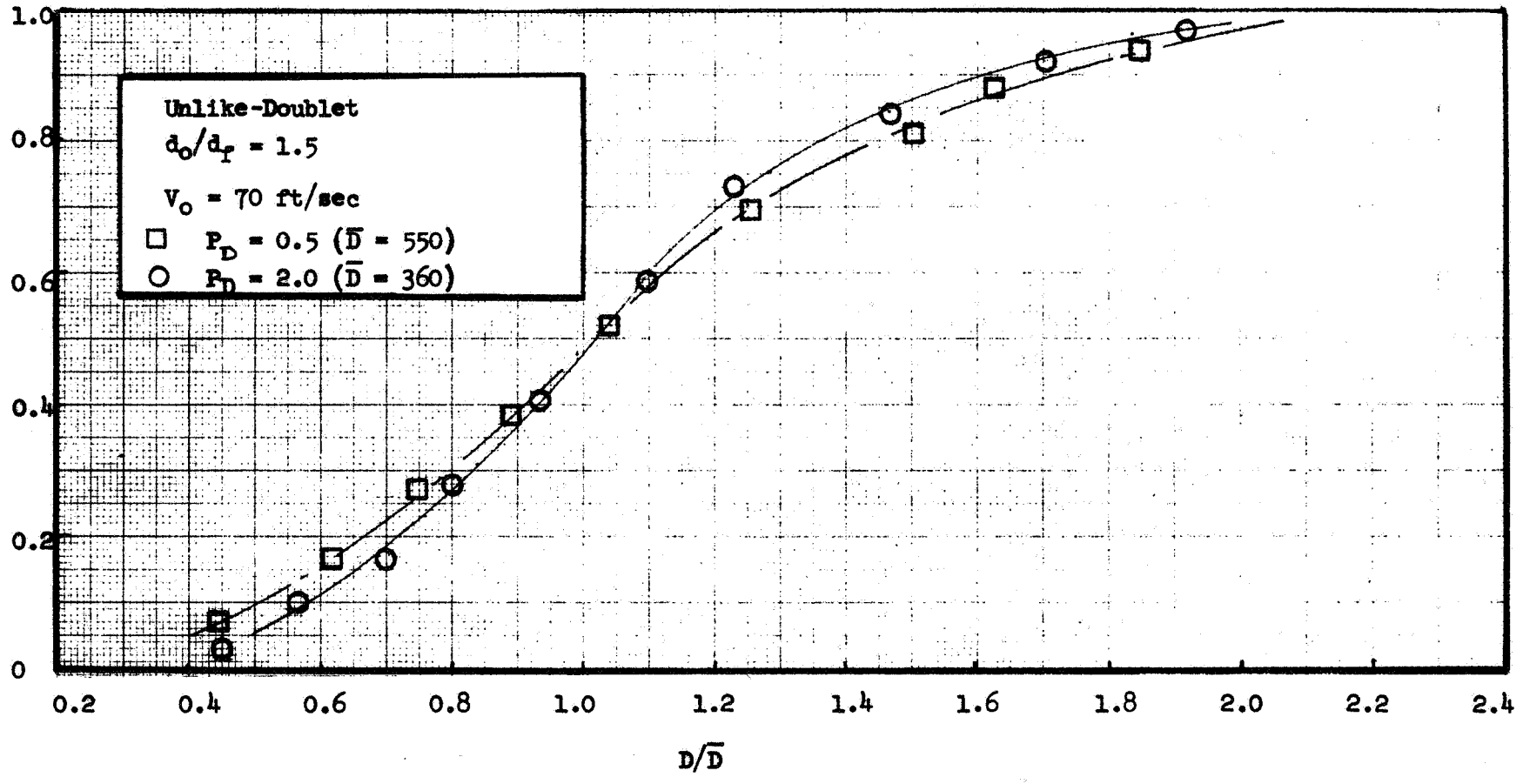

Figure 72. Influence of Dynamic Pressure Ratio on Oxidizer-Side Dropsize Distribution

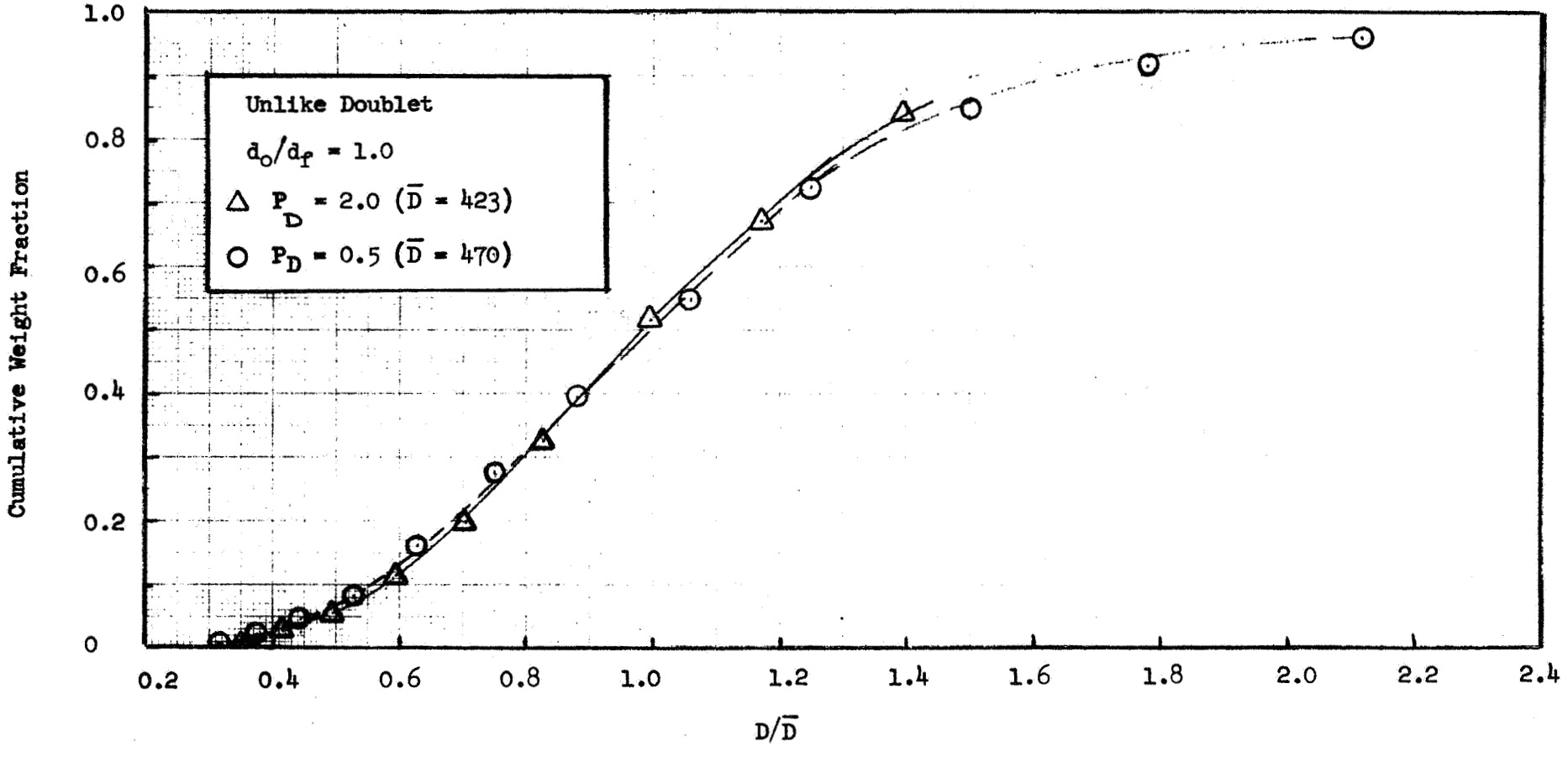

Figure 73. Influence of Dynamic Pressure Ratio on Dropsize Distribution (Equal - Diameter, Unlike Doublet)

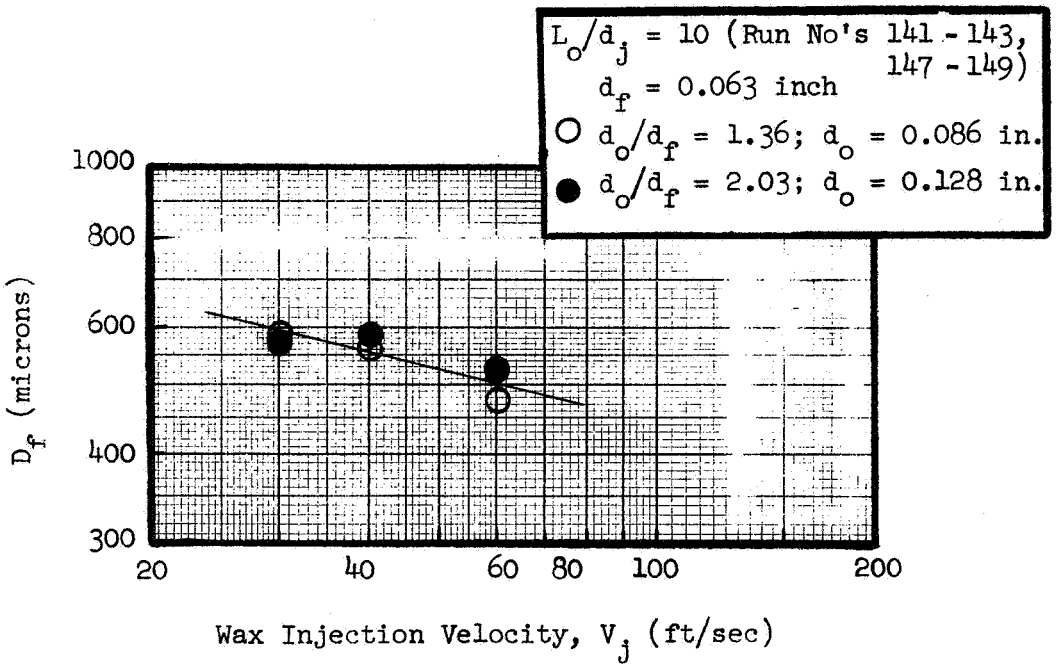

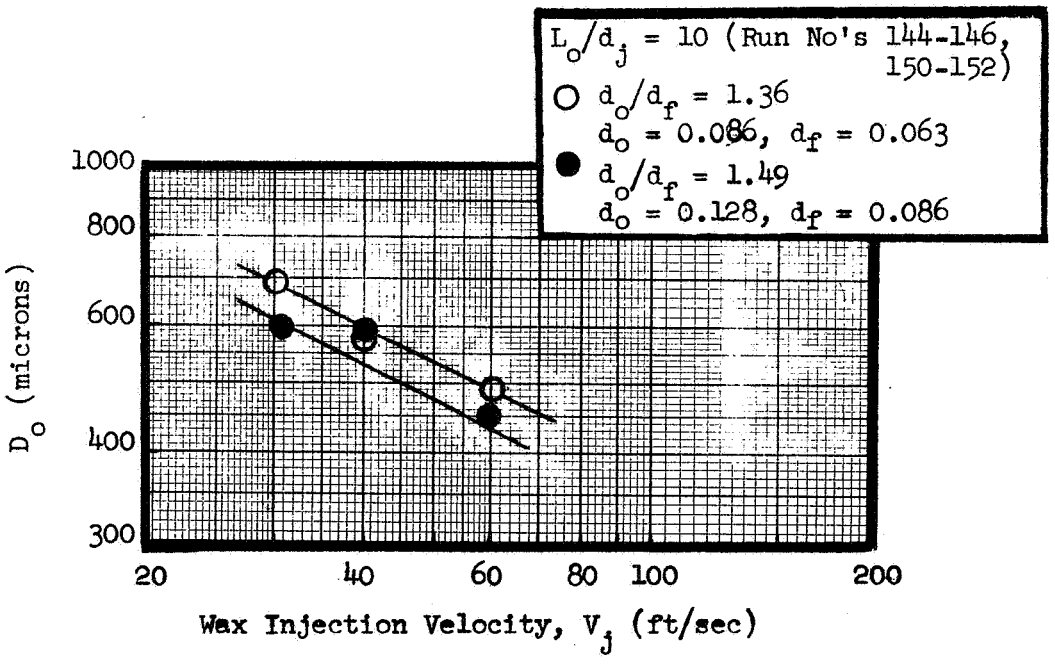

Figure 74. Influence of Diameter Ratio on Mass Median Dropsize

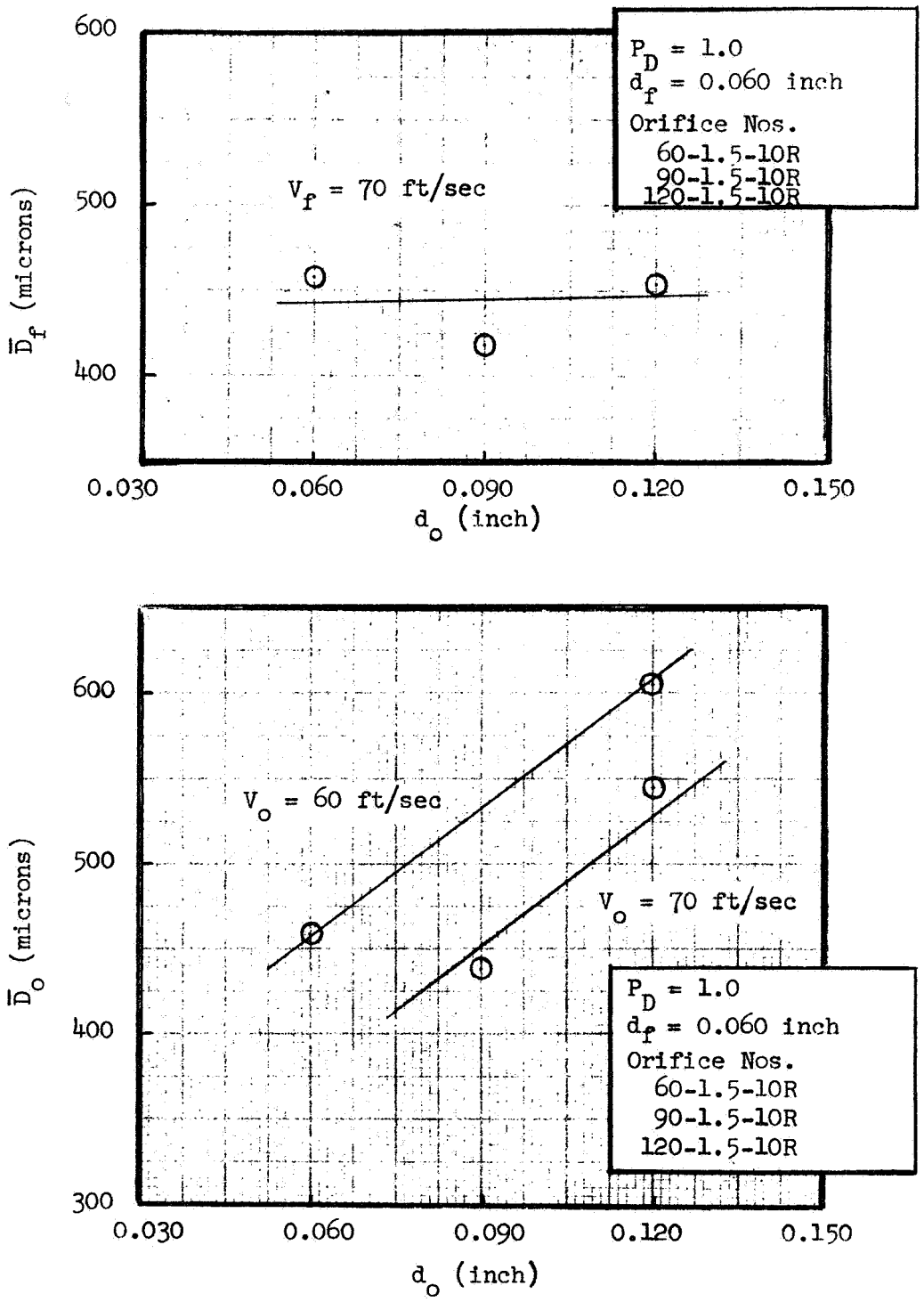

Figure 75. Influence of Oxidizer Orifice Diameter on Mass Median Dropsize

dynamic pressure ratio as a function of the oxidizer diameter. In these tests, the fuel orifice diameter was constant and equal to 0.060 inches. When presented in this manner it is readily seen that the fuel dropsize is not very sensitive to d_o while the oxidizer dropsize increases rapidly when the oxidizer orifice is enlarged.

Finally, the influence of diameter ratio on the overall spray dropsize can be evaluated from the wax/wax tests conducted in the miscibility studies. These data are shown on Fig. 76 as a function of injection velocity for the diameter ratios of 1.0, 1.28 and 1.91. The fuel orifice diameter was 0.067 inches in all the tests. As in the case of the oxidizer dropsizes, the overall spray dropsize increases with the oxidizer diameter.

The influence of diameter ratio on the dropsize distributions is presented on Fig. 77 for the case of miscible impingement and on Fig. 78 for immiscible impingement. Both figures present a comparison of the distribution curves obtained with the 1.0 and 1.91 diameter ratio elements. An examination of these data indicates that the effects of diameter ratio on the overall spray distribution was small and approximately the same for both miscible and immiscible impingement.

The effect of diameter on the individual fuel and oxidizer dropsizes can be determined from an examination of the distributions presented on Fig. 79 for the 1.28 and 1.91 diameter ratio elements. These data indicate that the smaller diameter orifice produces a more monodisperse distribution.

Propellant Miscibility. The evaluation of the effect of propellant miscibility on the atomization process is complicated by the large number of variables which could also affect the results. For instance, such parameters as the momentum level, orifice diameter ratio, and dynamic pressure ratio are known to effect the atomization characteristics. In addition, it is important to select a liquid which is immiscible with wax but which has similar physical properties. The fluid chosen for this study is an aqueous

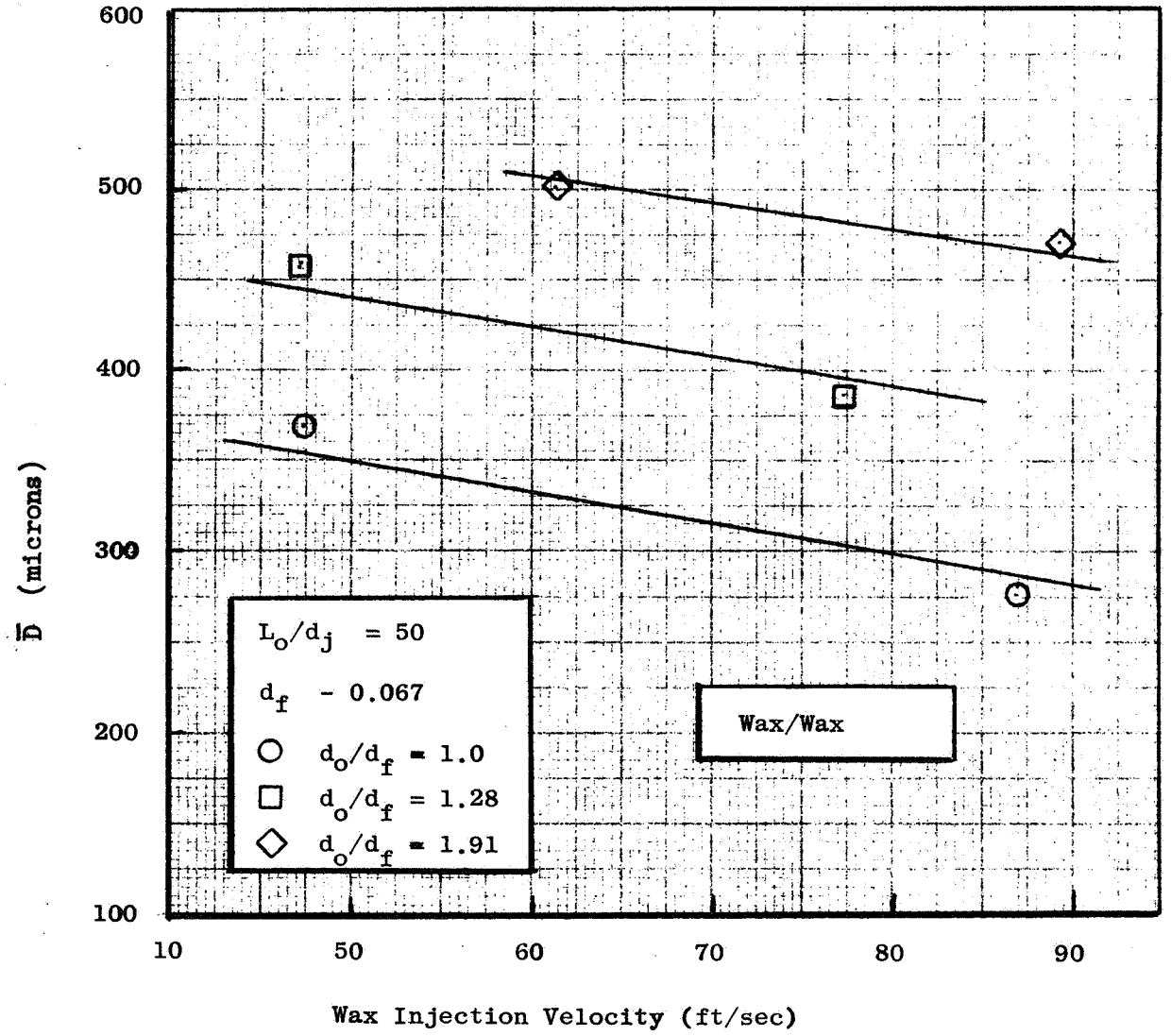

Figure 76. Influence of Diameter Ratio on Mass Median Dropsize (Miscible Propellants)

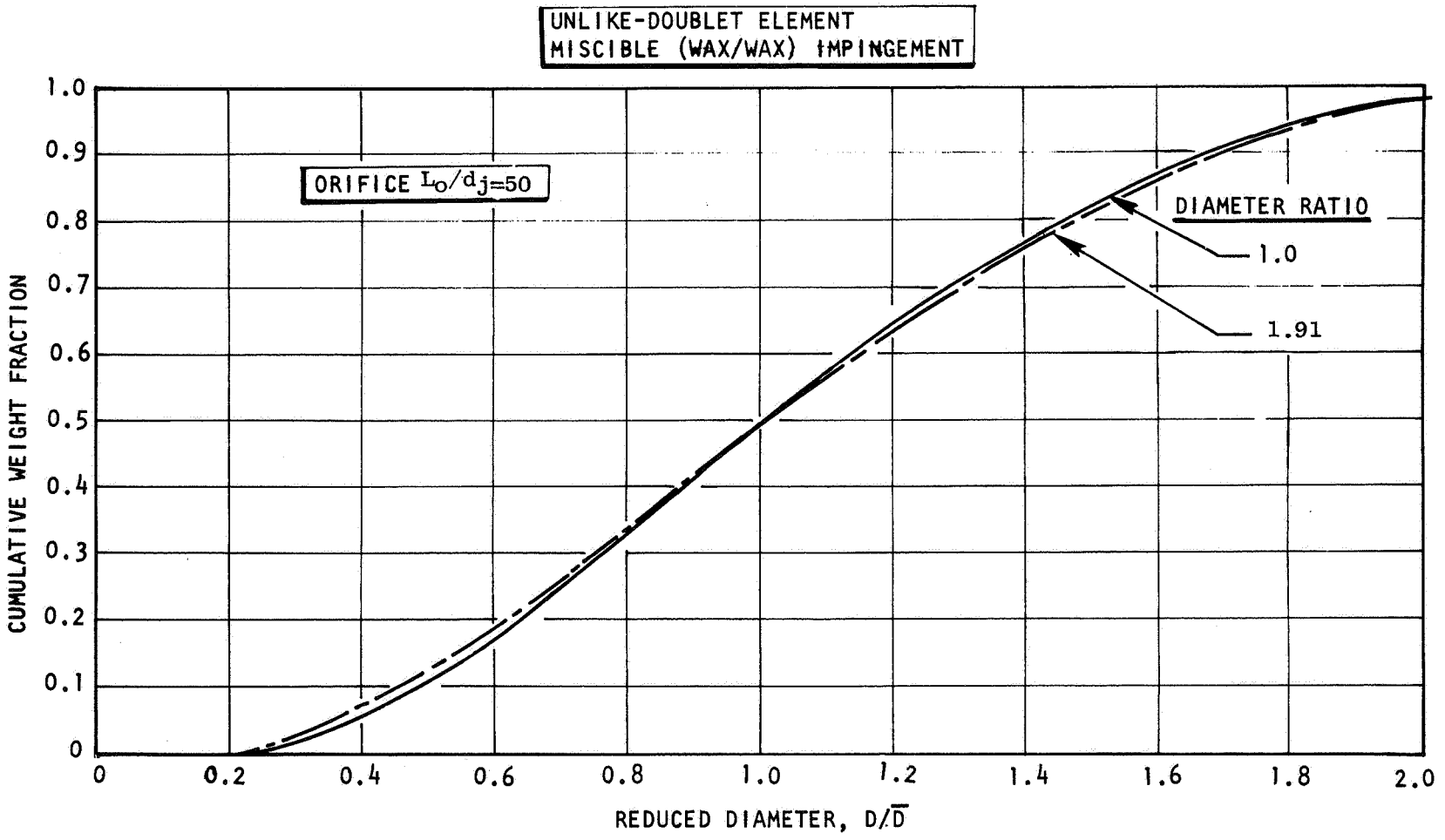

Figure 77. Normalized Distribution Curves Obtained for the Case of Miscible (Wax/Wax) Impingment

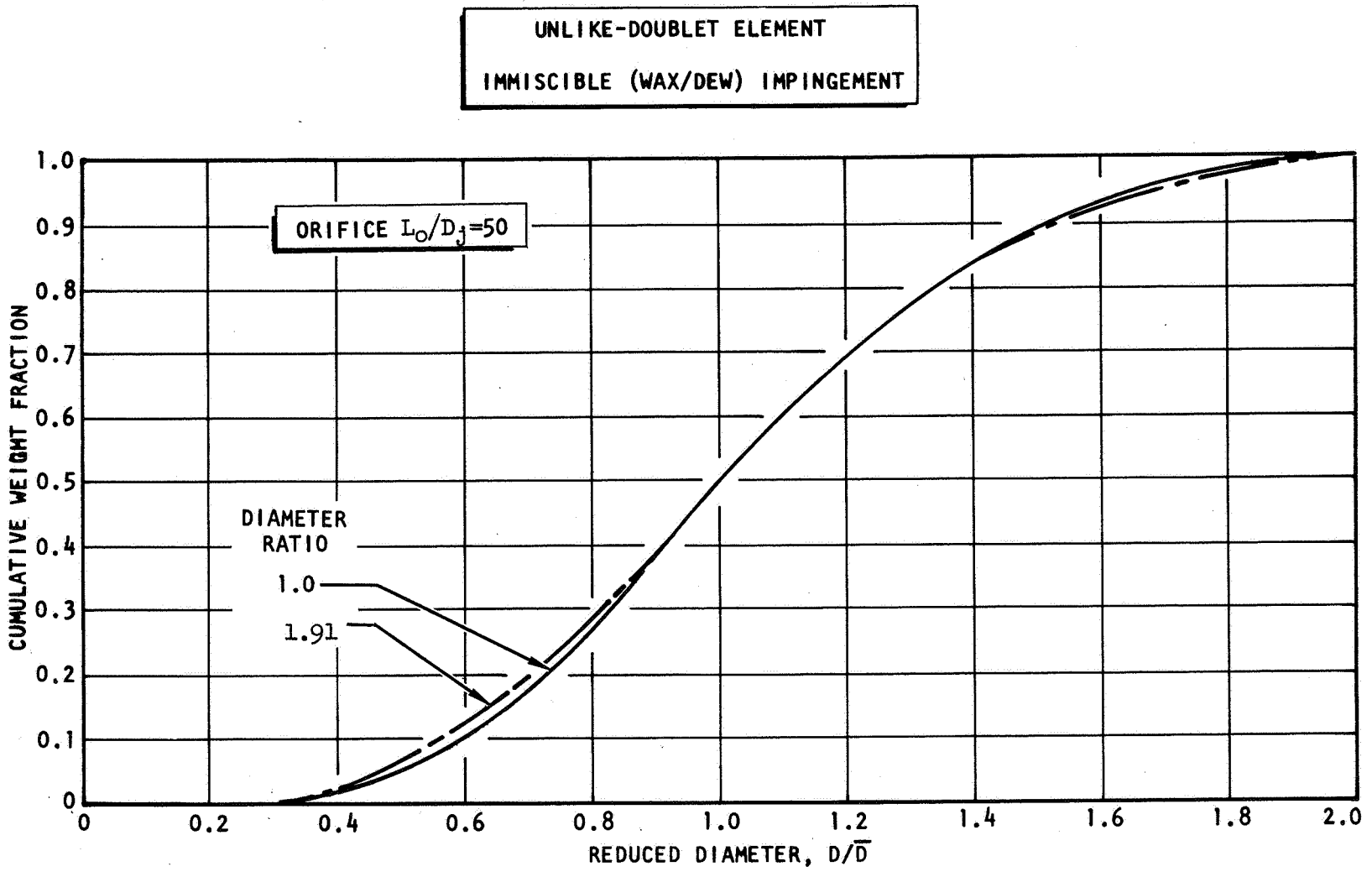

Figure 78 Normalized Distribution Curves Obtained for the Case of Immiscible (Wax/Dew) Impingement

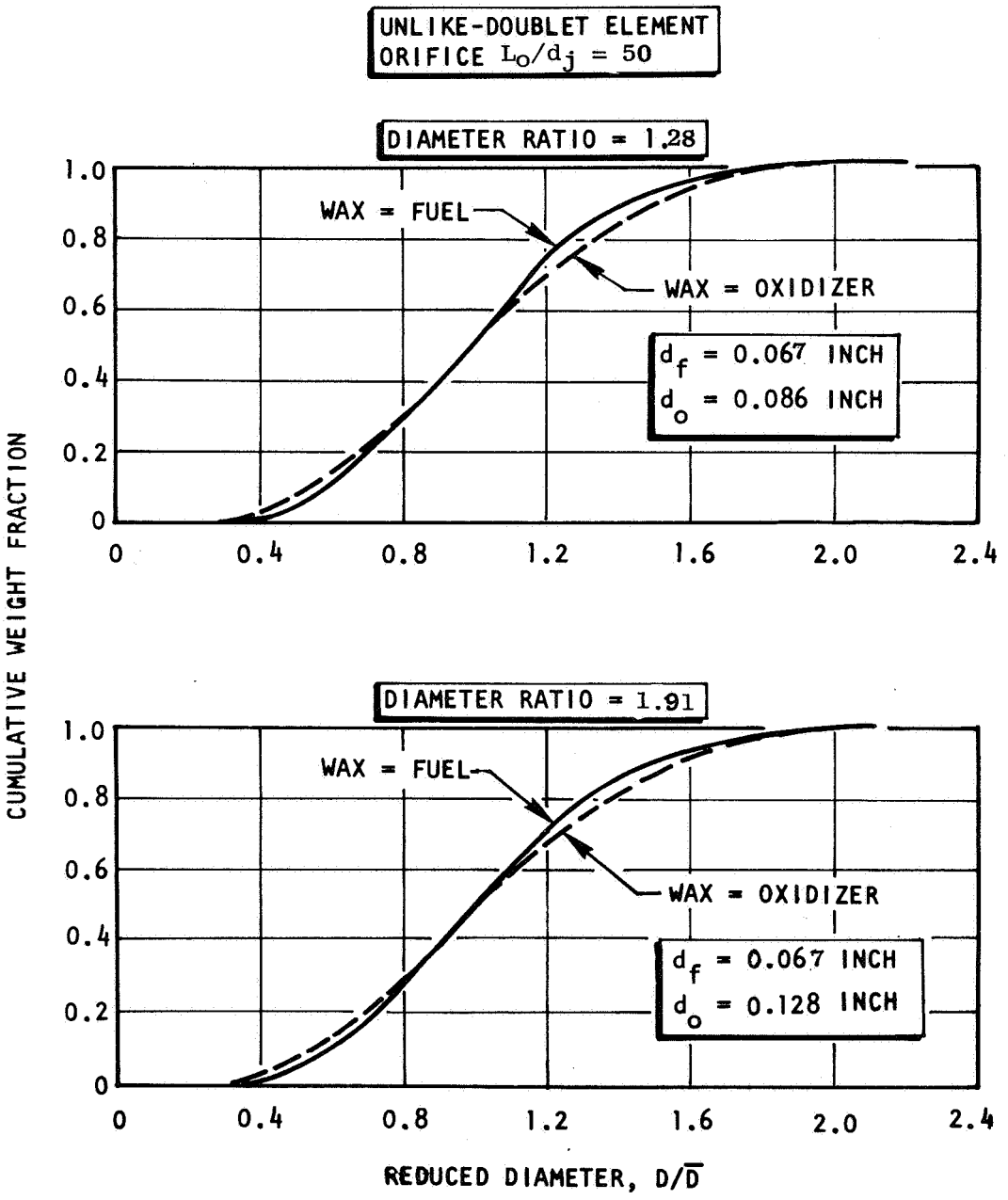

Figure 79. Fuel and Oxidizer Distribution Curves for Unlike-Doublet Elements Having Unequal Orifice Diameters

solution containing diethanolamine. The rationale leading to the selection of this fluid and its pertinent physical properties are presented in the discussion of propellant simulants, Section 3.2.

The study of propellant miscibility effects was conducted with both equal and unequal diameter, unlike-doublet elements. When equal diameter elements were used, two experiments were performed; in one, wax simulated both propellants (miscible impingement) while, in the second, wax was used as the fuel simulant and DEW as the oxidizer (immiscible impingement). In this manner, the influence of propellant miscibility on atomization can be ascertained by a direct comparison of the dropsizes obtained from each test. Two elements were used in this case; one was formed from 60-1.5-10R orifices while the 67-50-5R orifices comprised the second.

The experiments performed with the 1.5 L_o/d_j element were conducted at a constant total momentum flux of 9 ft-lbm/sec^2 while the dynamic pressure ratio was varied from 0.2 to 2.0. The test conditions and the results obtained from the immiscible, run numbers 105 to 112, and miscible impingement experiments, run numbers 113 to 116, are summarized in Table C2 of Appendix C. From the comparison of the mass median dropsizes previously presented on Fig. 68, it is apparent that a much larger dropsize is obtained when DEW, rather than wax, is used as the other propellant simulant.

The second set of equal diameter experiments were performed with a 50 L_o/d_j element over an injection velocity range of about 50 to 125 ft/sec. In these tests, the dynamic pressure ratio was held constant at unity; thus satisfying the criterion for optimum mixing. The results of the immiscible atomization experiments, run numbers 153 to 155, are given in Table C2 of Appendix C. In addition, three like-doublet experiments, run numbers 55 to 57 in Table C1, constituted the miscible atomization results. A comparison of the dropsizes obtained from the two sets of experiments is shown on Fig. 80. In contrast to the results obtained with the short element, these data indicate that, under the specific test conditions examined, the same size droplets are produced by miscible and immiscible impingement.

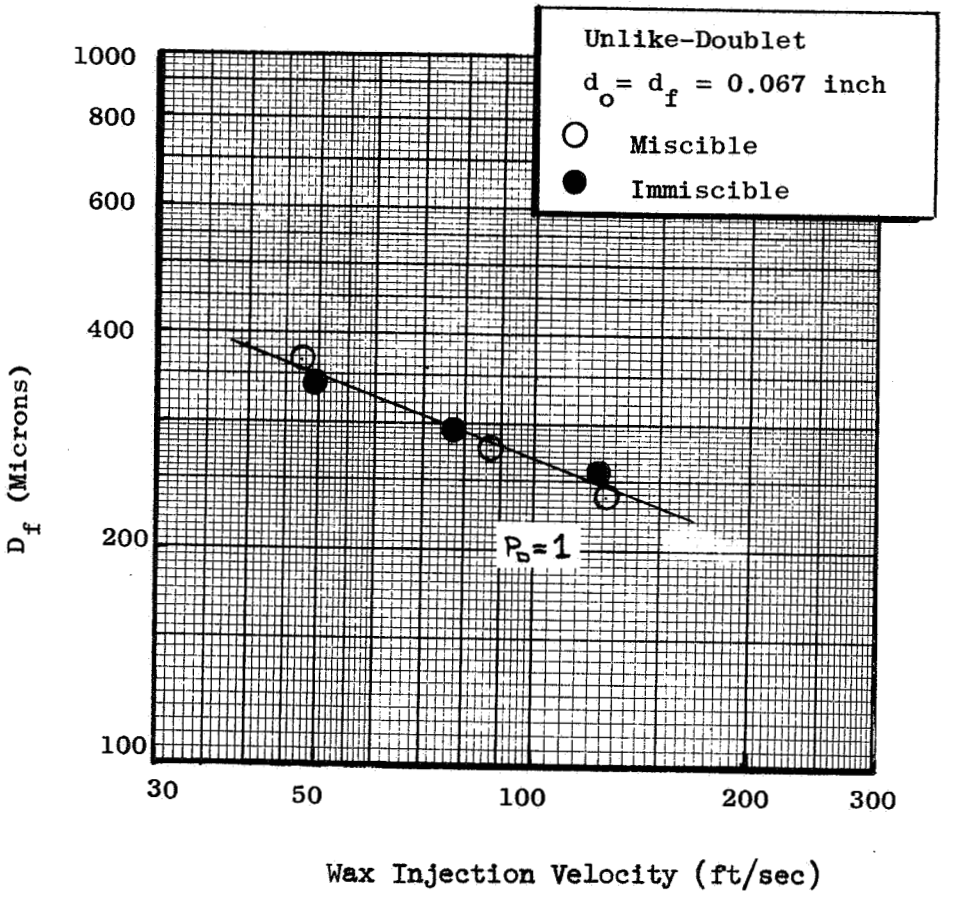

Figure 80. Comparison of Mass Median Dropsize for Miscible and Immiscible Impingement (L_o/d_f = 50)

In addition to the above, propellant miscibility effects were examined with unlike-doublet elements having diameter ratios of 1.28 and 1.91. These elements were formed from a combination of a 67-50-5R orifice with either an 86-50-5R or 128-50-5R orifice. With each element, molten wax experiments were conducted at nominal total momentum levels of 6, 20, and 40 ft-lbm/sec^2. In order to compare the dropsizes obtained from miscible and immiscible impingement at each momentum level, three separate tests were required. In two of the experiments, wax and DEW were alternately used to simulate the fuel and oxidizer. Combining the distributions obtained in the individual tests for the fuel and oxidizer dropsizes gives the total, mass-weighted distribution and mass median dropsize under conditions of immiscibility. This is accomplished by multiplying each point of the distributions of both the fuel and oxidizer by the wax flowrate divided by the total flowrate. The calculation procedure for obtaining the total dropsize and dropsize distribution is illustrated in Table 10.

For the case of miscible impingement, a third experiment was conducted utilizing molten wax as the simulant for both fuel and oxidizer. This experiment, which was conducted at approximately the same total jet momentum level as in the preceding immiscible tests, gives directly the overall distribution for miscible impingement.

The results of each experiment performed with the 1.29 d_o/d_f element, run numbers 162 to 167 and 174 to 176, and the 1.91 d_o/d_f element, run numbers 177 to 184, are presented in Table C2 of Appendix C. Insufficient freezing of the wax drops using the 1.92 diameter ratio element invalidated the data obtained at the low momentum level of 6 ft-lb/sec^2; hence, this data point was not included in Table C2. It should be noted that the experiments were not conducted under optimum mixing conditions ($P_d = d_o/d_f$).

The mass median dropsizes obtained with the unequal diameter ratio, unlike-doublet elements are shown in Table 11. The velocities in the table represent the average of the miscible and immiscible test velocities (experimental variation). As shown in Table 11, the mass median dropsizes $\bar{D}_1$ and $\bar{D}_2$ are

TABLE 10

CALCULATION PROCEDURE FOR OBTAINING TOTAL DROPSIZE DISTRIBUTION FOR IMMISCIBLE IMPINGEMENT

Sieve Size, microns	Run No. 8		Run No. 11		Total Weighted Fraction	$\overline{D}$ = 348 microns	
	Mass Fraction	Weighted Fraction	Mass Fraction	Weighted Fraction		Cumulative Fraction	$D/\overline{D}$
Pan	0.0005	0.00026	0.0008	0.00038	0.00064	--	--
88	0.0020	0.00104	0.0017	0.00081	0.00185	0.00064	0.253
105	--	--	0.0048	0.00230	0.00230	0.00249	0.302
125	0.0035	0.00182	0.0074	0.00354	0.00536	0.00479	0.359
149	0.0180	0.00938	0.0369	0.01768	0.02706	0.01015	0.428
177	0.0414	0.02157	0.0434	0.02079	0.04236	0.03721	0.509
210	0.1045	0.05444	0.1054	0.05049	0.10493	0.07957	0.604
250	0.1472	0.07669	0.1412	0.06763	0.14432	0.18450	0.719
297	0.2014	0.10493	0.1764	0.08450	0.18943	0.32882	0.854
354	0.2560	0.13338	0.1876	0.08986	0.22324	0.51825	1.017
420	0.1503	0.07830	0.1375	0.06586	0.14416	0.74149	1.207
500	0.0628	0.03272	0.1176	0.05633	0.08905	0.88565	1.437
590	0.0082	0.00427	0.0392	0.01878	0.02305	0.97470	1.696
710	0.0042	0.00219	--	--	0.00219	0.99775	2.040

different for each jet. It is interesting to note that the magnitude of the difference between the individual dropsizes is much greater for the larger diameter ratio element. However, the data were not obtained at flow conditions such that a direct comparison of the influence of diameter ratio or velocity can be made. Also included in the table for each test are the overall mass weighted average dropsizes for the entire spray. A comparison of the mass weighted immiscible and the miscible dropsizes indicates that, in these tests (50 L/D, $d_o/d_f > 1$), the use of DEW as a propellant simulant (i.e., immiscible jets) produced a smaller dropsize.

TABLE 11. COMPARISON OF MISCIBLE AND IMMISCIBLE DROPSIZES FOR UNEQUAL DIAMETER ELEMENTS*

d_1, inch	d_2 inch	Average V_1	Average** V_2	Immiscible			Miscible
				D_1, microns	D_2 microns	Mass Weighted $\bar{D}$, microns	$\bar{D}$ microns
0.067	0.086	54	41	443	434	438	453
		96	60	349	346	348	384
		131	93	274	294	285	302
0.067	0.128	40	34	558	591	583	---
		71	55	375	538	496	499
		101	83	272	448	405	457

*Immiscible and miscible experiments conducted at same operating conditions of velocity and mixture ratio.
**Average $V = (V_{miscible} + V_{immiscible})/2$

The dropsize distributions obrained with the 50 L_o/d_j equal and unequal diameter elements are shown on Figs. 81 to 83 for several momentum levels and for both immiscible (wax/DEW) and miscible (wax/wax) conditions. The data on Fig. 81 were obtained utilizing an equal diameter unlike-doublet at a dynamic pressure ratio of approximately one. In addition, since the orifice sizes are equal, the dropsize distribution determined for the orifice flowing wax is representative of the overall spray dropsize distribution.

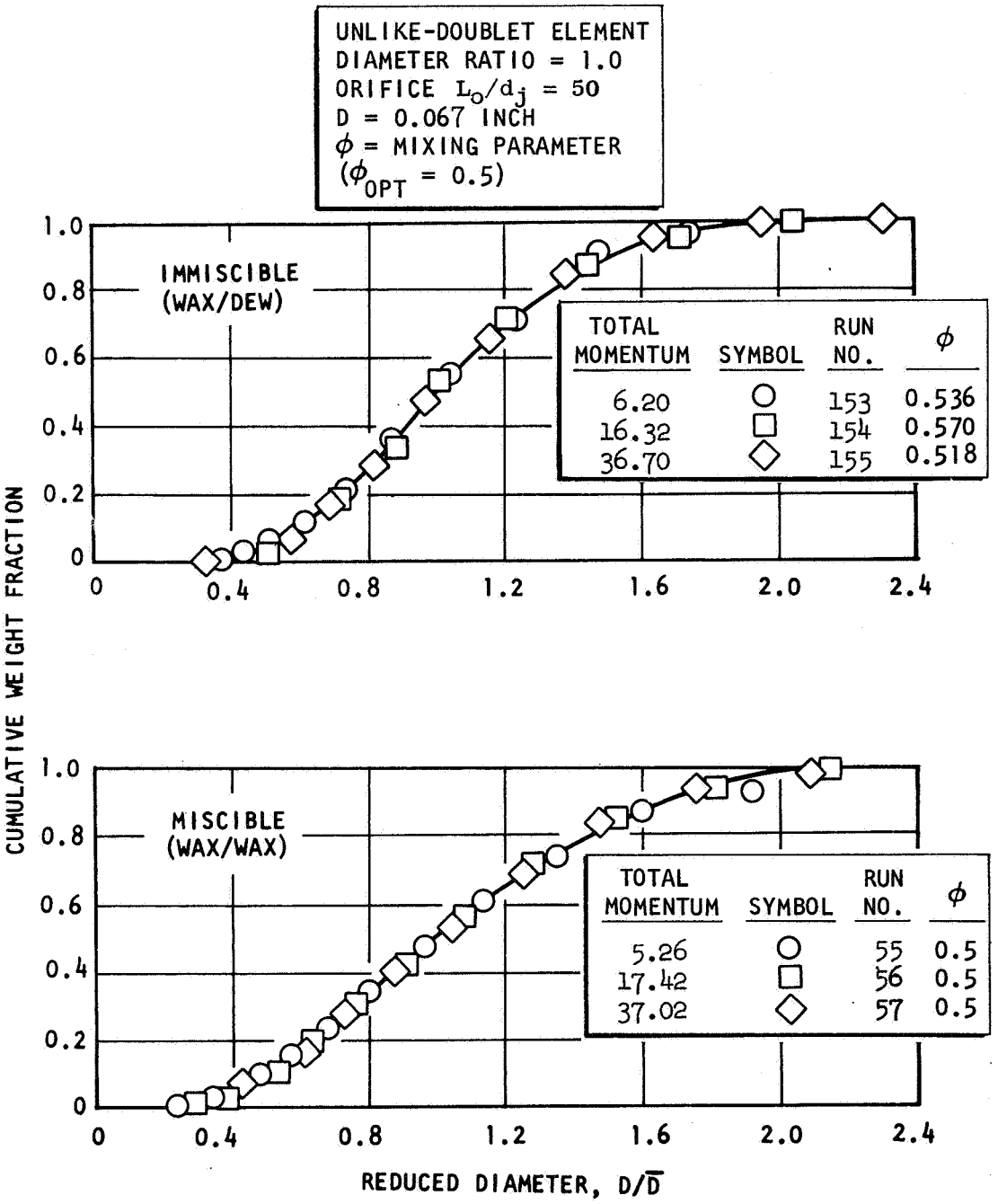

Figure 81. Normalized Distribution Curves for an Unlike-Doublet Element Having a Diameter Ratio of 1.0

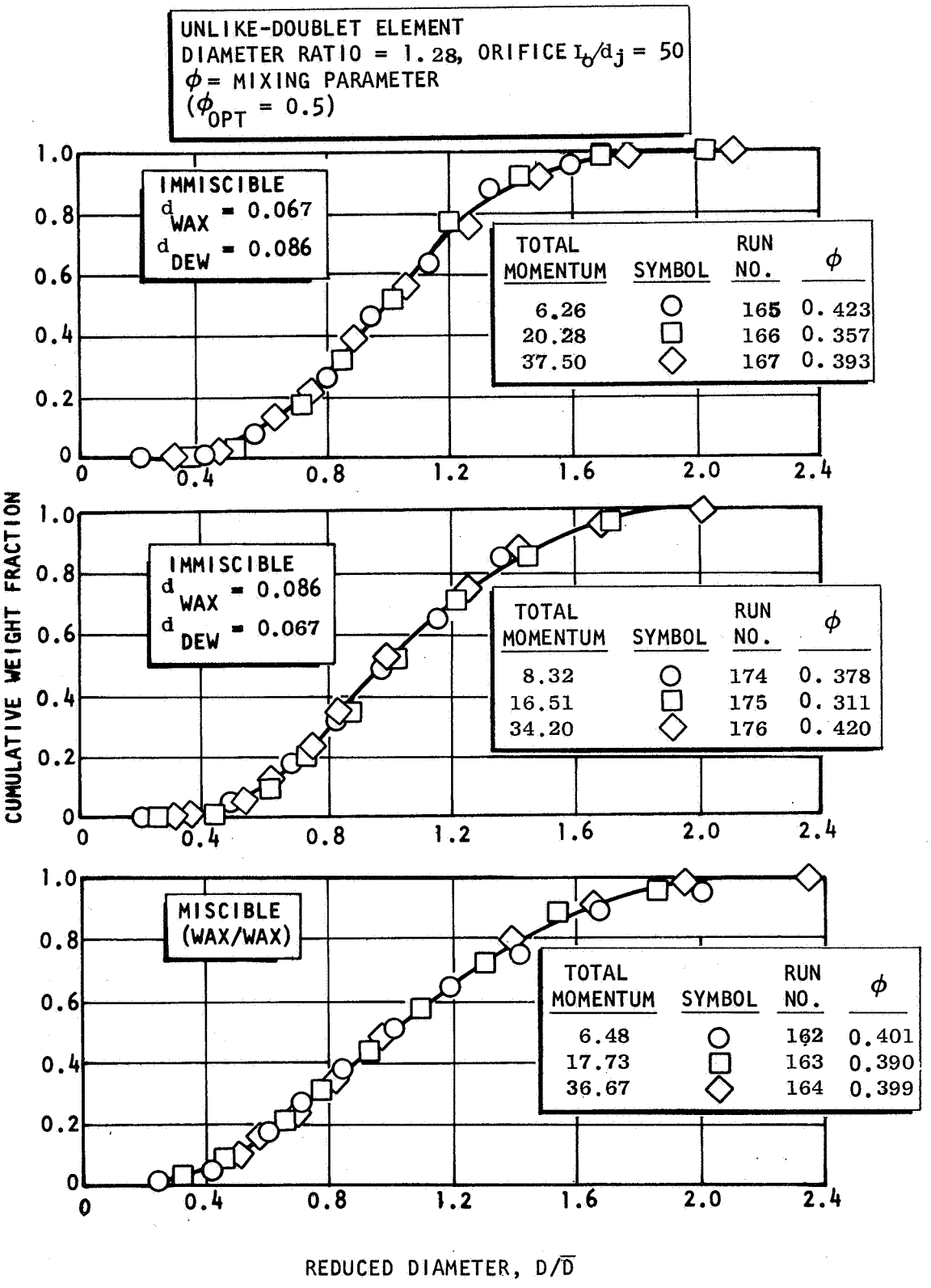

Figure 82. Normalized Distribution Curves for an Unlike-Doublet Element Having a Diameter Ratio of 1.36

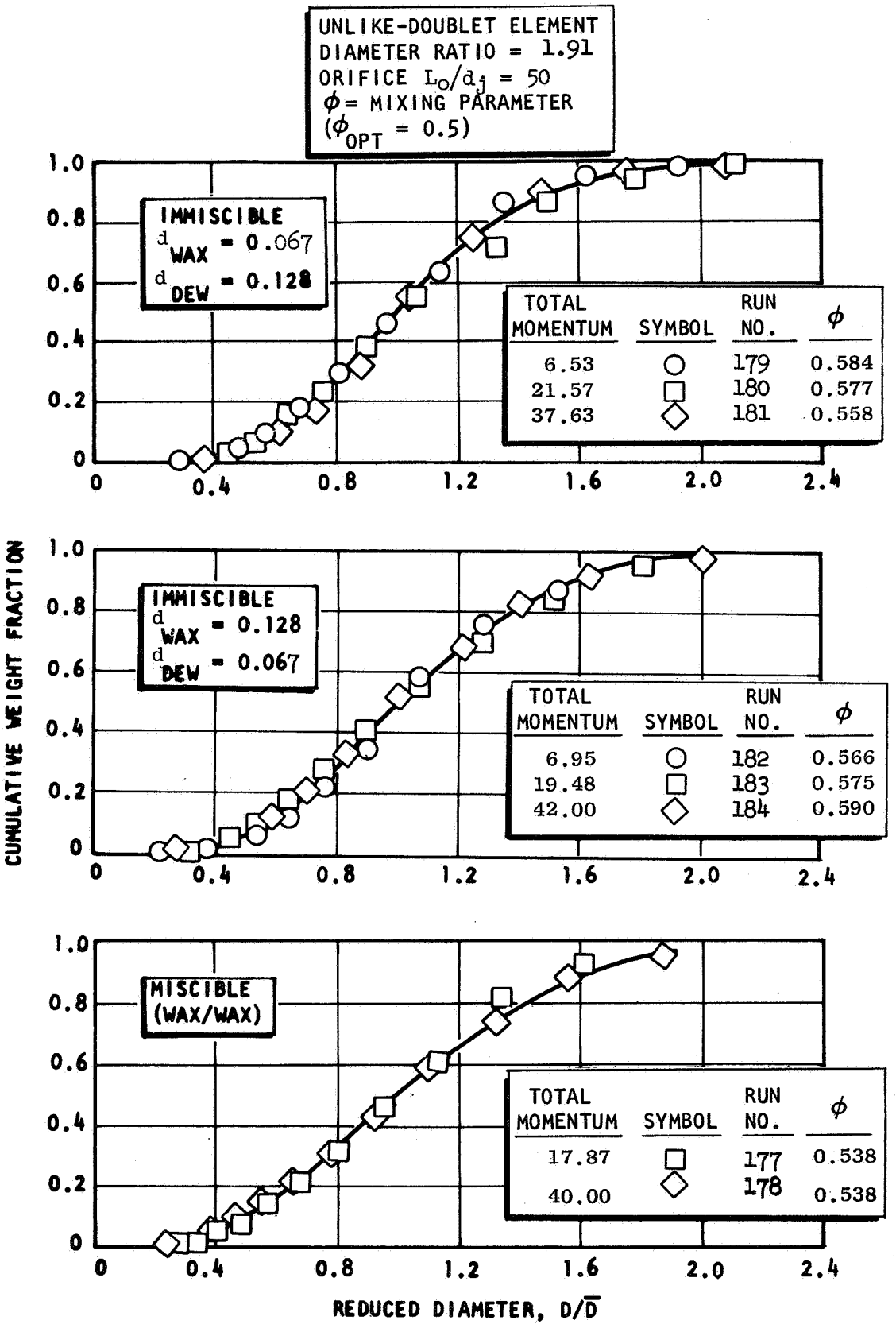

Figure 83. Normalized Distribution Curves for an Unlike-Doublet Element Having a Diameter Ratio of 2.03

The data presented for the 1.0 diameter ratio elements can be used directly to determine if miscibility has an effect on the dropsize distribution. In this case, it is only necessary to compare the distribution curves shown in the upper plot, obtained with wax flowing in one orifice and the immiscible fluid DEW in the other, with the lower curve obtained with wax flowing in both orifices. For the unequal diameter orifices (see Figs. 68, 69) it is first necessary to combine the distributions obtained from both the large and the small orifice to obtain an overall average distribution. This result can then be directly compared to the overall distribution shown in the lower curve obtained at near identical flow conditions and consequently nearly identical dynamic pressure ratio with wax flowing in both orifices. This was done for the 1.0 and 1.91 diameter ratio elements and the results are presented in Fig. 84. These results show that miscibility has an effect on the dropsize distribution. In addition, the condition of immiscibility results in a distribution closer to the monodisperse case (all droplets at one diameter) than does miscible impingement. It should be recalled however, that the unequal diameter experiments were conducted at non-optimum mixing conditions.

4.2.3 Triplet (2-on-1) Atomization Results

A series of 13 tests were conducted with a 50:1 L_o/d_j co-planar triplet element (i.e., two outer jets impinging on a central jet). The experiments were conducted over a range of injection velocities from 30 to 171 ft/sec using wax/water propellant simulants. This range was investigated because no data were known to exist for this type of element configuration. The orifice diameter ratio for these tests was constant at 1.0 ($d_f = d_{ox} = 0.067$ inch).

The test conditions and dropsize results from the triplet element are presented in Table C3 of Appendix C. The data are also presented as a function of the wax velocity on Fig. 85. The dashed line on the figure represents the slope of a pentad correlation developed in Ref. 14 while the equation number refers to a correlation evaluated in this program and presented in Section 5.2.3. The data show that almost identical dropsize versus velocity

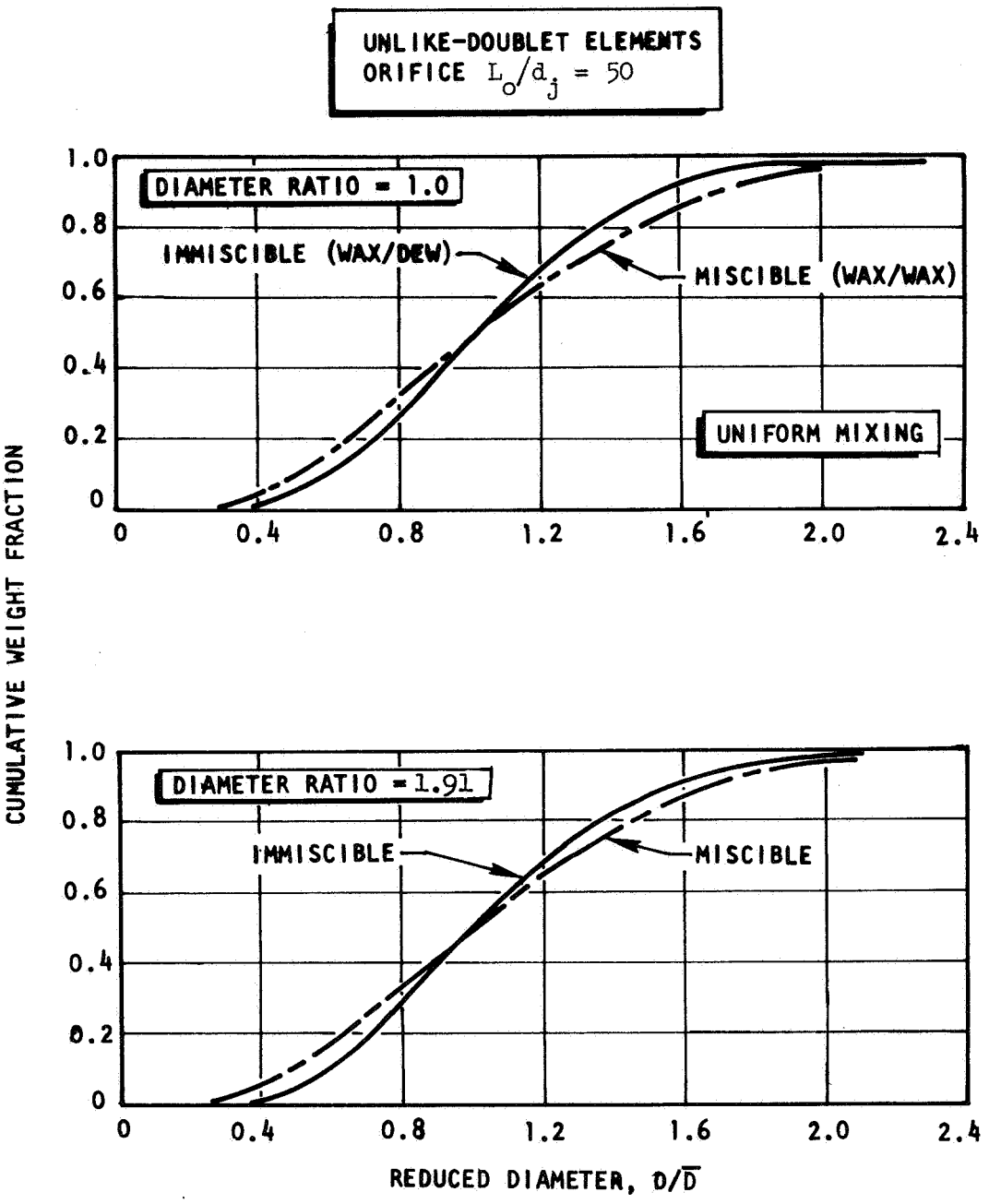

Figure 84. Normalized Distribution Curves for Miscible and Immiscible Impingement Using Unlike-Doublet Injection Elements

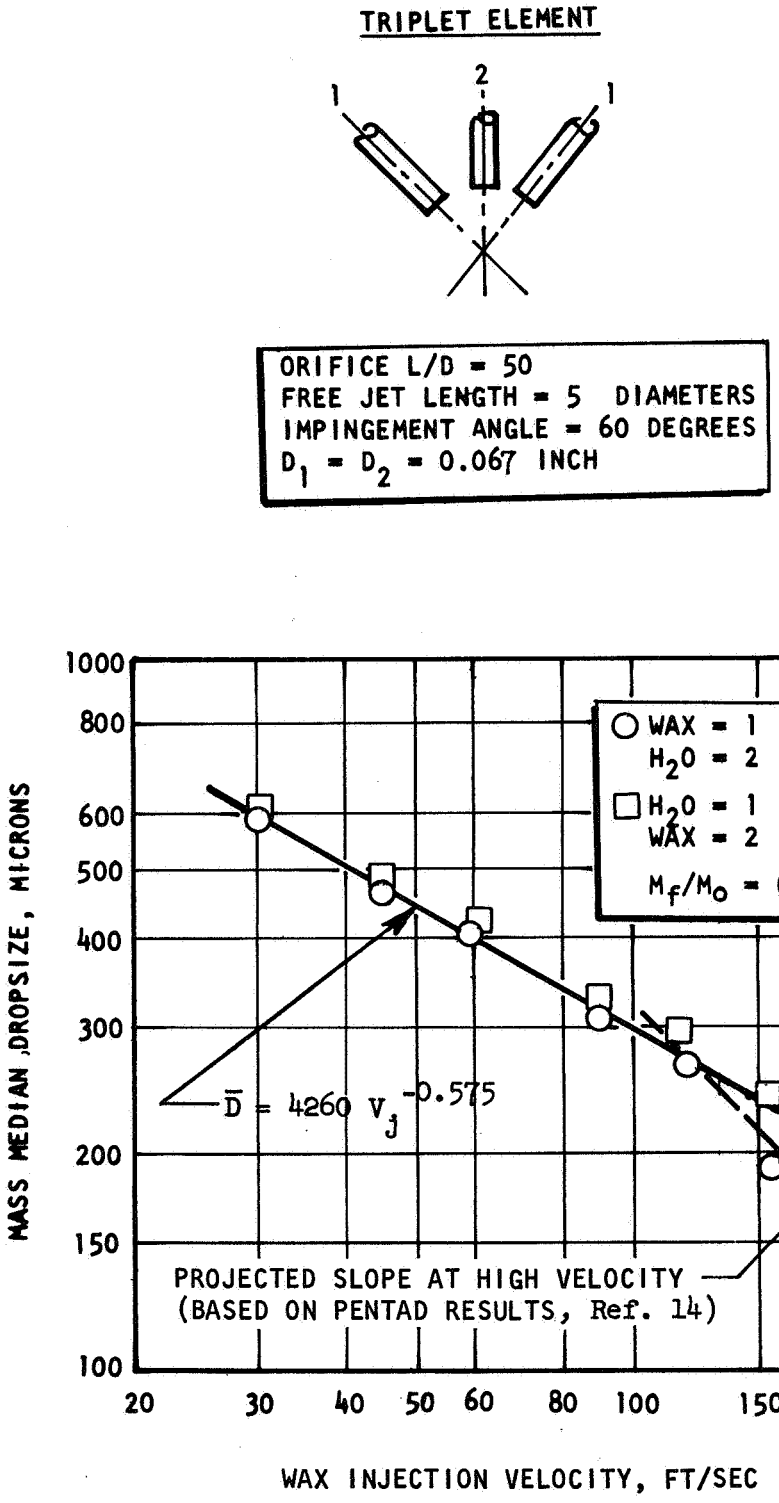

Figure 85. Mass Median Dropsize Versus Injection Velocity for a Triplet Element

relationships were obtained for both fuel (wax flowed through the central orifice) and oxidizer (wax flowed through the outer two orifices). This may be attributed to the fact that the two orifice diameters were equal and the injection velocities (computed on the basis of optimum mixing) are nearly equal.

Examination of Fig. 85 shows that the triplet element produced a linear dropsize-velocity relationship over the majority of the velocity regime investigated. A break in the curve is suggested; however, the exact point is not as well defined as those of the doublet elements.

4.2.4 Pentad (4-on-1) Atomization Results

Experiments were conducted with two pentad elements at nominal injection velocities of 30, 40 and 60 ft/sec. Both short (10:1) and long (50:1) orifice L_o/d_j elements were used. In each case, the central (fuel) orifice diameter was 0.086 inch. The oxidizer diameter for the short element was 0.063 inch and for the long element it was 0.067 inch. The orifice diameter ratios defined as d_{fuel}/d_{oxid}, were 1.365 for the short L/D element and 1.284 for the long L_o/d_j element. Molten wax and water were used as propellant simulants.

The results for the pentad element are presented in Table C4 and are plotted as a function of the wax injection velocity on Fig. 86. The tendency for the dropsize-velocity curve to steepen is again in evidence at injection velocities about 100 ft/sec. The correlations shown on Fig. 82 were developed in Ref. 14.

4.3 OCCURRENCE OF EMULSIFICATION

The objective of this study was to determine if an emulsion is formed at the interface of two jets flowing immiscible fluids. A detailed description of the experimental method for the quantitative determination of the extent of emulsification was given in Appendix B. Described below are (1) experiments conducted to verify that the quantitative measurements of emulsification were indeed the result of the amount of one propellant entrapped within a droplet of the other, and (2) the results of the emulsification experiments.

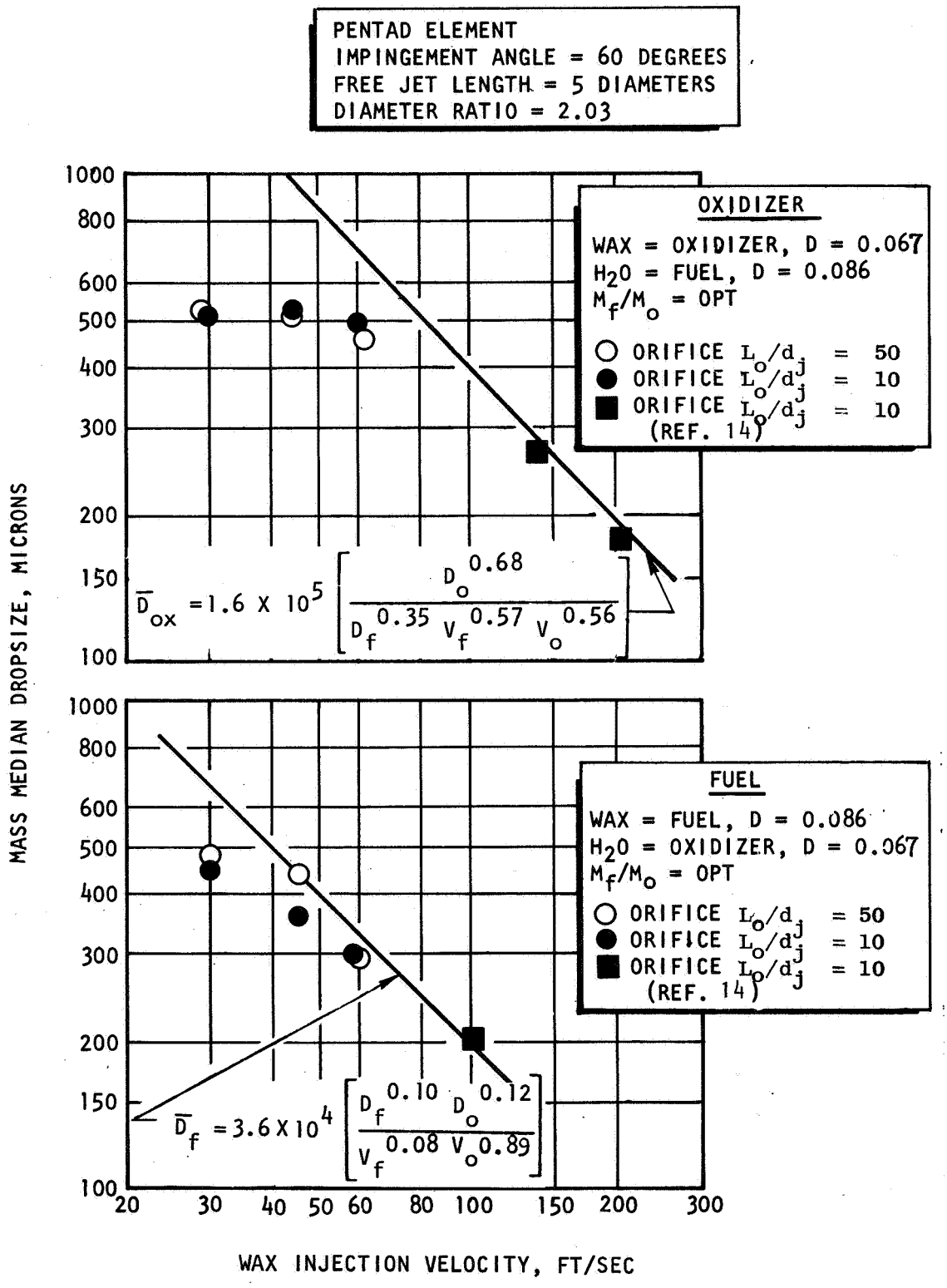

Figure 86. Mass Median Dropsize Versus Injection Velocity for a Pentad Element

Verification Tests

Molten wax and the diethanolamine-water (DEW1) mixture were used as propellant simulants in this study. The frozen wax particles resulting from unlike element tests were collected and thoroughly washed in water to remove any traces of diethanolamine (DEA) which might have adhered to the outside of the spherical particles. The quantity of remaining DEA contained in the wax was determined by mixing the wax with an equal amount of water, heating the mixture to the melting point of the wax, and allowing the mixture to separate. The amount of DEA originally included in the wax was then determined by a chromatographic analysis of the DEA-water mixture. A question was raised as to the effectiveness of the removal of DEA from the surface of the droplets. As discussed below, the amount of DEA measured was small and consequently small amount of DEA left on the surface of the droplet would have a large effect on the interpretation of the results. A controlled test was therefore conducted wherein wax droplet uncontaminated with DEA (formed from wax on wax impingement) were subjected to a DEA-H_2O solution for a period of 12 days. The droplets were then given the identical washing procedure as that for the emulsification tests. The wax was then subjected to chromatographic analysis to determine the amount of DEA in the droplets. The procedure employed in performing this analysis is presented in Appendix B. The results of the analysis showed that no detectable amount of DEA was present in the washed sample. This result verifies that the experimental procedure for washing of the wax droplets is sufficient to remove the DEA from the surface. Therefore, any DEA that is measured in subsequent experiments was indeed entrapped within the wax droplet and not on the surface.

Qualitative Measurement of Emulsification

Experiments were conducted to determine the emulsification characteristics over a range of momenta level employing both an unlike doublet and unlike pentad element injector. The unlike-doublet element incorporated a 1.28 diameter ratio, and the 4-on-1 pentad element had a d_{fuel}/d_{oxid} of 1.91 (four outer oxidizer streams impinging on a central fuel stream).

A total of six tests were conducted; three each for the two injector types. The experiments were conducted over a total injected momentum level of from about 7 to 50 ft-lb_m/sec^2.

The tests were conducted at nominal fuel/oxidizer momentum ratios of 0.42 and 0.98 for the unlike-doublet and pentad elements, respectively. The latter value roughly corresponds to the condition of optimum mixing for the pentad (optimum value = 0.82) whereas for the unlike doublet, due to a calculation error, the flow conditions were significantly off the optimum value of 0.73.

The data are summarized in Table C5 of Appendix C.

The results presented on Fig. 87 show a nominal level of 1-percent DEW1 imbedded in the wax droplets for both the unlike doublet and pentad elements. A repeat chromatographic analysis of the unlike-doublet droplets obtained at a total momentum of 20 ft-lb/sec^2 indicated a repeatability of ±25 percent from the mean. Using this error band, the amount of emulsification would appear relatively constant over the range of total momentum examined in this study.

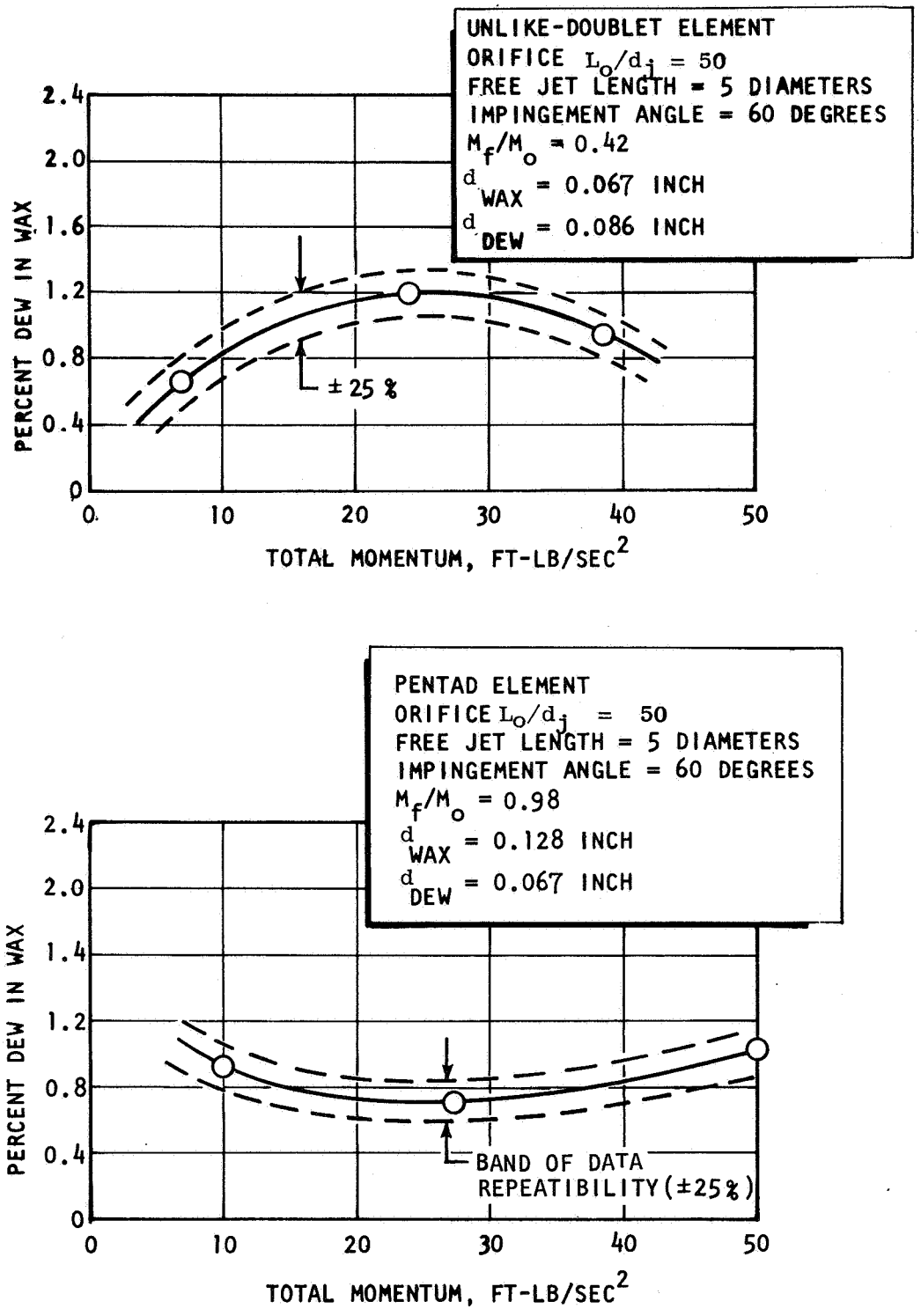

Figure 87. Percent DEW in Wax Versus Total Momentum for Unlike-Doublet and Pentad Elements

5.0 DISCUSSION OF RESULTS

The discussion of the results obtained in this study is divided into three sections: (1) the internal characteristics of the free jets and the influence of the geometry of the orifice producing these jets, (2) the influence of the variables examined in this study on the mass median dropsize, and dropsize distribution, and (3) the occurrence of emulsification.

5.1 FREE JET CHARACTERISTICS

The internal characteristics of liquid jets were found to influence atomization. In order to account for these effects in the design of injection systems, it is desirable to be able to determine a priori the characteristics of the jets over the range of injector operating conditions. This requires a knowledge of where transition from laminar to turbulent flow could occur, the extent of velocity profile development, the effect of manifold and orifice entrance conditions, and the variations of jet properties between the orifice exit and the impingement point.

It is well known from theoretical fluid mechanics that flow fields which are geometrically similar and which have identical initial conditions, are also dynamically similar if the Reynolds numbers are equal. The initial conditions are here considered to be those existing at the orifice entrance. In the current study, the entrance condition for most of the orifices examined was quiescent or near-quiescent. Because of the similarity of the entrance conditions, the jet characteristics at the orifice exit are a function of the orifice length and jet Reynolds number only.

However, in many rocket engine injection systems, a cross-flow exists at the orifice entrance and the assumption of static conditions at the entrance is not valid. The entrance effects will have a direct bearing on the Reynolds number of transition from laminar to turbulent flow within the orifice and will influence the velocity profile for some distance into the orifice. In

this case, the manifold Reynolds number and orifice entrance type as well as the orifice Reynolds number and length will contribute to the jet characteristics.

When the jets impinge at some distance from the orifice exit, variation of the free jet characteristics over this length and, in particular, the onset of jet disintegration will effect atomization. While it was not a specific objective of this program, some data on the influence of free jet length on jet characteristics were obtained.

The discussion of jet characteristics and their relation to: (1) Reynolds number and orifice length, (2) orifice entrance condition, and (3) free jet length is presented below.

5.1.1 Influence of Reynolds Number and Orifice Length on Jet Characteristics

The Reynolds number was perturbated by variations of orifice diameter and injection velocity. For the geometrically similar orifices ($1.5\ L_o/d_j$, d_j = 0.060, 0.090 and 0.120) the velocity profiles and the variation of profile with injection velocity were shown to be identical when compared at equal Reynolds numbers, demonstrating the validity of the assumption of dynamic similarity. Consequently, the velocity profile within a jet of any other fluid produced by an orifice geometrically similar to these (or any of the quiescent entrance orifices examined) can be deduced from the measurements presented in Section 4.1.

When the flow is in the laminar regime, the velocity profile at the exit plane of the orifice is a function of the orifice length as well as the Reynolds number. There are a number of theoretical solutions available to predict the velocity profile of laminar streams as a function of the orifice length and the Reynolds number of the flow. Two of these solutions, due to Langhaar, Ref. 26, and Boussinesq, Ref. 27, are shown on Fig. 88. The solutions are presented in terms of the variation of the centerline pressure ratio, p_c/p_j, with the combined non-dimensional parameters $(L_o/d_j\ N_R)$.

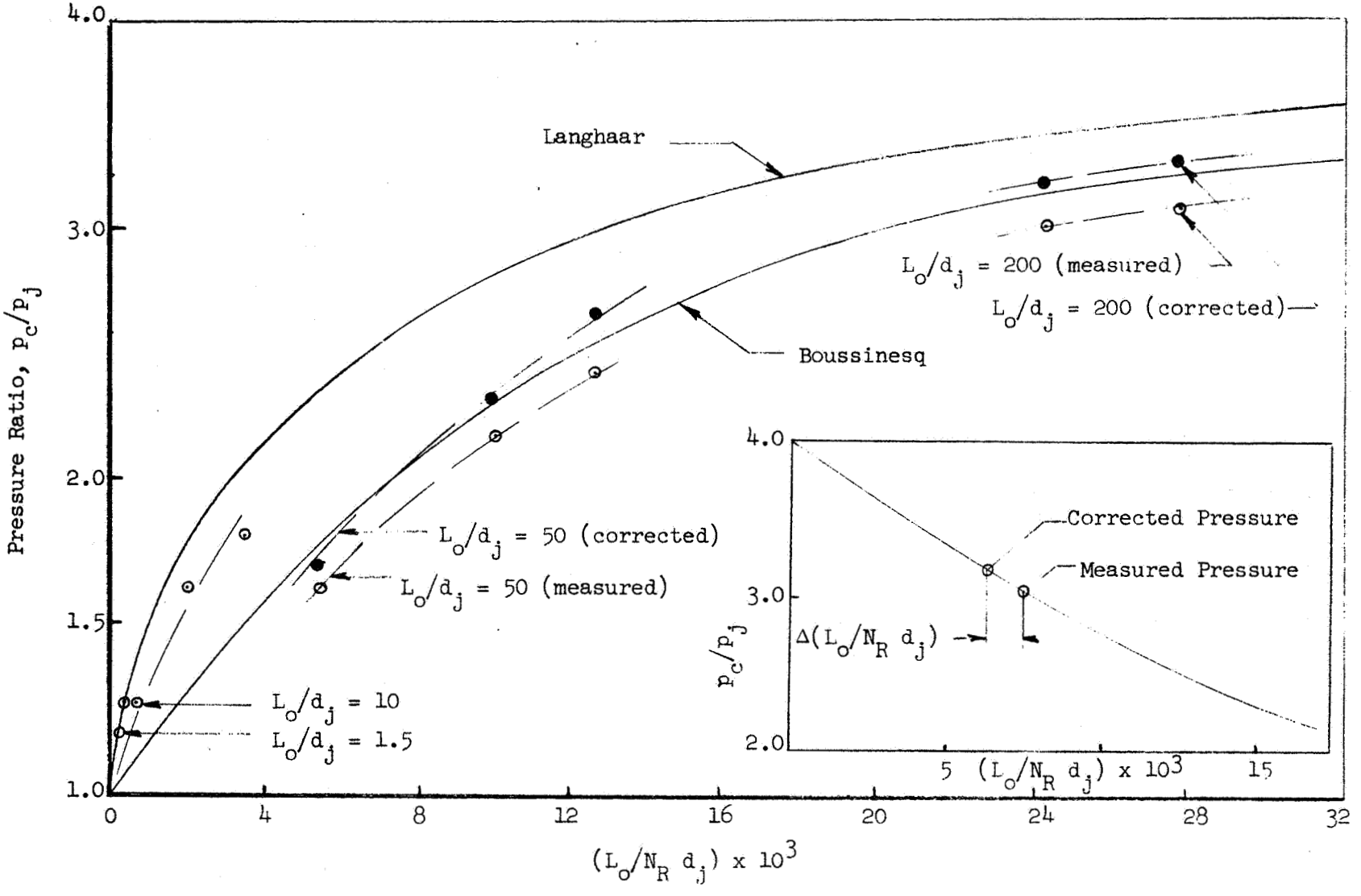

Figure 88. Comparison of Theoretical and Measured Centerline Pressure Ratios

The measured centerline pressure ratios for $N_R < 10{,}000$ obtained in this study are also shown on Fig. 88. As is readily seen, the pressures measured with the 1.5 and 10 L_o/d_j orifices fall within the range of theoretically predicted values. However, the centerline pressure ratios of the jets produced by the longer orifices are below the predicted range. The reason for this is that when substantial velocity profile development has occurred, a significant profile decay will occur even within short free jet lengths. If it is assumed that, at a given N_R, the profile decays in a manner inverse to the way it develops at the same Reynolds number, the measured centerline pressures can be corrected to the value existing at the orifice exit.* As shown on Fig. 88, the corrected pressure ratios for the 50 and 200 L_o/d_j orifices agree quite well with the theoretical solution of Boussinesq.

In turbulent flow, the velocity profile cannot be analytically determined as a function of orifice length. However, because of the interchange of momentum between streamlines in the turbulent fluid, the profile does not experience much development, attaining a maximum value of about 1.5 for the pressure ratio in a fully developed jet. It was found that an orifice length of 50 d_j was sufficient for the establishment of fully developed turbulent flow. Furthermore, the atomization tests indicated that the turbulent profile had a small effect on dropsize. Consequently, for the determination of dropsize, the turbulent profile can be considered to be uniform in velocity.

---

*Shown as an insert in Fig. 88 is the inverse of the solution obtained by Boussinesq. The curve represents the decay in the centerline pressure of a fully developed laminar jet with the non-dimensional jet length, $L_j/d_j N_R$. To illustrate the calculation procedure, assume that the measured centerline pressure is 3.0. This point is then located on the curve at a value of $L_j/d_j NR \times 10^3 = 7.5$. If the free jet length was 5 at a jet Reynolds number of 5000, the jet will have experienced decay over a non-dimensional free jet length of 1. Consequently, the pressure existing at the orifice exit is located on the curve at the point $L_j/d_j NR \times 10^3 = 6.5$.

The velocity above which laminar flow can cease to exist defines the upper critical Reynolds number. The lowest value that has been observed for this Reynolds number is 2300. In general, it is a function of the surface roughness, entrance conditions, surroundings, etc. For example, in rough tubes with controlled entrance conditions, an upper critical Reynolds number of 13,000 has been observed.

In this study, laminar flow was obtained with the 1.5 and 6 L_o/d_j orifices over the entire range of Reynolds numbers examined (up to $N_R < 15{,}000$). When the length of the orifice was 10 d_j, turbulence at the center of the jet was initially measured at a Reynolds number of 10,000. In the case of the 50 and 200 L_o/d_j orifices, an abrupt transition from laminar to fully developed turbulent flow occurred at about this Reynolds number. Since the method of fabrication and the material of these orifices are similar to rocket engine injectors, the transition from laminar to turbulent flow within operational, rounded entrance injectors with nearly quiescent entrance conditions can be presumed to occur at a Reynolds number of about 10,000. The importance of the qualification of nearly quiescent entry conditions in the above statement cannot be overemphasized. If this condition is not attained, turbulent flow will most probably exist at much lower Reynolds numbers.

5.1.2 Influence of Orifice Entrance Conditions on Jet Characteristics

The hydraulic and geometric conditions existing at the entrance to the orifice were found to have a pronounced effect upon the internal characteristics of the free jet. The specific geometrical conditions examined included sharp and round entrance orifices and the orifice manifold types illustrated on Fig. 16. The hydraulic conditions included the injection velocity and the manifold cross-velocity.

For the manifold type shown on Fig. 16a, the jet characteristics were examined as a function of injection velocity. When well rounded orifices were used, the inlet Reynolds number was less than 2300 when transition to turbulent flow

occurred in the jet. Since the inlet flow was definitely laminar, the origin of the turbulence was within the orifice. One exception to this was obtained with the like-doublet element No. 63/63-10-3LD (Fig. 27). In this case, the inlet Reynolds number was about 2900 and the inlet flow could conceivably have been turbulent. Thus, the origin of the jet turbulence may have been the entrance tube. It is interesting to note that the level of turbulence measured with this orifice was on the order of that obtained with a fully developed jet and more than five times greater than what was obtained with the L_o/d_j orifice No. 63-10-7R (also shown on Fig. 27).

When a sharp-edged orifice was used in conjunction with quiescent entry conditions, both the DEW (measured) and the wax (visual observation) jets were found to completely separate from the orifice walls. (This was observed with orifice L_o/d_j's up to 10. Longer, sharp-edged orifices were not examined.) The Reynolds number at separation ranged from 3300, for the 2 L_o/d_j, to 4500, for the 10 L_o/d_j orifice, for both fluids. However, these results cannot be generalized on the basis of Reynolds number since the fluid vapor pressure* will also govern the separation point. Jet separation becomes more likely to occur whenever the Reynolds number or fluid vapor pressure is increased. As will be noted later in this section, the manifold condition will also influence the occurrence of separation.

For the manifold type shown on Figs. 16b and 16c, the jet characteristics of both round and sharp entrance orifices were examined as a function of cross-velocity** while the orifice velocity was held constant. The length of the orifices in these experiments ranged from 6 to 100 diameters with a manifold

---

* Vapor pressure data was not available for either fluid.

**It should be recalled that the cross-velocity is defined as the velocity downstream of the orifice. For an orifice velocity of 120 ft/sec there is a difference of 1.67 ft/sec between the inlet and exit manifold velocities.

cross-flow from 0 to 20 ft/sec in velocity imposed for each combination of entrance type and L_o/d_j. Measurements of the characteristics of jets produced by orifices less than 6 d_j in length were attempted. However, the occurrence of jet disintegration precluded an accurate measurement of the turbulence and velocity profiles. The orifice velocity was 120 ft/sec, corresponding to a Reynolds number of 10,740.

Since the orifice Reynolds number was above 10,000, the existence of turbulent flow within the orifice was consistent with the results obtained with the manifold type shown on Fig. 16a. When the cross-velocity was zero, the Reynolds number upstream of the orifice was about 1500, which is below the minimum upper critical Reynolds number of 2300. Thus, as in the case of the manifold type shown on Fig. 16a, the orifice inlet flow was within the laminar regime. However, there was a basic difference in the orifice inlet flow for the two manifold types. In one case, the inlet velocity vector was parallel to the orifice axis while, in the other, it was orthogonal.

The results obtained with the two manifold types (at zero cross-velocity) and with round-entrance orifices were compared on Fig. 37. It is seen from this figure that the direction of the inlet velocity vector exerts an influence on the jet characteristics, particularly the turbulence level, when the orifice length is short; even though the magnitude of the inlet velocity is on the order of only 2 ft/sec. As would be expected, the inlet effect is damped as the length of the orifice is increased. Beyond an L_o/d_j of about 20, inlet effects were not discernible and identical jet characteristics were measured for both manifold types.

The results obtained with a sharp-edged orifice using a cross-feed manifold are also shown on Fig. 37. When compared to the round entrance orifice data (using the same manifold type), it is seen that much greater turbulence levels and lower centerline pressures were obtained with sharp entrance orifices. Above an L_o/d_j of about 25, orifice entrance effects were not discernible and identical jet characteristics were measured. In contrast to the sharp

entrance data obtained with parallel-feed manifolds (Fig. 34), jet separation over the entire orifice length was not attained with this combination of orifice entrance and manifold type in the L_o/d_j range examined (i.e., 6 to 100). This result is directly attributable to the direction of the inlet velocity. In the case of a parallel-feed manifold, the orifice entry flow is symmetric about the orifice axis and detached from the orifice wall in the proximity of the entrance. Whether or not the flow remains separated along the entire orifice length depends upon the Reynolds number, fluid properties and orifice L_o/d_j ratio. When a cross-feed manifold system is used, the entry flow is biased in the direction of the cross velocity vector. This bias leads to a displacement of the jet from the orifice axis in a direction parallel to the cross velocity, i.e., towards the orifice wall. While the flow can also be detached near the entrance in this case, the fluid momentum orthogonal to the orifice axis causes the flow to re-attach on one side thereby prohibiting completed detached flow.

With L_o/d_j's less than 6, complete separation could occur but this was not investigated. The influence of the transverse flow on the free jet characteristics will diminish as the orifice length is increased but, as is apparent from the non-symmetrical turbulence profile shown on Fig. 41, it is still felt at an orifice length of 10 d_j.

The primary effect of increasing the manifold cross-velocity was an exaggeration of the difference between the characteristics of the jets produced by the two manifold types. That is, as the cross-velocity was increased for a given orifice length and entrance type, the jets became more turbulent and a slight non-symmetry of the jets became apparent at the shorter orifice lengths. It was found that an orifice length of about 15 for round orifices and 25 for sharp was required to damp manifold effects regardless of the magnitude of the cross-velocity.

5.1.3 Influence of Free Jet Length on Jet Characteristics

When the length of the free jet is increased, two changes in the jet characteristics occur. The first is that the velocity profile becomes more uniform. Rupe, Ref. 23, experimentally showed that the profile of a laminar jet decays in a manner inverse to the way it develops. This fact was utilized previously in correcting the measured profile to that which would exist at the orifice exit. In this study it was found that the existence of turbulence within the free jet will result in a more rapid relaxation of the profile. For example, the pressure profiles of the laminar jets obtained with the 1.5 L_o/d_j orifice were invariant with free jet length. On the other hand, with the turbulent jets produced by geometrically identical orifices, a decrease in the centerline pressure ratio with free jet length was observed.

The second change that occurs is in the level of turbulence, which appears to increase with free jet length. Even for those cases where no measurable turbulence could be found at short free jet lengths (high velocity laminar jets, Fig. 20), pressure fluctuations were detected at lengths of 10 d_j. This apparent increase in the turbulence level is, in reality, a result of the oscillation of the jet about a fixed point, i.e., the probe, and thus corresponds to the "turbulence" which would be seen at the impingement point of two or more jets. These same oscillations contribute to the disintegration of the free jet.

The free jet length at which jet disintegration will occur was not fully established in this program. For the turbulent jet produced by the 50 L_o/d_j orifice, the turbulence measurements shown on Fig 33 indicate that, at an injection velocity of 100 ft/sec, disintegration occurred at a free jet length of about 5 d_j. For the turbulent jet produced by the 1.5 L_o/d_j orifice, the observed widening of the jet (see e.g., Fig. 25 or Fig. 26d) between the free jet lengths of 5 and 10 d_j could be interpreted as the onset of disintegration. Although these results are inconclusive, disintegration of turbulent jets above a free jet length of 5 d_j would appear to be a likely possibility and

should be a consideration in injector designs. With a laminar jet, disintegration did not occur within a length of at least 10 d_j.*

5.2 ATOMIZATION CHARACTERISTICS

The successful design of rocket engine injectors depends upon a thorough knowledge of the influence of injector and hydraulic operating conditions on atomization. The objective of this program was to examine a variety of the parameters that may influence atomization and obtain useful correlations for predicting the resulting dropsizes. These empirical correlations can then be utilized for the analysis of rocket engine performance characteristics.

An empirical correlation is, in essence, the experimental evaluation of the solution to the equations governing the atomization process. As such, it requires a knowledge of the parameters that would effect the solution, though not the exact form of the relationship between these parameters. This knowledge can be deduced from an examination of the physical processes.

From a fluid mechanic viewpoint, the complete atomization process occurs in several distinct phases beginning at the orifice entrance and ending with the formation of droplets. These phases are (1) the flow development through the orifice, (2) the interaction of the free jet with the surrounding atmosphere, (3) jet impingement and sheet formation, (4) the disintegration of the sheet into ligaments, and (5) the breakdown of the ligaments into droplets.

---

*Photographs presented in Ref. 23 show that fully developed laminar jets (N_R = 1395 and 2128) will disintegrate quite violently at L_j/d_j's above about 40 while nearly uniform velocity, laminar jets (N_R = 49,122 and 98,296) will remain relatively stable for a considerable distance (to an L_j/d_j of 50 or more). The photographs of fully developed turbulent jets (N_R = 52,789 and 105,589) illustrate substantial disturbances on the surface of the free jet but the onset of jet disintegration is not readily discernible.

Generally, theoretical and experimental interest has been centered on occurrences downstream of the impingement point. Analytic solutions have been obtained for this regime by employing specific simplifying assumptions (see e.g., Refs. 9 and 10). In an experimental investigation, one must supplement theory with physical and intuitive reasoning in order to select those parameters which can influence atomization. Essentially, this amounts to a specification of the parameters that would define the initial and boundary conditions required to obtain a solution to a generalized mathematical formulation of the phenomena.

For example, the initial conditions at the impingement point would be described by the number of jets, n, involved in the sheet formation, the velocity profile, V(r) and turbulence profile, T(r) (where r is the radial position measured from the jet center)*, of each jet and a set of parameters specifying the geometrical arrangement of the jets with respect to some coordinate system. The latter could be the angle, γ, between the jet axis and a fixed plane and the distance, Δ, from the origin of the coordinate system (which can be the impingement point) to the intercept of the jet axis with this plane. The above, together with the fluid physical properties, would be sufficient to uniquely describe the sheet formation. Subsequent sheet motion and disintegration would depend upon these parameters and, in addition, occurrences at the sheet interface with its surroundings. Thus, to complete the formulation of the problem, the dynamic and physical properties of the atmosphere around the sheet must be specified. In general then, one would expect the solution of the problem to be a function of the form

$$\overline{D} = \overline{D}\left[(V(r),\ T(r),\ \gamma,\ \Delta,\ \rho,\ \sigma,\ \mu)_{i=1,\ldots n},\ (V,\ p,\ \rho,\ \sigma,\ \mu)_{ATM}\right] \quad (1)$$

*This, of course, assumes cylindrically symmetric jets.

The utilization of the velocity and turbulence profiles, per se, is not essential to the development of an empirical correlation and, for convenience, they can be replaced by a set of parameters which describe the overall characteristics of the profiles. For example, the velocity profile can be characterized by the mean velocity, V_j, the maximum velocity (or equivalently, the centerline velocity, V_c, in circular jets), and a geometric scale factor which can be taken to be the jet diameter, d_j. Similarly, the turbulence intensity profile can be described by a characteristic turbulence level, e.g., the level at the jet center, T_c, and the jet diameter. Atmospheric properties were not varied in this program and these parameters may be deleted from an empirical correlation. Thus, Eq. (1) can be reduced to

$$\overline{D} = \overline{D}\left[(V_j,\ d_j,\ V_c,\ T_c,\ \gamma,\ \Delta,\ \rho,\ \mu,\ \sigma)_{i=1,\ldots n}\right] \qquad (2)$$

From dimensional analysis, it can be shown that a number of parameters can be reduced by an amount equivalent to the number of independent dimensions, i.e., mass, length and time. This analysis also shows that one set of dimensionless parameters would be the Reynolds number, $\left[\frac{\rho V_j d_j}{\mu}\right]_1$, the Weber number, $\left[\frac{d_j V_j^2}{\sigma}\right]_1$, and, $\left(\frac{V_c}{V_j}\right)_{j\,1}$ and $\left(\frac{\Delta}{d_j}\right)_{j\,1}^{*}$ for one of the jets, with the parameters of the remaining jets normalized by the appropriate parameter of the first jet, i.e., $\left(\frac{V_{j_2}}{V_{j_1}}\right)$, $\left(\frac{d_{j_2}}{d_{j_1}}\right)$, etc.

*The angle, γ, is dimensionless.

For the present purpose, it is more convenient to slightly modify the dimensionless quantities presented above in order to utilize the parameters actually measured experimentally. For example, instead of V_c/V_j, the dimensionless pressure, p_c/p_j is used and, similarly, ψ_c/p_j, in place of T_c/V_j. The dynamic pressure ratio, $P_{D_i} = (\rho V^2)_i/(\rho V^2)_1$, is also chosen in place of the velocity ratio $(V_j)_i/(V_j)_1$. Finally, since the Reynolds and Weber numbers were varied primarily by perturbations of velocity and diameter, these nondimensional parameters are replaced by the dimensional quantities, V_j and d_j. Hence, for the experimental study performed here, the parameters that should be included in any empirical correlation are

$$\bar{D} = \bar{D}\left[\left(V_j,\ d_j,\ \gamma,\ \frac{p_c}{p_j},\ \frac{\psi_c}{p_j},\ \frac{\Delta}{d_j}\right)_1,\ \left(P_{D_i},\ \frac{d_{j_i}}{d_{j1}},\ \frac{\psi_i}{p_{j1}},\ \frac{p_{c_i}}{p_{j1}},\ \frac{\Delta_i}{d_{j1}}\right)_{i=2,\ldots n}\right] \tag{3}$$

The parameters listed in Eq. (3) will directly influence the dropsize. However, additional parameters will indirectly effect $\bar{D}$ through their influence on the jets prior to impingement. Specifically, flow conditions at the entrance to the orifice, the orifice length, L_o, and the interaction of the jet with the atmosphere over the free jet length, L_j, will effect the velocity and turbulence profiles within the jets at the impingement point. Nevertheless, it is not necessary to include the above as separate parameters in Eq. (3) since their effects on $\bar{D}$ are taken into account by the velocity and turbulence profile parameters.

While the exact relationship between the parameters listed in Eq. (3) is not known, we can assume that the solution can be expressed by an infinite series, each term of which is simply the product of the various parameters raised to appropriate exponents and preceded by an unknown constant. A first order approximation to the solution is then obtained by empirically determining

the exponents and the constant of the first term in the series. The exponents were evaluated by a least squares fit of the equation

$$\bar{D} = C \prod_{i=1}^{N} (A_i)^{\alpha_i} \qquad (4)$$

to the experimental data. In the above equation, A_i represents the parameters listed in Eq. (3) (e.g., V_j, p_c/p_j, etc.) while α_i are the exponents to be determined. The constant C was determined after all the appropriate α_i were evaluated. To facilitate the data correlations, the experiments were conducted, in most cases, in a way such that only one parameter was varied in any series of tests.

In Section 4.2, the results of this study were presented according to element type. In the following paragraphs, the results obtained with each element type are also discussed separately and, where sufficient data was obtained, empirical correlations for the parameters listed in Eq. (3) are presented. In addition, the influence on dropsize of other parameters, such as free jet length, orifice entrance type and propellant miscibility, is discussed. The discussion of the median dropsize results is followed by a separate discussion of the dropsize distribution. The final section describes the results of the emulsification study.

5.2.1 Like-Doublet Atomization Characteristics

For a like-doublet element, the parameters of Eq. (3) expressing the characteristics of one jet relative to the other are all unity. The angle, γ , can also be conveniently defined as the included angle between the jets and, Δ , the distance between the jets at the impingement point. Hence, for this element, Eq. (4) becomes

$$\bar{D} = C\, V_j^{\alpha_1}\, d_j^{\alpha_2} \left(\frac{p_c}{p_j}\right)^{\alpha_3} \left(\frac{c}{p_j}\right)^{\alpha_4} \gamma^{\alpha_5} \left(1 - \frac{\Delta}{d_j}\right)^{\alpha_6} \qquad (5)$$

where the quantity $\left(1 - \frac{\Delta}{d_j}\right)$ was chosen to make $\bar{D}$ finite when $\Delta = 0$.

Influence of Single Jet Characteristics on Dropsize. The two parameters that are most commonly investigated in the experimental study of the atomization characteristics of impinging jets are the mean injection velocity and the orifice (or jet) diameter. It can be physically reasoned and has been verified experimentally (see e.g., Ref. 14) that the resulting dropsize is inversely proportional to the velocity and directly proportional to the orifice diameter. The velocity dependence generally ranges from $V_j^{-1/2}$ to $V_j^{-4/3}$ while the diameter dependence has been found to range from $d^{1/3}$ to d^1. The differences in the empirical correlations obtained from these studies can, in many cases, be attributed to the experimental technique, physical properties of the propellant simulants, or the mode of sheet disintegration, which is primarily governed by the fluid physical properties and injection velocity.

However, these two parameters do not uniquely specify the characteristics of a liquid jet. As a result, different dropsizes have been measured under conditions of identical injection velocity and orifice diameter using the same fluid and experimental technique. For example, it has been demonstrated by Dombrowski and Hooper, Ref. 12, that significant variations in dropsize are obtained when fully developed laminar as opposed to turbulent jets are used to produce atomization. In addition to the jet turbulence, Domborski et al. suggest that the distribution of velocity will contribute to the median dropsize. In this respect, it can be easily shown that, for the same diameter orifice and mass flowrate, the momentum flux of a fully developed laminar jet is 4/3 greater than that of a uniform velocity jet. Thus, it would be expected that the additional available energy alone would result in increased atomization.

Consequently, a study was undertaken to more closely examine the internal characteristics of the jets and their influence on droplet formation. The results of the jet characteristics study, discussed in Section 5.1, verified that the jets had velocity profiles ranging from nearly uniform to nearly fully developed. With the exception of the jets produced by the 1.5 L_D/d_j orifices, which were laminar unless turbulence was intentionally induced, the jets produced by the various orifices were generally laminar below an injection velocity of about 100 ft/sec and turbulent above this velocity.

The corresponding mass median dropsizes produced by the impingement of these jets are summarized on Fig. 45. As previously noted, the magnitude of the abscissa, p_c/p_j, was obtained from the pressure profile measurements of single jets. It is clearly seen on Fig. 45, that as the velocity profile of the jet develops (i.e., increasing p_c/p_j), while the injection velocity is held constant, the mass median dropsize decreases. It is also evident that the velocity profile exerts less influence on the dropsize when the jets are turbulent ($V_j > 100$ ft/sec) as opposed to when they are laminar.

Using a least squares technique to determine C_1, α_1, α_2 and α_3,* Eq. (5) was correlated with the laminar jet dropsize data shown on Fig. 45 and to the data obtained with the 0.081-inch diameter element (No. 81-10-3LD) shown on Fig. 52. The equation thus obtained is

$$D = 4.85 \times 10^4 \, V_j^{-0.75} \, d_j^{0.57} \left(\frac{p_c}{p_j}\right)^{-0.52} \qquad (6)$$

A comparison of the dropsizes calculated from Eq. (6) and the experimental data is presented on Table 12** and shown in graphical form on Figs. 43 and 46. When the flow is definitely laminar ($V_j < 80$ ft/sec), it is seen that the measured dropsizes agree quite well with the calculated values.

The influence on droplet formation of the turbulence intensity was also examined. This study was conducted with nearly uniform velocity jets in order to eliminate the effect of velocity profile. At a given injection velocity, the turbulence level at the impingement point was varied by changing the free jet length. Because of the technique used to generate and vary the turbulence level (Section 4.1), it is of interest to compare the turbulence intensity levels to those

---

* For laminar jets, α_4 is, of course, 0.

**Although by definition, the dynamic pressure ratio, P_D, of a like-doublet element is unity, all the tests performed with the 1.5 L_D/d_j elements were conducted at a dynamic pressure ratio of about 1.1. From a separate series of tests, discussed in a later section, it was found that for equal diameter, wax/wax impingement

$$\overline{D} \propto P_D^{-0.12} \text{ where } P_D = \left(\frac{V_2}{V_1}\right)^2 \quad (V_2 \leq V_1)$$

existing in turbulent jets produced by orifices where the turbulence is not artificially generated. Using a similar experimental technique, the turbulence intensity within free jets produced by round entrance orifices was measured by Rupe, Ref. 23. For an orifice L_o/d_j of 5.1, free jet length of 5 d_j, and a Reynolds number of 41,800, Rupe found the turbulence intensity level at the center of the jet to be approximately 0.5% of the mean pressure. At the same Reynolds number and free jet length, the intensity level was about 2.5% when the orifice length was increased to 15 d_j. For a fully developed turbulent jet, the intensity level is about 5% (see e.g., Fig. 29). On the other hand, when the turbulence generator was used in conjunction with the 1.5 L_o/d_j orifice, the intensity level was found to be 1 to 2% of the mean pressure at a free jet length of 4.5 d_j and as high as 14% at a free jet length of 10 d_j in the Reynolds number range of from 3000 to 10,000. Thus, the turbulence intensity levels (but not necessarily the scale of the turbulent eddies) within the jets used in the atomization study are characteristic of those found in turbulent jets produced by longer orifices.

The results of the atomization tests, shown on Fig. 48, revealed that the level of turbulence did not affect the dropsize. Consequently, α_4 (Eq. 5) is zero for both laminar and turbulent jets. However, it was found that the turbulent jets will produce a dropsize different from that obtained with laminar jets under otherwise similar flow conditions. This can be seen from a comparison of the laminar and turbulent jet data (runs 1 to 14 and 20 to 30 in Table C1) presented on Fig. 90. Further evidence of this effect is seen on Fig. 45 which demonstrates that the influence of velocity profile on dropsize also depends upon the flow regime.

In a manner analogous to the technique employed in the correlation of the laminar jet data, it was found that an empirical equation of the form

$$\overline{D} = 15.9 \times 10^4 \, V_j^{-1.0} \, d_j^{0.57} \left(\frac{p_c}{p_j}\right)^{-0.10} \qquad (7)$$

would fit the turbulent jet data quite well. The data utilized in this

correlation included all values of $\bar{D}$ obtained with the 10 and 50 L_o/d_j orifices as well as the data obtained with the 1.5 L_o/d_j element using the turbulence generator. Because of the small range of turbulent jet orifice diameters, the exponent of d_j was set equal to the value obtained from the laminar jet correlation.

The measured dropsizes are compared with Eq's.(6) and (7) in Table 12 and on Figs. 46 and 89. It is seen on Fig 46 that several data points, particularly those obtained with the 50 L_o/d_j orifices, do not conform to either the laminar or turbulent jet correlation in the velocity range from about 70 to 100 ft/sec. In these cases, it is possible that there was either intermittent laminar and turbulent flow or that one jet was flowing laminar and one turbulent.

The results of this study substantiate the findings of Dombrowski and Hooper, Ref. 12. They found that under identical geometric and hydraulic operating conditions, the sheet disintegration mechanism depended upon whether the jet was laminar or turbulent. In the latter case, sheet disintegration resulted from the formation of hydrodynamic (or "impact") waves for all operating conditions examined. When a fully developed laminar jet was used, an "unruffled" sheet was formed, the characteristics of which were determined by the impingement angle and jet velocity. For example, at an impingement angle of 50 degrees, the center of the sheet disintegrates through what appears to be impact waves; while the remainder of the sheet disintegrates by the action of aerodynamically generated waves. At larger impingement angles and low jet velocities, the impact waves at the center of the sheet disappear and disintegration occurs solely through the action of aerodynamic waves.

The mechanism by which droplets are formed by aerodynamically generated waves is fairly well understood (see e.g., Ref. 9, 10, and 12). However, little is known about the origin of impact waves. Since these waves were found to exist in a vacuum (Ref. 28), it is certain that they are not aerodynamically generated but are related to the inertial force of the jets at the impingement point. When the fluid inertia is increased, impact wave disintegration tends to dominate the droplet formation process.

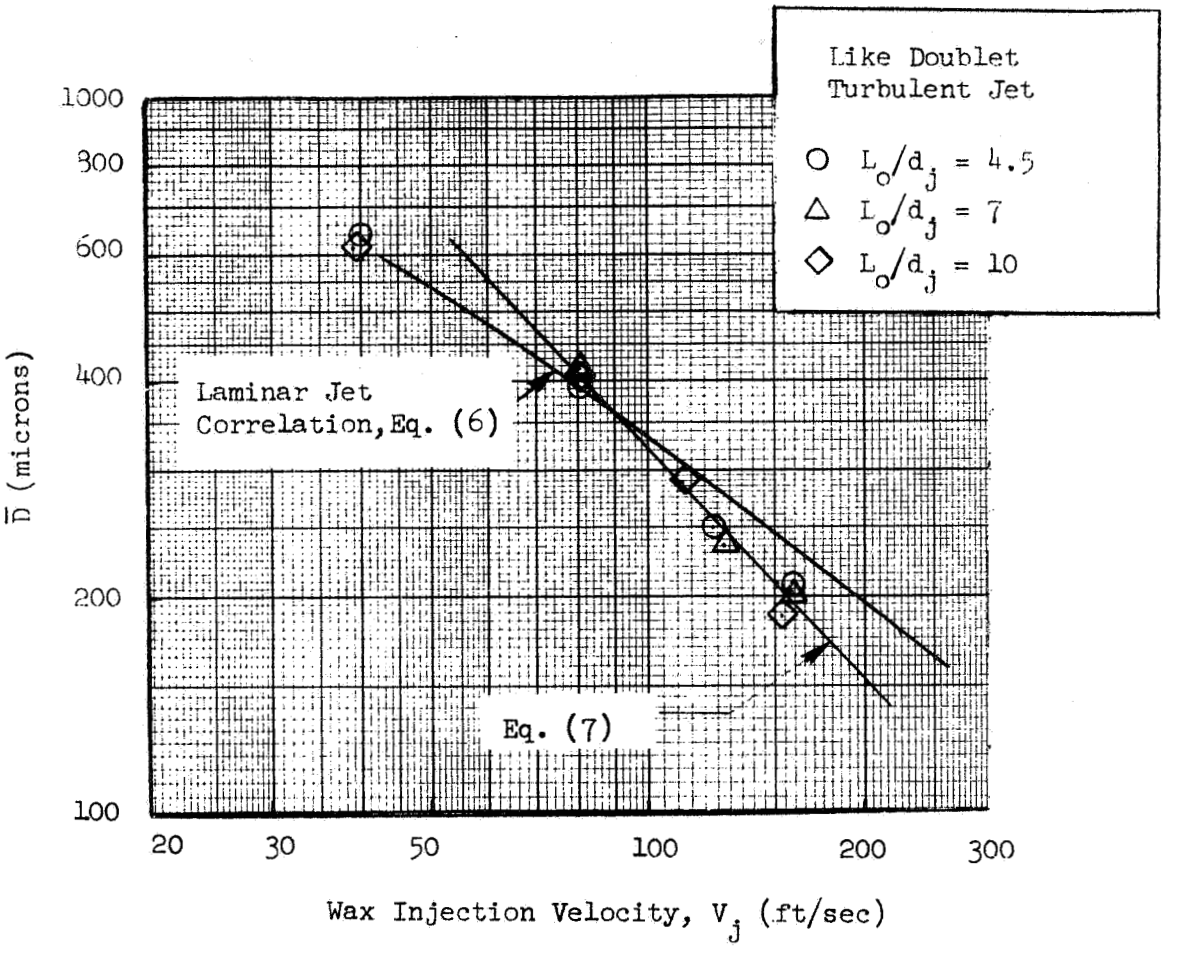

Figure 89. Comparison of Laminar and Turbulent Jet Atomization Result (Like Doublet)

TABLE 12

COMPARISON OF MEASURED AND CALCULATED DROPSIZES
FOR LIKE DOUBLET

Run No.	L_o/d_j	V_j	d_j	P_c/P_j	$\bar{D}_{meas}$	Equation 6		Equation 7	
						$\bar{D}_{calc}$	% Err	$\bar{D}_{calc}$	% Err
1	1.5	29.7	0.060	1.305	675	682	1.0	---	---
2		38.1		1.270	575	567	-1.4	---	---
3		52.8		1.220	482	451	-7.0	---	---
4		79.3		1.156	365	344	-6.0	---	---
5		127.4		1.093	240	257	6.6	---	---
6		166.5		1.060	196	206	5.0	---	---
7		214.0		1.030	170	175	2.8	---	---
8		36.9		1.273	615	587	-4.8	---	---
9		196.5		1.038	173	183	5.5	---	---
10		37.7		1.270	650	572	-13.6	---	---
11		78.3		1.166	340	345	1.3	---	---
12		107.5		1.115	265	278	4.7	---	---
13		213.0		1.030	173	174	0.7	---	---
14		51.6		1.220	445	456	2.3	---	---
31	6	37.4	0.061	1.505	520	526	1.1	---	---
32		73.0		1.330	375	340	-10.4	---	---
33		105.2		1.245	280	267	-4.7	---	---
34	10	40.1	0.063	1.705	470	476	1.3	---	---
35		79.5		1.460	315	309	-1.9	---	---
36		115.0		1.350	260	244	-6.5	---	---
37		152.5		1.305	187	201	7.0	---	---
38	10	30.0	0.063	1.765	463	582	20.4	---	---
39		40.4		1.680	423	477	11.4	---	---
40		59.8		1.552	387	371	-4.4	---	---
41		72.5		1.485	413	328	-25.8	436	5.3
42		78.1		1.460	415	313	-32.5	405	-2.4
43		100.1		1.340	337	---	---	319	-5.6
44		110.1		1.320	303	---	---	291	-4.2
45		129.9		1.280	256	---	---	247	-3.7
46		149.7		1.270	223	---	---	214	-4.0
47		29.8	0.081	1.770	505	649	22.2	---	---
48		38.5		1.694	493	556	11.3	---	---
49		58.4		1.558	438	422	-3.8	---	---
50	50	53.4	0.067	2.100	322	357	9.8		
51		35.3		2.430	421	451	6.7		
52		26.6		2.630	465	535	13.1		
53		156.6		1.425	205	---	---	195	-5.1
54		178.0		1.425	182	---	---	177	-2.7
55		47.4		2.200	369	381	3.1	---	---
56		86.8		1.650	276	281	1.9	---	---
57		125.8		1.420	238	---	---	261	9.0
86	200	61.1	0.069	3.160	276	265	-4.2	---	---
87		80.1		3.020	213	221	3.7	---	---
88		28.6		3.440	440	448	1.8	---	---
89		39.2		3.320	378	360	-4.9	---	---
90		97.6		1.440	315	281	-12.0	342	7.9
20	1.5	40.2	0.060	1.230	640	---	---	794	19.3
21		79.6		1.120	392	---	---	404	2.9
22		123.0		1.065	250	---	---	261	4.4
23		157.5		1.035	207	---	---	205	-1.1
24		79.9		1.095	415	---	---	401	-3.4
25		126.8		1.036	235	---	---	262	10.5
26		157.0		1.010	205	---	---	204	-0.5
27		38.9		1.130	605	---	---	824	26.5
28		80.1		1.065	398	---	---	401	0.8
29		112.9		1.025	288	---	---	289	0.2
30		151.8		0.905	186	---	---	209	10.9

From the photographs presented in Ref. 12, it can be seen that when turbulence exists within the jet, the entire sheet disintegrates through the action of impact waves. On the other hand, the disintegration of sheets produced by laminar jets is observed to result from either aerodynamically generated waves alone or a combination of aerodynamic and impact waves. It can thus be presumed that the presence of jet turbulence provides a mechanism for triggering impact wave disintegration. In the absence of internal jet turbulence, the local sheet velocity, or inertia, is the controlling factor in the mode of disintegration. When the flow is fully developed laminar, a parabolic velocity profile is established in the jet where the centerline velocity is twice the mean. This non-uniformity in the velocity distribution of the free jet persists as a non-uniform velocity distribution in the sheet. Dombrowski et al. have shown that the velocity in the center of the sheet produced by fully developed laminar jets is higher than the mean velocity. They suggest that the high-velocity core existing in the jet is the cause of the high-velocity stream in the sheet. Similarly, the low-velocity annuli of the jet form low-velocity laminae in the sheet adjacent to this stream. Because of its higher inertia, the center of the sheet will disintegrate through the action of impact waves. In the low-velocity regions of the sheet, aerodynamic disintegration will occur.

This phenomena provides an explanation for the variation of dropsize with jet velocity profile. Since the dropsize is inversely proportional to the velocity, the dropsize obtained from the center of the sheet will decrease as the velocity profile becomes more developed. Consequently, the center of the sheet, which contains the bulk of the mass flux, will dominate the overall size. As the velocity profile becomes more uniform in both the jet and the sheet, the overall dropsize will increase.

The difference in the exponents of the velocity profile parameter (p_c/p_j) in Eq's. (6) and (7) may be attributed to the different modes of sheet disintegration for turbulent and laminar jets. However, the shape of the profile, which is nearly flat for turbulent jets while becoming parabolic in fully developed laminar jets, may also be a contributing factor.

Because of the different physical processes by which aerodynamic and impact waves are amplified, it is to be expected that the critical wavelength and sheet thickness at the point of breakup, which in turn dictate the resulting dropsize, will be different functions of the jet (or sheet) velocity. In the case of turbulent jet impingement, the dropsize was proportional to V_j^{-1} while, for laminar jet impingement, the dropsize was proportional to $V_j^{-3/4}$. From the difference in the velocity exponents, it follows that a "critical" velocity exists above which the presence of turbulence enhances atomization. Similarly, laminar jet impingement will produce greater atomization when the injection velocity is below the critical. According to the results of this study, this velocity is 115 ft/sec, with $(p_c/p_j) = 1$, for molten wax.

At very high injection velocities, inertial forces should dominate breakup over the entire sheet regardless of whether the free jets were laminar or turbulent. Consequently, it is reasonable to expect that the dropsize produced by high velocity ($V_j >> 115$ ft/sec) laminar jet impingement would exhibit a velocity dependence similar to that obtained with turbulent jets. At very low injection velocities, surface tension rather than inertia forces are the controlling factor in sheet breakup and the tendency for impact wave disintegration to occur would diminish. Dombrowski et al. noticed that impact wave disintegration did not occur below the Weber number range of from 66 to 165. Similar observations were made by Taylor, Ref. 29, and Heidman et al., Ref. 30. For an impingement angle, γ, of 60 degrees, this corresponds to a velocity of about 6 to 10 ft/sec for wax and 17 ft/sec for water. As the injection velocity is decreased towards and below this value, free jet turbulence can be expected to exert a lesser influence on dropsize and the velocity dependence for turbulent jets would (hypothetically, at least) approach that of laminar jets.

An attempt was made to correlate the data obtained in this program and those of other investigators on the basis of Weber number. The above speculation as to the dropsize/velocity dependence outside the experimental range examined here and the Weber number correlation is discussed further in Appendix D.

The exponents of velocity and diameter in the dropsize correlation equations determined in this study are compared to those of several other investigators in Table 13. Dickerson et al., Ref. 14, using an experimental technique and propellant simulant identical to those of this work, obtained the same orifice diameter dependence, but a different velocity exponent. It is interesting to note, however, that in the Ref. 14 study the data were obtained in a velocity range extending into both the laminar and turbulent regimes (but were primarily turbulent) and that their exponent is almost an average of the exponents for laminar and turbulent flow obtained in this study.

The dropsize/velocity relations (Ref. 14 and Eq's. 6 and 7) are compared graphically on Fig. 90. Shown on Fig. 91 is a comparison of the dropsize data presented in Ref. 14 and the dropsize computed from either Eq. (6) or (7). Since the Ref. 14 data were obtained using molten wax and similar orifice geometry, the appropriate equation was chosen by assuming that all jets having Reynolds Numbers less than 10,000 were laminar while all those above this velocity were turbulent. As shown on Fig. 91, when the flow regime is taken into account, the Ref. 14 data agree quite well with the like-doublet correlations presented here.

In a series of experiments where the jets were known to be turbulent, Dombrowski and Hooper, Ref. 12, correlated the dropsize with $V_j^{-0.79}$. The difference between their exponent of velocity and that of Eq. (7) may be a result of the fact that, in Ref. 12, dropsizes were measured in the center of the sprayfield only.

Although the experiments of Hasson and Mizrahi, Ref. 16, were performed with spray fans rather than impinging jets, their data was selected for comparison because of the similarity of the experimental technique and propellant simulants. The physical properties of the molten wax used in their study were about the same as the wax used in this program and the tests were conducted over a similar velocity range (approximately 60 to 120 ft/sec). The complete

TABLE 13

COMPARISON OF DROPSIZE CORRELATIONS

$$\bar{D} = C\, V_j^{\alpha 1}\, d_j^{\alpha 2}\, (p_c/p_j)^{\alpha 3}$$

α_1	α_2	α_3	Remarks
-0.75	0.57	-0.52	Equation 6, Laminar
-1.0	0.57	-0.10	Equation 7, Turbulent
-0.85	0.57	----	Ref. 14, Laminar and Turbulent Fluid: Molten Wax Injector Type: Like Doublet
-0.79	----	----	Ref. 12, Turbulent Fluid: Water Injector Type: Like Doublet
-0.67	0.67	----	Ref. 16, Probably Laminar Fluid: Molten Wax Injector Type: Spray Fan
-0.67	0.67	----	Ref. 10, Theoretical Aerodynamic Wave Disintegration

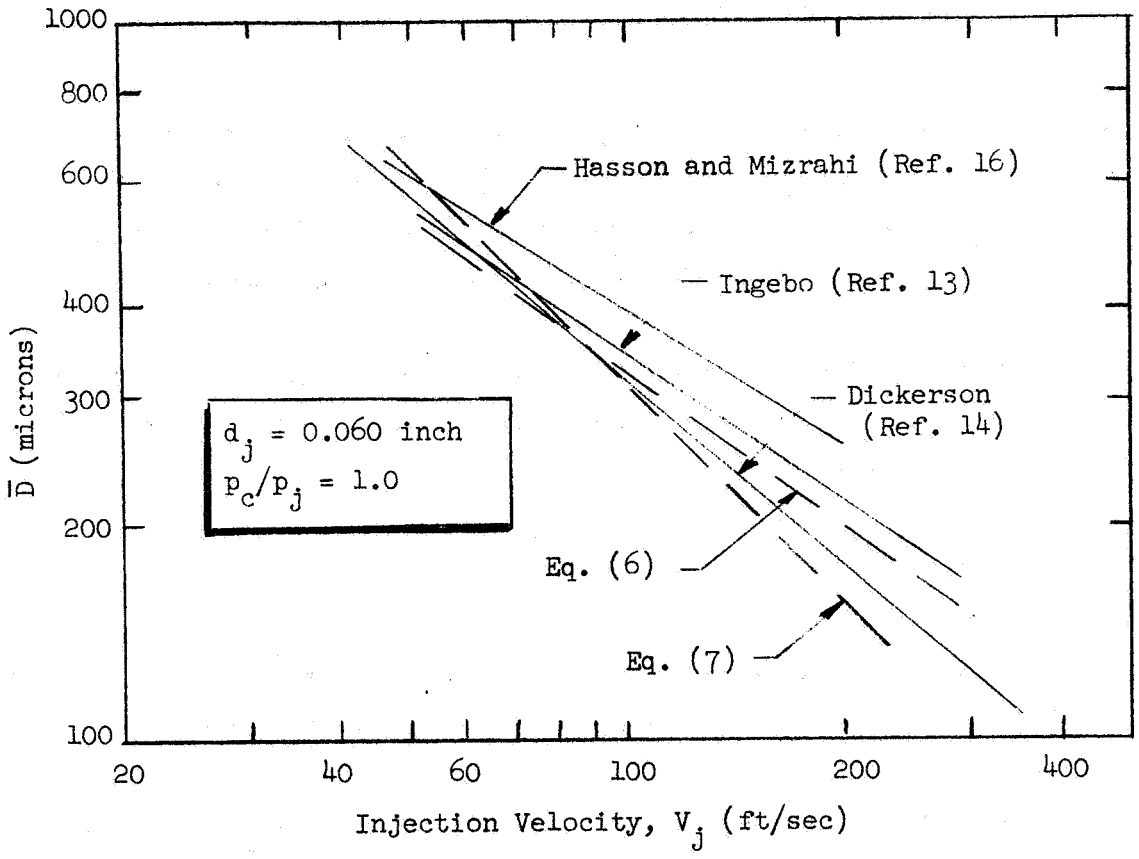

Figure 90. Comparison of Like Doublet Dropsize Correlations

correlating equation presented in Ref. 16 is given by

$$\bar{D}_{20} = 648 \left(\frac{\sigma K}{C_D \Delta P}\right)^{1/3} (\rho \mu)^{1/6} \qquad (8)$$

where K is the exit area of the spray nozzle and $\bar{D}_{20}$ is the surface mean diameter*, is compared to Eq's. (6) and (7) in Table 13 while the level of dropsize (corrected to $\bar{D}$) obtained from Eq. (8) is shown on Fig. 90. Considering the difference in the injector type, the agreement is quite good.

In a theoretical derivation of the dropsize resulting from the breakup of liquid sheets by the action of aerodynamic waves, Dombrowski and Johns, Ref. 10, found that

$$\bar{D} \propto (d_j/V_j)^{2/3} \qquad (9)$$

Their analysis is directly applicable to the work of Hasson and Mizrahi and, as shown in Table 13, identical exponents for d_j and V_j were obtained.

It is also interesting to note that the laminar jet correlating equation, Eq. (6), compares favorably with the parametric dependence obtained from the aerodynamic wave break-up model of Dombrowski. The slightly larger exponent of velocity expressed by Eq. (6) is consistent with the photographs indicating that impact disintegration, and its concomittant greater velocity dependence, also occurs over part of the sheet.

---

*In section 5.2.5, it is shown that, for the distributions obtained in this study, $\bar{D} = 2.82\ \bar{D}_{20}$. K was taken to be the cross-sectional area of a 0.060-inch-diameter jet. The units for Eq. (8) are: σ, dynes/cm; ρ, gm/cm^3; K, cm^2; μ, cP; $C_D \Delta P = \frac{1}{2} \rho V_j^2$, psig.

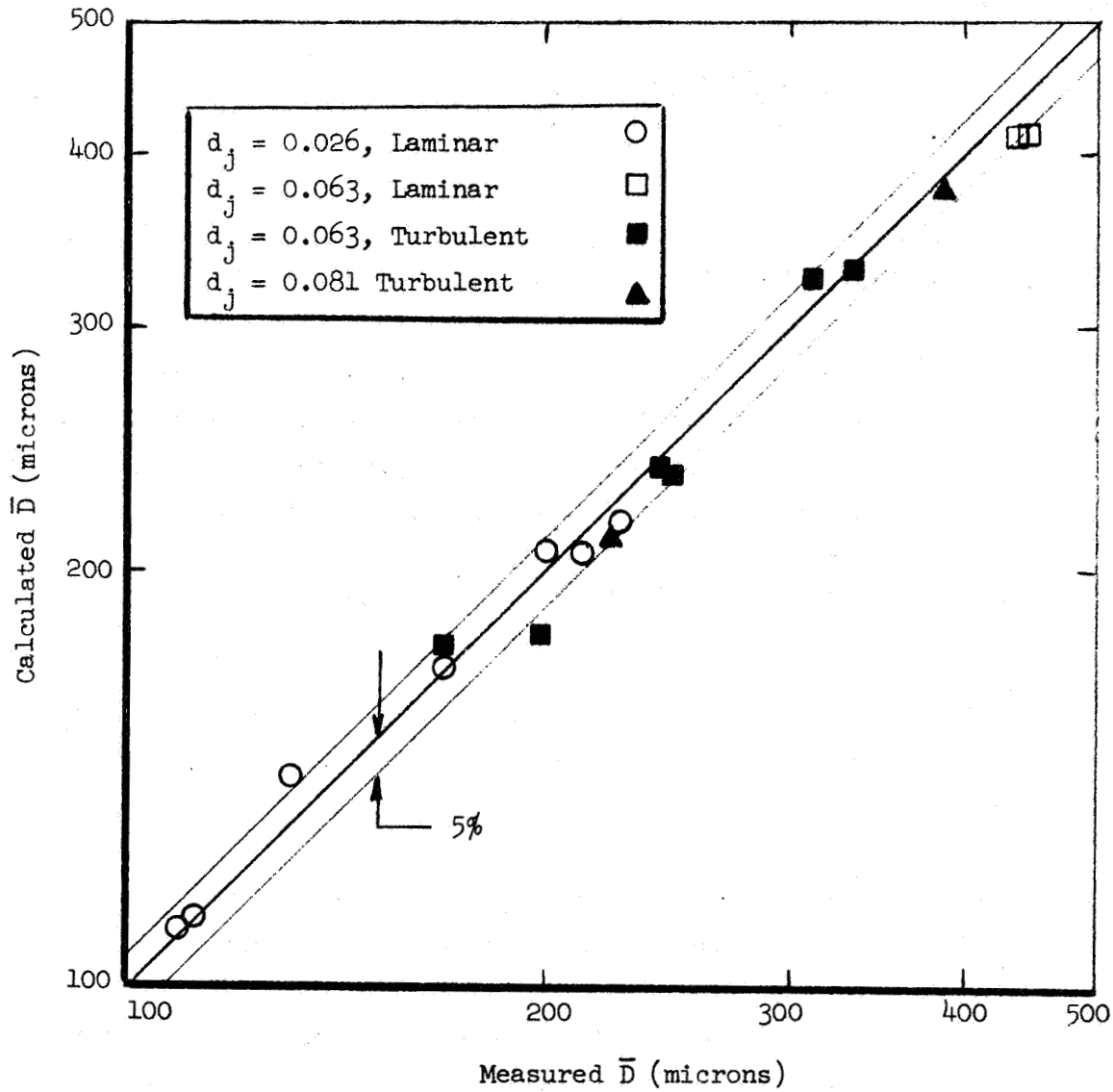

Figure 91. Comparison of Measured (Ref. 14) and Calculated Mass Median Dropsizes for Like Doublet

A final comparison, now shown on Table 13, is made with the work of Ingebo, Ref. 13. His data, which were obtained using n-heptane in air, gave the following relation

$$D_{30} = \frac{2.54 \times 10^4}{2.64\sqrt{V_j/d_j} + 0.97\ K|\Delta V|} \qquad (10)$$

where D_{30} is the volume mean droplet diameter, K is a function of liquid properties and ΔV is the relative air/liquid velocity.*

To compare Ingebo's expression with the current data, a modification of his relation was necessary to account for the effects of fluid physical properties on the relative velocity term. Other work by Ingebo indicated that the effects of liquid viscosity, density and surface tension could be accounted by (Ref. 36)

$$K = \left[\left(\frac{\mu\sigma}{\rho}\right)_{\text{n-heptane}} / \left(\frac{\mu\sigma}{\rho}\right)_{\text{wax}}\right]^{1/4} = 0.52$$

Using the above value for K and taking $|\Delta V|$ to be equal to the injection velocity (i.e., zero air velocity), Ingebo's expression was plotted on Fig. 90, and shows reasonable agreement with Eq's. (6) and (7).

Influence of Injector Geometry on Dropsize. Of practical importance in the design and fabrication of injection systems, is the criticality of orifice spacing, alignment and manifolding on atomization. For most injector types, the impingement angle and free jet length may affect both propellant atomization and face splashing. The latter can be a serious problem resulting in face burnout while long free jet lengths result in the impingement of streams that may be already partially disintegrated. Orifice misalignment will result in inefficient momentum exchange between the jets, leading to decreased atomization. It has already been shown that manifold and orifice entrance conditions

*The units of velocity are ft/sec, jet diameter is in inches while the dropsize is in microns. The correction factor for $\bar{D}$ is $\bar{D} = 2.2\ \bar{D}_{30}$.

exert considerable influence on the free jet characteristics, which in turn affect atomization.

Using two orifice entrance types, sharp and round, in combination with orifice lengths ranging from 1.5 to 10 diameters, molten wax experiments were performed to determine orifice entrance effects on dropsize and droplet distribution.

In all cases, an essentially quiescent reservoir, where the fluid velocity was approximately 2% of the jet velocity, was located upstream of the orifices. The results obtained with round entrance orifices were discussed above where it was shown that the mass median dropsizes could be correlated with either Eq. (6) or (7).

Velocity profile measurements of the jets produced by the sharp edge orifices presented in Section 4.1.1 revealed that the jets were separated from the orifice walls. It was shown there that by properly accounting for the increase in jet velocity and decrease in jet diameter resulting from the separation, the velocity profile of the jet could be reduced to a nearly uniform velocity jet. The mass median dropsizes obtained with the sharp edge orifices are shown in Fig. 54 where the abscissa represents the mean injection velocity ($V_j = \dot{w}/\rho A$).

Since the separated jets were laminar, it would be expected that, if the corrected velocity and diameter, V_s and d_s, were substituted into Eq. (6), the mass median dropsizes obtained with the sharp entry orifices could be predicted. To make this comparison, it is convenient to first modify Eq. (6). From the definition of the contraction coefficient, C_c, and continuity of mass, d_s and V_s can be defined as

$$d_s = \sqrt{C_c\, d_j}$$

and

$$V_s = V_j/C_c$$

Replacing V_j and d_j in Eq. (6) by the above definitions for d_s and V_s yields

$$\overline{D} = 4.85 \times 10^4 \, (C_c)^{1.035} \, V_j^{-0.75} \, d_j^{0.57} \, \left(\frac{p_c}{p_j}\right)^{-0.52} \qquad (11)$$

where V_j and d_j retain their previous definitions of mean velocity (based on flowrate) and orifice diameter respectively.

Assuming a uniform velocity profile, the mean velocity of the separated jet, V_s, can be computed from $V_s/V_j = \sqrt{p_c/p_j}$, where p_c/p_j is obtained from the pressure profile measurements shown on Fig. 34. From continuity of mass the separated jet/orifice diameter ratio is given by $d_s/d_j = \sqrt{V_j/V_s}$ which yields a diameter for the separated jet of about 0.049 inch; corresponding to a contraction coefficient of 0.645. Using this value of C_c, Eq. (11), when compared to the sharp orifice entry data on Fig. 92, is found to yield dropsizes 20-25% high. However, an excellent correlation was obtained when C_c was set equal to 0.52 (corresponding to a jet diameter of 0.045). The difference between the calculated value of C_c and that which correlates with the dropsize data may be attributed to the fact that the estimated value of C_c was based on measurements of DEW jets instead of wax. Since the diameters of the jet were not measured, this was not verified.

Additional experimental data on the effect of sharp entry orifices were obtained by Nurick and McHale, Ref. 19. These data are discussed in the section dealing with unlike-doublet atomization characteristics.

The influence of misimpingement on atomization was examined using both sharp and round entrance orifices. The results, previously presented on Fig. 56, are replotted on Fig. 93 where the ordinate is the non-dimensional dropsize $\overline{D}_\Delta / \overline{D}_{\Delta = 0}$. Kuykendal, Ref. 17, also examined the effects of misimpingement on dropsize and obtained a correlation of the form

$$\frac{\overline{D}_\Delta}{\overline{D}_{\Delta = 0}} = (1 - \Delta/d_j)^{-0.19} \qquad (12)$$

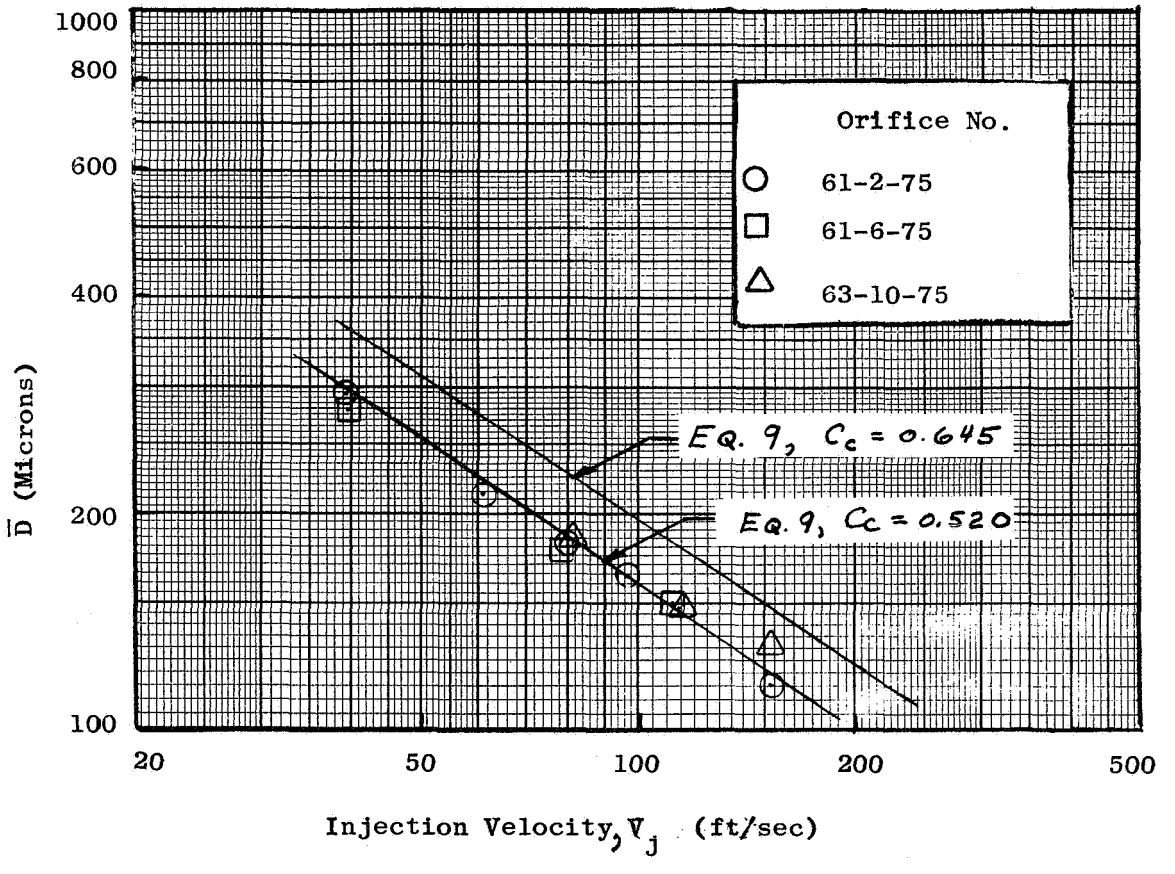

Figure 92. Comparison of Empirical Correlation With Mass Median Dropsizes Obtained With Sharp Entrance Orifices

As shown on Fig. 93 , Eg. (12) also agrees with the present results for both the sharp and round entrance orifices. It should be recalled that jet separation occurred when sharp entrance orifices were used. Because of the smaller jet diameter, the actual percentage of misimpingement is larger. Based on the real jet diameter, d_s, the misimpingement is

$$\frac{\Delta}{d_s} = \frac{\Delta}{\sqrt{C_c\, d_j}}$$

since $d_s = \sqrt{C_c\, d_j}$. With $C_c = 0.52$, a Δ/d_j of 0.50 corresponds to a misimpingement of 70% of the jet diameter.

The experimental study of the influence of <u>free jet length</u> on atomization revealed that with an orifice L_o/d_j of 1.5, no variation of dropsize was obtained. On the other hand, with 50 L_o/d_j orifices, an increase in dropsize on the order of 40% occurred when the free jet length was increased from 5 to 10 d_j. It is unlikely that the cause was misimpingement. As shown on Fig. 93, a 40% increase would require a misalignment of the jets of approximately 75%. Rather, it is believed that the cause of the decrease in atomization was jet disintegration. To verify this, the characteristics of the jet produced by the 50 L_o/d_j orifice were examined as a function of free jet length. The variations of the centerline pressure ratio and turbulence intensity at an injection velocity of 100 ft/sec are shown on Figs. 32 and 33, respectively. These measurements indicated that jet disintegration was initiated at an L_o/d_j of 5 and that the dropsizes obtained at the free jet L_o/d_j's of 10 were produced by the impingement of disintegrated or nearly disintegrated jets. From these experimental data, it appears that jet disintegration is more detrimental to atomization than a jet misimpingement of as much as 50 or 75%!

The experimental data on the effect of <u>impingement angle</u> on dropsize (also shown on Fig. 64) and curves based on the correlating equations of Dombrowski and Hooper (Ref. 12) and Fry, Thomas, and Smart (Ref. 18) relating dropsize to impingement angle, are summarized on Fig. 94. It is interesting to note

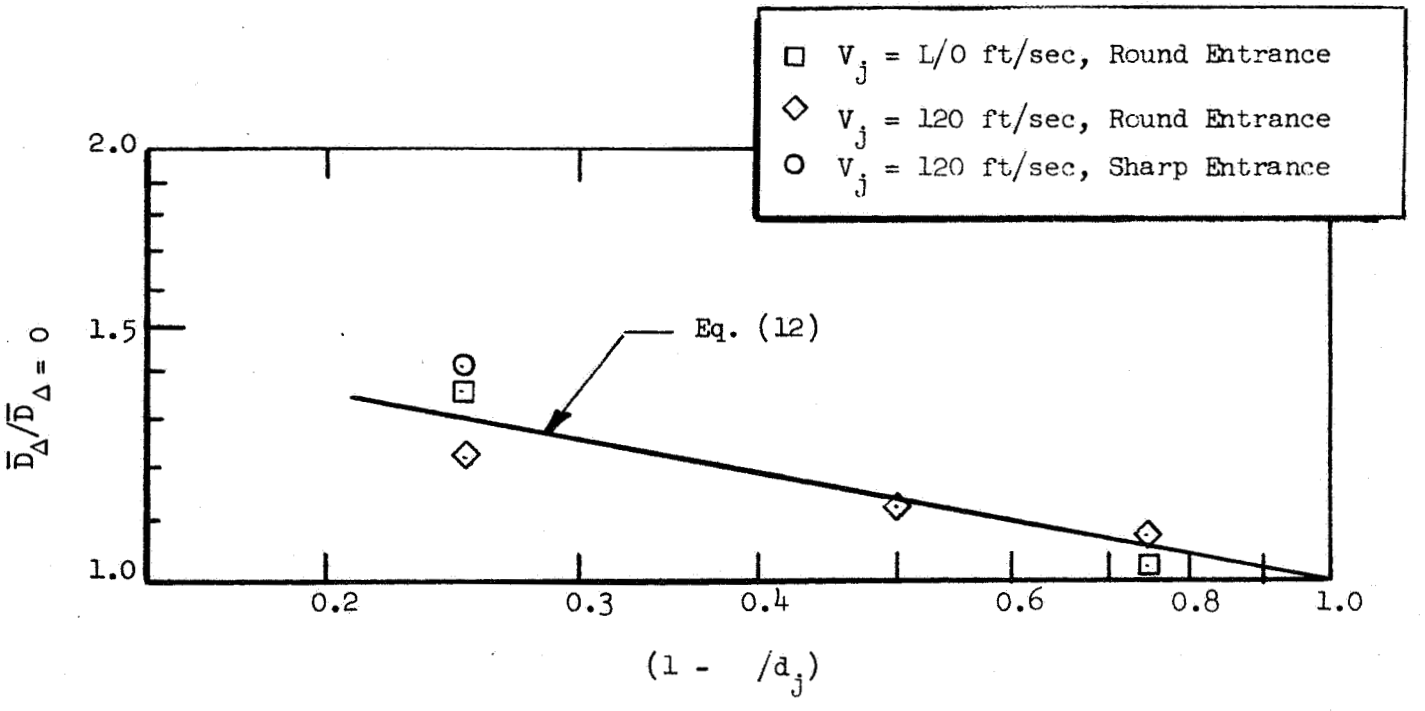

Figure 93. Correlation of Mass Median Dropsize and Jet Misalignment for a Like-Doublet

the wide discrepancy in the two correlations, particularly at the impingement angle of 45 degrees. Although both investigators used a photographic technique to measure particle sizes, Dombrowski and Hooper investigated only the central portion of the spray field. This could account for the large droplet sizes reported by Dombrowski and Hooper at the lower impingement angles.

Examination of Fig. 94 shows agreement of the current data with the correlation of Fry et al., to within ±10% for impingement angles of 45 to 90 degrees. It was found that a correlation of the form (instead of the form expressed by Eq. (5))

$$\overline{D}\,\gamma = (1.44 - 0.0073\,\gamma)\,\overline{D}_{60} \qquad (13)$$

where $\overline{D}_{60}$ is the dropsize obtained at 60 degrees while $D\,\gamma$ is the dropsize at γ degrees, would fit the experimental data of this program quite accurately.

The influence of a cross-velocity manifold on dropsize was not examined. Nevertheless, cross velocity effects can be deduced from the characteristics of jets obtained with this manifold type.* Since similar velocity profiles were obtained with both round and sharp entrance orifices, similar dropsizes could also be expected. Also, the non-symmetry of the jets obtained with high cross velocity and short L_o/d_j is probably too small to influence dropsize to any extent.

It should be recalled, however, that when short $(L_o/d_j < 6)$, both sharp and round entrance orifices were employed with the cross-flow manifold, the jets were so degraded that their characteristics were essentially unmeasurable. Under these conditions, a prediction of the atomization characteristics of these jets would be highly questionable. Atomization data obtained with jets

*This discussion is, of course, limited in scope since only one injection velocity (120 ft/sec) was examined.

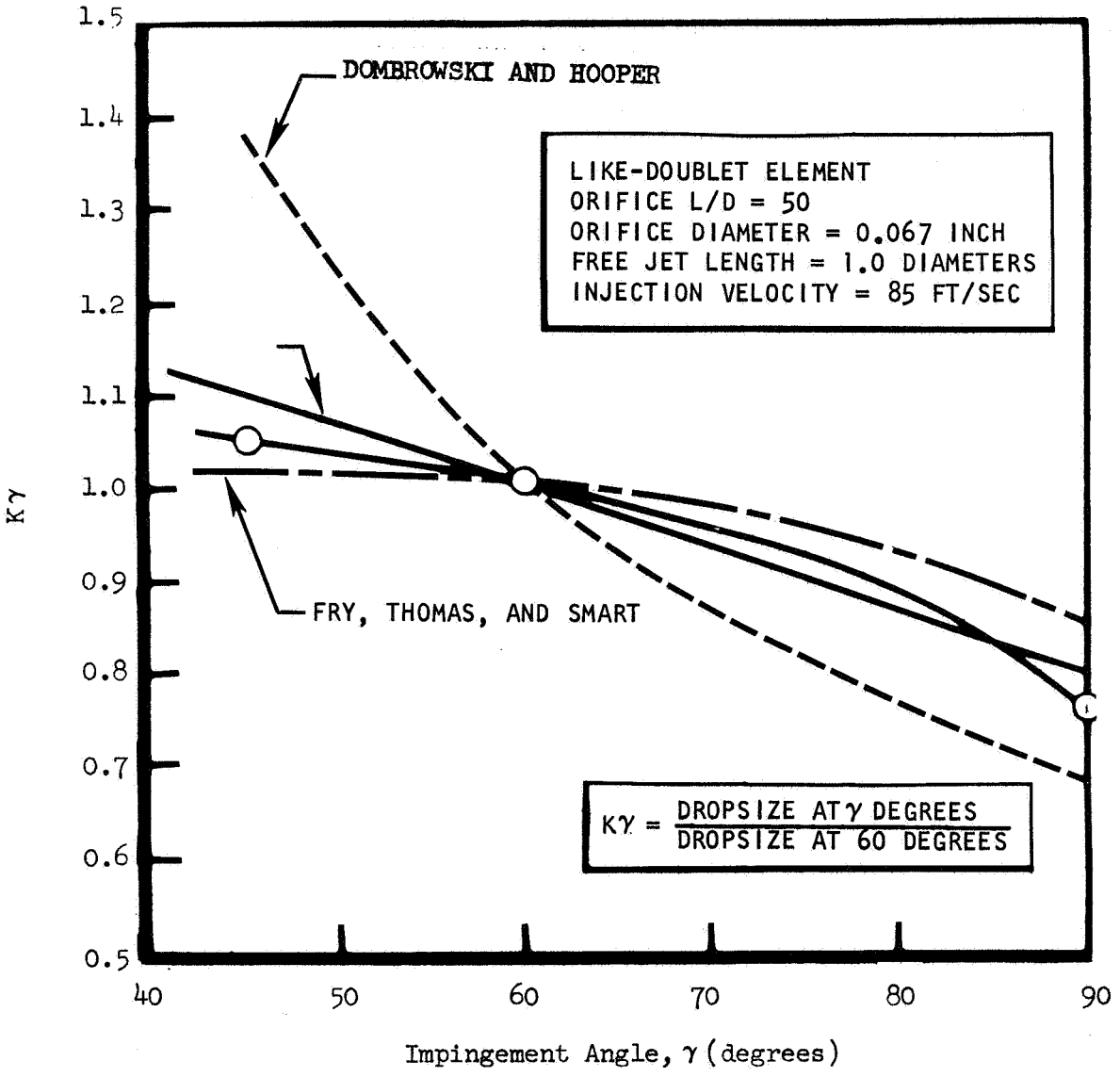

Figure 94. Correlation of Mass Median Dropsize with Impingement Angle for a Like-Doublet

that experienced partial disintegration prior to impingement indicated a substantial increase in dropsize above that which would be obtained if jet disintegration had not occurred. This strongly suggests that the impingement of jets issuing from short orifices fed by a cross velocity manifold would exhibit a similar decrease of atomization.

5.2.2 Unlike-Doublet Atomization Characteristics

Because of the propellant mixing, as well as atomization, that is achieved when liquid jets are impinged, unlike-doublets are commonly used as injector elements in rocket design. However, with a few exceptions, the bulk of the experimental studies of atomization have been conducted with like-doublet elements. One of the principle reasons for this is that, since photographic techniques are generally employed, it is difficult, at best, to distinguish the identity of the propellant simulants. Consequently, only an overall dropsize, which is of limited interest in rocket engine injector design, can be obtained. In this respect, the molten wax technique offers a unique advantage in that propellant simulants can be easily separated and the dropsize obtained from each orifice can be readily determined.

In order to attain the proper oxidizer/fuel mixture ratio in the combustion chamber, the propellants are generally injected through the orifices of an unlike-doublet at different flowrates. Thus, in addition to the single jet parameters which alone are sufficient to characterize like-doublet atomization, a study of unlike-doublets must include the effects of the velocity and orifice diameter differences between the inpinging jets. Obviously, the use of dissimilar fluids and their attendant physical property differences will also effect the droplet formation process. However, a complete physical property study was beyond the objectives of the current program. What was examined in this respect was the influence of propellant miscibility (discussed below) and the occurrence of an emulsion (discussed in Section 5.2.5.).

In order to obtain a correlation of the unlike doublet experimental data and the independent parameters, the empirical equation selected must include parameters that describe the characteristics of both jets. These parameters, according to Eq. (3) include: (1) a set of variables which describe the characteristics of one of the jets; namely, the mean injection velocity, orifice diameter and the velocity profile parameter, and (2) a set describing the characteristics of this jet relative to the equivalent parameters of the opposing jet; taken here to be the orifice diameter ratio and the dynamic

pressure ratio.* The influence of impingement angle and misimpingement were not examined with this element type. Hence, expressed in terms of the above parameters, the unlike-doublet correlating equation assumes the form

$$D_m = C_m (V_j)_m^{\alpha 1m} (d_j)_m^{\alpha 2m} \left(\frac{P_c}{P_{j_m}}\right)^{\alpha 3m} P_D^{\alpha 4m} \left(\frac{d_o}{d_f}\right)^{\alpha 5m} \qquad (14)$$

where the subscript m corresponds to the wax jet (which can represent either the fuel or oxidizer). The quantity d_o/d_f is the oxidizer-to-fuel diameter ratio. The dynamic pressure ratio is defined as the ratio (ρV_j^2) fuel/(ρV_j^2) ox where the oxidizer simulant is taken to be the liquid (either DEW or wax) issuing from the larger diameter orifices.

Influence of Opposing Jet Characteristics on Dropsize. The study of dynamic pressure ratio effects on atomization was performed with nearly uniform velocity profile jets using both equal and unequal diameter doublets. The results of these tests, shown on Figs. 68, 69, and 70, were used to determine the exponents of dynamic pressure ratio and diameter ratio for both the fuel and oxidizer dropsize correlations. For the fuel (i.e., when wax was flowing through the smaller diameter orifice) the correlation obtained was

$$D_f \propto P_D^{.165} \left(\frac{d_o}{d_f}\right)^{-0.023} \qquad (d_f \leq d_o) \qquad (15)$$

while for the oxidizer (wax flowing through the larger diameter orifice) the correlation becomes

$$D_o \propto P_D^{-0.25} \left(\frac{d_o}{d_f}\right)^{-0.168} \qquad (d_f < d_o) \qquad (16)$$

---

*An additional parameter, representing the relative effect of the velocity profiles of the opposing jets, should also be included. However, velocity profile effects were not a specific objective in the unlike doublet experiments and, as a consequence, in the bulk of the tests the velocity profile of the jet opposing the wax jet did not vary by an amount that was sufficient to obtain a meaningful correlation.

In those tests where molten wax was used to simulate both propellants (equal diameter orifices only), the overall dropsize depended upon P_D according to

$$D \propto P_D^{-0.12} \quad (P_D \leq 1) \tag{17}$$

where, by definition, P_D ($= V_2^2/V_1^2$) is always less than unity. A comparison of the above equations to the experimental data and the correlations obtained by Dickerson, Ref. 14, is presented in the next section. The influence of the characteristics of the wax jet (whether it is a fuel or oxidizer simulant) on atomization is also discussed in the following section.

For the present, it is of interest to examine the effects of the diameter and velocity of the opposing jets. Assuming that the wax jet parameters are held constant and employing the definition of P_D, Eq. (15) can be written as

$$D_f \propto \frac{d_o^{0.023}}{V_o^{0.33}}$$

while Eq. (16) becomes

$$D_o \propto \frac{d_f^{0.17}}{V_f^{0.50}}$$

From the above, it is seen that atomization of one of the jets of an unlike-doublet is enhanced by either an increase in the velocity or a decrease in the diameter of the opposing jet.

An understanding of the mechanisms governing the disintegration of liquid sheets produced by the impingement of circular jets can be obtained by examining the mechanisms leading to the disintegration of plane sheets. Dombrowski and Johns, Ref. 10, analyzed this problem and developed an analytical model relating the mean dropsize to the physical and dynamic properties of the sheet. Their model was extended in this study to include cases where the single sheet emanating from the impingement point is replaced by two sheets separated by a contact

discontinuity in velocity and physical properties. The double sheet could result, for example, from the impingement of immiscible fluids or of miscible fluids at different velocities. A detailed derivation of the model is presented in Appendix E. It should be noted that the derivation of the model is limited to plane sheets and as such is not directly applicable to an analysis of sheets produced by the impingement of circular jets. Nevertheless, it illustrates the dependence of dropsize on pertinent physical and dynamic parameters.

For small sheet velocities, the equation obtained from this model can be reduced to

$$D_o = 0.96 \left[\frac{2K_o^2 \bar{\sigma}^2}{V_o^4 \rho_a \bar{\rho}_L (1 + P_D \frac{\rho_o}{\rho_f})} \right]^{1/6} \qquad (18)$$

where $\bar{\sigma} = \sigma_o + \sigma_f$ is the surface tension ρ_a is the air density and $\bar{\rho}_L = \rho_o + \frac{h_f}{h_o} \rho_f$ is an average sheet density, while h_f and h_o are the sheet thicknesses. The constant K is a characteristic thickness of the sheet which, for example, could be the sheet thickness at the impingement point. Equation (16) yields the dropsize that would be obtained from the breakup of the oxidizer sheet. Similarly, the dropsize obtained from the fuel sheet would be given by:

$$D_f = 0.96 \left[\frac{2K_f^2 \bar{\sigma}^2 P_D (h_o/h_f)}{V_f^4 \rho_a \bar{\rho}_L (P_D + \frac{\rho_o}{\rho_f})} \right]^{1/6} \qquad (19)$$

In both equations the dynamic pressure ratio, P_D, has been defined as $(\rho V^2)_f/(\rho V^2)_o$. From Eq. (19) it is seen that as P_D is increased while V_f is held constant, the dropsize, D_f, increases. This is consistant with the empirical correlation expressed by Eq. (15). Similarly, an increase in P_D (Eq. 18) while holding V_o constant results in a decrease in the oxidizer dropsize. This is consistant with EQ. (16).

The reason for the observed behavior of dropsize with dynamic pressure ratio can be ascertained from an examination of Eq. (18) when cast in slightly different form. If it is noted that, by definition

$$1 + P_D \frac{\rho_o}{\rho_f} = \frac{V_o^2 + V_f^2}{V_o^2} \tag{20}$$

Eq. (18) may be rewritten as

$$D_o = 0.96 \left[\frac{K_o^2 \bar{\sigma}^2}{V_o^2 \rho_a \bar{\rho}_L \frac{V_o^2 + V_f^2}{2}} \right]^{1/6} \tag{21}$$

The quantity $\sqrt{1/2(V_o^2 + V_f^2)}$ can be taken to represent an average velocity of the sheet, $\bar{V}$. From Eq. (20) it is seen that when P_D is increased while V_o is held constant, V_f must increase or, equivalently, $\bar{V}$ increases. According to Eq. (21), the dropsize, D_o, will decrease. In an analogous manner, it can be shown from Eq. (19) that as P_D is increased $\bar{V}$ will decrease, while the dropsize, D_f, will get larger. Thus, the dropsize obtained from either sheet is inversely proportional to $\bar{V}$. It would be expected that if $(V_o^2 + V_f^2)$ is held constant while P_D is changed, the dropsize will not vary. In this case, holding V constant is approximately equivalent to maintaining a constant total momentum. (It would be exact if equal density fluids and equal diameter jets were utilized.) As shown on Figs. 69 and 70, the dropsize exhibits a small dependence on P_D when the total momentum is constant.

Similarly, the influence of the sheet thickness ratio, h_o/h_r on $\bar{D}$ is in agreement with the diameter ratio effect expressed by Eqs. (15) and (16). From Eq. (19), $\bar{D}_f \propto (\rho_o + \rho_f h_o/h_f)^{-1/6}$ while, from Eq. (19), $\bar{D}_f \propto (h_o/h_f)^2/(\rho_o h_o/h_f + \rho_f)$.

A consideration in the impingement of unequal diameter and/or unequal dynamic pressure ratio jets is the manner in which the individual sheet thicknesses influence the dropsize. This is of special importance when operating at a condition of near unity dynamic pressure ratio. At this condition, oscillations

about $P_D = 1$ will result in the stagnation of first one jet and then the other leading to rapid changes in the sheet thicknesses. This could then result in equally rapid variations in the dropsize. However, the experimental results indicate that there is no uniqueness associated with a unity dynamic pressure ratio condition. Indeed, while dynamic pressure ratio was used as a correlating parameter, its influence on dropsize can be explained equally well by a consideration of velocity effects.

Influence of Single Jet Characteristics on Dropsize. By applying a least squares technique[7] to all of the unlike-doublet data, the complete correlation equation (Eq. 14) was found to be

$$\bar{D}_f = 2.91 \times 10^4 \, V_f^{-0.76} \, d_f^{0.29} \left(\frac{p_c}{p_j}\right)_f^{-0.65} P_D^{0.165} \left(\frac{d_o}{d_f}\right)^{0.023} \quad (d_f \leq d_o) \tag{22}$$

for the fuel dropsizes and

$$D_o = 2.72 \times 10^4 \, V_o^{-0.57} \, d_o^{0.65} \left(\frac{p_c}{p_j}\right)_o^{-0.30} P_D^{-0.25} \left(\frac{d_o}{d_f}\right)^{-0.17} \quad (d_f \leq d_o) \tag{23}$$

for the oxidizer dropsizes.*

The study of velocity profile effects was not a specific objective of the unlike-doublet characterization. However, in order to correlate the data it was necessary to incorporate profile effects. From the above correlations, it is seen that as the velocity profile of a liquid jet develops, the dropsize obtained from that jet decreases. This result is analogous to that of the like-doublet.

---

* In the case of equal diameter unlike-doublets, Eq. (22) should be used to compute both fuel and oxidizer dropsizes.

Dropsizes calculated from the above equations are compared to the experimental data in Tables 14 and 15 for the fuel and oxidizer dropsizes respectively. A comparison is also made on Figs. 68, 69, and 70. In general the calculated values of $\bar{D}$ are quite good. An exception to this is the dropsize obtained when the opposing jet was water.

With the exception of those experiments where water was used as a propellant simulant (and, perhaps, 2 or 3 wax/DEW1 tests) the unlike-doublet study was performed primarily with laminar jets. Consequently, it can be presumed as in the case of like-doublets, that liquid sheet breakup was caused by either aerodynamic waves or the combined action of aerodynamic and impact wave instability. In fact, the similarity of the velocity exponents of the like-and unlike-doublet correlating equations, shown in Table 16, tend to support this. It is also of interest to note that the previously discussed breakup model, where disintegration resulted from aerodynamic instability, yields a comparable velocity exponent (-0.67).

On the other hand, the unlike-doublet experiments of Dickerson, Ref. 14, (using a wax/H_2O propellant simulant combination) were performed with primarily turbulent wax jets while the water jets were always turbulent. As shown in Table 16, identical exponents of P_D, d_f and d_o were obtained between this work and Ref. 14 for the fuel-side dropsize. Also, the velocity exponent of the Ref. 14 fuel dropsize correlation coincides almost exactly with the like-doublet turbulent jet velocity exponent (-1.07 vs -1.0). The oxidizer correlations of Ref. 14 and this program are considerably different. This may be attributed to the difference in the flow regime of the two studies; however, it was noted in Ref. 14 that the quantity of data was too small to obtain an accurate correlation for $\bar{D}_o$ so the Ref. 14 $\bar{D}_o$ correlation must remain somewhat suspect.

The level of dropsize obtained from Eq's. (22) and (23) and the correlating equation presented in Ref. 14, are compared on Fig. 95 as a function of injection velocity for both fuel and oxidizer dropsize. An orifice diameter or 0.060 inch, P_D = 1.0, and uniform velocity profile jets were assumed. As shown there, the injection velocity at the intersection of the two lines is comparable to the velocity at the intersection of the laminar and turbulent like-doublet correlations.

TABLE 14

COMPARISON OF MEASURED AND CALCULATED FUEL DROPSIZES FOR UNLIKE DOUBLET

Run	L_o/d_j	d_{wax}	d_o/d_f	V_{wax}	$(p_c/p_j)_{wax}$	P_D	Propellants	$\bar{D}_{meas}$	Equation 22		Equation 24	
									$\bar{D}_{calc}$	% Err	$\bar{D}_{calc}$	% Err
105	1.5	0.060	1.0	55.1	1.210	0.442	Wax/Dew 2	470	457	-2.9	---	---
106				70.4	1.175	0.970		457	439	-4.0	---	---
107				80.2	1.155	1.990		423	453	6.6	---	---
108				69.1	1.175	0.951		444	444	0	---	---
109				69.7	1.175	0.994		456	445	-2.6	---	---
110				55.6	1.210	0.451		473	455	-3.9	---	---
111				80.2	1.155	1.960		435	452	3.7	---	---
112				68.6	1.175	0.930		464	445	-4.2	---	---
117	1.5	0.060	1.5	55.9	1.210	1.065	Wax/Dew 2	536	527	-1.6	---	---
118				41.7	1.250	0.500		525	571	8.0	---	---
119				66.2	1.185	2.010		480	522	8.0	---	---
120				66.3	1.185	1.055		418	468	10.8	---	---
121				70.0	1.175	0.546		395	405	2.5	---	---
122				79.1	1.155	4.510		402	529	24.0	---	---
129	1.5	0.060	2.0	66.3	1.185	1.040	Wax/Dew 2	505	470	-7.4	---	---
130				48.6	1.230	0.503		455	517	12.0	---	---
131				80.5	1.155	1.830		480	452	-6.1	---	---
132				70.0	1.175	1.000		455	451	0.9	---	---
133				70.0	1.175	0.502		310	402	24.9	---	---
134				66.5	1.185	1.850		550	516	-6.6	---	---
141	10	0.063	1.36	30.6	1.760	1.365	Wax/Water	585	692	15.4	583	-0.3
142				40.0	1.682	1.290		560	575	2.6	530	-5.7
143				60.0	1.550	2.150		474	483	2.0	509	-7.0
147	10	0.063	2.03	30.6	1.760	2.113	Wax/Water	507	750	21.8	633	7.2
148				39.8	1.685	1.952		591	623	5.1	573	-3.1
149				60.4	1.545	1.779		526	471	-11.6	498	-5.6
156	50	0.067	1.28	52.7	2.120	1.714	Wax/Water	416	427	2.5	431	3.4
157				35.7	2.420	1.020		424	484	12.5	430	1.3
158				26.9	2.620	1.055		488	574	15.0	464	-5.1
153	50	0.067	1.0	49.6	2.17	0.87	Wax/Dew 1	339	391	13.4	---	---
154				77.5	1.76	0.95		290	323	10.3	---	---
155				123.0	1.42	0.93		257	260	1.1	---	---
165	50	0.067	1.28	52.5	2.12	1.75	Wax/Dew 1	443	429	-3.2	---	---
166				101.0	1.49	2.31		349	342	-1.9	---	---
167				132.5	1.42	1.98		274	280	2.1	---	---
168				39.2	2.35	1.03		384	460	16.6	---	---
169				76.8	1.78	0.96		321	326	1.7	---	---
170				109.5	1.38	0.98		291	294	0.9	---	---
171				39.8	2.34	0.58		421	415	-1.5	---	---
172				70.8	1.85	0.56		352	309	-13.9	---	---
173				96.5	1.54	0.71		292	286	-2.2	---	---
179	50	0.067	1.91	35.9	2.84	1.36	Wax/Dew 1	558	481	-16.0	---	---
180				73.2	1.82	1.40		375	357	-4.9	---	---
181				99.4	1.52	1.51		272	322	15.5	---	---

TABLE 15

COMPARISON OF MEASURED AND CALCULATED OXIDIZER DROPSIZES FOR UNLIKE DOUBLET

Run	L_o/d_j	d_{wax}	d_o/d_f	V_{wax}	$(p_c/p_j)_{wax}$	P_D	Propellants	$\bar{D}_{meas}$	Equation 23		Equation 25	
									$\bar{D}_{calc}$	% Err	$\bar{D}_{calc}$	% Err
123	1.5	0.090	1.67	58.8	1.14	0.518	Wax/Dew 2	612	589	-4.0	---	---
124	↓	↓	↓	53.2	1.15	1.000	↓	540	538	-2.2	---	---
125				46.7	1.18	2.060		490	471	-4.0	---	---
126				70.0	1.12	0.426		550	563	2.4	---	---
127				70.5	1.12	1.040		437	449	2.7	---	---
128				70.0	1.12	1.910		360	387	7.0	---	---
135	1.5	0.120	2.0	60.0	1.08	1.985	Wax/Dew 2	500	483	-3.5	---	---
136	↓	↓	↓	64.0	1.10	1.080	↓	605	543	-11.4	---	---
137				50.0	1.05	4.050		470	446	-5.5	---	---
138				69.9	1.10	0.910		545	546	0.1	---	---
139				70.0	1.10	0.505		698	627	-11.4	---	---
140				70.0	1.10	1.860		430	452	4.9	---	---
144	10	0.086	1.36	29.9	1.67	1.413	Wax/Water	697	592	-17.6	641	-8.7
145	↓	↓	↓	40.1	1.58	1.413	↓	568	510	-11.5	584	2.7
146				60.2	1.45	1.428		495	414	-19.7	514	3.7
150	10	0.128	1.49	31.2	1.53	1.929	Wax/Water	596	666	10.5	607	1.8
151	↓	↓	↓	40.2	1.45	2.110	↓	584	672	-2.0	545	-7.1
152				59.4	1.30	2.210		455	468	2.8	485	6.2
159	50	0.086	1.28	59.8	1.77	1.771	Wax/Water	392	375	-4.7	429	8.6
160	↓	↓	↓	39.7	2.20	1.755	↓	489	513	4.7	486	0.06
161				29.8	2.36	1.773		521	511	-20.0	484	-7.7
174	50	0.086	1.28	43.6	2.17	2.11	Wax/Dew 1	434	404	-7.5	---	---
175	↓	↓	↓	56.1	1.83	2.84	↓	346	342	-1.0	---	---
176				92.6	1.42	1.77		294	312	5.7	---	---
182	50	0.128	1.91	34.1	1.93	1.46	Wax/Dew 1	591	639	7.5	---	---
183	↓	↓	↓	57.4	1.42	1.41	↓	538	525	-2.4	---	---
184				84.9	1.42	1.33		448	427	-5.0	---	---

TABLE 16

SUMMARY OF MOLTEN WAX DROPSIZE CORRELATIONS

Element Type	Exponents				Flow Regime	Reference
	V_{wax}	d_{wax}	P_D	d_o/d_f		
Like-Doublet	-0.75	0.57	---	---	Laminar	Eq. 6
	-1.0	0.57	---	---	Turbulent	Eq. 7
	-0.85	0.57	---	---	Lam. & Turb.	Ref. 14
Unlike-Doublet Fuel Side	-0.76	0.29	0.165	0.023	Laminar	Eq. 22
	-1.07	0.29	0.165	0.023	Lam. & Turb.	Ref. 14
Unlike-Doublet Oxidizer Side	-0.57	0.65	-0.25	-0.17	Laminar	Eq. 23
	-2.05	-0.38	-0.59	0	Lam. & Turb.	Ref. 14

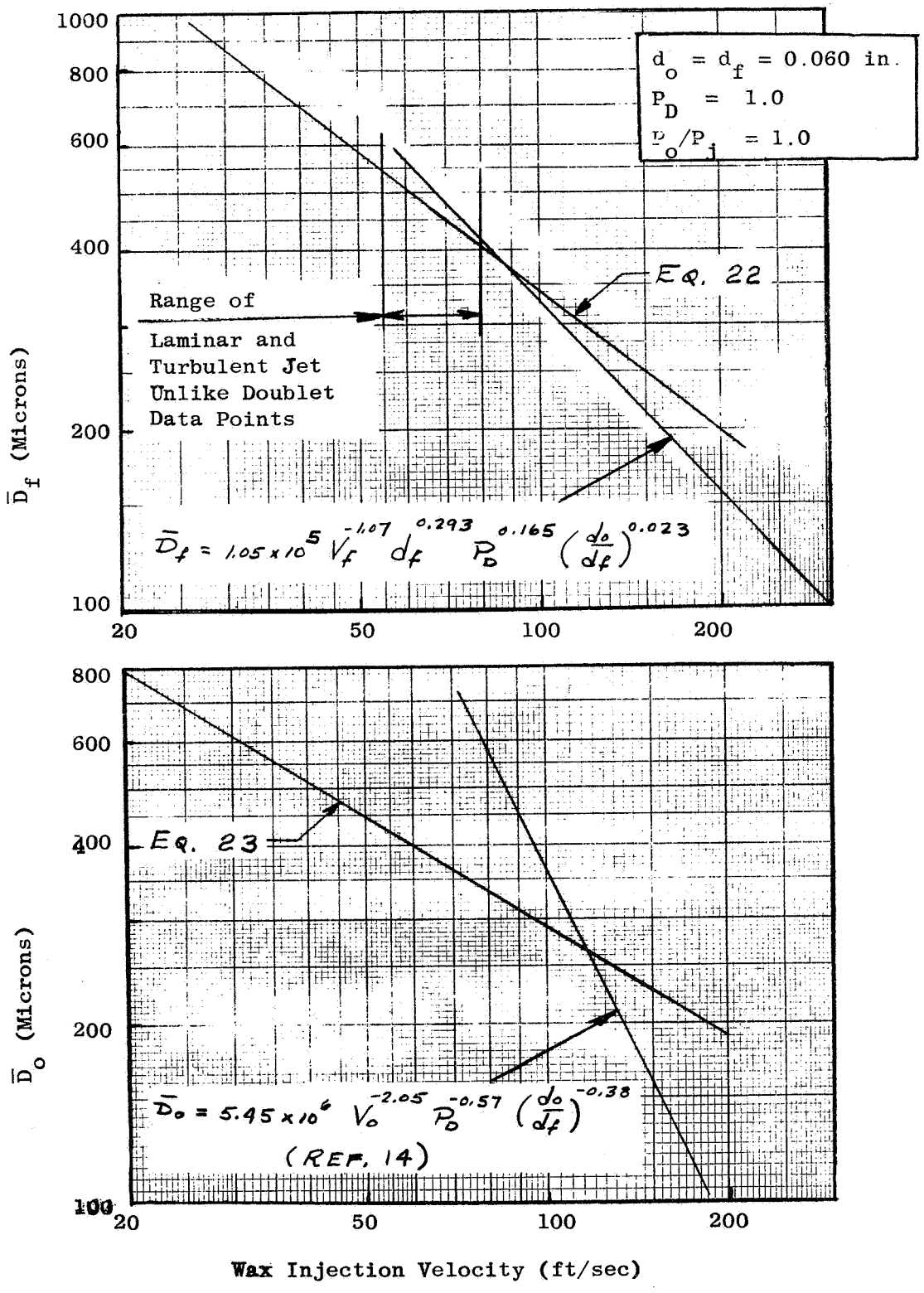

Figure 95. Comparison of Unlike -Doublet Dropsize Correlations

From the correlations obtained in this program and those of Ref. 14, it is evident that the unlike-doublet atomization characteristics will be a function of the flow regime (i.e., laminar or turbulent). In the discussion concerning the mechanisms of sheet disintegration in the two flow regimes for the like-doublet element, it was noted that the disintegration mechanism depended upon the Weber number regime as well. (Below the Weber number range of 66 to about 165 only aerodynamic wave disintegration has been observed.) For the unlike-doublet experiments conducted in this program, the Weber number* regime for the wax (assuming $d_j = 0.060$) was about 600 to 16,000. Surface tension data for the diethanolamine/water solution was not available. However, diethanolamine is a hydrocarbon which characteristically has a surface tension of about 20-30 dynes/cm. Since the DEW solution is primarily diethanolamine, a surface tension of 30 dynes/cm was arbitrarily assumed. This value yields a Weber number regime of about 1100 to 12,000 for the DEW. In the Ref. 14 program, the Weber number range for the wax was about 14,000 to 64,000. For the water, it ranged from 6,000 to 24,000. Thus, the differences in the correlations obtained in this program and Ref. 14 may be a result of not only a different Reynolds number regime but a different Weber number range as well. (This is discussed further in Appendix D.)

The above discussion is, of course, speculative. However, it is interesting to note that the wax/water data obtained in this program did not correlate well with the unlike-doublet correlation equations (see Tables 14 and 15). The discrepancy may, of course, be simply due to experimental error or because the water jet was turbulent while the wax jet was laminar. On the other hand, it may be a result of the Weber number regime in which these tests were conducted. For these experiments, the Weber number range for water was about 200 to 3500; the lower end of which is close to the critical Weber number regime mentioned above. The Weber number range for the wax was 1400 to 16,000. Thus, it is conceivable that the presence of water sufficiently lowered the sheet Weber number such that the dominant breakup mechanism was aerodynamic in spite of the existance of turbulence in the water jet. It was found that the wax/water dropsize correlation could be

$$*N_W = \frac{d_j V_j^2 \sin^2 (\gamma/2)}{\sigma}$$

significantly improved by changing the velocity exponent of Eqs. (22) and (23) while retaining the exponents of the other parameters. The correlation equations obtained are

$$\bar{D}_f = 7910\ V_f^{-0.44}\ d_f^{0.29}\left(\frac{p_c}{p_j}\right)^{-0.65}\ P_D^{0.165}\ \left(\frac{d_o}{d_f}\right)^{0.023}\quad (\text{wax}/H_2O) \qquad (24)$$

and

$$D_o = 10{,}050\ V_o^{-0.44}\ d_o^{0.65}\ \left(\frac{p_c}{p_j}\right)^{-0.30}\ P_D^{-0.25}\ \left(\frac{d_o}{d_f}\right)^{-0.17}\quad (\text{wax}/H_2O) \qquad (25)$$

As shown in Tables 14 and 15, the above equations give a much better correlation than Eqs. (22) and (23).

When the influence of dynamic pressure ratio was examined using turbulent jets, no difference in dropsize between the turbulent and laminar jet impingement was observed over a fairly large range of P_D. The results of these tests are shown on Fig. 67. However, it appears that the reason for this is an unfortunate choice of injection velocity. Shown on Fig. 95 are the correlating equations of Dickerson and this work for the fuel dropsize. The curves were plotted assuming $d_o = d_f = 0.060$ inch and $P_D = 1$. As shown there, the two correlations intersect in the proximity of the laminar and turbulent jet data points. Thus, it is possible that had the experiments been conducted at either a higher or lower velocity, effects of turbulence would have been observed. It may be assumed that these data points would have followed the correlation of Dickerson.

Influence of Orifice Geometry on Dropsize. Injector design effects were also not a specific objective in the study of unlike-doublet atomization. Consequently, until data is available to explicitly determine their influence on this element type, the empirical equation defining the effects of misimpingement and impingement angle for the like-doublet may be assumed to be applicable. It is also reasonable to expect similar free jet length and orifice entrance effects on atomization.

With respect to the latter, experimental dropsize measurements obtained by Nurick and McHale, Ref. 19, using sharp entrance, unequal diameter doublets and wax/water propellant simulants, were found to be substantially smaller than would be predicted from the correlations of this program or Ref. 14. In view of the results obtained with sharp entrance orifices during the current program, their measurements were probably influenced by jet separation.

Measurements of the separated jets produced in this program indicated that they were laminar and possessed a nearly uniform velocity profile. Therefore, the like-doublet, laminar jet correlation was used to correlate the sharp entrance data obtained here. As previously noted, a good correlation was obtained; particularly in the slope of the dropsize/velocity relation. However, when Eq. (22) (the laminar, fuel dropsize correlation) was applied to the Ref. 19 data, a good fit could not be obtained. It was found that a fairly good correlation could be obtained when the fuel-side correlation presented in Ref. 14 was used.*

Assuming that the Ref. 19 data was obtained with separated jets, Dickerson's equation becomes

$$\bar{D}_f = 10^5 \, (C_c)^{1.215} \, V_f^{-0.74} \, V_o^{-0.33} \, d_f^{-.27} \, d_o^{.023} \qquad (26)$$

after correcting for velocity and jet diameter changes resulting from separation by means of the contraction coefficient. As shown on Fig. 96, the results presented in Ref. 19, correlate quite well with the above equation if a value of 0.60 is assumed for C_c. Thus, it appears that for unlike-doublets, as in the case of the like-doublet, the effect of jet separation on dropsize can be

---

*The reason for this anomaly is uncertain. However, upon examining the Ref. 19 data and orifice geometry, it was found that the Reynolds number of the water in the entrance tube was 11,000 or greater. Hence, the flow was probably turbulent upstream of the orifice. Even though the jet separated, turbulence in the free jet may have altered the sheet breakup mechanism. If this was the case, the correlation with the Ref. 14 equation would be reasonable.

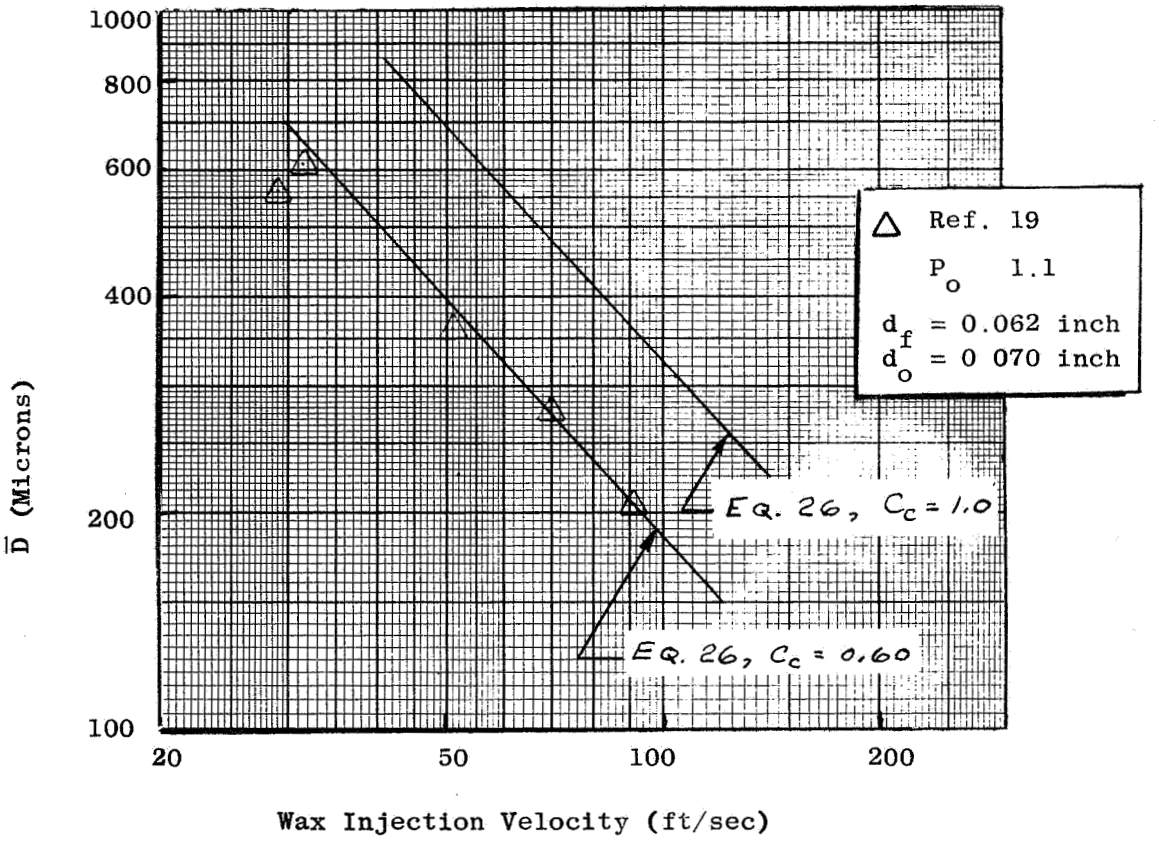

Figure 96. Comparison of Sharp Orifice Dropsize Data with Empirical Correlation (Unlike Doublet)

accounted for by a simple correction of the unseparated jet correlating equation.

Influence of Propellant Miscibility on Dropsize. When immiscible liquid jets impinge, it is reasonable to assume that the droplet formation mechanisms will be altered if only because of the physical property differences of the liquids forming the spray fan. In the investigation of the influence of propellant miscibility on dropsize, three sets of experiments were performed. The procedures employed to obtain and reduce the data are described in Section 4.2.2.

In the first series of tests, nine experiments were performed using equal diameter, short (L_o/d_j = 1.5) orifices; five of which used wax/DEW2 as the propellant simulants while the remainder used wax/wax. Because of the short orifice length the velocity profiles were nearly uniform. The results of these tests, which were performed at different dynamic pressure ratios but constant total momentum, are shown on Fig. 68. It is evident that, with the wax/DEW2 combination, the molten wax dropsize obtained from one DEW2 and one wax jet was substantially larger than the overall dropsize obtained from the two wax jets.

In the second series of tests, six tests were required to obtain a miscible versus immiscible dropsize comparison for any given operating condition. Six dropsize comparisons were obtained using two different diameter ratio, 50 L_o/d_j doublets operating at various total momentum levels. The results of the tests are presented in tabular form on Table 11. Whereas in the first series of tests, immiscible liquid jets produced larger dropsizes than miscible jet impingement, the converse was found to be true from this last test series.

An explanation for this anomaly is provided by a comparison of the empirical correlations of the dropsizes obtained from like- and unlike-doublet elements, Eqs. (6) and (22). For equal diameter elements, at the same injection velocity and unity dynamic pressure ratio, the ratio of Eqs. (6) and (22) becomes

$$\frac{\bar{D}_{L.D.}}{\bar{D}_{U.D.}} = 1.67\, V^{0.016} \left(\frac{P_c}{P_j}\right)^{0.13} d^{0.28} \qquad (27)$$

From this it is seen that the ratio of the dropsizes obtained when $P_D = 1$ and with miscible and immiscible propellants depends primarily on the velocity profile development and the orifice diameter.

In the first series of tests described above, the orifice diameter was 0.060 inches and the velocity profile was nearly uniform. Substituting these values and neglecting the (weak) velocity effect Eq. (27) reduces to

$$\frac{\overline{D}_{L.D.}}{\overline{D}_{U.D.}} = 0.76$$

From Fig. 68, the ratio of the experimentally measured miscible and immiscible propellant dropsizes at $P_D = 1$ can be shown to be 0.79. Thus the correlating equations correctly predict larger immiscible propellant dropsizes under these test conditions.

In the second series of tests, long orifices, and consequently jets with non-uniform velocity profiles were used. To evaluate the relative dropsizes obtained from miscible and immiscible jet impingement, the correlating equations were compared at an arbitrarily selected velocity of 50 ft/sec. For the 0.067-inch diameter, 50 L_o/d_j orifices, this velocity corresponds to a centerline pressure ratio of 2.2. Under these conditions, and with $P_D = 1$, Eq. (27) becomes

$$\frac{\overline{D}_{L.D.}}{\overline{D}_{U.D.}} = 0.93$$

With the occurrence of a suitable amount of velocity profile development, the correlating equations would predict nearly equal miscible and immiscible propellant dropsizes which is in agreement with the experimental results shown in Fig. 80.

Because of the manner in which the third series of tests were performed, the simple analysis employed in the above two cases is not readily applicable However, it is not difficult to conceive of a situation in which, with a proper combination of parameters, the miscible jet dropsizes would be larger than those obtained with immiscible jets.

While the correlating equations proved useful in demonstrating that what appeared to be inconsistant data were actually consistent with the rest of the unlike doublet results, they do not afford a physical explanation of the reasons for the differences. Furthermore, from the results of this study, it cannot be concluded unconditionally that the condition of propellant miscibility will influence the mass median dropsize. The reason for this is that, while an immiscible propellant combination is obtained when one of the wax jets is replaced by DEW, the liquid physical properties and, as a consequence, the forces which result in spray fan disintegration, have also been altered. It can be concluded however, that wax/DEW impingement (or any other dissimilar fluid combination) will, in general, result in a dropsize different from that of wax/wax impingement. The extent and direction of this difference will be a function of the specific operating conditions.

5.2.3 Atomization Characteristics of Triplet and Pentad Elements

As in the case of the unlike-doublet, the atomization characteristics of triplet and pentad elements have received little attention. An exception to this is the work of Dickerson, et al., Ref. 14, which included a characterization of pentad elements.

All of the parameters which influence unlike-doublet atomization (e.g., velocity profile, dynamic pressure ratio, diameter ratio, etc.) can also be presumed to influence the triplet and pentad atomization characteristics. However, only a limited number of tests were performed with these element types and the injection velocity was the only parameter which was varied over a significant range. Velocity profile changes occurred over the injection velocity range examined but the quantity of data points was insufficient to include this parameter in a correlation. The influence of velocity profile is

particularly evident from the pentad oxidizer results, Fig. 82, which illustrates the difference in velocity dependence between the high and low velocity range.

From Fig. 81 it is seen that approximately the same oxidizer and fuel dropsizes were obtained with the triplet element. The empirical equation

$$\bar{D} = 4260\ V_{wax}^{-0.575}$$

which exhibits a velocity dependence similar to that of the unlike-doublet oxidizer correlation, Eq. (23), was found to fit the data quite well. The two oxidizer data points at the injection velocity of 150 ft/sec suggest a high velocity slope of approximately V^{-1} which would be in agreement with the high velocity correlations of the like and unlike doublets.

The fuel (center orifice) dropsize data obtained with the pentad element, Fig. 82, were found to agree quite well with the correlation of Dickerson, Ref. 14. The decreasing slope at lower velocity is presumably due to the effect of velocity profile; however, this was not verified experimentally. On the other hand, the oxidizer (four outer orifices) dropsize exhibits a considerable deviation from the Ref. 14 correlation at the lower injection velocities. This, again, is a result of the aforementioned velocity profile variations. The oxidizer dropsizes are seen to be influenced more by velocity profile than are the fuel dropsizes at comparable velocities. This is probably due to the fact that, in measuring the oxidizer dropsize, four laminar molten wax jets are opposed by a single turbulent water jet, while the opposite occurs when the fuel dropsizes are measured. The result is that the flow regime of the four jets (laminar for the oxidizer and turbulent for the fuel) appears to dominate the droplet formation process.

It is interesting to note that the Ref. 14 correlations, which were obtained in a high velocity (and probably turbulent) regime, exhibit a velocity dependence

of about V_j^{-1}. * (That is to say the sum of the fuel and oxidizer velocity exponents is about -1.) The similarity of the dropsize dependence on velocity for all element types suggests that the mechanisms governing sheet disintegration are independent of the number of impinging jets involved in the spray formation.

5.2.4 Correlations of Dropsize Distributions

In general, the dropsize distributions about the mass median dropsize did not significantly vary as the geometric (including element type) and hydraulic operating conditions were changed. In those cases where some variation did occur, the dropsize distribution became more monodisperse (i.e., approaching a state of uniform dropsize) under the following conditions:

1. immiscible propellant combinations
2. increased total momentum (or injection velocity)
3. as the diameter ratio approached unity
4. when misimpingement was decreased

It was found that, for a given element type and injection velocity, the impingement angle, turbulence and free jet length had a minimal effect on the distribution.

No single distribution function was found that would precisely fit all the distributions. Rather than seek a unique distribution function for each droplet distribution curve, a single function was determined and deviations of the measured distributions from this function were specified in tabular form. Assuming that it is more important from the standpoint of combustion analysis to accurately fit the larger dropsizes in the distribution, a Rossin-

---

* Note that $\bar{D}_o \propto V_o^{-.57} V_f^{-.56} \propto V_o^{-1.13} P_D^{-.285}$

and

$\bar{D}_f \propto V_f^{-.08} V_o^{-.89} \propto V_f^{-.97} P_D^{.445}$

Rammler (Ref. 32) distribution function was found that would reasonably fit most the wax droplet distribution curves obtained in this study. This function is given by:

$$\frac{d(\dot{w}/\dot{w}_{TOT})}{d(D/\bar{D})} = \frac{2.46\ (D/\bar{D})^{1.46}}{(1.21)^{2.46}}\ \text{EXP}\ -\frac{D/\bar{D}}{1.21}^{2.46} \qquad (29)$$

where

$\dot{w}/\dot{w}_{TOT}$ = cumulative mass fraction

and

$D/\bar{D}$ = normalized mass median dropsize

The integral of Eq. (29) is shown on Fig. 97, The deviations of the measured data from this function are defined by

$$\left(\frac{D}{\bar{D}}\right)_{meas} = \left(\frac{D}{\bar{D}}\right)_{calc} + \triangle\frac{D}{\bar{D}}$$

The differences between the measured and calculated values of $\triangle(D/\bar{D})$ for various hydraulic and geometric perturbations are listed in Table 17 for like and unlike doublets.

In the utilization of median droplet size and dropsize distributions it is often more convenient to employ a definition of mean droplet diameter other than the mass median dropsize, e.g., surface mean or volume mean diameters. Once a dropsize distribution based on croplet mass is obtained, a straightforward procedure (see e.g., Mugele and Evans, Ref. 33) can be used to

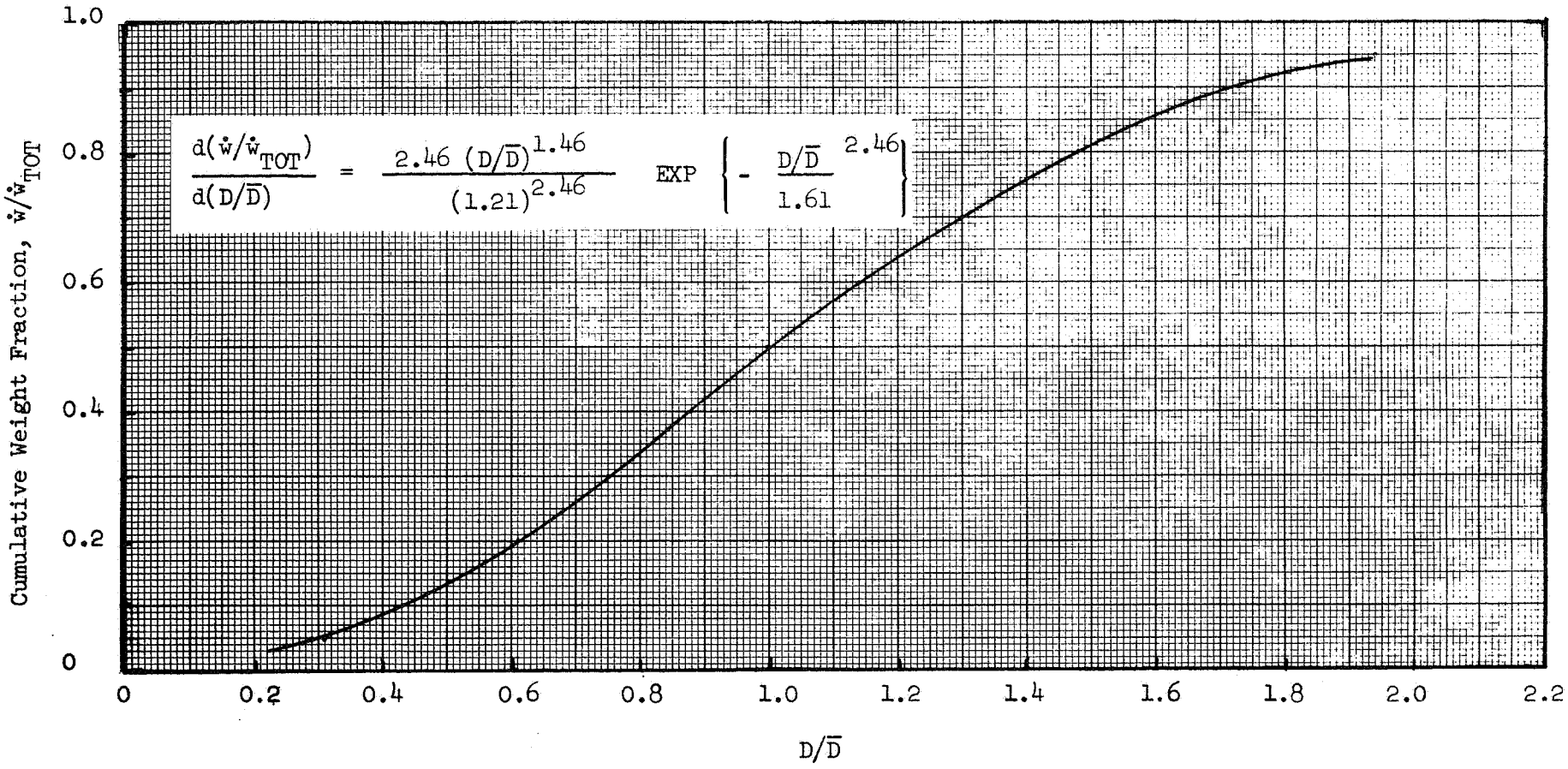

Figure 97. Rosin-Rammler Normalized Distribution Function

TABLE 17. SUMMARY OF DROPSIZE DISTRIBUTIONS

EQUATION 29 $\frac{\dot{w}}{\dot{w}_{TOT}}$	D/$\bar{D}$	$\triangle(D/\bar{D})$									
		LIKE-DOUBLET				UNLIKE-DOUBLET					
						FUEL-SIDE		OXIDIZER SIDE			
		$L_o/d_j = 1.5$ $V_j = 80$ ft/sec $\Delta/d_j = 0$	$L_o/d_j = 1.5$ $V_j = 166$ ft/sec $\Delta/d_j = 0$	$L_o/d_j = 200$ $V_j = 90$ ft/sec $\Delta/d_j = 0$	$L_o/d_j = 1.5$ $V_j = 80$ ft/sec $\Delta/d_j = 0.75$	$d_o/d_f = 1.5$ $V_L = 70$ ft/sec $P_D = 0.5$	$d_o/d_f = 1.5$ $V_f = 70$ ft/sec $P_D = 2.0$	$d_o/d_f = 1.5$ $V_o = 70$ ft/sec $P_D = 0.5$	$d_o/d_f = 1.5$ $V_o = 70$ ft/sec $P_D = 2.0$	$d_o/d_f = 1.0$ $P_D = 1.5$	$d_o/d_f = 1.0$ $P_D = 2.0$
0.05	0.31	0.04	0.17	0.09	0.04	0.18	0.10	0.09	+0.19	0.15	0.17
0.10	0.43	0.07	0.14	0.06	0.07	0.15	0.08	0.07	0.15	0.12	0.15
0.20	0.61	0.05	0.10	0.03	0.05	0.11	0.05	0.05	0.11	0.07	0.09
0.30	0.75	0.04	0.07	0.04	0.04	0.08	0.05	0.05	0.08	0.04	0.05
0.40	0.88	0.04	0.03	0.03	0.03	0.05	0.03	0.03	0.05	0.01	0.01
0.50	1.0	0.0	0.0	0.0	0.0	0.0	0.0	0.0	0.0	0.0	0.0
0.60	1.14	-0.01	-0.05	-0.01	0.19	-0.04	-0.02	-0.02	-0.02	-0.03	-0.06
0.70	1.3	-0.01	-0.08	-0.03	0.20	-0.09	-0.05	-0.04	-0.10	-0.08	-0.10
0.80	1.48	-0.02	-0.08	-0.06	0.27	-0.11	-0.04	-0.03	-0.04	-0.11	-0.15
0.90	1.73	-0.05	-0.05	-0.10	0.42	-0.12	-0.02	-0.01	-0.12	-0.10	-0.22
0.95	1.94	-0.10	-0.01	-0.18	0.51	-0.14	-0.02	-0.06	-0.13	+0.01	-0.28

determine all other mean diameters. From Ref. 33, the mean diameter D_{P_a} is related to $\bar{D}$ through

$$D_{PQ} = \bar{D} \left(\frac{X_P}{X_Q}\right)^{\frac{1}{P-Q}} \tag{30}$$

where P and Q are integers that define the mean diameter to be determined, e.g., the volume mean diameter, D_{30} (P = 3, Q = 0). The quantities X_P and X_Q are obtained from

$$X_i = \int_0^1 \frac{6\pi}{\rho D^3} \left(\frac{D}{\bar{D}}\right)^i \frac{d(w/w_{TOT})}{d(D/\bar{D})} \, d\left(\frac{D}{\bar{D}}\right) \quad (i = P \text{ or } Q) \tag{31}$$

where $d(w/w_{TOT})/d(D/\bar{D})$ is defined by the mass distribution function. Substituting the Rossin-Rammler distribution, Eq. (29), the integrals, X_i, were evaluated numerically for values of i ranging from 0 through 5. The results are listed in Table 18.

TABLE 18

MEAN DIAMETER CONVERSION FACTORS

i	X_i
0	10.35
1	2.85
2	1.31
3	0.98
4	1.00
5	1.24

As an example of the use of this Table, the volume mean diameter will be evaluated. From Eq. (3) and Table 18,

$$D_{30} = \bar{D} \left(\frac{X_3}{X_0}\right)^{1/3} = \bar{D} \left(\frac{0.98}{10.35}\right)^{1/3}$$

or

$$D_{30} = 0.455 \bar{D}$$

5.3 OCCURRENCE OF EMULSIFICATION

When liquid atomization is produced by the impingement of two dissimilar fluids, the question arises as to how the atomization is affected by the interaction of the fluids. Since unlike impinging elements are designed such that the liquid fuel and oxidizer impinge with considerable dynamic force, it is conceivable that an emulsion may be formed. The occurrence of an emulsion at the interface would be extremely important to any model describing mixing, atomization, or reactive stream blowapart.

The results of this study, shown in Fig. 87, indicate that a nominal level of 1-percent DEW-1 was imbedded in the wax droplets at all test conditions. Based on these results, it is indicated that, even though an emulsion is formed when two immiscible liquids collide, the level of emulsification is relatively invarient with either momentum level or element type. While this level of emulsification will, in all probability, not effect the median dropsize, it may be important when hypergolic propellant combinations are employed. Even a 1-percent emulsification could result in ignition within the sheet and, hence, lead to cyclic blowapart.

6.0 CONCLUDING REMARKS

Previous investigations of the atomization characteristics of impinging stream injectors have generally been limited to a study of the effects of orifice diameter, injection velocity, and impingement angle on mean dropsizes. The results of this study have shown that additional parameters such as orifice and free jet geometry, free jet internal characteristics, dynamic pressure ratio and propellant miscibility are also important. Aside from presenting dropsize correlations with these various parameters, it was also shown that apparent discrepancies between the correlations of other investigators could be resolved by a consideration of the effects of flow regime and orifice entrance type on the internal characteristics of the jets and their concomittant influence on atomization.

In order to properly apply the dropsize correlations presented herein, the flow regime of the liquid jets must be delineated. It was found that, with nearly quiescent* inlet conditions, a Reynolds number of 10,000 is a practical upper limit for laminar flow. A lower limit for turbulent flow is, of course, the upper critical Reynolds number of 2300. In contemporary injector manifold systems (e.g., cross-flow manifold) non-quiescent flow at the orifice entrance is almost always present. Under these conditions, turbulent flow can be expected whenever the jet Reynolds number exceeds 2300.

*A quiescent entry flow would exist for example, when the orifice is fed from an essentially statis reservoir. In this case, the jet characteristics are free of any manifold effects. With non-quiescent entrance conditions, turbulence and velocity gradients generated within the manifold (resulting from, for example, cross-flow) are introduced into the orifice.

Results of this work point out that in the design of injection systems, the geometric parameters of orifice length, free jet length, and orifice entrance type should be considered from the standpoint of atomization because of their influence on the individual jet characteristics. From these results, guidelines from the selection of the above parameters can be established. For example, since the jet disintegration which occurred at the longer jet lengths resulted in decreased atomization, free jet lengths greater than 5 orifice diameters should be avoided. If quiescent or nearly quiescent inlet conditions exist, the orifice length can be as short as 1 to 2 orifice diameters. With non-quiescent entry conditions, however, an orifice length greater than 15 diameters is required in order to insure that manifold conditions will not significantly influence atomization. When the orifice length is between 6 to 15 diameters, the jet characteristics will exhibit some degree of manifold effects; but since atomization under these conditions was not examined, the corresponding influence on dropsize is not known. Orifice lengths less than 6 diameters should be avoided when the entry flow is non-quiescent, because of the possible occurrence of jet disintegration.

The recommended orifice entrance type depends upon the manifold type and orifice length. If a cross-flow manifold is used with an orifice 15 d_j or greater in length, either a round or sharp entrance is acceptable. (A point in favor of rounded over sharp entrances is the lower ΔP required for a given flowrate.) For orifice lengths less than 15 d_j, a round entrance orifice is recommended in order to achieve some control over jet characteristics. This is particularly true when the orifice length is less than 6 d_j since the occurrence of hydraulic flip, and hence jet misimpingement, is quite likely with sharp entrance orifices.

With quiescent inlet conditions, sharp entrance orifices should be avoided (unless the orifice length is greatly in excess of 10 d_j) because of the possible occurrence of jet separation. Although, on the surface it might appear that, because of the increase in atomization, sharp entrance orifices offer a decided advantage over rounded entrance types, it should be noted

that the same result can be obtained, with nearly the same injection Δp, by using round entrance orifices with a diameter and injection velocity equivalent to those of the separated jet. The disadvantage of sharp entrance orifices is that it is entirely possible that some of the jets would be separated while others would be flowing "full". The resulting variation of propellant atomization and flowrate could seriously affect combustion performance.

The empirical correlations presented in this report are, of course, directly applicable to molten wax only. In order to convert the dropsize computed from these equations to a propellant dropsize, a physical property correction factor is required. Unfortunately, there is a distinct lack of consistant data regarding physical property effects on dropsize. Until such data is available, the physical property correction factors suggested by, e.g., Wolfe and Anderson, Ref. 35, or Ingebo, Ref. 36, may be used.

It is concluded that the molten wax technique is an excellent tool for the cold-flow evaluation of the mechanisms governing atomization. This conclusion is based on the following reasons. (1) The entire spray field is readily analyzed and, consequently, the dropsize and size distribution results are therefore not influenced by such factors as depth of field and measurement location which are encountered with photographic techniques. (2) Through the use of immiscible liquids, the wax technique permits the direct measurement of both fuel and oxidizer sprays resulting from unlike impinging injector elements. (3) This technique is economical primarily because of the simple sieve analysis used to determine the spray size distribution.

Recommendations for future work resulting from observations in this study are as follows:

1. It was found that the non-quiescent conditions existing within a corss-flow manifold will significantly influence the jet characteristics. A concomittant influence on atomization can be expected; but this effect was not examined. Since adverse

manifold conditions are almost always present in rocket engine injection systems, additional studies are suggested to further define manifold effects on jet characteristics; particularly with regard to manifold geometry and flow conditions, injection velocity, and inlet geometry (e.g., angle between jet axis and manifold flow direction). The results of these tests would then be used to direct atomization studies in those areas where manifold conditions may contribute to droplet size and size distribution.

2. The like-doublet unlike-doublet, triplet and pentad are equally important elements in the design of contemporary injectors. In this program, a comprehensive study of the like-doublet atomization characteristics was performed. While a considerable amount of dropsize data was generated for these other element types, their atomization characteristics remain not as well defined as those of the like doublet. Consequently, additional atomization experiments for the unlike-doublet, triplet and pentad elements are recommended. Suggested areas of study include entrance geometry, jet characteristics, jet misalignment, and impingement angle for all three element types and dynamic pressure ratio, orifice diameter, and diameter ratio for the triplet and pentad elements. Since the molten wax technique has been proven to be uniquely suitable to the study of unlike-impinging injector elements, the method is recommended as the experimental technique for this study.

3. The influence of fluid physical properties on atomization is not well known. This information is required if quantitative predictions of propellant dropsizes are to be accurately made. Experimental studies to dilineate the effects of, e.g., liquid density, surface tension, and viscosity on dropsize are thus recommended. It is suggested that particular attention be paid to correlating dropsize with non-dimensional parameters, such as the Weber and/or Reynolds number, that incorporate both the physical and dynamic properties of the impinging jets.

REFERENCES

1. Lord Rayleigh (J. W. Strutt), "On the Instability of Jets," Proc. of London Math Soc., V10, 1878, p. 4.
2. Lord Rayleigh (J. W. Strutt), On the Stability of a Cylinder of Viscous Liquid Under Capillary Force, Phil. Mag., V37, 1892, p. 153.
3. Weber, C., "On the Breakdown of a Fluid Jet," Ninth Progress Report, V11, 1931, Project MX-833, Sect. II, University of Colorado, Boulder, Colorado.
4. Baron, T., Atomization of Liquid Jets and Droplets; University of Illinois Technical Report No. 4., February 15, 1949.
5. Borodin, V. A., and Dityakin, Unstable Capillary Waves on the Surface of Separation of Two Viscous Liquids, NACA Tech. Memo No. 1281, April 1951.
6. Balje, O. E., and Larson, The Mechanism of Jet Disintegration, AAF Air Material Command, Engineering Division Memorandum Report No. MCREXE-664-531B; GS-USAF-Wright-Patterson No. 179, August 1949.
7. Heidmann, M. R., Priem, R., and Humphrey, J., A Study of Sprays Formed by Two Impinging Jets, NACA TN 3835, March 1957.
8. Dombrowski, N., and Fraser, R., A Photographic Investigation Into the Disintegration of Liquid Sheets, British Chemical Engineering, V247, A-924, September 1954, p. 101.
9. Hagerty, W. W., and Shea, J., A Study of the Stability of Plane Fluid Sheets, Journal of Applied Mechanics, December 1955, p. 510.
10. Dombrowski, N., and Johns, W. R., The Aerodynamic Instability and Disintegration of Viscous Liquid Sheets, Chem. Eng. Sci., V18, pp. 203-214, 1963.

11. Tanasawa, Y., The Atomization of Liquid by Means of Flat Impingement, Preprint No. 356-56, American Rocket Society, 1956.
12. Dombrowski, N., and P. Hooper, A Study of the Sprays Formed By Impinging Jets in Laminar and Turbulent Flow, Journal of Fluid Mechanics, V18, Part 3, pp. 392-400, 1964.
13. Ingebo, R. D., Dropsize Distributions for Impinging-Jet Breakup in Airstreams Simulating the Velocity Conditions in Rocket Combustors, NACA TN 4222, March 1958.
14. Dickerson, R., Tate, K., and Barsic, N., AFRPL-TR-68-147, Correlation of Spray Injector Parameters with Rocket Engine Performance, Final Technical Report, Rocketdyne, A Division of North American Rockwell Corporation, Canoga Park, California, June 1968.
15. Schweitzer, P. H., Factors in Diesel Spray Nozzle Design in the Light of Recent Oil-Spray Research, ASME Transactions, V52, 1930, p. 121.
16. Hasson, D., and Mizrahi, J., The Drop Size of Fan Spray Nozzles: Measurements by the Solidifying Wax Method Compared With Those Obtained by Other Sizing Techniques, Trans. Instr. Chem. Engrs., Vol. 39, p. 415, 1961.
17. Kykendal, W. B., The Effect of Injector Design Variables on Average Dropsize for Impinging Jets, Technical Report AFRPL-TR-70-53, May 1970.
18. Fry, F., Thomas, P., and Smart, P., Institute of Fire Engineers, Edinborough, England, 1954.
19. Nurick, W. H., and McHale, R. M., NASA CR-108570, Noncircular Orifice Holes and Advanced Fabrication Techniques for Liquid Rocket Injectors, Phase I, Rocketdyne, A Division of North American Rockwell Corporation, Canoga Park, California, 1969.

20. Dannenbrink, R. W., Shell Chemical Company, private communication.
21. Rupe, J. H., A Dynamic Head Probe for Evaluating the Properties of Free Liquid Jets, Progress Report No. 20-299, Jet Propulsion Laboratory, Pasadena, California, 23 March 1956.
22. LeClerc, A., Deflection of a Liquid Jet by a Perpendicular Boundary, M. S. Thesis, University of Iowa, 1948.
23. Rupe, J. H., On the Dynamic Characteristics of Free-Liquid Jets and Partial Correlation with Orifice Geometry, TR 32-207, Jet Propulsion Laboratory, Pasadena, California, 15 January 1962.
24. Schlichting, H., Boundary Layer Theory, McGraw-Hille, New York, 1960.
25. Rupe, J. H., A Correlation Between the Dynamic Properties of a Pair of Impinging Streams and the Uniformity of Mixture-Ratio Distribution in the Resulting Spray, Progress Report No. 20-209, Jet Propulsion Laboratory, Pasadena, California, 28 March 1956.
26. Langhaar, H. L., Trans. ASME 64, A55, 1942.
27. Boussinesq, J., Compt. Rend. 113, 9, 49, 1891.
28. Dombrowski, N. and Hooper, P., The Performance Characteristics of an Impinging Jet Atomizer in Atmospheres of High Ambient Density, Fuel, 41, 1962, p. 323.
29. Taylor, G. I., Proc. Roy. Soc. A, 259, 1, 1960.
30. Heidman, M. F., Priem, R. J. and Humphrey, J. C., NACA Tech. Note, No. 3835, 1957.
31. Milne-Thomson, L. M., Theoretical Hydrodynamics, The MacMillan Co., New York, 1960.
32. Rosin, P., and Rammler, E. Z., Ver. duet. Ing. 71, 1, 1927 (J. Inst. Fuel, 1, 29, 1933).
33. Mugele, R. A., and Evans, H. D., Droplet Size Distribution in Spray, Indus. and Eng. Chem., 43, 6, 1951, p. 1317.

34. Merrington, A. C., and Richardson, E. G., The Breakup of Liquid Jets, The Phys. Soc., Vol. 59, Part 1, No. 331, January 1947.

35. Wolfe, H. E., and Anderson, W. H., Kinetics, Mechanism, and Resultant Droplet Sizes of the Aerodynamic Breakup of Liquid Droplets, Report 0395-04(18)S. Aerojet General Corporation, Downey, California, April, 1964, AD 43740.

36. Ingebo, R. D., et al., Dropsize Distribution for Crosscurrent Breakup of Liquid Jets in Airstreams, NACA TN 4087, 1957.

APPENDIX A

JET CHARACTERISTICS FACILITY

A schematic diagram of the experimental facility designed to obtain the turbulence and velocity profile measurements is shown on Fig. A1. The major components of the facility include: (1) a supply tank (25 gal capacity) with pressurizing and fill equipment, (2) a flow metering system, (3) fine control and fast shut-off valves, (4) the flat plate pressure probe assembly, and (5) a traversing mechanism supporting the probe assembly and a catch pan to collect and return the fluid to the supply tank.

The frequency output of the turbine flowmeters and the voltage output of the supply tank and injection pressure transducers are displayed on a digital counter. The output of the Kistler transducer is a high-impedance charge signal. A charge amplifier is used to convert the charge signal to a low-impedance voltage. The dc-voltage, which is proportional to the mean pressure applied on the diaphragm of the transducer, is displayed on an oscilloscope. A Hewlett-Packard voltmeter is used to measure the ac-voltage produced by the pressure fluctuations.

Since the transducer output is generated by pressure changes, the dc-voltage signal will decay under prolonged application of a constant pressure. The time required for the signal to decay to zero is on the order of 10 minutes. Therefore, consecutive mean pressure measurements can be made only by removing the pressure source. Initially, a thin metal plate was placed directly over the probe entrance to interrupt the flow. Pressure measurements were then obtained by grounding the charge amplifier and removing the metal plate. However, it was found that identical results could be obtained more easily by using a solenoid valve to provide fast on-off control of the flow. In this case, the readings are delayed a few seconds to allow the flow to stabilize.

The test fluid was an aqueous solution of diethanolamine containing 35 percent (by volume) water. At room temperatures, this solution has a kinematic viscosity equivalent to that of paraffin wax at a temperature of 200°F. During the test, the solution was collected by the catch pan, returned to the supply tank and recycled through the system.

Experimental Procedure

In each experiment, the objective was to measure the mean pressure distribution on the flat plate probe, $p(r)$, and the RMS deviation from the mean, $X(r)$, produced by a jet issuing from a particular orifice at a specified flowrate. The measurements were made along two perpendicular lines passing through the centerline of the jet. Along each line, $p(r)$ and $X(r)$ were measured at spatial intervals of approximately 0.1 times the jet radius.

One stagnation point exists in the flowfield produced by the impingement of a cylindrical jet on the flat plate. This point coincides with the centerline of the jet and is the maximum pressure point in the pressure distribution. The location of the center point in the x-y plane parallel to the flat plate probe is determined by first measuring the pressure along the line $x = x_1$. Designating the coordinates of the maximum pressure point along this line by (x_1, y_1), pressure measurements are then made along the line $y = y_1$. The centerline of the jet is located by consecutively measuring in alternate directions.

The specific procedures employed to measure the pressures $p(r)$ and $X(r)$ are outlined below:

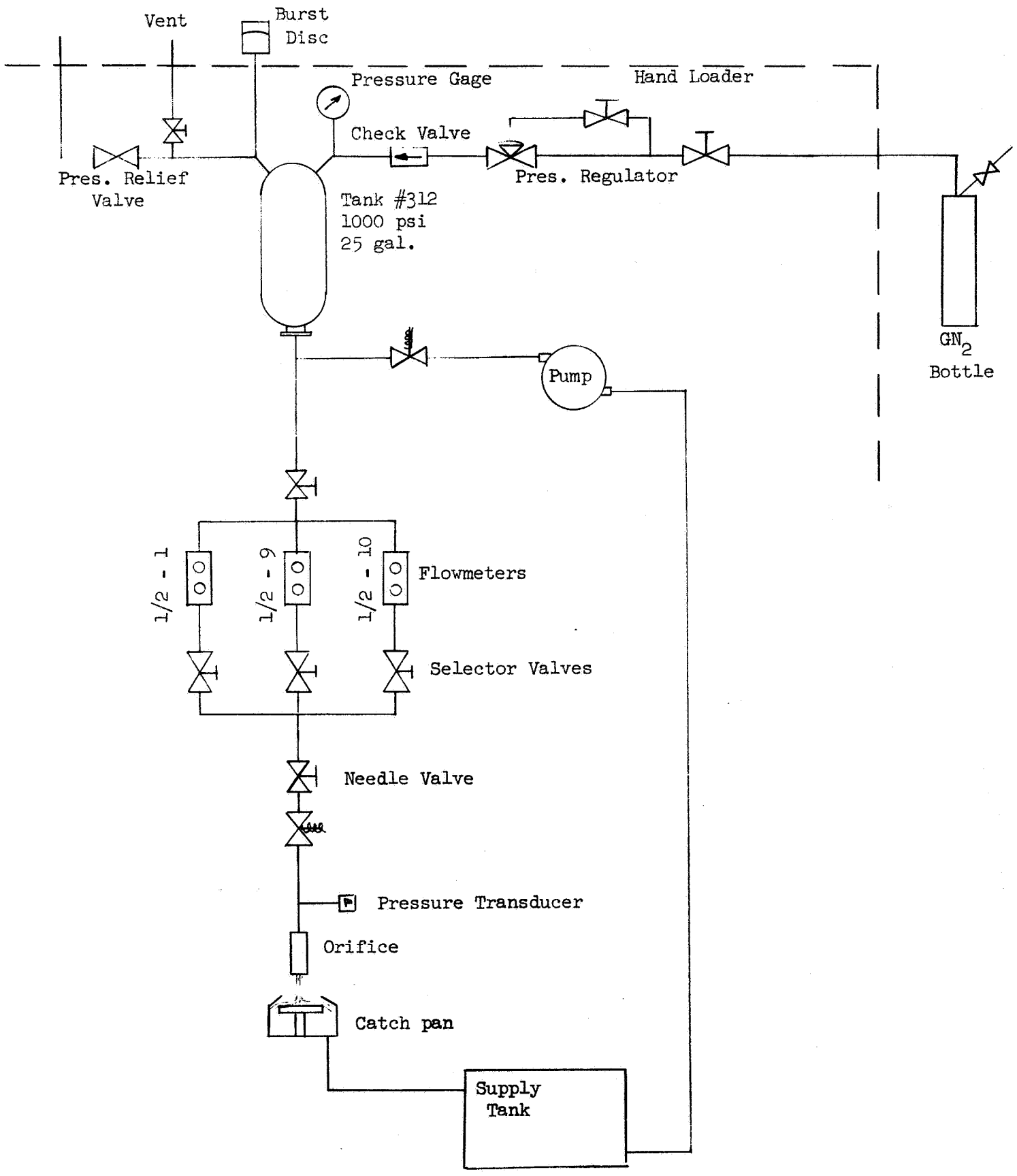

Figure A1. Schematic Diagram of Turbulence Measurement Facility

1. Fill and pressurize supply tank (see Fig. A1).
2. Open one of three flowmeter selector valves.
3. Open solenoid valve and adjust needle valve to desired flowrate.
4. Close solenoid valve.
5. Using the traversing mechanism, position the probe opening at desired radial location.
6. Open solenoid valve and allow flow to stabilize (5 - 10 seconds).
7. Record dc- and ac-voltage output of Kistler transducer.
8. Reposition probe and repeat steps 6 and 7.

The recorded dc-voltage is converted to a pressure according to the relation

$$(\text{psi}) = \frac{\text{volts} \times k_a}{k_s}$$

where k_a is the charge amplification (generally 100 mv/pCb) and k_s is the Kistler sensitivity (0.29 pCb psi). The RMS value of the pressure fluctuation is obtained from the ac-voltage measurement in the same manner.

APPENDIX B

WAX FLOW FACILITY

The wax flow facility used for the dropsize measurements is shown on Fig. B1a and B1b. The overall system consisted of wax and water supply tanks immersed in a hot oil bath container and a particle collector which catches the frozen wax particles. Instrumentation used to measure pressure, flowrate and temperature consisted of strain gauge transducers, turbine flowmeters and iron-constantan thermocouples, respectively.

Each wax and water tank had an independent pressurizing and vent system. Also, as illustrated on Fig. B2 and B3, each product outline had three flowmeters, thermocouples, and hand shutoff valves arranged in parallel so a wide range of flowrates could be obtained. The hot oil bath, shown schematically on Fig. B4, was heated by means of a 30 kilowatt, thermostatically controlled heater. An electrically operated pump circulated the oil from the oil bath container through the heater and back. Hot oil was forced through jacketed run lines and valves to ensure that the wax did not freeze in the feed lines.

The particle collector, shown on Fig. B1b, is an 18 by 50 foot epoxy-coated wooden platform which is located under a roofed structure. During Tasks I and II, the injector end of the collector was surrounded by a large canvas (not shown on the figure) to reduce wind currents which would cause the smaller particles to be blown away. Prior to the initiation of Task III this end of the facility was permanently enclosed.

Wax Spray Procedure

The experimental procedure for droplet size measurement was as follows:

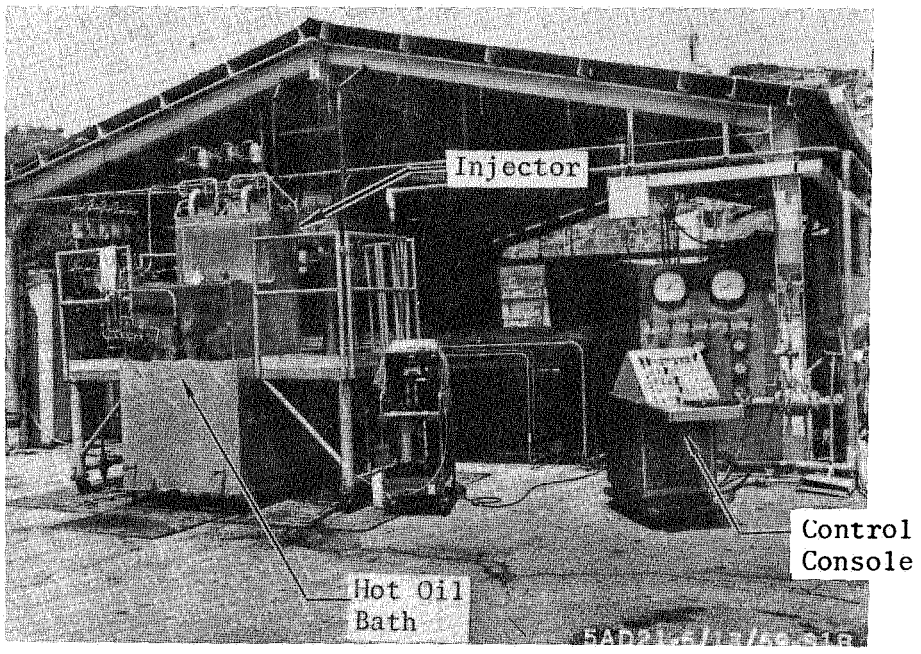

a. Wax Flow System

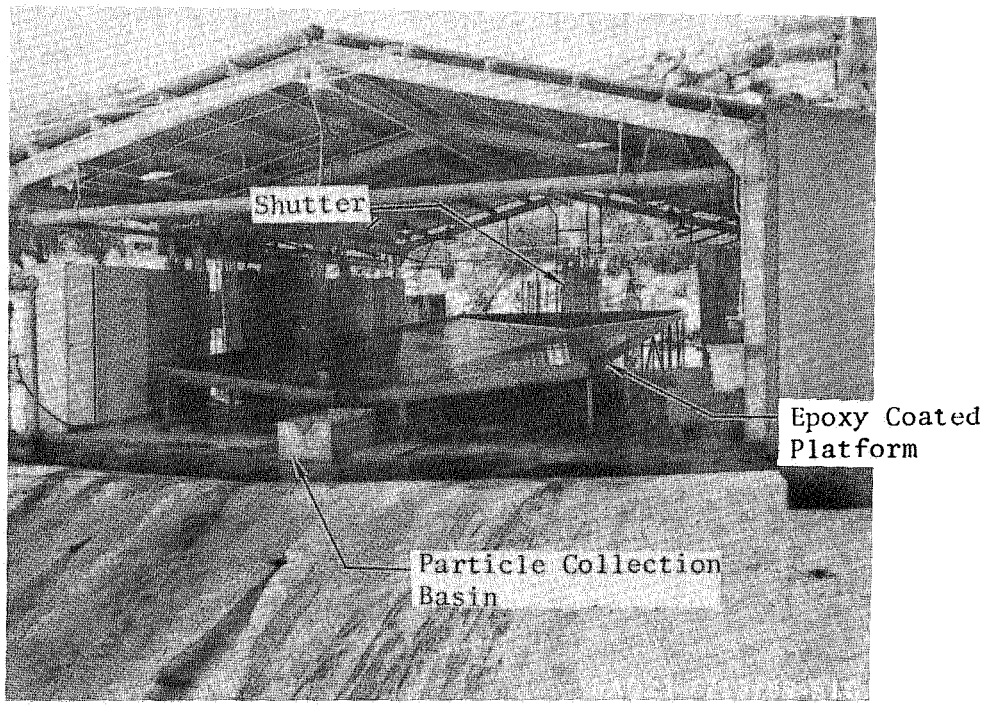

b. Particle Collector

Figure B1. Wax Flow Facility

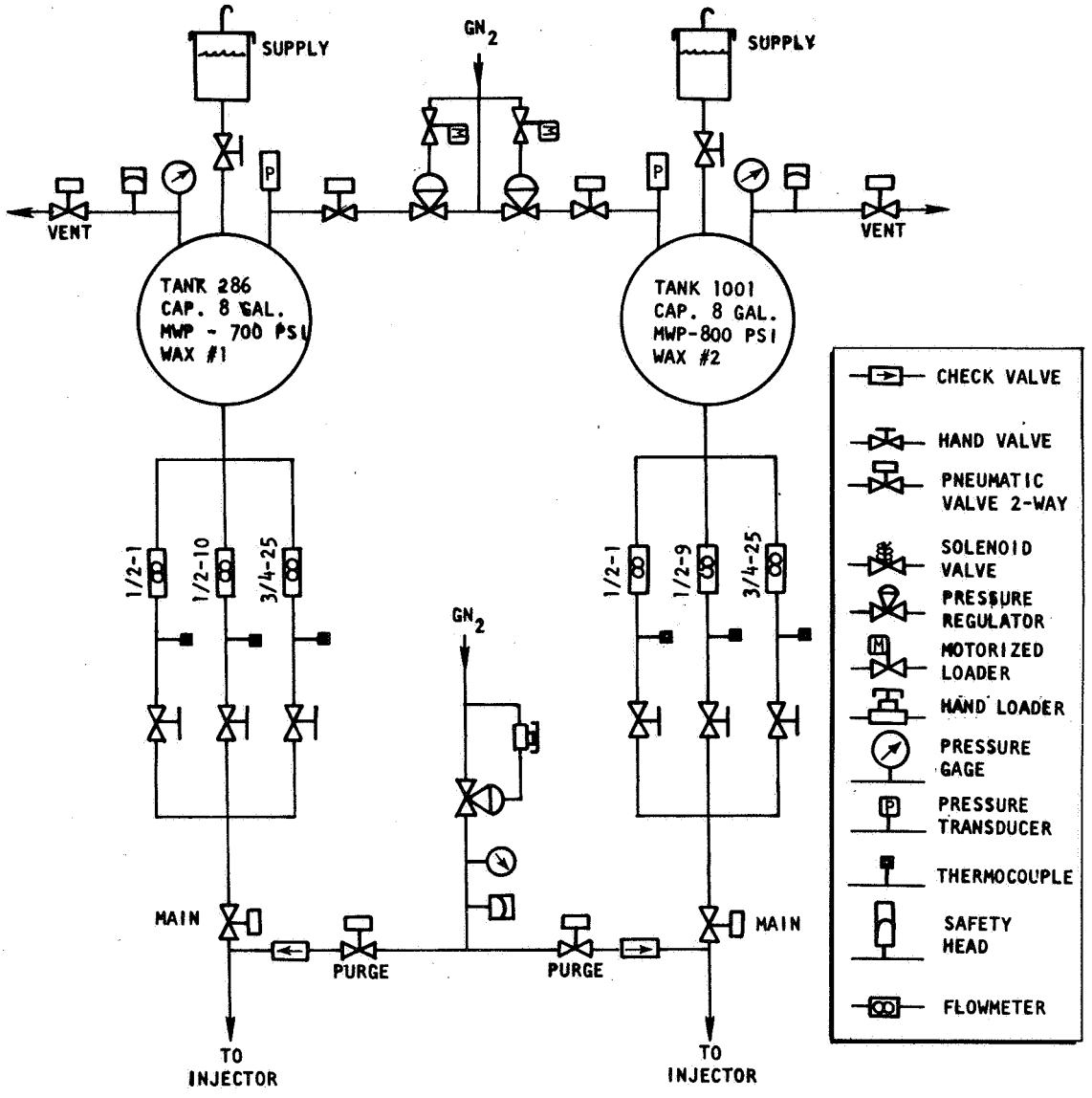

Figure B2. Schematic of Hot Wax System

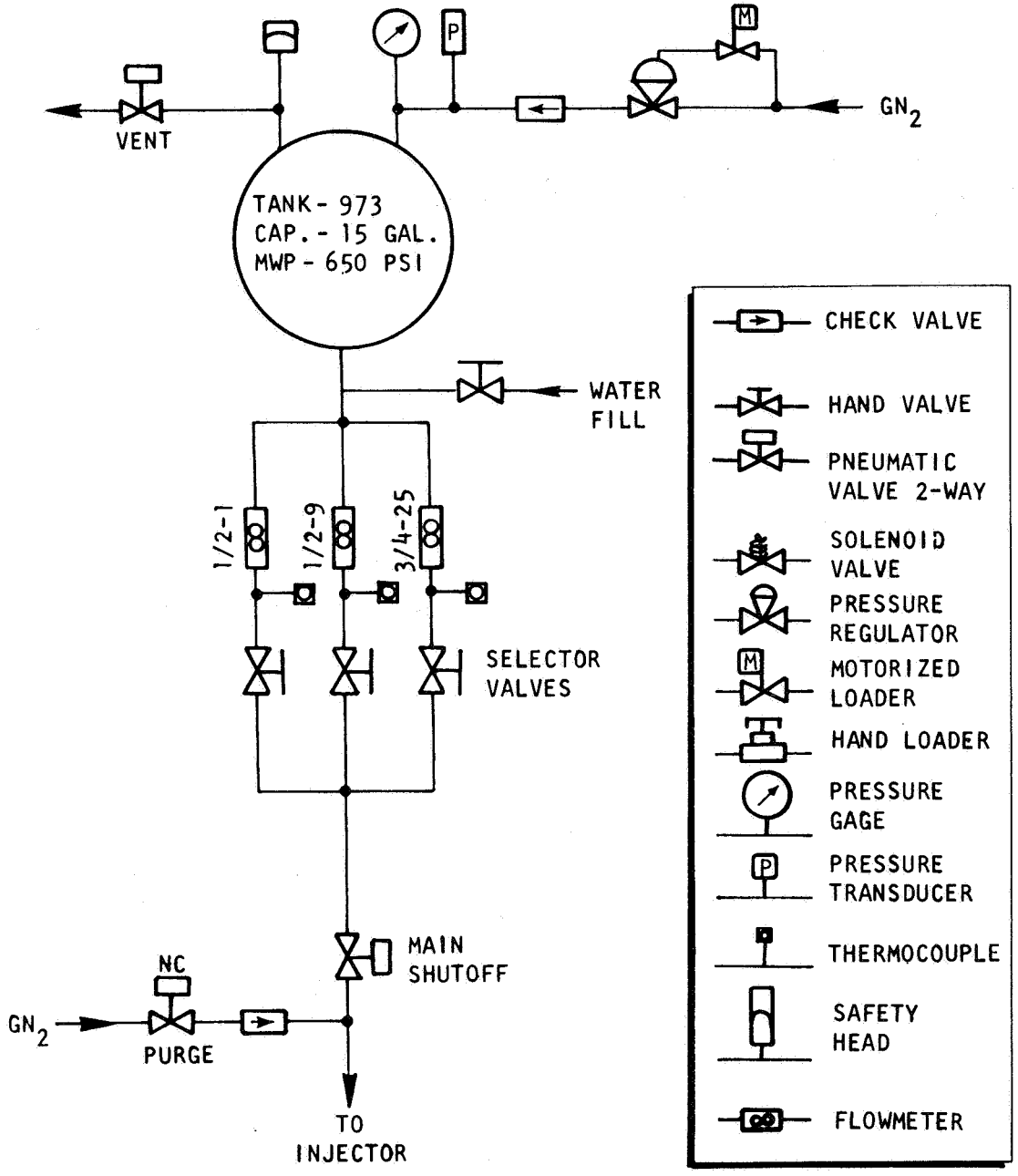

Figure B3. Schematic of Hot Water System

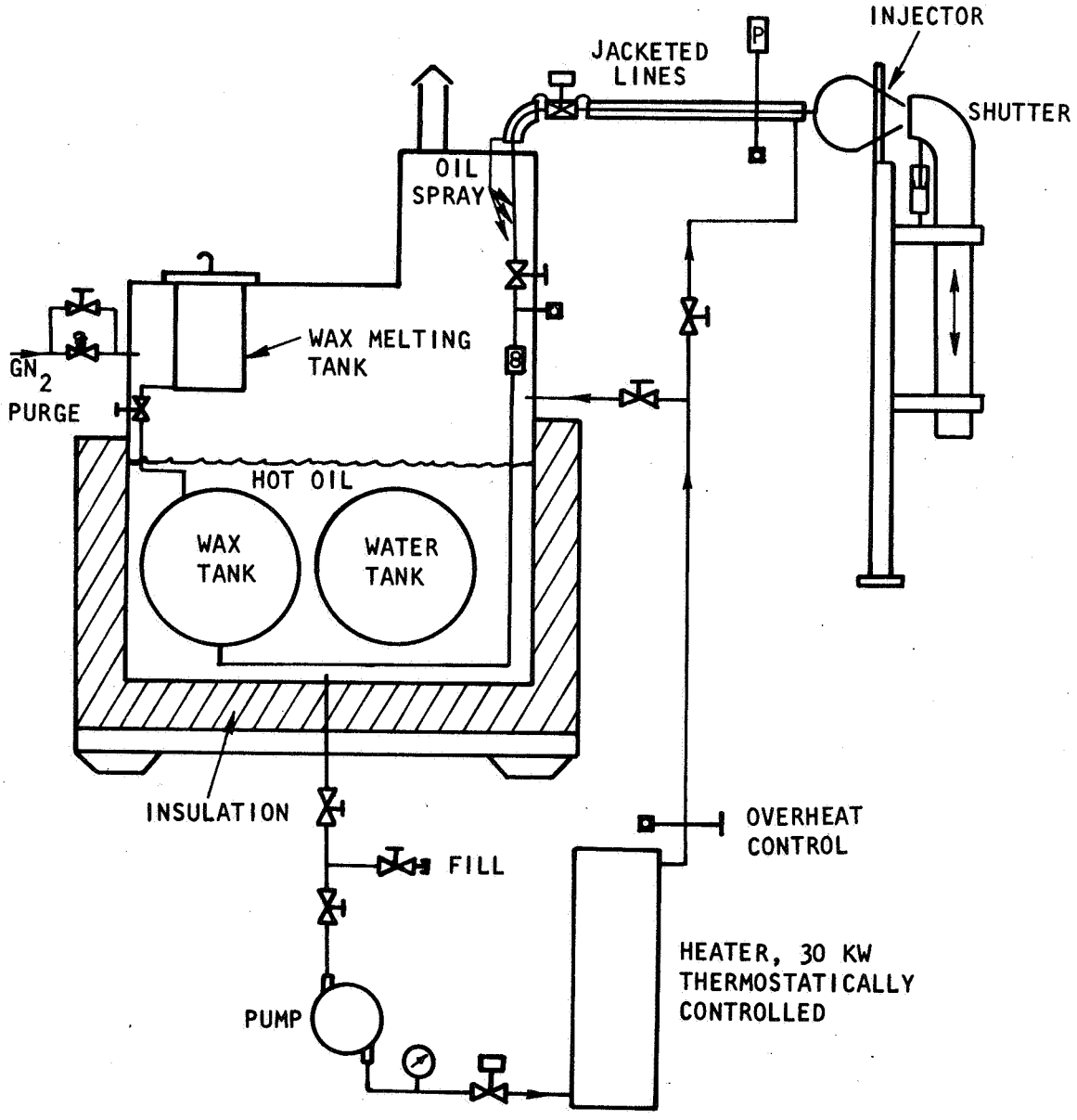

Figure B4. Schematic of the Hot Oil System

1. The injector configuration was installed on the wax facility so that the wax spray created by the orifices after freezing during its ballistic trajectory strikes the particle collector.

2. The electrical oil heater and pump were turned on to bring the propellant simulant tanks and run lines up to 210°F.

3. After all parts of the system were heated and instrumentation requirements checked, the run tanks were heated and the run tanks were pressurized.

4. With the piston operated shutter in the up position, the test was initiated by actuating the main penumatic shutoff valves. When the flowrates and injection pressures reached a steady condition, the shutter was actuated and the wax particles were allowed to spray onto the particle collector. The use of the shutter minimized the influence of start and stop transients on the size distribution of the collected particles.

5. The injector flow was continued for approximately 10 seconds. The shutter was then actuated to the up position and main shut-off valves closed.

6. The tanks were then vented and systems secured.

7. The particles were washed from the collector into the catch basin, where they were scooped from the surface of the water and placed in a plastic bag for temporary storage.

Particle Sample Analysis

The following procedure was used for the analysis of the particles:

1. A 100-gram sample of wax particles was placed in a Buchner funnel and subjected to suction for removal of water.

2. After the particles had been partly dried by suction, they were placed on a large tray in a vacuum chamber for a period of at least 48 hours to ensure that the particles were completely dry.

3. After drying, a random 10-gram sample was selected to be sieved. A series of 23 standard testing sieves ranging in size from 53 to 2380 microns was used. For any particular sample, only 12 of the sieves were used; the particular sieve sizes used depended upon the anticipated size range of the particle sample. The sieves were shaken on a "RO-TAP" automatic sieve shaker for 30 minutes, during which time the shaking was stopped every 6 minutes and each sieve struck sharply several times to help release any particles which had become wedged in the sieve screens.

4. After the sieving operation was completed, the mass of particles retained on each sieve was weighed on an electric balance. It was found that with considerable care in transferring the wax from the sieves into the weighing pan, a total recovery of 97 to 99 percent of the mass originally introduced into the sieves was possible. The photographs shown in Fig. B5 are typical of the uniformity of sizes of the solid wax particles obtained by the sieving operation.

5. These data were then converted into the total fraction of mass having a particle size smaller than each of the sieve sizes. An example of the raw data and converted data is shown in Table B1. The data shown in Table B1 are also shown plotted in Fig. B6.

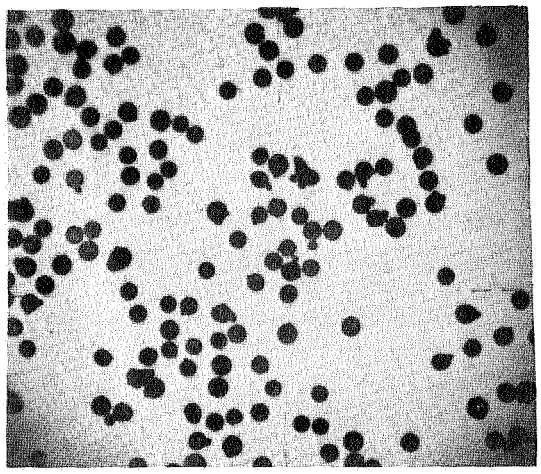

500 Microns

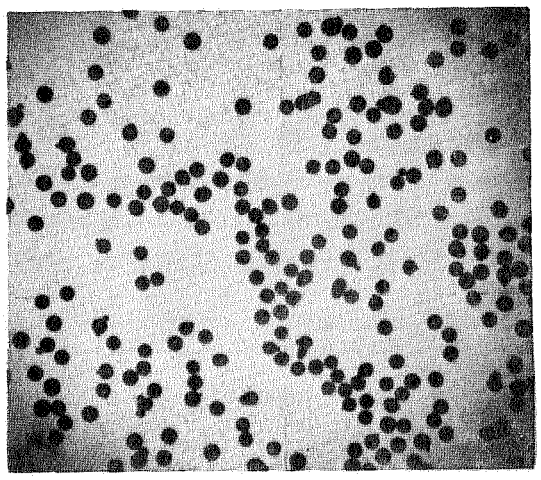

420 Microns

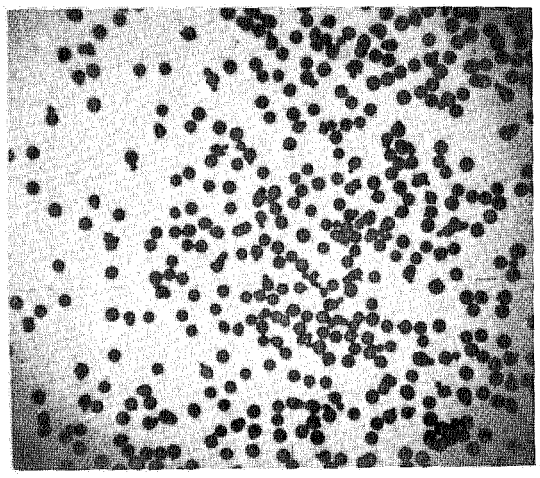

354 Microns

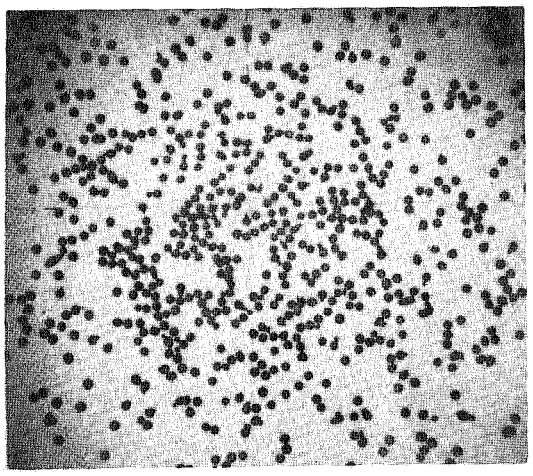

250 Microns

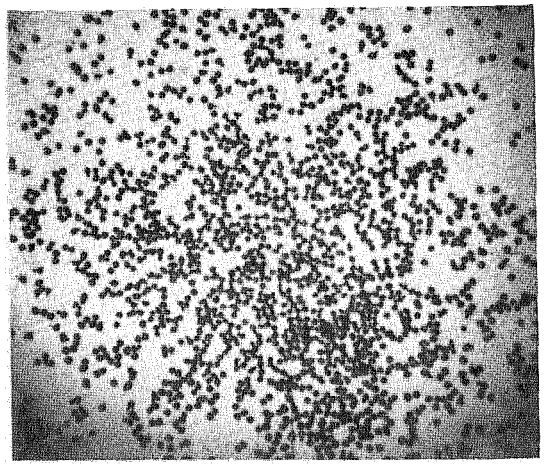

177 Microns

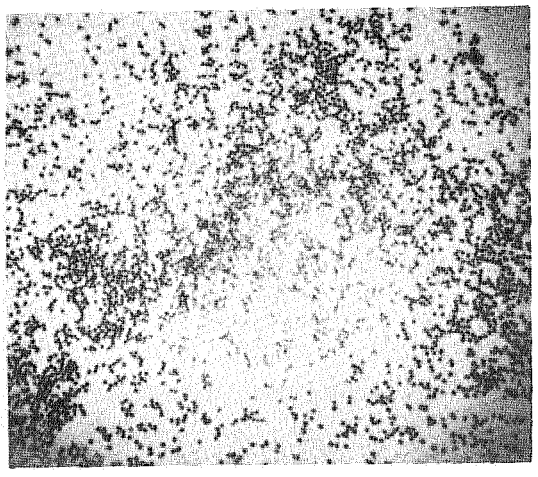

125 Microns

Figure B5. Photographs of Solidified Wax Droplets Using a 0.063-Inch-Diameter Like-Doublet Element

TABLE B1

TYPICAL RESULTS FROM SIEVING ANALYSIS*

Sieve Size, microns	Mass in Sieve, grams	Fraction of Total Mass	Cumulative Fraction of Total Mass Having Particle Size Smaller Than Sieve Size
Catch Pan	0.156	0.0153	--
88	0.139	0.0141	0.0153
105	0.169	0.0170	0.0293
125	0.208	0.0211	0.0464
149	0.667	0.0674	0.0674
177	0.591	0.0598	0.1348
210	1.042	0.1053	0.1946
250	1.201	0.1214	0.2999
297	1.490	0.1507	0.4212
354	1.609	0.1627	0.5719
420	1.138	0.1150	0.7346
500	1.155	0.1168	0.8496
590	0.332	0.0336	0.9664

*0.063-inch-diameter like-doublet injector with free jet length of 5 diameters and P = 100 psi.

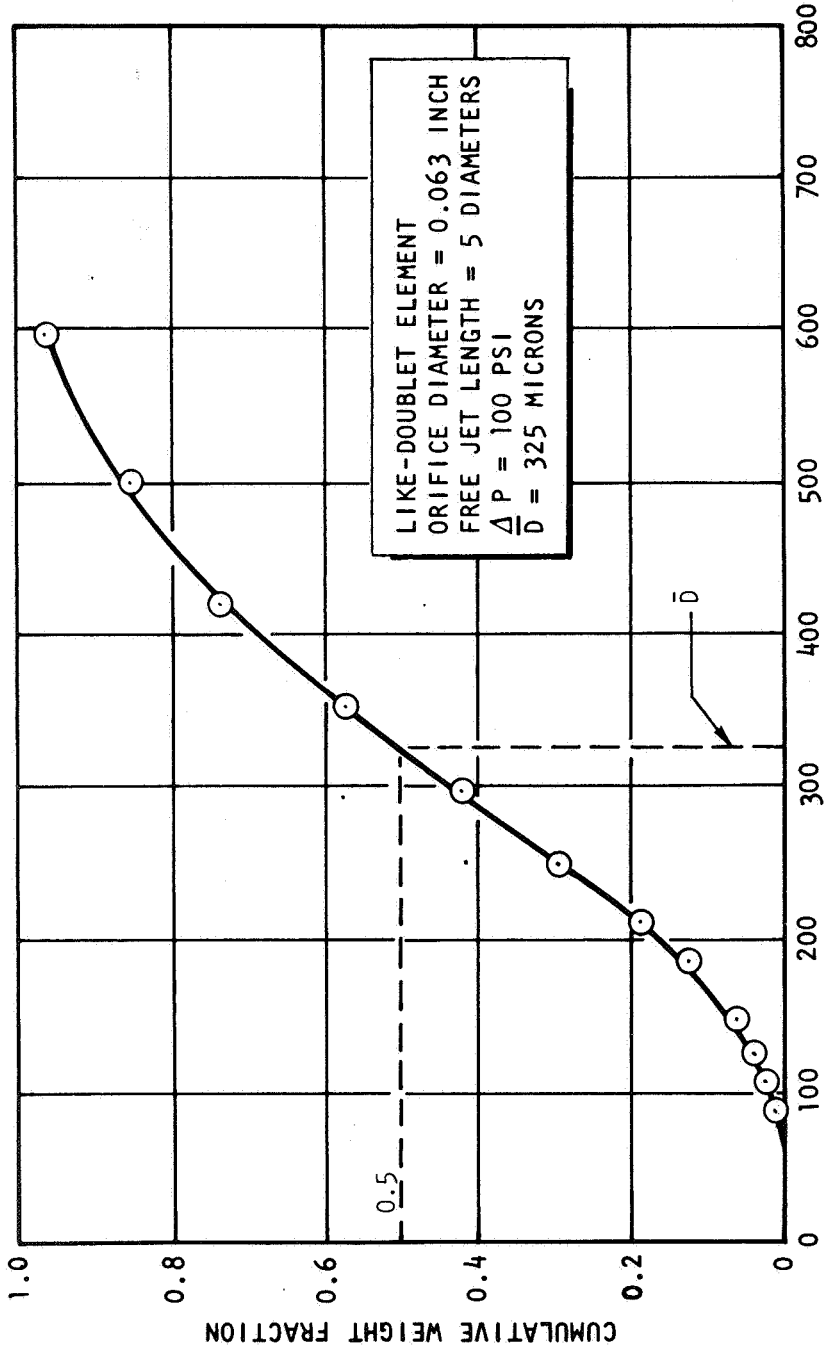

Figure B6. Typical Particle Size Distribution Data Obtained Using the Frozen Wax Technique

Determination of Diethanolamine Entrapped in Wax Droplets

The method developed for the determination of diethanolamine (DEA) entrapped in the wax droplets involved three phases:

1. Removal of the surface DEA
2. Extraction of the entrapped DEA
3. Analysis of the extract solution for DEA

The removal of the surface DEA required repeated washing of the droplet samples using room temperature distilled water in a large extraction funnel. A gas chromatographic analysis for residual DEA was performed after each wash until complete removal was verified. Minimal rinse volumes were used to preclude dilution below analytical detection limits. Experiments were also conducted to verify that DEA was not soluble in the paraffin wax. These experiments included long-term (12 days) surface contact with pre-formed wax droplets at room temperature to indicate surface uptake and possible solubility. The 12-day soak period revealed no entrapped DEA.

Extractions of the entrapped DEA were performed on a weighed portion of the wax droplets at a temperature such that the wax was molten. The sample was placed in an Erlenmeyer flask on a hotplate and the solution agitated to ensure thorough mixing. This arrangement permitted repeated aqueous extractions of the molten wax. Each portion of the aqueous extract was placed in a volumetric flask for dilution to a known total volume. Precipitates had been observed with low-level DEA solutions during the preparations for the calibrations. The addition of several drops of ammonium hydroxide precluded acidic-carbonate interference and ensured the free base was in solution.

Analysis of the aqueous extract for DEA was accomplished by gas chromatography as follows:

Instrument:	Aerograph 600-D with flame ionization detector
Column:	5 percent DC550 on 40/60 Fluoropak-80, 10 foot by 1/8 inch
Temperature:	Column = 150 C isothermal, injection port = 180 C
Flowrates:	Carrier N_2 = 25 ml/min; H_2 = 25 ml/min, Air - 250 ml/min
Readout:	Sargent SR recorder, 0 to 1 mv, with Disc Integrator

The absence of chromatographically detectable substances was verified by examinations of aqueous extractions of the bulk wax and droplets formed by wax-wax injector impingement. Positive identification of DEA response using these stated parameters was continuously verified by injection of DEA standards in the range of 0.2 to 1.0 weight percent.

Calibrations were performed using 2- 2- (2- ethoxy ethoxy) ethoxy ethanol as an empirically derived internal standard. The addition of a known concentration of this standard to the prepared DEA/H_2O calibration mixtures yielded a linear nomograph (see Fig. B7), which w was independent of minor instrumental and injected sample size differences. The standard was similarly added to the extraction samples, approximating the calibration concentrations.

The selection of 2- 2- (2- ethoxy ethoxy) ethoxy ethanol as an internal standard was made to meet the criteria established by the chromatographic parameters required for DEA detection. Lower homologs of this compound had been used successfully under these same conditions, demonstrating symmetrical peaks and reproducible retention times.

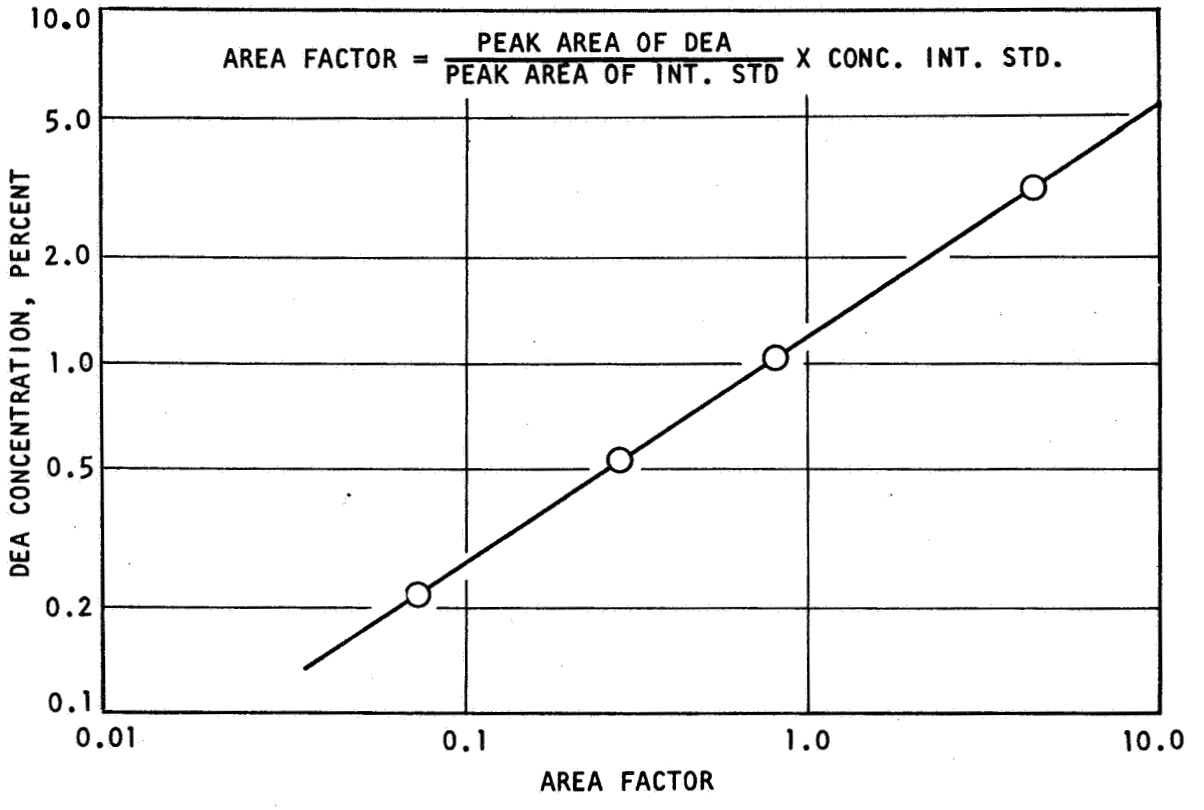

Figure B7. Diethanolamine Calibration Using an Internal Standard

The ethoxy ethanols are typically water soluble and have demonstrated both chemical and thermal stability under these chromatographic conditions. The addition of each ethoxy group to the parent ethanol increases the molecular weight which allows predictable retention times in relationship to DEA.

Sample Calculation

Chromatogram. A typical analysis chromatogram with peaks for DEA and the internal standard is shown in Fig. B8. Note the absence of a water peak even though the sample was an aqueous extract. This is because of the fact that the flame ionization detector responds only to carbon containing organic compounds.

Calculations. The entrapped DEA in wax concentration was calculated from the known wax sample weight, the total extraction volue, and the concentration of DEA in the extract. A stepwise sample calculation is presented below.

1. Weight of dry wax sample (surface DEA removed), grams = 38.96
2. Total Volume of Extract, milliliter = 30.0
3. Concentration of Internal Standard, percent = 0.728
4. From sample chromatogram, $\frac{\text{Peak Area of DEA}}{\text{Peak Area of Int. Std.}}$ = 1.06
5. Area Factor = $\frac{\text{Peak Area of DEA x Concentration of Internal Standard}}{\text{Peak Area of Internal Standard}}$
6. From the nomograph

   Area Factor 0.772 = 1.0% DEA in the 30.0-ml extract which weighed 30 grams

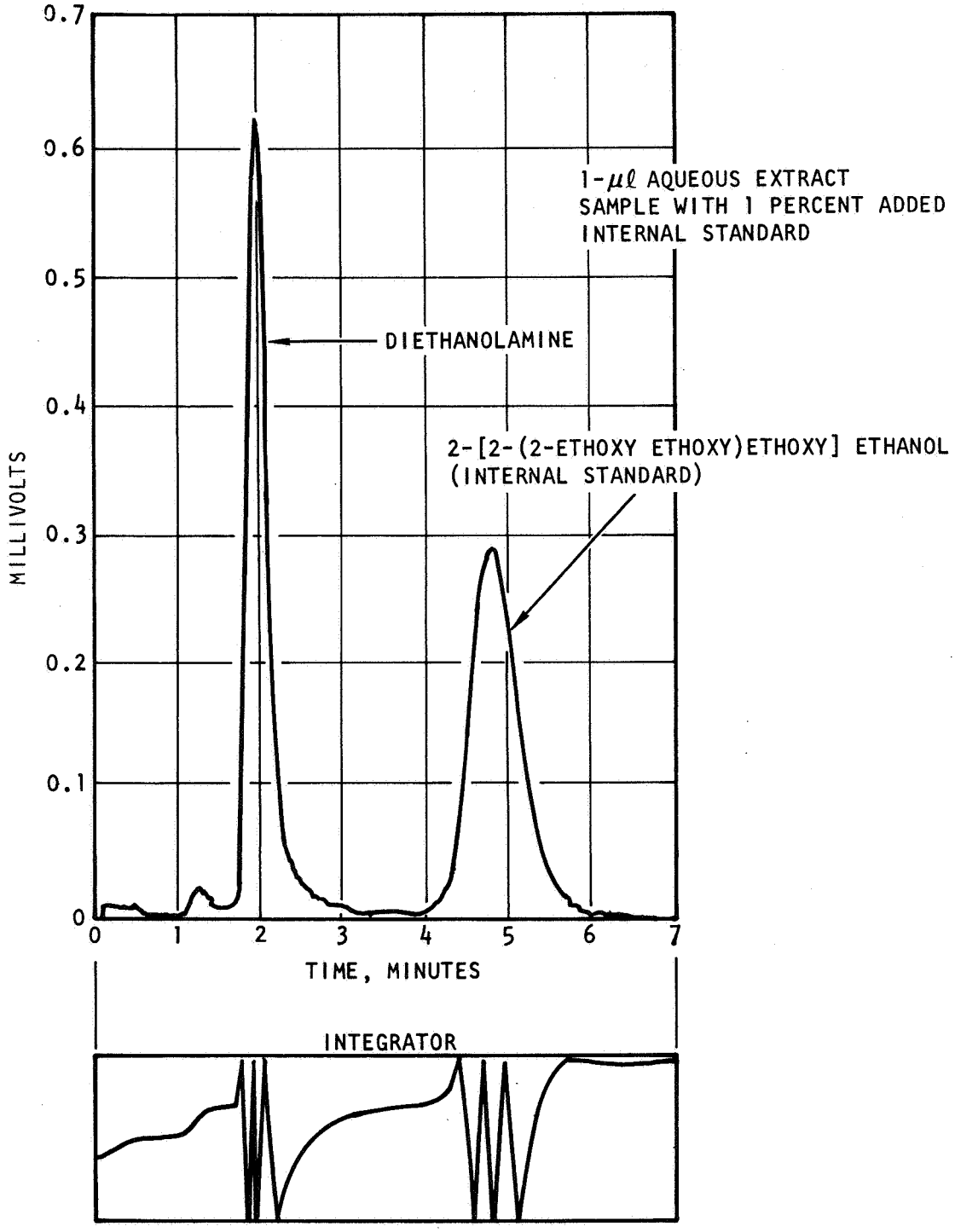

Figure B8. Diethanolamine Analysis Chromatogram

7. Concentration of DEA in Wax Sample = $\frac{\text{(1\% DEA) (Weight of extract)}}{\text{Weight of Original Sample}}$

Concentration of DEA* in Wax Sample = $\frac{(1.0\%)\ (30.0\ gm)}{38.96\ gm} = 0.8\%$

8. Concentration of DEW* in Wax Sample = % DEA/0.75

Concentration of DEW in Wax Sample = $\frac{0.8}{0.75} = 1.07\%$

*DEW denotes the DEA-H_2O solution.

TABLE C-1

LIKE-DOUBLET ATOMIZATION RESULTS

Orifice No. 60-1.5-10R (γ = 60 degrees)

Run No.	Free Jet L/D	Orifice No. 1		Orifice No. 2		Mean Velocity	MT	ϕ	P_D	$\bar{D}$
		$\dot{w}$	V_j	$\dot{w}$	V_j					
1	4.5	0.0290	31.0	0.0265	28.4	29.7	1.65	0.456	1.19	675
2		0.0350	37.4	0.0362	38.8	38.1	2.71	0.481	1.08	575
3		0.0495	53.0	0.0490	52.5	52.8	5.19	0.495	1.02	482
4		0.0756	81.0	0.0725	77.5	79.3	11.7	0.477	1.095	365
5		0.1300	139.0	0.1080	115.8	127.4	30.6	0.410	1.44	240
6		0.1590	170.0	0.1520	163.0	166.5	51.8	0.479	1.09	196
7		0.2070	222.0	0.1926	206.0	214.0	85.6	0.463	1.16	170
8	7.0	0.0360	38.5	0.0330	35.3	36.9	2.55	0.456	1.19	615
9	7.0	0.1850	198.0	0.1820	195.0	196.5	72.1	0.493	1.03	173
10	10.0	0.0360	38.5	0.0345	36.9	37.7	2.66	0.479	1.09	650
11		0.0740	79.1	0.0725	77.5	78.3	11.5	0.490	1.04	340
12		0.1020	109.0	0.0990	106.0	107.5	21.6	0.485	1.06	265
13		0.2030	217.5	0.1950	208.5	213.0	84.8	0.479	1.09	173
14		0.0480	51.3	0.0485	51.8	51.6	4.97	0.505	0.98	445

Orifice No. 60-1.5-10R (γ = 60 degrees)

											% Mis. ($100\Delta/d_j$)
15	5	0.038	40.6	0.036	38.5	39.6	2.92	0.527	0.90	770	75
16		0.0365	39.0	0.0359	38.4	38.7	2.80	0.508	0.97	590	25
17		0.1125	120.5	0.118	126	123.3	28.40	0.520	0.92	302	75
18		0.1115	119.2	0.118	126	122.6	28.10	0.513	0.95	280	50
19		0.1125	120.5	0.118	126	123.3	28.40	0.521	0.92	265	25

TABLE C-1 (Cont.)

Orifice No. 60-1.5-10R (with Turbulence Generator) (γ = 60 degrees)

Run No.	Free Jet L/d	Orifice No. 1		Orifice No. 2		Velocity	M_T	ϕ	P_D	$\bar{D}$	ψ/P_c
		$\dot{\omega}$	V_j	$\dot{\omega}$	V_j						
20	4.5	0.0770	82.3	0.0720	77.0	79.6	11.9	0.468	1.14	392	0.012
21	↓	0.1210	129.5	0.1090	116.5	123.0	28.4	0.476	1.1	250	0.018
22	↓	0.1485	159.0	0.1460	156.0	157.5	46.4	0.476	1.1	207	0.0165
23	↓	0.0390	41.7	0.0362	38.8	40.2	3.03	0.463	1.16	640	0.012
24	7.0	0.0766	81.8	0.0729	78.0	79.9	11.9	0.476	1.10	415	0.029
25	↓	0.1290	138.0	0.1080	115.5	126.8	30.3	0.413	1.42	235	0.040
26	↓	0.1480	158.0	0.1460	156.0	157.0	46.2	0.495	1.02	205	0.034
27	10.0	0.0766	81.8	0.0735	78.5	80.1	12.0	0.479	1.09	398	0.06
28	↓	0.1062	113.9	0.1045	111.9	112.9	23.8	0.490	1.04	288	0.118
29	↓	0.1490	159.5	0.1350	144.0	151.8	43.3	0.439	1.28	186	0.092
30	↓	0.03750	40.1	0.0353	37.8	38.9	2.83	0.472	1.12	605	0.054

Orifice No. 61-6-7R (γ = 60 degrees)

31	5	0.0359	37.4	0.0359	37.4	37.4	2.68	0.5	1.0	520
32	↓	0.0758	73.0	0.0758	73.0	73.0	11.05	↓	↓	375
33	↓	0.1090	105.2	0.1090	105.2	105.2	22.90	↓	↓	280

Orifice No. 63-10-7R (γ = 60 degrees)

34	5	0.0385	37.5	0.0385	37.5	37.5	3.08	0.5	1.0	470
35	↓	0.0765	75.0	0.0765	75.0	75.0	12.20	↓	↓	315
36	↓	0.1105	107.5	0.1105	107.5	107.5	23.70	↓	↓	260
37	↓	0.1570	153.0	0.1570	153.0	153.0	48.00	↓	↓	187

TABLE C-1 (Cont.)

Orifice No. 63-10-3LD (γ = 60 Degrees)

Run No.	Free Jet L/d_j	Orifice No. 1		Orifice No. 2		Mean Velocity	M_T	ϕ	P_D	$\bar{D}$
		$\dot{w}$	V_j	$\dot{w}$	V_j					
38	0.5	0.0310	30.0	0.0310	30.0	30.0	1.86	0.5	1.0	463
39	↓	0.0417	40.4	0.0417	40.4	40.4	3.37	↓	↓	423
40		0.0618	59.8	0.0618	59.8	59.8	7.38			387
41		0.150	72.5	0.150	72.5	72.5	21.65			413
42		0.162	78.1	0.162	78.1	78.1	25.3			415
43		0.202	100.1	0.202	100.1	100.1	40.8			337
44		0.227	110.0	0.227	110.0	110.0	50.0			303
45		0.268	129.9	0.268	129.9	129.9	69.6			256
46	↓	0.309	149.7	0.309	149.7	149.7	92.5	↓	↓	223

Orifice No. 81-10-3LD (γ = 60 Degrees)

47	0.5	0.0508	29.8	0.0508	29.8	29.8	3.03	0.5	1.0	505
48	↓	0.0656	38.5	0.0656	38.5	38.5	5.05	↓	↓	493
49		0.0996	58.4	0.0996	58.4	58.4	11.6			438

Orifice No. 67-50-5R (γ = 60 Degrees)

50	0.5	0.0624	53.4	0.0624	53.4	53.4	6.66	0.5	1.0	322
51	↓	0.0413	35.3	0.0413	35.3	35.3	2.92	↓	↓	421
52		0.0311	26.6	0.0311	26.6	26.6	1.65			465
53		0.1835	156.6	0.1830	156.6	156.6	57.3			205
54		0.2085	178.0	0.2080	178.0	178.0	74.1			182
55		0.0555	47.4	0.0555	47.4	47.4	5.26			369
56		0.1017	86.8	0.1017	86.8	86.8	17.42			276
57	↓	0.1475	125.8	0.1475	125.8	125.8	37.02	↓	↓	238

TABLE C-1 (Cont.)

Orifice No. 67-50-5R

Run No.	Impingement Angle, degrees	Free Stream, L/D	Flowrate, lb/sec	Injection Velocity, ft/sec	$\bar{D}$, microns
58	45	1	0.1245	106.0	265
59			0.1009	86.1	275
60			0.0657	56.0	440
61		5	0.1225	104.2	290
62			0.0981	83.9	320
63			0.0715	61.1	430
64		10	0.1230	105.0	340
65			0.0970	82.9	420
66			0.0706	60.4	495
67		1	0.0715	61.0	370
68			0.0990	86.6	295
69			0.1274	169.0	250
70	60	5	0.0764	65.4	422
71			0.1000	85.5	325
72			0.1225	105.0	268
73		10	0.1220	104.0	317
74			0.1019	87.0	383
75			0.0725	62.0	400
76	90	1	0.1215	104.0	195
77			0.1245	106.5	195
78			0.1021	87.1	197
79			0.0686	58.6	306
80		5	0.1213	104.0	210
81			0.1008	86.0	205
82			0.0708	60.4	282
83		10	0.1254	107.0	278
84			0.0988	84.5	272
85			0.0715	61.1	270

TABLE C-1 (Cont.)

Orifice No. 69-200-9R (γ = 60 degrees)

Run No.	Free Jet L/d_j	Orifice No. 1 $\dot{w}$	Orifice No. 1 V_j	Orifice No. 2 $\dot{w}$	Orifice No. 2 V_j	Mean Velocity	M_T	ϕ	P_D	$\bar{D}$
86	5	0.0758	61.1	0.0758	61.1	61.1	9.28	0.5	1.0	276
87	↓	0.0995	80.3	0.0995	80.1	80.1	15.9	↓	↓	213
88		0.0354	28.6	0.0354	28.6	28.6	2.02			440
89		0.0485	39.2	0.0485	39.2	39.2	3.8			378
90		0.1209	97.6	0.1209	97.6	97.6	23.6			315

Orifice No. 61-2-7S (γ = 60 degrees)

91	5	0.0376	39.2	0.0376	39.2	39.2	2.94	0.5	1.0	296
92	↓	0.0585	61.0	0.0585	61.0	61.0	7.15	↓	↓	212
93		0.0780	81.2	0.078	81.2	81.2	12.75			185
94		0.0931	97.2	0.0931	97.2	97.2	25.4			165
95		0.0935	115.0	0.0935	115.0	115.0	29.0			150
96		0.1470	153.0	0.1470	153.0	153.0	45.0			115
97		0.0985	118.0	0.0985	118.0	118.0	30.5			150

(Δ = 0.5 d_j)

Orifice No. 61-6-7S

98	5	0.0384	40.0	0.0384	40.0	40.0	4.00	0.5	1.0	281
99	↓	0.0758	78.8	0.0758	78.8	78.8	11.90	↓	↓	180
100		0.1095	114.0	0.1095	114.0	114.0	25.00			152

Orifice No. 61-10-7S (γ = 60 degrees)

101	5	0.0376	39.2	0.0376	39.2	39.2	2.95	0.5	1.0	496
102	↓	0.0775	80.6	0.0775	80.6	80.6	12.50	↓	↓	192
103		0.1105	115.0	0.1105	115.0	115.0	25.4			150
104		0.1470	153.0	0.1470	153.0	153.0	45.0			135

TABLE C-2

UNLIKE-DOUBLET ATOMIZATION RESULTS

Orifice No.'s 60-1.5-10R/60-1.5-10R (γ = 60 degrees, L_j/d_j = 5)

Run No.	Fuel				Oxidizer				M_T	ϕ	P_b	$\bar{D}$
	d_f	$\dot{\omega}$	V_j	Fluid	d_o	$\dot{\omega}$	V	Fluid				
105	0.060	0.0515	55.1	Wax	.060	0.0902	71.5	Dew	9.29	0.694	0.442	470
106		0.0657	70.4			0.0780	61.8		9.45	0.507	0.970	457
107		0.0750	80.2			0.0620	49.2		9.46	0.334	1.990	423
108		0.0646	69.1			0.0774	61.4		9.22	0.513	0.951	444
109 (turb)		0.0651	69.7			0.0761	60.5		9.15	0.501	0.994	456
110 (turb)		0.0520	55.6			0.0900	71.5		9.32	0.690	0.451	473
111 (turb)		0.0750	80.2			0.0624	49.5		9.09	0.338	1.960	435
112 (turb)		0.0642	68.6			0.0775	61.5	"	9.17	0.518	0.930	464
113		0.0665	71.0			0.0665	71.0	wax	9.45	0.500	1.0	358
114		0.0540	57.8			0.072	77.0		8.65	0.641	0.560	375
115		0.0520	55.6			0.0755	80.9		8.99	0.679	0.475	390
116	"	0.0370	39.6	"	"	0.0790	84.5	"	8.04	0.821	0.219	420

TABLE C-2 (Cont.)

Orifice No's. 60-1.5-10R/90-1.5-10R (γ = 60 degrees, L_j/d_j = 5)

Run No.	Fuel				Oxidizer				M_T	O	P_D	$\bar{D}$
	d_f	$\dot{W}$	V_j	Fluid	d_o	$\dot{W}$	V_j	Fluid				
117	0.060	0.0522	55.9	Wax	0.090	0.1320	46.7	Dew	9.08	0.585	1.065	536
118	↓	0.0390	41.7	↓	↓	0.1431	50.7	↓	9.00	0.750	0.500	525
119	↓	0.0619	66.2	↓	↓	0.1139	40.3	↓	8.67	0.428	2.010	480
120	↓	0.062	66.3	↓	↓	0.1575	55.7	↓	12.87	0.587	1.055	418
121	↓	0.0655	70.0	↓	↓	0.2510	81.8	↓	23.50	0.733	0.546	395
122	↓	0.0740	79.1	↓	↓	0.0910	32.2	↓	8.80	0.250	4.510	402
123	↓	0.0456	36.3	Dew	↓	0.1235	58.8	Wax	8.95	0.755	0.518	612
124	↓	0.0576	46.1	↓	↓	0.1115	53.2	↓	8.64	0.589	1.000	540
125	↓	0.0729	58.1	↓	↓	0.0985	46.9	↓	8.95	0.410	2.06	490
126	↓	0.0496	39.6	↓	↓	0.147	70.0	↓	12.31	0.770	0.426	550
127	↓	0.0776	62.0	↓	↓	0.148	70.5	↓	15.21	0.595	1.040	437
128	↓	0.1045	83.5	↓	↓	0.147	70.0	↓	19.21	0.435	1.910	360

TABLE C-2 (Cont.)

Orifice No's. 60-1.5-10R/120-1.5-10R (γ = 60 degrees, L_j/d_j = 5)

	Fuel					Oxidizer						
Run No.	d_f	$\dot{W}$	V_j	Fluid	d_o	$\dot{W}$	V_j	Fluid	M_T	ϕ	P_D	$\bar{D}$
129	0.060	0.0620	66.3	Wax	0.120	0.142	56.1	Dew	20	0.658	1.03	505
130	↓	0.0455	48.6	↓	↓	0.150	59.3	↓	19.91	0.800	.503	455
131	↓	0.0754	80.5	↓	↓	0.130	51.4	↓	19.32	0.523	1.83	480
132	↓	0.0655	70	↓	↓	0.152	60.4	↓	22.87	0.668	1.00	455
133	↓	0.0655	70	↓	↓	0.216	85.4	↓	41.07	0.800	.502	310
134	↓	0.0622	66.5	↓	↓	0.107	42.2	↓	13.14	0.520	1.85	550
135	0.060	0.0921	73	Dew	0.120	0.112	60	wax	20.16	0.502	1.985	500
136	↓	0.0725	57.4	↓	↓	0.120	64	↓	19.47	0.650	1.08	605
137	↓	0.110	87	↓	↓	0.0935	50	↓	18.85	0.331	4.05	470
138	↓	0.0718	56.8	↓	↓	0.129	68.9	↓	21.78	0.690	0.91	545
139	↓	0.0443	43	↓	↓	0.131	70	↓	20.7	0.799	0.505	698
140	↓	0.104	82.5	↓	↓	0.131	70	↓	26.88	0.519	1.86	430

TAB. J-2 (Cont.)

Orifice No's. 63/86-10-3UD, 86-128-10-3UD (γ = 60 degrees, L_j/d_j = 5)

Run No.	d_f/d_o	Fuel				Oxidizer				M_T	ϕ	P_D	$\bar{D}$
		d_f	$\dot{W}$	V_j	Fluid	d_o	$\dot{W}$	V_j	Fluid				
141	1.36	0.063	0.0316	30.6	Wax	0.086	0.0554	22.9	H_2O	2.24	0.500	1.365	585
142			0.0413	40.0			0.0747	30.8		3.95	0.514	1.290	560
143			0.0620	60.0			0.0867	35.8		6.82	0.389	2.150	474
144			0.0404	31.1	H_2O		0.0575	29.9	Wax	2.98	0.492	1.413	697
145			0.0542	41.7			0.0771	40.1		5.35	0.492	1.413	568
146			0.0818	62.9			0.1158	60.2		12.12	0.490	1.428	495
147	2.03		0.0316	30.6	Wax	0.128	0.0990	18.4	H_2O	2.79	0.490	2.113	587
148			0.0411	39.8			0.1335	24.9		4.97	0.510	1.952	591
149			0.0624	60.4			0.2128	39.6		12.19	0.533	1.779	526
150	1.49	0.086	0.0493	37.9	H_2O		0.1328	31.2	Wax	6.01	0.437	1.928	596
151			0.0665	51.1			0.1713	40.2		10.29	0.416	2.110	584
152			0.1005	77.2			0.2534	59.4		22.80	0.403	2.210	455

Orifice No's. 67-50-5R/67-50-5R (γ = 60 degrees, L_j/d_j = 5)

153	1.0	0.067	0.0582	49.6	Wax	0.067	0.0723	46.1	Dew	6.20	0.536	0.87	339
154			0.0906	77.5			0.1210	77.0		16.32	0.570	0.95	290
155			0.1440	123.0			0.1728	110.0		36.70	0.518	0.93	257

Orifice No's. 67-50-5R/86-50-5R (γ = 60 Degrees, L_j/d_j = 5)

156	1.28	0.067	0.0616	52.7	Wax	0.086	0.0849	35.0	H_2O	6.23	0.428	1.714	416
157			0.0417	35.7			0.0749	30.9		3.80	0.562	0.020	424
158			0.0315	26.9			0.0556	22.9		2.13	0.548	1.055	488
159			0.0814	69.6	H_2O		0.1150	59.8	Wax	12.53	0.420	1.771	392
160			0.0538	46.0			0.0763	39.7		5.51	0.423	1.755	489
161			0.0406	34.7			0.0573	29.8		3.12	0.420	1.773	521

TABLE C-2 (Cont.)

Orifice No's. 67-50-5R/86-50-5R (γ = 60 degrees, L_j/d_j = 5)

Run No.	d_f/d_o	Fuel				Oxidizer				M_T	ϕ	P_D	$\bar{D}$
		d_f	$\dot{W}$	V	Fluid	d_o	$\dot{W}$	V_j	Fluid				
162	1.28	0.067	0.0637	54.6	Wax	0.086	0.0761	39.5	Wax	6.48	0.401	1.915	453
163			0.1066	91.4			0.1241	64.5		17.73	0.390	2.01	384
164			0.1519	130.0			0.1807	93.9		36.67	0.399	1.93	302
165			0.614	52.5	Wax		0.0883	34.3	Dew	6.26	0.423	1.75	443
166			0.1175	101.0			0.1473	57.1		20.28	0.357	2.31	349
167			0.1545	132.5			0.2097	81.3		37.5	0.393	1.98	274
168			0.0457	39.2	Wax		0.0861	33.4	Dew	4.67	0.555	1.03	384
169			0.0894	76.5			0.1741	67.5		18.58	0.572	0.96	321
170			0.1277	109.5			0.2465	95.6		37.6	0.567	0.98	291
171			0.0465	39.8			0.1159	45.0		7.05	0.689	0.58	421
172			0.0826	70.8			0.2105	81.7		23.05	0.697	0.56	352
173			0.1126	96.5			0.2545	98.7		35.95	0.643	0.71	292
174			0.0854	54.7	Dew		0.0840	43.6	Wax	8.32	0.378	2.11	434
175			0.1279	81.8			0.1080	56.1		16.51	0.311	2.84	346
176			0.1663	106.2			0.1782	92.6		34.2	0.420	1.77	294

Orifice No's. 67-50-5R/128-50-5R (γ = 60 degrees, L_j/d_j = 5)

177	1.91	0.067	0.0805	68.9	Wax	0.128	0.2293	53.8	Wax	17.87	0.538	1.64	499
178			0.1203	103.0			0.3430	80.5		40.00	0.538	1.64	457
179			0.0467	39.9	Wax		0.1583	29.5	Dew	6.53	0.584	1.36	558
180			0.0856	73.2			0.2865	53.4		21.57	0.577	1.40	375
181			0.1162	99.4			0.3740	69.7		37.63	0.558	1.51	272
182			0.0559	35.6	Dew		0.1455	34.1	Wax	6.95	0.566	1.46	591
183			0.0924	58.9			0.2445	57.4		19.48	0.575	1.41	538
184			0.1330	84.8			0.3620	84.9		42.00	0.590	1.33	448

TABLE C-3

TRIPLET ATOMIZATION RESULTS

Orifice No. 67-50-5R ($L_j/d_j = 5$)

Run No.	d_f/d_o	Fuel				Oxidizer				M_T	ϕ	P	$\bar{D}$
		d_f	$\hat{W}$	V_j	Fluid	d_o	$\hat{W}$	V_j	Fluid				
185	1.0	0.067	0.0457	29.9	H_2O	0.067	0.0624	26.7	Wax	3.04	0.379	1.640	583
186			0.0700	45.8			0.0936	40.0		7.02	0.369	1.710	470
187			0.0943	61.6			0.1243	53.1		12.4	0.363	1.760	412
188			0.1408	92.1			0.1861	79.5		27.8	0.363	1.755	307
189			0.1853	121.2			0.2439	104.3		47.9	0.363	1.760	266
190			0.2393	156.5			0.3210	137.2		81.5	0.370	1.700	190
191			0.2583	169.0			0.3540	151.3		97.3	0.380	1.630	195
192			0.0315	26.9	Wax		0.0528	17.3	H_2O	1.76	0.353	1.837	606
193			0.0465	39.8			0.0793	25.9		3.90	0.357	1.805	484
194			0.0629	53.8			0.1021	33.4		6.79	0.335	1.984	425
195			0.0935	80.0			0.1542	50.4		15.3	0.342	1.928	333
196			0.1201	102.7			0.2093	68.5		26.7	0.367	1.722	297
197			0.1572	134.4			0.2583	84.5		43.0	0.341	1.937	238

TABLE C-4

PENTAD ATOMIZATION RESULTS

Orifice No. 86/63-10-3P

Run No.	d_f/d_o	Fuel				Oxidizer				M_T	ϕ	P_D	$\bar{D}$
		d_f	$\dot{W}$	V_j	Fluid	d_o	$\dot{W}$	V_j	Fluid				
198	1.365	0.086	0.0526	21.7	H_2O	0.063	0.1211	29.6	Wax	4.63	0.511	0.702	517
199			0.0780	32.2			0.1880	45.5		11.06	0.528	0.655	522
200			0.1019	42.0			0.2494	60.4		19.33	0.537	0.632	498
201			0.0577	30.0	Wax		0.1780	34.2	H_2O	7.82	0.554	0.588	451
202			0.0862	44.8			0.2643	50.8		17.28	0.553	0.594	364
203			0.1082	56.2			0.3599	69.2		30.98	0.592	0.505	299

Orifice No's. 86-50-5R/67-50-5R ($L_j/d_j = 5$)

Run No.	d_f/d_o	Fuel				Oxidizer				M_T	ϕ	P	$\bar{D}$
		d_f	$\dot{W}$	V_j	Fluid	d_o	$\dot{W}$	V_j	Fluid				
204	1.284	0.086	0.1037	42.8	H_2O	0.067	0.2534	54.7	Wax	18.30	0.494	0.798	451
205			0.0773	31.0			0.1860	40.2		9.89	0.500	0.776	503
206			0.0507	20.9			0.1206	26.0		4.20	0.480	0.842	535
207			0.1156	60.1	Wax		0.3659	59.9	H_2O	28.87	0.502	0.772	292
208			0.0860	44.7			0.2623	42.9		15.10	0.484	0.830	432
209			0.0583	30.3			0.1815	29.7		7.16	0.495	0.796	488

TABLE C-5

EMULSIFICATION RESULTS

Task I Run No.	Element Type	Wax System			Dew System			Total Momentum, ft-lb/sec^2	$\frac{M_{wax}}{M_{Dew}}$	Percent Dew in Wax
		Orifice Diameter, Inch	Flowrate, lb/sec	Injection Velocity, ft/sec	Orifice Diameter, inch	Flowrate, lb/sec	Injection Velocity, ft/sec			
210	Unlike-Doublet	0.067	0.0465	45.0	0.086	0.1159	45.0	7.31	0.40	0.67
211		0.067	0.0826	79.9	0.086	0.2105	81.7	23.80	0.38	1.20
212		0.067	0.1126	109.0	0.086	0.2545	98.7	37.39	0.49	0.84
213	Pentad	0.128	0.0856	20.1	0.067	0.1839	44.5	9.91	0.84	0.93
214		0.128	0.1482	34.8	0.067	0.2988	72.3	26.76	0.95	0.67
215		0.128	0.2189	51.4	0.067	0.4030	97.5	50.54	1.15	1.00

Free Jet Length = 5 diameters
Impingement Angle = 60 degrees
Unlike-Doublet Element No. 67/86-50-3UD
Pentad Element No. 67/128-50-3P

APPENDIX D

WEBER NUMBER CORRELATION

Because of its importance in specifying the mode of sheet disintegration, an attempt was made to correlate the median dropsize with the Weber number. Shown on Fig. D1 is a plot of the empirical correlations for a like doublet (Eqs. (6) and (7)) and the Weber number range of the experiments in this program. The ordinate of Fig. D1 is the normalized dropsize $\bar{D}/D_R$ where D_R (1.89 d_j) is the dropsize obtained from a Rayleigh jet, Ref. 1. The latter represents the maximum dropsize for a given diameter jet at very low Weber numbers. At higher Weber numbers, the upper limit for the dropsize obtained from a single jet was measured by Richardson, Ref. 34, and is also shown on Fig. D1.

The dropsize obtained from impinging jets will, of course, be smaller than the dropsize predicted from these two limiting cases. However, as the Weber number goes to either zero or infinity, the impinging jet dropsize should approach either the Rayleigh or Richardson data, respectively. Thus, at very high Weber numbers, both the laminar and turbulent jet dropsizes should approach a velocity dependence similar to that expressed by the Richardson correlation. Similarly, at low Weber numbers, both dropsizes should become independent of velocity.

The decreasing velocity dependence at lower Weber numbers may be the reason why many experimental investigations with high surface tension fluids have yielded a smaller velocity dependence of dropsize than was obtained in this program. For example, Dombrowski et. al., Ref. 12,

obtained $\bar{D} \quad V^{-.79}$ with turbulent water jets as compared to V^{-1} in this program. If their data is corrected from D_{20} to $\bar{D}$ (Section 5.2.4) and plotted on Fig. D1, it is seen that good agreement is obtained with the turbulent jet correlation, Eq, (7), extrapolated to low Weber numbers.

Because of the uncertainty in the correction of any other mean dropsize to a mass median dropsize and the possibility that the results may have been influenced by the experimental technique, the correlation was not attempted with the data of investigators other than Dombrowski. Hence, the above result may be fortuitous. Nevertheless, the generation of a Weber number/dropsize relation would seem to be a plausible starting point for an investigation of physical property effects on dropsize.

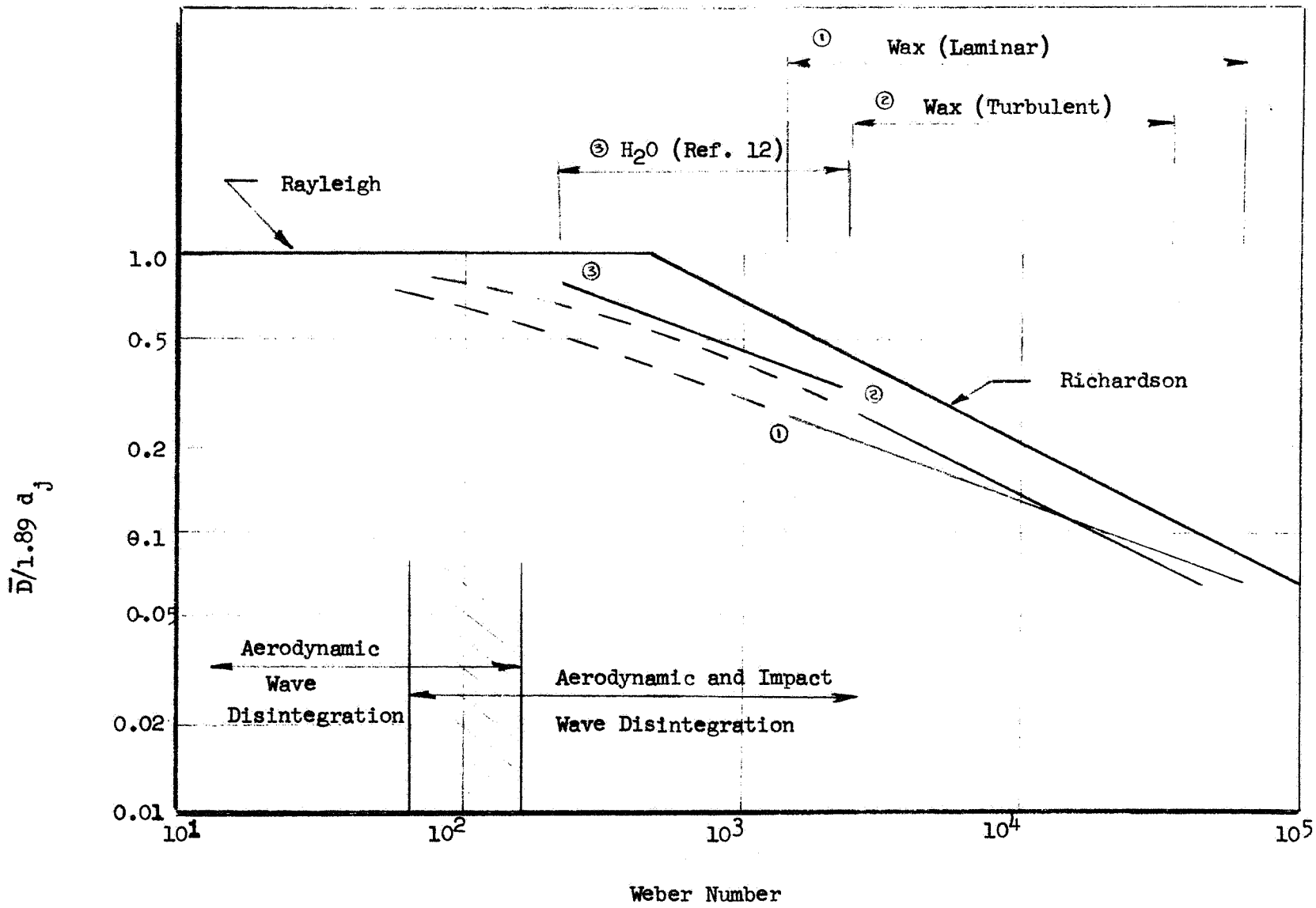

Figure D1. Mass Median Dropsize Versus Weber Number

APPENDIX E

DERIVATION OF SHEET BREAK-UP MODEL

The mechanism by which a liquid sheet disintegrates into droplets depends upon the specific operating conditions. In the derivation of this model it is assumed that the cause of the instabilities leading to sheet breakup is due to the amplification of small disturbances by the interaction of the sheet with the surrounding atmosphere. When the waves generated by this interaction reach a critical amplitude, fragments of the sheet are torn off. The fragments contract into ligaments and finally break down into droplets.

If the sheet is formed from the impingement of immiscible fluids, it can be assumed to be comprised of two adjacent sheets. The upper sheet, of thickness h_1, moves at a velocity V_1 and lower sheet, of thickness h_2, has a velocity V_2. In the derivation of the model it is further assumed that the sheets retain separate identities but remain in contact at the interface at all times.

The movement of the atmosphere above and below the sheet is caused solely solely by the wave motion of the sheet. If the gas is inviscid and incompressible and the sheets are of infinite width, the gas flow is irrotational and is defined by the Laplace equation in two spatial dimensions

$$\frac{\partial^2 \psi}{\partial x'^2} + \frac{\partial^2 \psi}{\partial y'^2} = 0 \qquad \text{(E-1)}$$

where ψ is the velocity potential. The local components of velocity, u and v, are defined by

$$u = \frac{\partial \psi}{\partial X}, \quad v = \frac{\partial \psi}{\partial y'} \tag{E-2}$$

A solution to Eq. (E-1) for a sinusoidal disturbance of increasing amplitude and velocity V moving along the X-axis is given by

$$\psi = \psi \text{ EXP} \left[(a + in)(X - Vt)\right]$$

where

$$\psi = \psi \quad (y')$$

while a and n are the wave growth per unit distance and the wave number respectively.

Combining Eqs. (E-1) and (E-3) and integrating yields

$$\psi = \psi_o \text{ EXP} \left[i(a + in)y'\right] \tag{E-4}$$

Combining Eqs. (E-3) and (E-4) yields the solution

$$\psi = \psi_o \text{ EXP} \left[(a + in)(X - Ut) + i(a + in)y'\right] \tag{E-5}$$

For an incompressible, inviscid fluid the pressure gradient in the y direction is related to the acceleration of the gas through the linearized equation

$$-\frac{1}{\rho}\left(\frac{\partial P}{\partial y'}\right) = \frac{\partial v}{\partial t} \tag{E-6}$$

The velocity, v, can be written in terms of the rate of displacement of a gas streamline by

$$v = \frac{\partial \delta}{\partial t} \tag{E-7}$$

From Eq. (E-2), the velocity component is also given by

$$v = \frac{\partial \Psi}{\partial y'} \tag{E-8}$$

If we define $\psi = \frac{\partial \phi}{\partial t}$, Eq. (E-8) can be written as

$$v = \frac{\partial}{\partial t} \left(\frac{\partial \phi}{\partial y'} \right) \tag{E-9}$$

Equating Eqs. (E-7) and (E-9) yields

$$\delta = \frac{\partial \phi}{\partial y'} \tag{E-10}$$

While Eq. (E-6) becomes

$$\frac{1}{\rho} \frac{\partial P}{\partial y} = - \frac{\partial^2}{\partial t^2} \left(\frac{\partial \phi}{\partial y'} \right)$$

or, after integration

$$P = - \rho \frac{\partial^2 \phi}{\partial t^2} \tag{E-11}$$

Substituting the definition of ψ, into Eq. (E-5) and performing the integration yields

$$\phi = - \frac{\psi_o}{(a + in)V} \text{ EXP } \left\{ (a + in) (X - Vt) + i(a + in)y' \right\} \tag{E-12}$$

From Eqs. (E-10) and (E-12), the displacement of a gas streamline is given by

$$= - \frac{i \psi_o}{v} \text{ EXP } \left[(a + in) (X - Vt) + i(a + in)y' \right] \tag{E-13}$$

Similarly, the pressure is obtained from Eqs. (E-11) and (E-12).

$$P = \rho(a + in)\, V\psi_o \;\; EXP \left[(a + in)\,(X - Vt) + i(a + in)y'\right] \qquad (E\text{-}14)$$

Combining Eqs. (E-13) and (E-14) the gas pressure can be expressed in terms of the velocity, wave number and displacement by

$$P = - \rho V^2 n\delta \qquad (E\text{-}15)$$

Following Dombrowski, Ref. 10, consider a sheet moving in the X-direction and decreasing in thickness. For a sinusoidal wave motion, the position of the interface is given by

$$y = T(t) \sin(nX + \epsilon) \qquad (E\text{-}16)$$

where T, the wave amplitude, is a function of time only while ϵ is the phase angle.

The motion of the interface of the two sheets is governed by the forces caused by the gas pressure, surface tension, liquid inertia and viscosity.

The displacement, δ, of the upper surface of the sheet from the undisturbed position is $(y_1 - h_1)$. The pressure exerted by the gas on the sheet is, from Eq. (E-15),

$$P_u = n \rho V_1^2 (y_1 - h_1)$$

and the force is therefore

$$P_u\, dA = n \rho V_1^2 (y_1 - h_1)\, Z dx = n \rho V_1^2 y\, Z dx$$

Similarly, the force on the lower surface is

$$P_L dA = N \rho V_2^2 (y_2 + h_2) Zdx = n \rho V_1^2 y Zdx$$

The total pressure force is therefore

$$F_p = n \rho (V_1^2 + V_2^2) y Zdx \qquad \text{(E-17)}$$

For the upper sheet, the force caused by surface tension (F_σ) has a component in the y-direction given by

$$F_{\sigma_1} = \sigma_1 Z \left(\frac{\partial y_1}{\partial X} + \frac{\partial y}{\partial X}\right)$$

Similarly, for the lower sheet the force is

$$F_{\sigma_2} = \sigma_2 Z \left(\frac{\partial y_2}{\partial X} + \frac{\partial Y}{\partial X}\right)$$

Since $y_1 = y + h_1$ and $y_2 = y - h_2$, the net force along a length dx is

$$F = \lim_{\Delta X \to 0} \frac{\Delta (F_1 + F_2)}{\Delta X} =$$

$$\frac{\partial}{\partial X}\left\{2(\sigma_1 + \sigma_2) \frac{\partial y}{\partial X} + \left(\sigma_1 \frac{\partial h_1}{\partial X} - \sigma_2 \frac{\partial h_2}{\partial X}\right)\right\} Zdx \qquad \text{(E-18)}$$

The inertia force is given by the rate of change of momentum of a liquid element, i.e., for the upper sheet,

$$F_{I_1} = \frac{\partial}{\partial t}\left[(\rho_{L_1} h_1 Zdx)v\right]$$

or, since $v = \frac{\partial y}{\partial t}$

$$F_{I_1} = \rho L_1 \left[h_1 \frac{\partial^2 y}{\partial t^2} + \frac{\partial h_1}{\partial t} \frac{\partial y}{\partial t} \right] Z dx$$

for the lower sheet

$$F_{I_2} = - \rho L_2 \left[h_2 \frac{\partial^2 y}{\partial t^2} + \frac{\partial h_2}{\partial t} \frac{\partial y}{\partial t} \right] Z dx$$

The total inertia force is thus

$$F_I = - \left[(\rho L_1 h_1 + \rho L_2 h_2) \frac{\partial^2 y}{\partial t^2} + (\rho L_1 \frac{\partial h_1}{\partial t} + \rho L_2 \frac{\partial h_2}{\partial t}) \frac{\partial y}{\partial t} \right] Z dx \qquad \text{(E-19)}$$

To determine the viscous force we note that the shear stress at X for the upper sheet is

$$(\tau_{xy})_x = \mu_1 \left(\frac{\partial v}{\partial x} \right)_x$$

while at X + dx it is

$$(\tau_{xy})_{x + dx} = \mu 1 \left(\frac{\partial v}{\partial X} \right)_{x + dx}$$

Hence, the net shear force along a length d_x becomes

$$F_{\mu 1} = \frac{\Delta \tau_{wy}}{\Delta X} \, dA \, dx = \frac{\partial}{\partial X} \left[\mu_1 \, Zh_1 \, \frac{\partial v}{\partial X} \right] dx$$

Similarly, the shear force for the lower sheet is

$$F_{\mu 2} = \frac{\partial}{\partial X} \left[\mu_2 \, Zh_2 \, \frac{\partial v}{\partial X} \right] dx$$

Substituting, $v = \frac{\partial y}{\partial t}$, and summing, the total viscous force becomes

$$F_{\mu} = \frac{\partial}{\partial X} \left[\mu_1 \, h_1 \, \frac{\partial^2 y}{\partial t \partial X} + \mu_2 \, h_2 \, \frac{\partial^2 y}{\partial t \partial X} \right] = dx$$

or

$$F_{\mu} = \left[(\mu_1 H_1 + \mu_2 h_2) \, \frac{\partial^3 y}{\partial t \, X^2} + (\mu_1 \frac{\partial h_1}{\partial X} + \mu_2 \frac{\partial h_2}{\partial X} \, \frac{\partial^2 y}{\partial t \partial X} \right] Z dx \qquad \text{(E-20)}$$

The force balance for the sheet is then given by the sum of Eqs. (E-17) to (E-20). The resulting equation can be simplified under those conditions where the rate of change of the displacement of the interface from the undisturbed position is much greater than the rate of change of the sheet thickness. In order to examine when this occurs, the sheet thicknesses are assumed to vary according to

$$h_i = K_i X^r = K_i V_i^r t^r \qquad \begin{matrix} (i = 1,2) \\ (r \leq 0) \end{matrix} \qquad \text{(E-21)}$$

where K_i is a constant representing a characteristic sheet thickness. The position of the interface is given by Eq. (E-16).

The ratio of the first and second terms in Eq. (E-18) is

$$\frac{2\,(\sigma_1 + \sigma_2)\,\dfrac{\partial^2 y}{\partial X^2}}{\dfrac{\partial^2}{\partial X^2}\,(\sigma_1 h_1 + \sigma_2 h_2)}$$

Using Eq. (E-16), the numerator of the above becomes

$$2(\sigma_1 + \sigma_2)\,\frac{\partial^2 y}{\partial X^2} = -2(\sigma_1 + \sigma_2)\,\eta^2 y$$

The denominator can be evaluated from Eq. (E-21), which yields

$$(\sigma_1 h_1 + \sigma_2 h_2)\; r\,(r-1)\; X^{-2}$$

The ratio then becomes

$$\frac{2(\sigma_1 + \sigma_2)y}{(\sigma_1 h_1 + \sigma_2 h_2)} \qquad \frac{(\eta X)^2}{r(r-1)}$$

According to the above, the surface tension force resulting from a variation in h can be neglected when

$$(\eta X)^2 >> \left[\frac{r(r-1)\;(\sigma_1 h_1 + \sigma_2 h_2}{-2\,(\sigma_1 + \sigma_2)y}\right]$$

which can be simplified to

$$(\eta X)^2 >> \frac{h_1}{y}$$

for $r = -1$ and $h_1 \approx h_2$.

Dombrowski, et al, note that for inviscid sheet breakup

$$\eta = \frac{\rho V^2}{2\sigma}$$

For wax at a typical injection velocity of 50 ft/sec, η is on the order of 10^6 ft^{-1}. Consequently, even for small sheet lengths, X, and displacements, y, the second term of Eq. (E-18) can be neglected.

By noting that $\frac{\partial}{\partial t} = \frac{\partial X}{\partial t} \quad \frac{\partial}{\partial X} = \frac{\partial}{\partial X}$, and again using Eqs. (E-16) and (E-21), Eq. (E-19) can be rewritten as

$$F_I = -\Big[(\rho_{L_1} h_1 + \rho_{L_2} h_2) (-\eta^2 T \sin (\eta X + \epsilon)) V^2$$

$$+ (\rho_{L_1} h_1 + \rho_{L_2} h) (rX^{-1}) (\eta T \cos (\eta X + \epsilon)) \Big] V^2$$

The ratio of the maximum values of the first and second terms of the above Eq. is X/r. As before, the inertia force resulting from changes in the sheet thickness can be neglected for a sufficiently large wave number , η . An identical result is obtained when the viscous forces of Eq. (E-20) are compared.

Thus, for large η, the sum of the forces acting on the sheet can be reduced to

$$F_P + F_\sigma + F_I + F_\mu = \Big[\eta\rho(V_1^2 + V_2^2)y + 2(\sigma_1 + \sigma_2) \frac{\partial^2 y}{\partial X^2}$$

$$- (\rho L_1 h_1 + \rho_{L_2} h_2) \frac{\partial^2 y}{\partial t^2} + (\mu_1 h_1 + \mu_2 h_2) \frac{\partial^3 y}{\partial t \partial X^2} \Big] Z dx = 0 \qquad \text{(E-22)}$$

Substituting Eq. (E-16) and letting $T = T_o$ EXP (f) where f is the total wave growth, Eq. (E-22) becomes

$$\eta\,\rho(V_1^2 + V_2^2) - 2(\sigma_1 + \sigma_2)\,\eta^2 - (\rho_{L_1} h_1 + \rho_{L_2} h_2)\left(\frac{\partial f}{\partial t}\right)^2$$

$$- (\sigma_1 h_1 + \sigma_2 h_2)\eta^2 \left(\frac{\partial f}{\partial t}\right) = 0 \qquad \text{(E-23)}$$

Equation (E-23) can be put into a form identical to the force balance obtained for a single sheet by defining the fluid properties as

$$\begin{aligned} 2V^2 &= (V_1^2 + V_2^2) \\ \bar{\sigma} &= (\sigma_1 + \sigma_2) \\ \bar{\rho}_{L_1} &= (\rho_{L_1} + h_2/h_1\ \rho_{L_2}) \\ \bar{\mu}1 &= (\mu_1 + h_2/h_1\ \mu_1) \end{aligned} \qquad \text{(E-24)}$$

or

$$\begin{aligned} \bar{\rho}_{L_2} &= (\rho_{L_1} h_1/h_2 + \rho_{L_2}) \\ \bar{\mu}_2 &= (\mu_1 h/h_2 + \mu_2) \end{aligned}$$

Substituting the above into Eq. (E-23) yields

$$2\rho V^2 - 2\bar{\sigma}\eta^2 - \bar{\rho}_{L_1} h_1 \left(\frac{\partial^2 f}{\partial t^2}\right) - \bar{\mu}_1 h_1 \eta^2 \left(\frac{\partial f}{\partial t}\right) = 0 \qquad \text{(E-25)}$$

and

$$2\rho V^2 - 2\bar{\sigma}\eta^2 - \bar{\rho}_{L_2} h_2 \frac{\partial^2 f}{\partial t^2} - \bar{\mu}_2 h_2 \eta^2 \left(\frac{\partial f}{\partial t}\right) = 0$$

Thr form of Eqs. (E-25) is identical to Eq. (24) of Ref. 10. Consequently, the relations for the size of the ligaments and droplets resulting from the wave disintegration of a double sheet are also identical in form to that obtained for a single sheet and can be written directly from the results presented in Ref. 10.

In their analysis, Dombrowski, et al, considered the cases where the exponent, r, of Eq. (E-21) is either 0 or -1. The case of interest here is that of an attenuating sheet where r = -1 or

$$h = \frac{K_i}{X} = \frac{K_i}{V_i t} \quad (i = 1,2) \tag{E-26}$$

According to Ref. 10, the diameter of cylindrical ligaments produced by the wave disintegration of a single sheet is given by

$$D_L = 0.9614 \left[\frac{k^2 \sigma^2}{\rho \rho_L V^2} \right]^{1/6} \left[1 + 2.6 \mu^3 \sqrt{\left(\frac{k \rho^4 V^8}{72 \rho_L^2 \sigma^5} \right)} \right]^{1/5} \tag{E-27}$$

where

$k = K/V$.

The diameter of the droplets resulting from the breakdown of the ligaments is given by (see Ref. 10),

$$\bar{D} = 1.88 \; D_L \left[1 + \sqrt{\frac{3\mu}{(\rho_L \sigma D_L)}} \right]^{1/6} \tag{E-28}$$

From Eq. (E-27) the ligament diameters produced from the upper sheet, D_{L_1}, can be obtained by substituting Eqs. (E-24) and noting that $k_1 = K_1/V_1$.

Hence

$$D_{L_1} = 0.9614 \left[\frac{K_1^2}{V_1^2} \quad \frac{\bar{\sigma}^2}{\rho \bar{\rho}_{L_1} V^2} \right]^{1/6} \left[1 + 2.6 \mu_1^3 \sqrt{\left(\frac{K_1 \rho^4 V^8}{72 V_1 \bar{\rho}_{L_1}^2 \bar{\sigma}^5} \right)} \right]^{1/5} \tag{E-29}$$

Similarly, the diameter of the ligaments produced by the lower sheet is

$$D_{L_2} = 0.9614 \left[\frac{K_2^2}{V_2^2} \quad \frac{\bar{\sigma}^2}{\rho \rho_{L_2} V^2} \right]^{1/6} \left[1 + 2.6 \mu_2^3 \left(\frac{K_2 \rho^4 U^8}{72 V_2 \bar{\rho}_{L_2}^2 \bar{\sigma}^5} \right)^{1/5} \right]$$

, (E-30)

For small sheet velocities and correspondingly large ligament diameters, the second terms of Eqs. (E-28) to (E-30) can be neglected in comparison to the first and the dropsizes approximated by

$$D_i = 1.88 \ (0.9614) \left[\frac{K_i^2}{V_i^2} \quad \frac{\bar{\sigma}^2}{\rho \bar{\rho}_{L_i} V^2} \right]^{1/6} \qquad (i = 1,2) \qquad \text{(E-31)}$$

By noting that

$$V^2 = (V_1^2 + V_2^2)/2$$

$$\rho_{L_2} = \frac{h_1}{h_2} \rho_{L_1}$$

and defining the dynamic pressure ratio of the two sheets by

$$P_D = \frac{(\rho V^2)_2}{(\rho V^2)_1}$$

Eq. (D-31) can be rewritten as

$$D_1 = 1.81 \left[\frac{2K_1^2 \ \bar{\sigma}^2}{V_1^4 \ \rho \bar{\rho}_{L_1} (1 + P_D \frac{\rho_1}{\rho_2})} \right]^{1/6} \qquad \text{(E-32)}$$

and

$$D_2 = 1.81 \left[\frac{2K_2^2 \ P_D \ \bar{\sigma}^2 \ h_2/h_1}{V_2^4 \ \rho \bar{\rho}_{L_1} (\frac{\rho_1}{\rho_2} + P_D)} \right]^{1/6} \qquad \text{(E-33)}$$

APPENDIX F

DISTRIBUTION LIST FOR FINAL REPORT
(Contract NAS7-726)

Recipient	Copies
NASA Headquarters Washington, D. C. 20546	
Contracting Officer	1
Patent Office	1
NASA Lewis Research Center 21000 Brookpark Road Cleveland, Ohio 44135	
Office of Technical Information	1
NASA Manned Spacecraft Center Houston, Texas 77058	
Office of Technical Information	1
J. Thibodaux, Jr.	1
NASA Marshall Space Flight Center Huntsville, Alabama 35812	
Dale Burrows, S+E-ASTN-PJ	1
NASA Ames Research Center Moffett Field, California 94035	
Patents and Contracts Management	1
Jet Propulsion Laboratory 4800 Oak Grove Drive Pasadena, California 91103	
Jack Rupe	1
Raymond Kushida	1
Richard M. Clayton	2
Robert Riebling	1
Manager, Liquid Rocket Propulsion Technology, RPL Office of Advanced Research and Technology NASA Headquarters Washington, D. C. 20546	3
Director, Technology Utilization Division Office of Technology Utilization NASA Headquarters Washington, D. C. 20546	1

Recipient	Copies
NASA Scientific and Technical Information Facility P.O. Box 33 College Park, Maryland 20740	1 25
Director, Launch Vehicles and Propulsion, SV Office of Space Science and Applications NASA Headquarters Washington, D. C. 20546	1
Director, Advanced Manned Missions, MT Office of Manned Space Flight NASA Headquarters Washington, D. C. 20546	1
Mission Analysis Division NASA Ames Research Center Moffett Field, California 24035	1
Ames Research Center Moffett Field, California 94035 Hans M. Mark	1
Goddard Space Flight Center Greenbelt, Maryland 20771 Merland L. Moseson, Code 620	1
Jet Propulsion Laboratory California Institute of Technology 4800 Oak Grove Drive Pasadena, California 91103 Henry Burlage, Jr. Propulsion Division 38	2
John F. Kennedy Space Center, NASA Cocoa Beach, Florida 32931 Dr. Kurt H. Debus	2
Langley Research Center Langley Station Hampton, Virginia 23365 Ed Cortwright, Director	2
Lewis Research Center 21000 Brookpark Road Cleveland, Ohio 44135 E. W. Conrad Allen J. Metzler Dr. Abe Silverstein	2
Marshall Space Flight Center Huntsville, Alabama 35812 Hans G. Paul, Code R-P+VED	2

Recipient	Copies
Manned Spacecraft Center Houston, Texas 77058 H. Pohl	2
Arnold Engineering Development Center Arnold Air Force Station Tullahoma, Tennessee 37388 Dr. H. K. Doetsch	1
Air Force Rocket Propulsion Laboratory Research and Technology Division Air Force Systems Command Edwards, California 93523 RPRPD/Mr. H. Main R. R. Weiss	2
Aeronautical Systems Division Air Force Systems Command Wright-Patterson Air Force Base Dayton, Ohio 45433 D. L. Schmidt, Code ASRCNC-2	1
Defense Documentation Center Headquarters Cameron Station, Building 5 5010 Duke Street Alexandria, Virginia 22314 Attn: TISIA	1
Bureau of Naval Weapons Department of the Navy Washington, D. C. 20546 J. Kay, RTMS-41	1
U.S. Naval Ordnance Test Station China Lake, California 93557 D. Couch	1
Picatinny Arsenal Dover, New Jersey 07801 I. Forsten, Chief Liquid Propulsion Laboratory	1
U.S. Army Missile Command Redstone Arsenal Alabama 35809 Mr. Walter Wharton	1
U.S. Bureau of Mines 4800 Forbes Avenue Pittsburgh, Pennsylvania 15213 Library	1

Recipient	Copies
Air Force Office of Scientific Research 1400 Wilson Boulevard Arlington, Virginia 22209 B. T. Wolfson	1
Chemical Propulsion Information Agency Applied Physics Laboratory 8621 Georgia Avenue Silver Spring, Maryland 20910 Tom Reedy	1
Aerojet-General Corporation P.O. Box 296 Azusa, California 91703 W. L. Rogers	1
Aerojet-General Corporation Space Division 9200 East Flair Drive El Monte, California 91734 S. Machlawski	1
Aerospace Corporation 2400 East El Segundo Boulevard P.O. Box 95085 Los Angeles, California 90045 O. W. Dykema	1
Atlantic Research Corporation Edsall Road and Shirley Highway Alexandria, Virginia 22314 Dr. Ray Friedman	1
Bell Aerosystems Company P.O. Box 1 Buffalo, New York 14240 W. M. Smith	1
Boeing Company P.O. Box 3999 Seattle, Washington 98124 J. D. Alexander	1
Wright Aeronautical Division Curtiss-Wright Corporation Wood-Ridge, New Jersey 07075 C. Kelley	1
Research Center Fairchild Hiller Corporation Germantown, Maryland Ralph Hall	1

Recipient	Copies
Missile and Space Systems Center General Electric Company Valley Forge Space Technology Center P.O. Box 8555 Philadelphia, Pennsylvania F. Mezger F. E. Schultz	1
Grumman Aircraft Engineering Corporation Bethpage, Long Island New York 11714 Joseph Gavin	1
Honeywell, Inc. Aerospace Division 2600 Ridgway Road Minneapolis, Minnesota Mr. Gordon Harms	1
Hughes Aircraft Company Aerospace Group Centinela and Teale Streets Culver City, California 90230 E. H. Meier V.P. and Division Manager Research + Dev. Div.	1
Arthur D. Little, Inc. 20 Acorn Park Cambridge, Massachusetts 02140 Library	1
Lockheed Propulsion Company P.O. Box 111 Redlands, California 92374 Library	1
The Marquardt Corporation 16555 Saticoy Street Van Nuys, California 91409 Howard McFarland	1
Denver Division Martin Marietta Corporation P.O. Box 179 Denver, Colorado 80201 Dr. Morganthaler A. J. Kullas	1
Astropower Laboratory McDonnell Douglas Aircraft Company 2121 Paularino Newport Beach, California 92663 Dr. George Moc, Director - Research	1

Recipient	Copies
Missile and Space Systems Division McDonnell Douglas Aircraft Company 3000 Ocean Park Boulevard Santa Monica, California 90406 Mr. R. W. Hallet, Chief Engineer Adv. Space Technology	1
Space and Information Systems Division North American Rockwell Corporation 12214 Lakewood Boulevard Downey, California 90241 Library	1
Northrop Space Laboratories 3401 West Broadway Hawthorne, California 90250 Dr. William Howard	1
Stanford Research Institute 333 Ravenswood Aven ue Menlo Park, California 94025 Dr. Gerald Marksman	1
TRW Systems Group TRW Incorporated One Space Park Redondo Beach, California 90278 G. W. Elverum R. N. Porter	1
Research Laboratories United Aircraft Corporation 400 Main Street East Hartford, Connecticut 06108 Erle Martin	1
United Technology Center 587 Methilda Avenue P.O. Box 358 Sunnyvale, California 94088 Dr. David Altman	1
Pratt-Whitney Aircraft Florida Research - Development Center P.O. Box 2691 West Palm Beach, Florida 33402 G. D. Lewis	1
Defense Research Corporation P.O. Box 3587 Santa Barbara, California 93105 Mr. Gray	1

Recipient	Copies
AiResearch Manufacturing Company 9851 Sepulveda Boulevard Los Angeles, California 90009 Library	1
Aerojet -General Corporation P.O. Box 1947 Sacramento, California 95809 Library	1
Dynamic Science 2400 Michelson Drive Irvine, California 92664 Library	1
Mathematical Applications Group, Inc. 180 South Broadway White Plains, New York 10605 Dr. S. Z. Burstein	1
Ohio State University Department of Aeronautical Engineering Columbus, Ohio 43210 R. Edse	1
Pennsylvania State University Mechanical Engineering Department 207 Mechanical Engineering Boulevard University Park, Pennsylvania 16802 G. M. Faeth	1
University of Southern California Department of Mechanical Engineering University Park Los Angeles, California 90007 M. Gerstein	1
Princeton University Forrestal Campus Guggenheim Laboratories Princeton, New Jersey 08540 D. Jarrje I. Glassman	1
University of Wisconsin Mechanical Engineering Department 1513 University Avenue Madison, Wisconsin 53705 P. S. Myers	1
University of Michigan Aerospace Engineering Ann Arbor, Michigan 48104 J. A. Nicholls	1

Recipient	Copies
University of California Department of Chemical Engineering 6161 Etcheverry Hall Berkeley, California 94720 A. K. Oppenhiem R. Sawyer	1
Purdue University School of Mechanical Engineering Lafayette, Indiana 47907 Library	1
Sacramento State College Engineering Division 60000 J. Street Sacramento, California 95819 E. H. Reardon	1
Illinois Institute of Technology Room 200 M.H. 3300 S. Federal Street Chicago, Illinois 60616 T. P. Torda	1
Polytechnic Institute of Brooklyn Graduate Center Route 110 Farmingdale, New York V. D. Agosta	1
Georgia Institute of Technology Atlanta, Georgia 30332 B. T. Zinn	1
University of Denver Research Institute Denver, Colorado Library	1
New York University Department of Chemical Engineering University Heights New York 53, New York Leonard Dauerman	1
The Johns Hopkins University Applied Physics Laboratory 8621 Georgia Avenue Silver Springs, Maryland 20910 W. G. Berl	1
Dartmouth University Hanover, New Hampshire 03755 Library	1

Recipient	Copies
Massachusetts Institute of Technology Department of Mechanical Engineering Cambridge, Massachusetts 02139 T. Y. Toong	1
The University of Sheffield Department of Fuel Technology St. George's Square Sheffield 1, Yorks, England Mr. J. Swithenbank	1
Motorlar Enstitusu Professor Zubeyir Demirgue Director of Engine Institute Istanbul - Gumussuyu	1
Instituto Nacional de Tecnica Aeroespacial Carlos Sanchez-Tarifa Seranno 43 Madrid, Spain	1